GEOTILL Inc.

Geotechnical Engineering • Subsurface Exploration • Environmental Services • Construction Testing and Material Engineering

GEOTECHNICAL ENGINEERING LIBRARY

GEOTILL

USA

GEOTILL

ENGINEERING, INC.

Phone 317-449-0033 Fax 317- 285-0609

info@geotill.com

Toll Free: 844-GEOTILL

Geotechnical, Environmental and Construction Materials Testing Professionals

www.geotill.com

Offices Covering all USA

School of Civil and Environmental Engineering

Profiling the Overconsolidation Ratio of Clays by Piezocone Tests

Barry Shiyo Chen, PhD, P.E.

Paul W. Mayne, PhD, P.E.

National Science Foundation

August 1994

Report No. GIT-CEEGEO-94-1

Profiling the Overconsolidation Ratio of Clays by Piezocone Tests

prepared by

Barry Shiyo Chen, PhD, P.E.
Research Assistant

and

Paul W. Mayne, PhD, P.E.
Principal Investigator

GTRC Project No. E20-648/X51

Georgia Tech Research Corporation
Georgia Institute of Technology
School of Civil & Environmental Engineering
Atlanta, Georgia 30332-0355

for

NSF Grant No. MSS-9108234

National Science Foundation
Geomechanical, Geotechnical
and Geoenvironmental Program
4201 Arlington Boulevard
Arlington, Virginia 22230

August 1994
Reissued November 1994

Profiling the Overconsolidation Ratio of Clays by Piezocone Tests

NSF Grant No. MSS-9108234

B.S-Y. Chen and P.W. Mayne

Executive Summary

The capability of utilizing piezocone tests for evaluating the magnitude of yield stress in natural clays is examined using experimental, analytical, and statistical methods. Results are expressed in terms of the overconsolidation ratio and normalized piezocone parameters.

Experimental field studies are performed using paired sets of piezocones with differing positions of the porous filter elements and special dual- and triple-element penetrometers that can measure penetration pore water pressures simultaneously at more than one location along the cone. Two field test programs involved a soft to firm lacustrine clay at Port Huron, Michigan and a stiff desiccated deltaic clay in Baton Rouge, Louisiana.

Empirical expressions relating stress history to measured piezocone parameters are derived from regression analyses using a database compiled from 205 clay sites worldwide.

An analytical approach was developed based on spherical cavity expansion theory and constitutive soil models that follow the concepts of critical state soil mechanics. The effects of initial stress state, undrained strength anisotropy, stress path loading, and strain rate are considered in the approach. Formulations are presented to address piezocones having different positions for measuring pore water pressure, including: (1) face/tip and (2) shoulder elements.

ACKNOWLEDGMENTS

The authors extend sincere gratitude and appreciation to a number of individuals who provided support and encouragement throughout this research effort. In particular, Dr. Mehmet T. Tumay, Program Director at NSF, provided the research funding over the past three years. Kaare Senneset of the Norwegian Institute of Technology, Trondheim, provided the triple-element piezocone for use in the experimental work. Messrs. Paul Griffin and J.B. Esnard of the Louisiana Dept. of Transportation and Development and Mr. Bill Tierney of the Louisiana Transportation Research Center helped complete the testing and sampling in Baton Rouge. Messrs. John S. Jones, Jr., David A. Panich, and Ken Abbott provided the opportunity to collect piezocone data in Port Huron. Dr. Alan J. Lutenegger of the University of Massachusetts-Amherst and Mr. Carl Davey of Clarkson University assembled the cone penetrometers for the GT testing system. The second author is grateful to Dr. Wayne Clough for lending the miniature electric cone for chamber tests conducted at Cornell.

A guidance committee assisted the first author during his residency as a graduate research assistant on this project including: Dr. Richard D. Barksdale, Dr. Glenn J. Rix, Dr. Wan-Lee Yin, and Dr. Nader S. Rad. Helpful comments and criticism for improving the final product was offered by Dr. Jean-Lou Chameau, now of Golder Associates. Advice was also provided by Drs. J. David Frost, Emir J. Macari, and James S. Lai of Georgia Tech.

A number of graduate students assisted during several different stages of the project, including: Doug N. Brown, Susan E. Burns, Wes Spang, Kevin Sutterer, Jorge Alba, Chun-Yi Kuo, Yasser Hegasy, Erol Tutumluer, and others. Thanks are extended to Ms. Vicki Clopton and Lee Wilder for helping to prepare the final report and to Karen Mayne for proof-editing versions. Appreciation is also given to Messrs. Ken Thomas, Larry Westbrooks, and Seth Scott for assisting in the mechanical and testing details.

Several individuals contributed data, interesting discussion, and/or words of wisdom to the authors during the project: Jay Auxt, Ming-Fang Chang, J.C. Chern, Ramesh Gupta, Greg Hamadock, An-Bin Huang, Ray Franz, Mike Jamiolkowski, Ilan Juran, Demetrious Koutsoftas, Steve Kraemer/H&A, Steve Kramer/Univ. of Wash., Suzanne Lacasse, Rolf Larrson, Jerry Leonards, Serge Leroueil, Mike Lewis, Tom Lunne, Jim Niehoff, Hideki Ohta, Dennis O'Meara, John Powell, Brian Taylor, Stevan Vidic, George Voyiadjis, Andrew Whittle, as well as the late Charles Peter Wroth.

TABLE OF CONTENTS

McClelland-Type Piezocone With Apex Element.

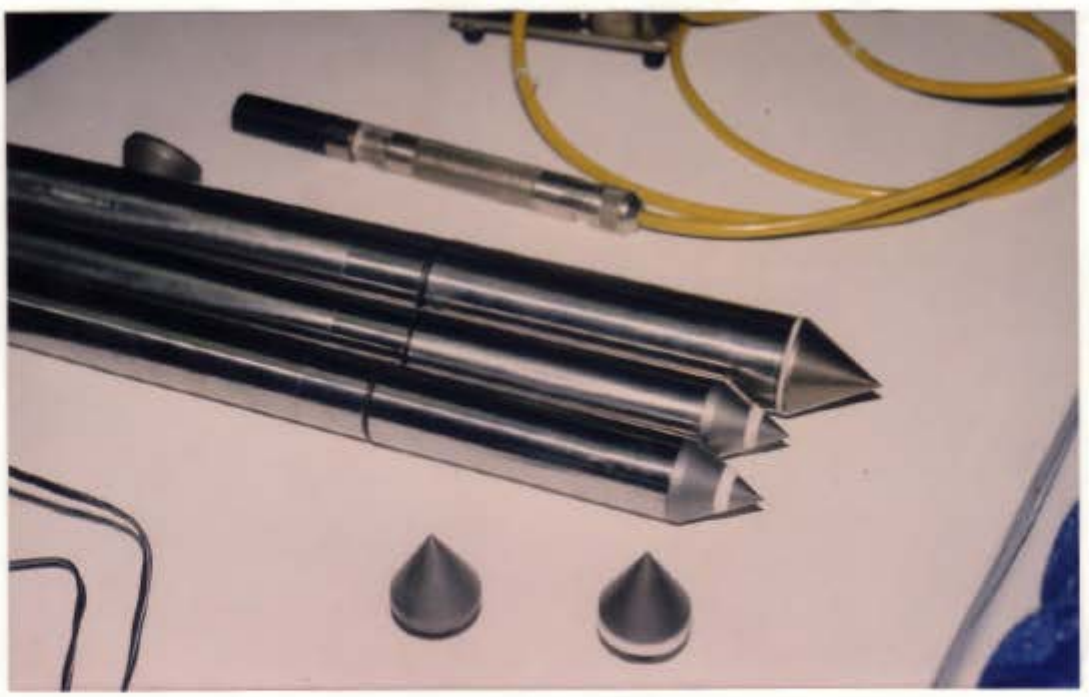

Penetrometers (10-cm^2 and 15-cm^2) with Interchangeable Tips and Elements.

Fugro-Type Triple-Element Piezocone (courtesy Kaare Senneset, NTH).

Quad-Element Piezocone (courtesy Gillian Sills, Oxford University).

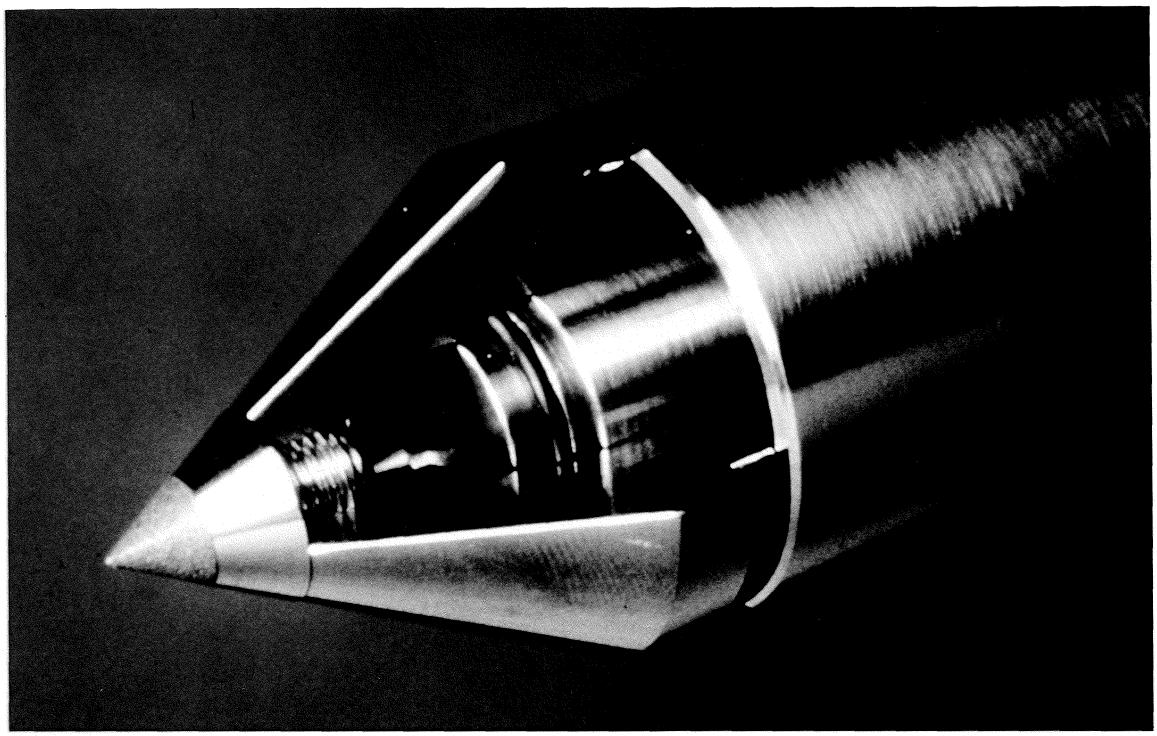

McClelland-Type Piezocone With Apex Element.

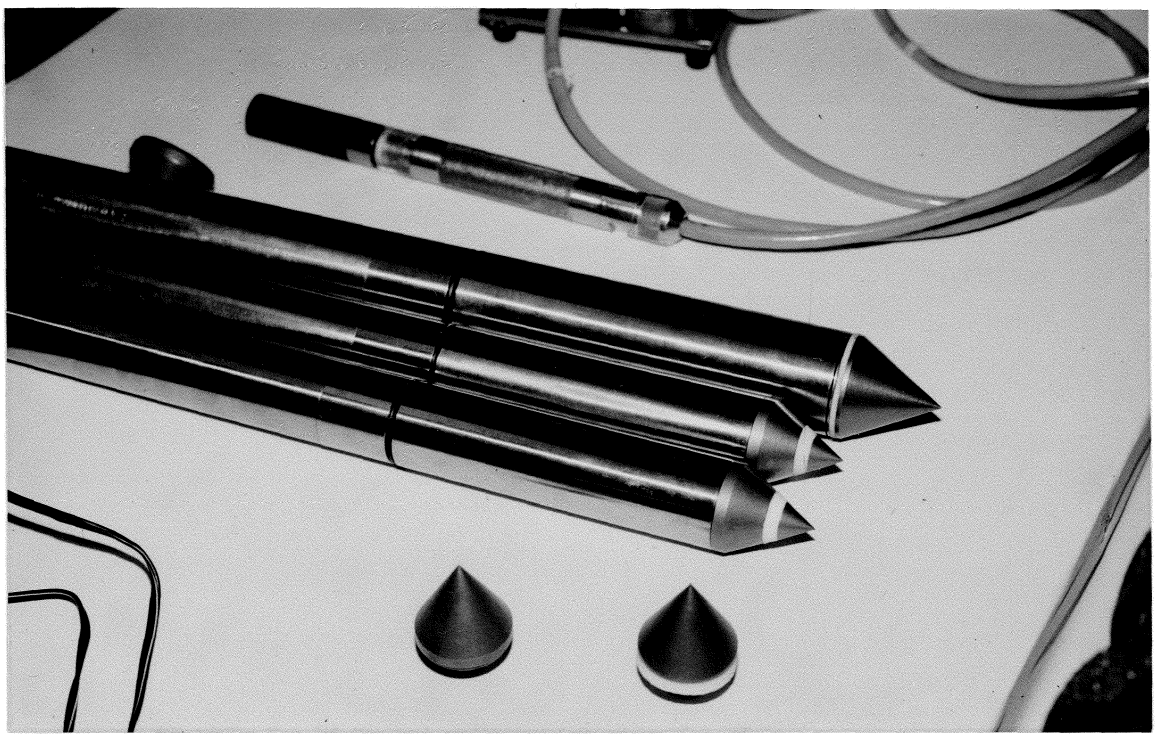

Penetrometers (10-cm^2 and 15-cm^2) with Interchangeable Tips and Elements.

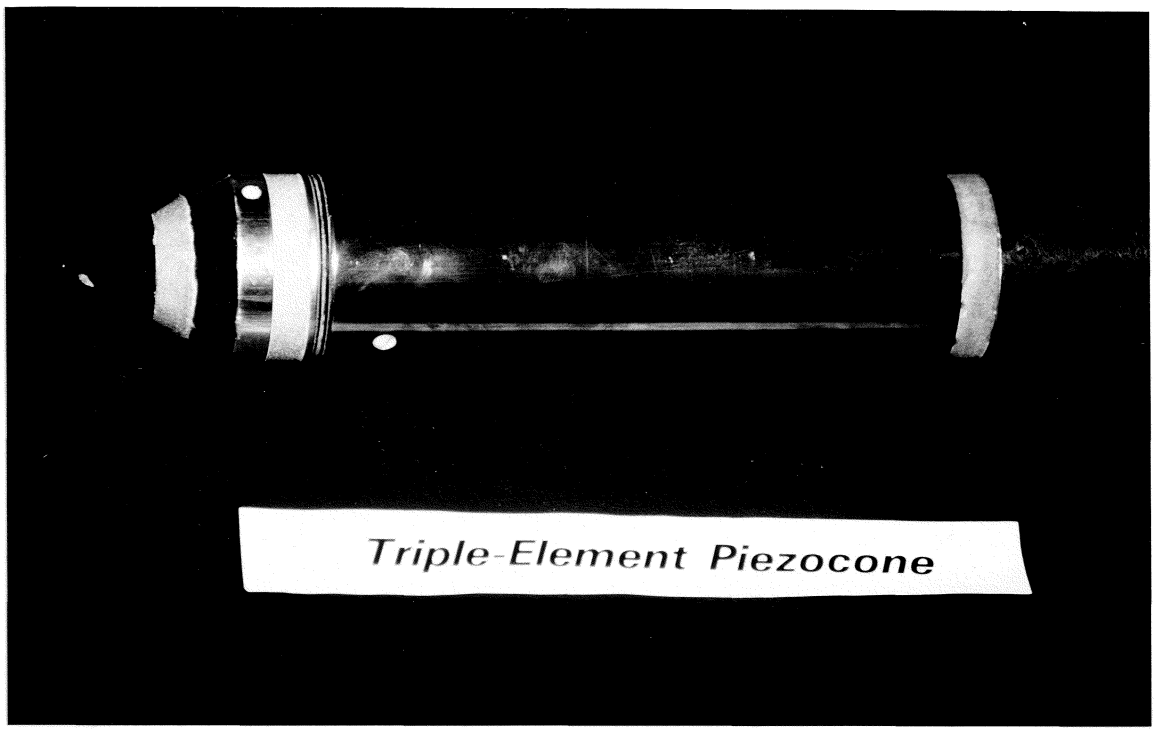

Fugro-Type Triple-Element Piezocone (courtesy Kaare Senneset, NTH).

Quad-Element Piezocone (courtesy Gillian Sills, Oxford University).

LIST OF SYMBOLS

A = Skempton's pore pressure parameter.
A_{bs} = sleeve end area behind sleeve.
A_{bt} = sleeve end area behind tip.
A_s = surface area of friction sleeve.
A_t = projected surface area of cone tip (usually 10 cm^2 or 15 cm^2).
B_q = piezocone pore pressure parameter = $\Delta u/(q_T-\sigma_{vo})$.
a = net area ratio.
a_k = factor in Modified Cam Clay equation (also: a).
a' = attraction = $c'\cot\phi'$.
a^* = empirical factor term for K_o.
b = factor in plane strain version of Modified Cam Clay.
b^* = empirical factor term for K_o.
C_c = virgin compression index.
C_r = recompression index.
C_s = swelling index.
$C_{\alpha e}$ = coefficient of secondary compression.
c_v = coefficient of consolidation.
c' = effective cohesion intercept.
D = constrained modulus = $(1/m_v)$.
e = void ratio.
e_o = initial void ratio.
F = normalized sleeve friction = $f_T/(q_T-\sigma_{vo})$.
f_s = measure sleeve friction.
f_T = corrected sleeve friction.
G = shear modulus.
G_s = specific gravity of solids.
I_o = octahedral stress = σ_o.
I_p = plasticity index (also PI).
I_r = G/s_u = rigidity index (undrained).
K_{45} = anisotropic strength ratio = $s_u(DSS)/s_u(TC)$.
K_o = lateral stress coefficient = $\sigma_{ho}'/\sigma_{vo}'$.
k = permeability or hydraulic conductivity.
LL = liquid limit (also w_L).
M = failure line in Cambridge q-p' space = $(6\sin\phi')/(3-\sin\phi')$.
m_v = coefficient of volumetric compressibility.
N_c = specific cone bearing factor.
N_{kT} = cone bearing factor = $(q_T-\sigma_{vo})/s_u$.
N_{qc} = specific cone bearing factor.
N_{qu} = cone bearing factor = $(q_T-u)/s_u$.
N_u = cone pore pressure factor = $\Delta u/s_u$.
n = number of data sets.

OCR	=	overconsolidation ratio = σ_p'/σ_{vo}'.
PI	=	plasticity index (also I_p).
PPD	=	normalized pore pressure.
p	=	mean stress or octahedral stress = $\frac{1}{3}(\sigma_1+\sigma_2+\sigma_3)$.
p'	=	mean effective stress.
p_o	=	lift off pressure from dilatometer test.
p_1	=	expansion pressure from dilatometer test.
Q	=	normalized net cone tip resistance = $(q_T-\sigma_{vo})/\sigma_{vo}'$.
q	=	deviatoric stress = $(\sigma_1-\sigma_3)$.
q_c	=	measured cone tip resistance.
q_T	=	corrected cone tip resistance = $q_c + (1\text{-}a)u_2$
r^2	=	coefficient of determination from regression.
s_u	=	undrained shear strength.
u_m	=	measured penetration pore water pressure.
u_o	=	hydrostatic pore pressure.
u_1	=	penetration pore water pressure measured on cone face/tip (also u_t).
u_2	=	penetration pore water pressure measured at shoulder (also u_{bt}).
u_3	=	penetration pore water pressure measured behind sleeve (u_{bs}).
v	=	specific volume = (1+e).
w_n	=	natural water content.
α	=	regression term.
α	=	pore pressure ratio = u_1/u_2.
ß	=	regression term.
ß	=	normalized pore pressure term.
$d\epsilon/dt$	=	strain rate (percent per hour).
Δu	=	excess pore water pressure.
δ	=	interface friction angle between soil and material.
ϵ	=	axial strain.
γ	=	unit weight; shear strain.
κ	=	isotropic swelling index.
Λ	=	plastic volumetric strain ratio = $1\text{-}\kappa/\lambda$.
λ	=	isotropic compression index.
σ	=	normal stress.
σ_h'	=	effective horizontal stress.
σ_o'	=	effective octahedral stress = p'.
σ_p'	=	effective preconsolidation stress or yield stress (P_c' or σ_{vmax}').
σ_v	=	total vertical stress.
σ_v'	=	effective vertical stress.
σ_{vo}'	=	current effective vertical stress.
ϕ'	=	effective stress friction angle.
τ	=	shear stress.
Θ	=	½ apex angle of cone (Θ = 30° for standard cone).

CHAPTER 1
INTRODUCTION

The piezocone test has become an important tool for site characterization and the evaluation of soil engineering properties in-situ. Data from the test can be used either qualitatively and/or quantitatively in evaluating the subsurface conditions on geotechnical projects. Specific advantages of the piezocone include: (1) testing under the in-situ ambient stress state, (2) unparalled stratigraphic detailing, (3) continuous profiling, (4) fast operation, and (5) relatively low cost. Nevertheless, it has limitations of not being suitable for all soil types (particularly gravel), soil samples are not retrieved, and it requires a higher level of field expertise to conduct than most other in-situ tests. Over the last two decades, substantial improvements in equipment design, field operation, and data interpretation have occurred and will continue as the piezocone becomes increasingly popular.

1.0. Development of Piezocone Penetrometer

A standard cone penetrometer provides continuous measurements of tip resistance (q_c) and sleeve friction (f_s) as the probe is pushed vertically into the ground. The piezocone originates from the static cone penetrometer, with an additional capability of measuring pore water pressures. The historical and chronological development of the cone penetrometer has been discussed in detail by Vlasblom (1985), with synopses also provided by Broms and Flodin (1988) and Briaud and Miran (1992).

Wissa et al. (1975) and Torstensson (1975) developed piezometer probes for the direct measurement of penetration pore water pressures. Separate soundings were required for cone resistance and piezometer measurements. Janbu and Senneset (1974) and Senneset (1974) of the Norwegian Institute of Technology (NTH) modified a standard cone penetrometer by installing a pressure transducer with a filter element positioned on the shaft just behind the cone tip. In this manner, simultaneous measurements of q_c, f_s, and u_m could be obtained from a single sounding, thus optimizing data collection.

Today, piezocones exist in a variety of designs and configurations (Lunne et al. 1986a; Campanella and Robertson, 1988). The standards governing the geometry and testing method of electric cones also apply to piezocones, as specified by the International Symposium on Penetration Testing (DeBeer et al., 1988) and the American Society of Testing Materials (ASTM D-3441-86).

Most modern piezocones are characterized as having a conical tip with projected area of 10 cm^2 and apex angle of 60°, although many of the piezocones used in offshore applications have projected tip areas of 15 cm^2 (Bayne and Tjelta, 1987; Sandven, 1990). The friction sleeve, located immediately above the tip, typically has a surface area of 150 cm^2 for the 10 cm^2 tip cone and 200 cm^2 for the 15 cm^2 tip cone. The standard rate of penetration for advancing the cone during the test is 20 mm/sec. The tip resistance and sleeve friction are typically monitored using electric strain gages, and the pore water pressures are measured using a pressure transducer that is connected to a porous filter element. Some piezocones are also equipped with an inclinometer to monitor the verticality and/or a temperature sensor to record thermal variations.

Recent advances in piezocone technology have resulted in cone designs which are capable of measuring pore pressures at more than one location. Dual-element (Juran and Tumay 1989), triple-element (Skomedal and Bayne 1988; Sandven, 1990), and quad-element (Sills et al. 1988) piezocones are available that allow the simultaneous measurement of pore pressure at two, three, and four different locations, respectively. Piezocones capable of measuring additional properties such as shear wave velocity (Campanella et al. 1986; Lunne, et al. 1992), lateral stress (Huntsman et al. 1986), and resistivity (Campanella and Weemes 1990) have also been developed.

1.1. Piezocone Measurements

A standard piezocone penetration test measures cone tip resistance (q_c), sleeve friction (f_s), and pore water pressure (u_m) in separate but simultaneous recordings. These stress measurements are depicted on the schematic penetrometer shown in Figure 1.1. Aspects of each measurement are discussed in the following sections.

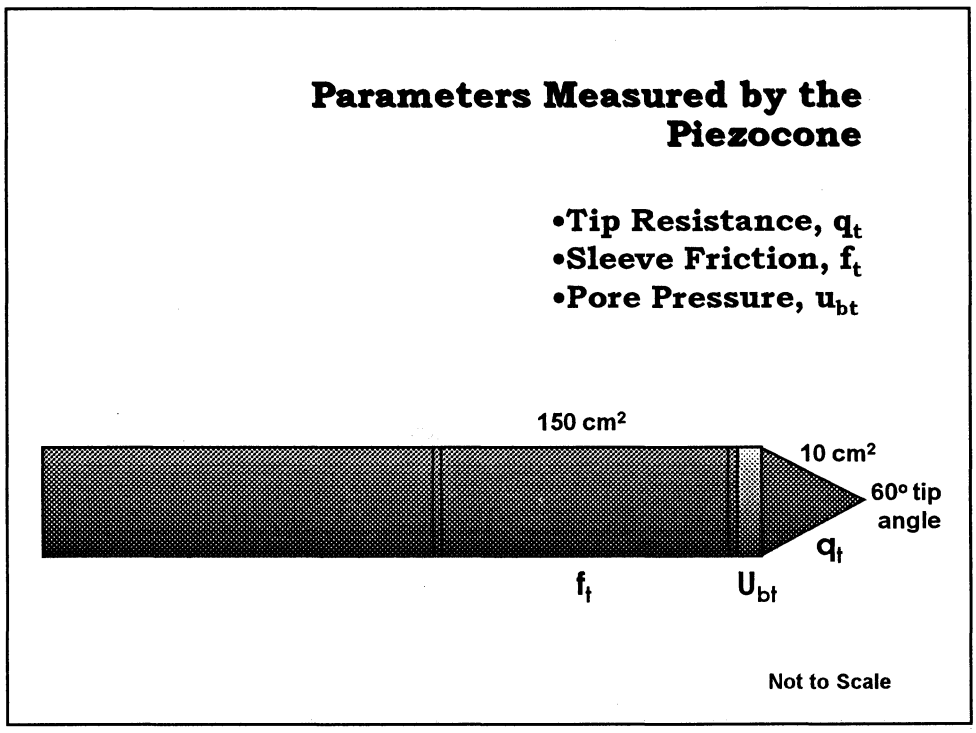

Figure 1.1. Separate and Simultaneous Readings Obtained from Piezocone Tests.

1.1.1. Cone Tip Resistance: Campanella et al. (1982) indicated the importance for correcting the measured cone tip resistance ($q_{c)}$ for pore pressures acting on the unequal end area behind the cone tip. The significance of this correction was later supported by other researchers (Jamiolkowski et al. 1985; Aas, et al., 1986; Lunne et al. 1986a; Powell et al. 1988). Pore pressures generated during cone penetration act on the back of the cone tip as well as on the face, resulting in a measured value of q_c that is less than the full magnitude of the total vertical resistance. The corrected tip resistance (q_T) is determined from:

$$q_T = q_c + (1-a)\, u_{bt} \qquad [1.1]$$

where $a = A_n/A_t$ = net area ratio and u_{bt} ($= u_2$) is the pore pressure measured behind the tip, as illustrated in Figure 1.2. The net area ratio "a" is a function of the particular cone design (Battaglio et al. 1986). Measurements of the net area ratio via the calculated cone geometry often lead to erroneous results (Nyirenda and Sills, 1988). Instead its value should

be determined by inserting the cone into a sealed triaxial chamber, applying a known pressure, and recording the q_c and u_{bt} responses.

1.1.2. <u>Sleeve Friction</u>: The measured sleeve friction can also be corrected to account for pore pressures acting on unequal end areas of the upper (A_{bs}) and lower (A_{bt}) ends of the friction sleeve (as illustrated in Figure 1.2). Different corrections for sleeve resistance measurements, (f_T), have been proposed (Campanella, et al. 1982; Jamiolkowski, et al. 1985; and DeBeer, et al. 1988), with the latter suggesting the following:

$$f_T = f_s + \frac{u_{bs}A_{bs} - u_{bt}A_{bt}}{A_s} \qquad [1.2]$$

where u_{bt} ($= u_2$) and u_{bs} ($= u_3$) are pore pressures measured behind the tip and the friction

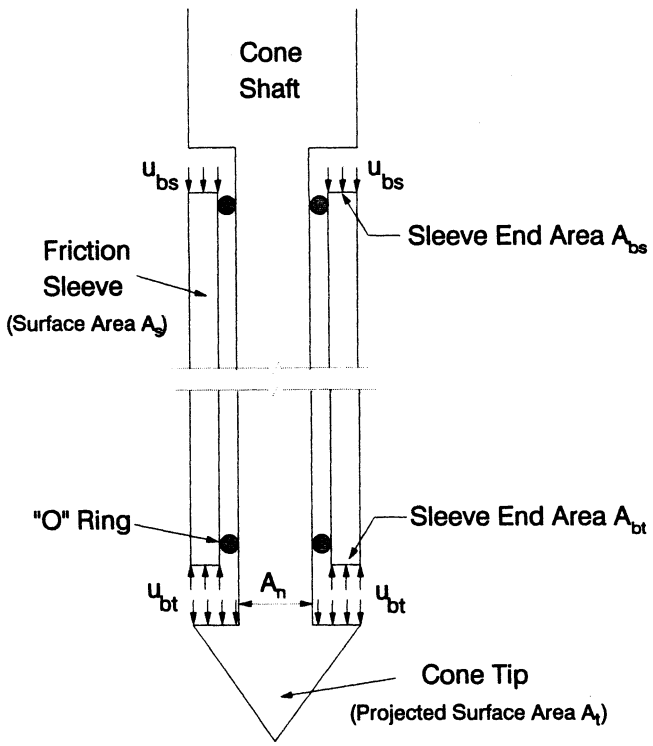

$$q_T = q_c + (1-a)\, u_{bt}$$

$$f_T = f_s + \frac{u_{bs}A_{bs} - u_{bt}A_{bt}}{A_s}$$

Figure 1.2. Unequal End Areas of Electric Cone Used for Correcting q_c and f_s. (Modified after DeBeer, et al. 1988)

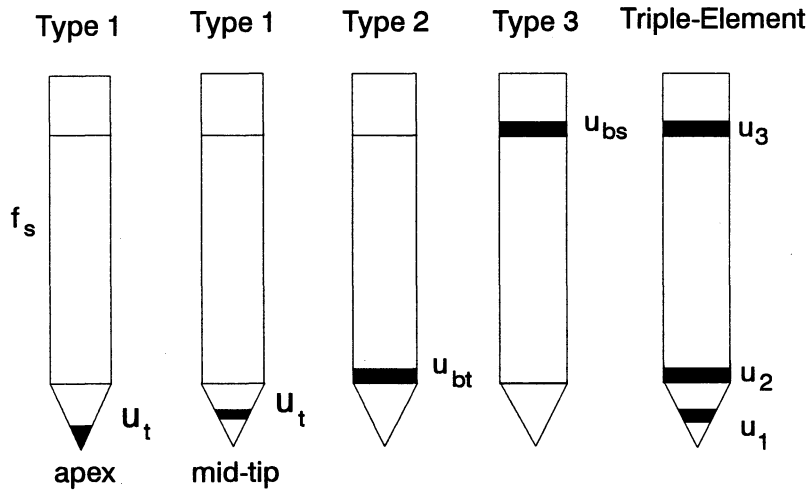

Figure 1.3. Schematic Showing Common Locations of Porous Filter Element.

sleeve, and A_s is the surface area of the friction sleeve. However, the correction is often small if same end areas are used on the sleeve.

1.1.3. **Pore Pressure Measurements**: One important aspect of the piezocone that has not yet been standardized is the location of the porous element. Piezocones used in current practice have three common locations for the porous elements: (1) on the cone face/tip (u_1 or u_t), (2) just behind the tip (u_2 or u_{bt}), and (3) behind the friction sleeve (u_3 or u_{bs}), as illustrated in Figure 1.3. The magnitude of pore pressure varies depending on the specific location of the filter element and large gradients in pore pressures can exist behind the tip, as shown theoretically by Levadoux (1980) and experimentally by Campanella et al. (1986a), Campanella and Robertson (1988), Powell et al. (1988), and Larsson and Mulabdić (1991).

Data from normally-consolidated clays, lightly overconsolidated sensitive clays, cemented clays, and stiff, fissured materials show that the highest pore pressures exist on

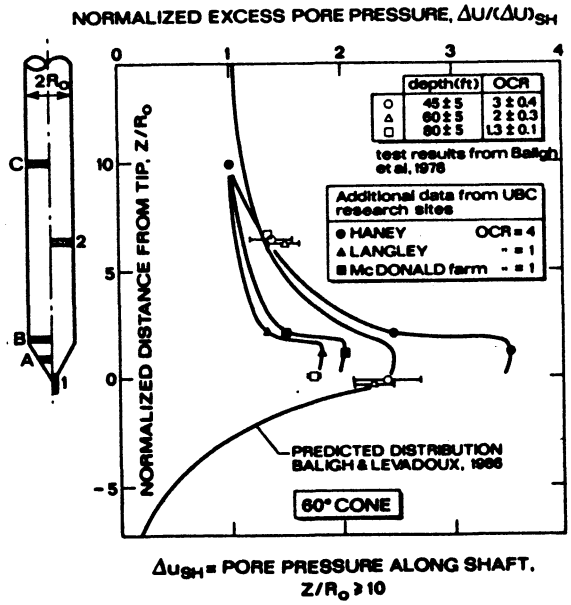

Figure 1.5. Distribution of Measured and Predicted Normalized Excess Pore Pressures During Penetration. (Baligh and Levadoux, 1986; Campanella and Robertson, 1988).

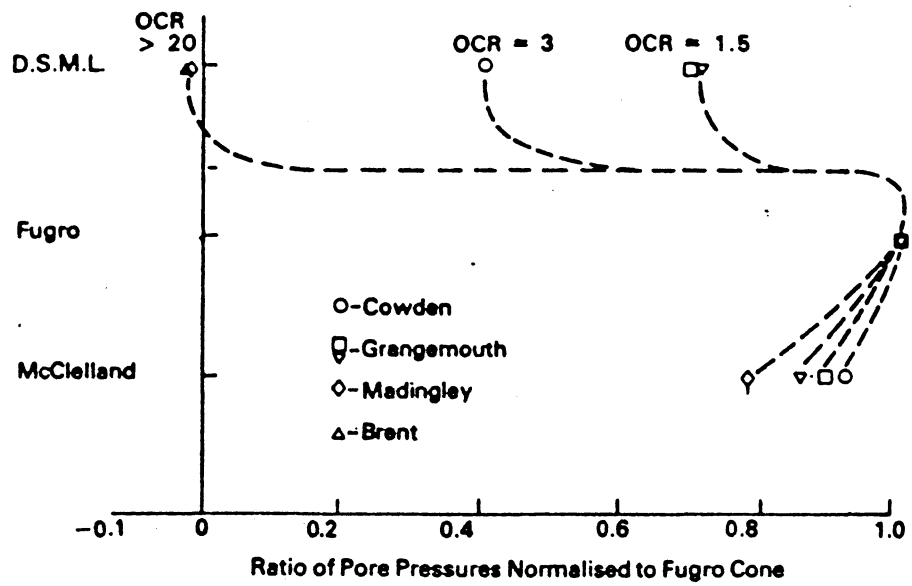

Figure 1.6. Effect of OCR on Penetration Pore Pressure Distribution. (Powell et al. 1988).

the cone face and the magnitude of pore pressure decreases dramatically with the filter located on the shaft of the cone, especially for the heavily overconsolidated London Clay, as illustrated by Figure 1.4. The strain path method predicts the excess pore pressure distribution along the cone is shown in Figure 1.5, which is generally supported using pore pressure data from Boston Blue Clay and three clay sites in British Columbia, Canada. Figure 1.6 shows similar trends of pore pressure distribution with data from clay sites in the U.K. in which the OCRs range from 1.5 to greater than 20. Finally, the distribution of pore pressures shown in Figure 1.7 indicates that the pore pressure measured along the shaft decreases gradually away from the tip.

Discussions regarding which is the most appropriate location for the filter element on piezocones are still in disagreement (Wroth 1984; Jamiolkowski et al. 1985; Houlsby 1988; Campanella and Robertson, 1988). Although there remains debate, it seems appropriate to have the porous element positioned behind the cone tip, since u_2 is required in order to correct the measured value of tip resistance for pore pressure effects. However,

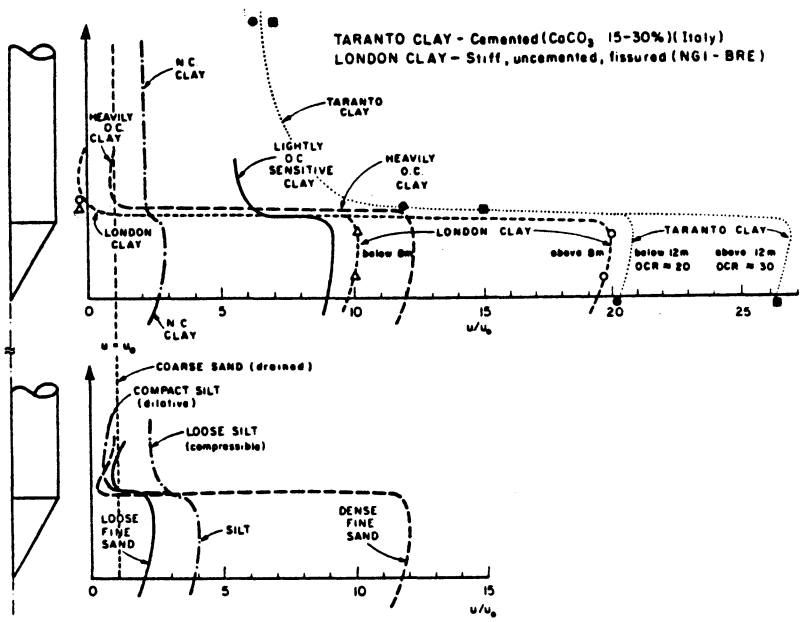

Figure 1.4. Measured Distributions of Normalized Water Pressures During Penetration (Campanella et al. 1986a; Robertson et al. 1986).

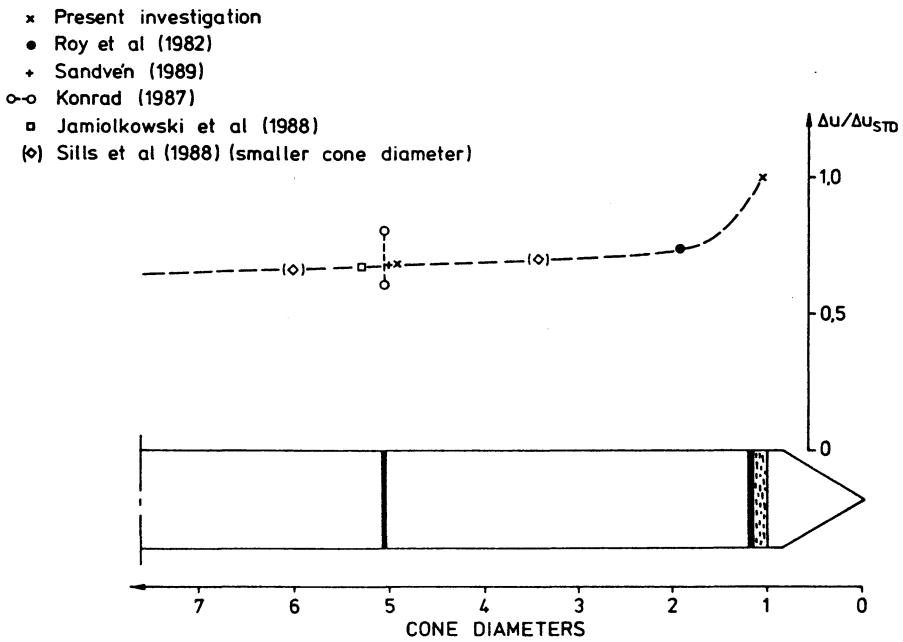

Figure 1.7. Distribution of Penetration Pore Pressures on Shaft Behind Cone Tip. (Larsson and Mulabdic 1991).

in some areas where stiff, fissured cohesive materials are present in the local geology, the use of u_1 appears to be more popular for stratigraphic profiling in practice because the u_2 response becomes small, and therefore, the correction $q_c \rightarrow q_T$ is not significant. The correction for q_T is of primary significance in soft to firm clays or in deep soundings where u_2 measurements are of high magnitude.

Additional details concerning piezocone equipment, saturation, calibration, and operating procedures are given in Appendix A of this report.

1.2 Interpretation of Piezocone Data

Piezocone data are interpreted to assess soil stratigraphy and engineering parameters for use in geotechnical design. There are several interpretation methods which can vary from empirical correlations to analytical approaches. For clays, Table

1.1 summarizes some of the more common soil parameters that are extracted from piezocone test results in clays and cites selected references that document the interpretation procedures. Complete state-of-the-art reports on the interpretation of piezocone tests are given by Jamiolkowski et al. (1985; 1988), Robertson and Campanella (1988, 1989), Leroueil and Jamiolkowski (1991), Jamiolkowski, Leroueil, and LoPresti (1991), and Lunne, Lacasse, and Rad (1992). Detailed reports concerning piezocone testing in clays are provided by Sandven (1990) and Larsson and Mulabdic (1991).

Table 1.1. List of Soil Parameters Interpreted from Piezocone Data in Clays.

Soil Parameter	Reference
Soil Classification	Robertson (1990); Senneset & Janbu (1985)
In-Situ Stress State (K_o)	Mitchell & Masood (1994); Brown & Mayne (1993)
Effective Friction Angle (ϕ')	Senneset & Janbu (1985); Sandven, (1990)
Constrained Modulus ($D=1/m_v$)	Kulhawy & Mayne (1990)
Shear Modulus (G_{max})	Mayne & Rix (1993)
Stress History (σ_p' or OCR)	See Chapter 2 of this report
Sensitivity (S_t)	Robertson & Campanella (1988)
Undrained Strength (s_u)	Aas et al. (1986); Konrad & Law (1987)
Hydraulic Conductivity (k)	Robertson et al. (1992)
Coefficient of Consolidation (c_h)	Houlsby & Teh (1988)
Unit Weight (γ_T)	Larsson & Mulabdic (1993)
Effective Cohesion Intercept (c')	Senneset et al. (1989)

1.3 Purpose of Study

The advent of the piezocone penetration test (PCPT) circa 1974 initiated an extensive search for the most appropriate parameter for reliably profiling the in-situ stress history of

clay deposits. Specifically, can piezocone data be used to evaluate the magnitude of prestress or preconsolidation of natural clays in-situ? The intensity of this ambition is evidenced by the wide range of piezocone parameters proposed in geotechnical literature. Most of these parameters have been suggested merely from an empirical standpoint and are based on specific trends observed at a particular site or within a geologic setting. Very few of the parameters have been derived from a theoretical point of view.

It was a primary objective of this study to obtain a theoretically sound but practical approach for evaluating the stress history of natural cohesive deposits using piezocone data. For this purpose, an analytical model is developed and calibrated against a large database containing clays worldwide that have wide ranges in frictional characteristics, compressibility, consistency, geologic origin, age, mineralogy, plasticity, sensitivity, and stiffness. Although each of these facets were not directly addressed in the assessment of this study, they have been implicitly included in a general sense.

Chapter 2 provides background information and review of several methods for evaluating the preconsolidation stress from conventional laboratory oedometer tests, as well as a compilation of the existing methods for interpreting stress history of clays using piezocone data. Empirical correlations with emphasis on specific piezocone parameters are reviewed in chronological order. A few theoretically-based analytical models are also examined. Finally, several numerical approaches, such as the strain path method, flow field method, and finite element method, are briefly reviewed.

Chapter 3 describes a large piezocone database which contains over 600 digitized piezocone soundings from 205 clay sites around the world. Several piezocone parameters which have been used for evaluating overconsolidation ratio (OCR) and preconsolidation pressure (σ_p') are examined using selected data from the database. Direct correlations between the prominent piezocone parameters and OCR (or σ_p') are generated from simple and multiple regression analyses. The main objective for compiling the database is to provide data for the calibration of developed piezocone models for evaluating stress history and undrained strength of clay deposits.

Chapter 4 presents the results of an experimental field testing program which contain series of piezocone and laboratory tests at two major test sites: (1) soft to firm glacial

lacustrine clay in Port Huron, Michigan, and (2) stiff overconsolidated and desiccated clay in Baton Rouge, Louisiana. Piezocone penetrometers with the porous filter element located on the cone face (Type 1 or u_1) or immediately behind the cone base (Type 2 or u_2) were used at the Port Huron site, whereas single-, dual-, and triple-element piezocones with u_1, u_2, and u_3 (filter behind the friction sleeve) were used at the Baton Rouge site. Laboratory tests for the latter site included index, fall cone, miniature vane shear, one-dimensional consolidation, and consolidated undrained triaxial compression tests.

Chapter 5 describes a precursory isotropic model which combines spherical cavity expansion theory and Modified Cam Clay for the prediction of stress history in clays using PCPT data. Data from laboratory calibration chamber tests, experimental field tests, and the compiled database are used for the model verification. The model has the advantages of being simple and closed-form. Several important influencing factors, such as initial stress state, strength anisotropy, and strain rate, are not considered, however.

Utilizing the concepts developed in Chapter 5, the capabilities for evaluating the undrained shear strength of clays are discussed in Chapter 6. The predicted undrained strength is comparable to that determined from isotropically-consolidated triaxial compression tests, and approaches are outlined for evaluating strengths corresponding to anisotropic triaxial compression and field vane.

Chapter 7 presents the development of a more rigorous soil behavioral model derived from spherical cavity expansion (Vesić 1972, 1977) and anisotropic Modified Cam Clay theory (Wroth 1984) that incorporates considerations such as initial stress state, stress path, strength anisotropy, strain rate, and the potential use of other constitutive soil models. This soil behavior model distinguishes between different types of piezocones where pore pressures are measured on the cone face (Type 1) and behind the cone tip (Type 2) or both. The model requires an iterative solution when used in its generic format, but can be simplified to approximate closed-form through parametric studies. Calibration comparisons using data from the two experimental test sites and a significant number of clay sites indicate that the model provides a reasonable estimate of OCR.

Chapter 8 summarizes the conclusions of this NSF research effort and recommends the directions for future research and testing regarding piezocone applications in clays.

Additional features and extensions of the aforementioned methodology are also outlined.

Several appendices are provided to detail supplementary information and materials for this study. Appendix A documents the development of the piezocone penetration testing system currently used at Georgia Institute of Technology. Appendix B provides reference backup information on the piezocone database. Finally, a spreadsheet which contains approximately 1500 data points with digitized piezocone and associated soil engineering parameters is listed in Appendix C.

CHAPTER 2

REVIEW OF EXISTING METHODS FOR INTERPRETING STRESS HISTORY IN CLAYS FROM PIEZOCONE TESTS

2.0. Conventional Laboratory Evaluation of Stress History in Clays

The stress history of clays governs many aspects of soil behavior including volume change during consolidation, stress dilatancy, induced pore pressures, peak strength, and time-dependent behavior during undrained shearing. The soil response in many geotechnical problems is approximately described by elastic-plastic models. In this regard, the conventional preconsolidation stress (σ_p') is considered a yielding point that separates elastic (recoverable) from plastic (irrecoverable) behavior.

A three-dimensional yield surface marks the boundary of the elastic and plastic domains, as illustrated in Figure 2.1. If the soil is normally-consolidated (NC), its current stress state can be represented by a point on the yield surface (point A). Removal of the overburden stress, groundwater rise, or sampling process could cause unloading (point A to point B) and result in overconsolidation of the soil. The change of stress state (such as

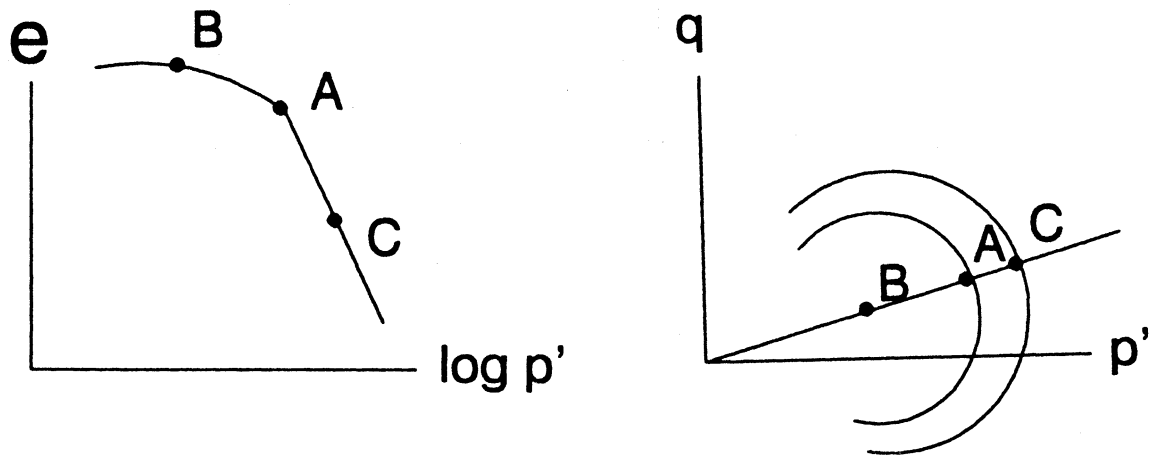

Figure 2.1. Change of Stress State during Consolidation.

reloading) inside the yield surface is considered to occur within the elastic range. Once the loading exceeds the yield point, permanent plastic deformations occur and the yield surface expands to a new stress state (point C). While the soil is inside the yield surface, it tends to "memorize" the previous maximum stress state or the preconsolidation pressure (σ_p'). The relative magnitude of prestress is commonly described by a normalized parameter termed the overconsolidation ratio, OCR = σ_p'/σ_{vo}', in which σ_{vo}' is the current effective vertical stress in the ground. The OCR is conventionally and practically expressed in terms of vertical stresses, although it can also be addressed using mean effective stresses or horizontal effective stresses.

2.1 Profiles of Stress History

There are many reasons why a natural soil deposit may be overconsolidated. Since effective stress governs soil behavior, any changes in either total stress or pore water pressure could cause overconsolidation. Geoenvironmental factors can also contribute to an apparent preconsolidation effect. Examples of overconsolidation caused by reductions in total stress include: (a) erosion, (b) glaciation, and (c) removal of overburden (such as excavation and past structures). Overconsolidation caused by changes in pore water pressures could be due to (a) fluctuations of the groundwater table, (b) change in pressures due to underdrainage, pumping, or artesian flow, and (c) desiccation due to surface drying or capillary flow. In addition, changes in soil structure due to aging and chemical alterations causing cementation can result in overconsolidation-like effects. The common mechanisms of overconsolidation or apparent preconsolidation are reviewed in Figure 2.2. In reality, the final overconsolidation may have been caused by more than one mechanism and the actual profile of stress history can therefore be rather complicated.

Prior to equilibrium conditions, a gradient exists such that the soil is underconsolidated (OCR $<$ 1), such as during sedimentation. A reference profile for equilibrium conditions is the state for normally-consolidated (NC) clays when OCR = 1. Shown here as Figure 2.2(a), the soil deposit has achieved a compression state corresponding to the end of primary consolidation (t_p). For NC clays, the preconsolidation stress equals the effective vertical overburden stress and the profile of OCR = 1 is constant with depth.

If a normally-consolidated deposit is subjected to groundwater lowering, such as during a drought condition, and then the water table returns, a resulting profile of constant OCR = γ_{total}/γ' with depth occurs, as shown in Figure 2.2(b). The occurrence of this phenomenon in soft clays has been discussed by Parry (1970).

Soft normally-consolidated clays can also develop a quasi-preconsolidation effect by the processes of aging or secondary compression effects (Bjerrum 1972). Here, a divergence of σ_p' and σ_{vo}' profiles is indicated by a profile of constant OCR that relates to the age of clay (t), the time required to attain end-of-primary consolidation (t_p), compressibility parameters (C_c and C_r), and the coefficient of secondary compression ($C_{\alpha e}$), as shown in Figure 2.2(c). This phenomenon has been discussed by Mesri and Choi (1979).

Often, capillarity effects and solar phenomenon result in the desiccation of NC deposits near the ground surface (Parry 1970). This results in a crustal layer, generally within the upper 1 to 5 meters, as illustrated by Figure 2.2(d). Below the crust, the soil may be normally-consolidated or possibly lightly overconsolidated due to the aforementioned processes related to aging and groundwater effects. The crustal layer usually has a high variability over short distances, both vertically and laterally.

Perhaps the most common means of overconsolidation occurs by simple unloading. The amount of prestress removed ($\Delta\sigma_v$) corresponds to the natural erosion rates or past glacial activity, such as the geologic loading of London clay (Skempton 1961). Figure 2.2(e) illustrates the basic profile of σ_p' which parallels the current effective stress regime (σ_{vo}') and shows the associated decreasing trend of OCR with depth caused by mechanical overconsolidation. An intentional increase in OCR can be man-made by this mechanism if preloading, surcharging, or excavation is applied to a site.

Many clay deposits located in sun-belt regions are desiccated throughout their entire depth because of prolonged exposure to high heat and temperature, as shown in Figure 2.2(f). These include the expansive Beaumont clays in Texas and Louisiana, as well as hard desiccated deposits in southern California and Florida. In these cases, the profile of σ_p' may be somewhat constant with depth, resulting in a profile of OCR that decreases with depth but at a faster rate than caused by single unloading.

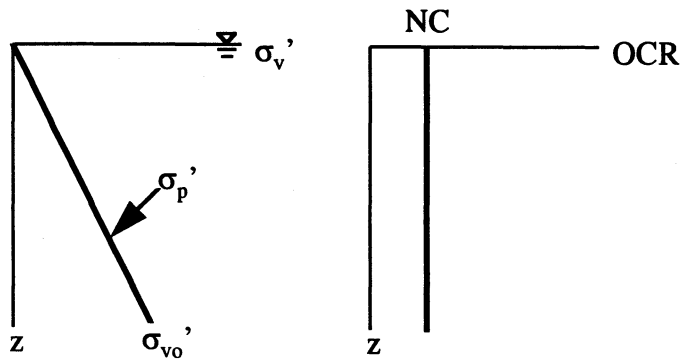

(a) Normally Consolidated Deposits

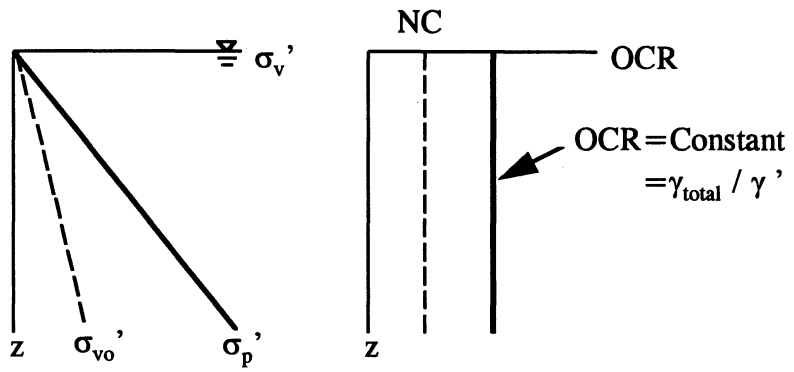

(b) Groundwater Fluctuation

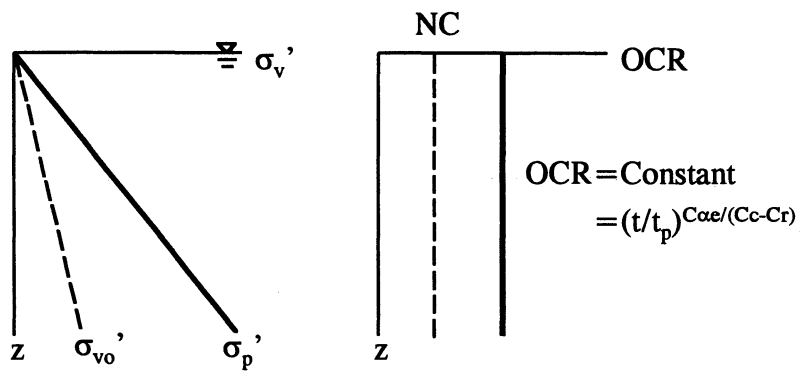

(c) Aged NC Deposits

Figure 2.2 Profiles of Stress History Caused by Different Mechanisms.

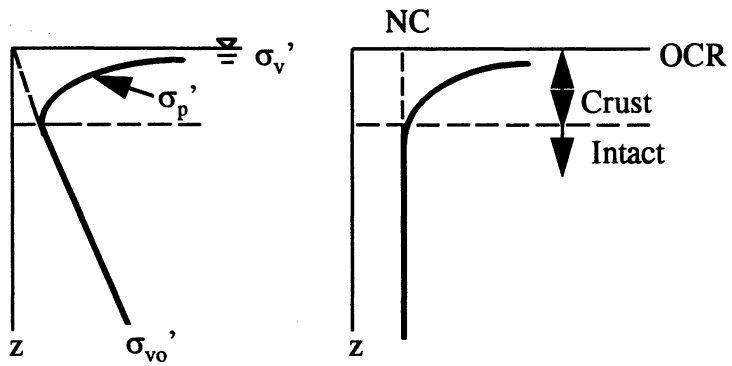

(d) NC Deposits with Crustal Layer

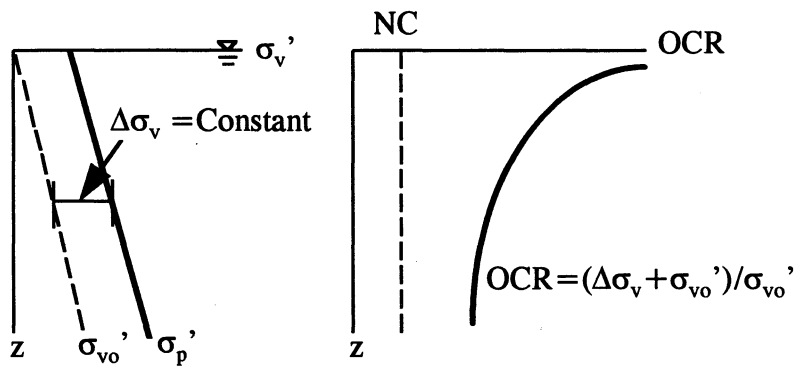

(e) Overconsolidated Deposits Prestressed by Mechanical Means (Erosion, Glacial Action, and Excavation)

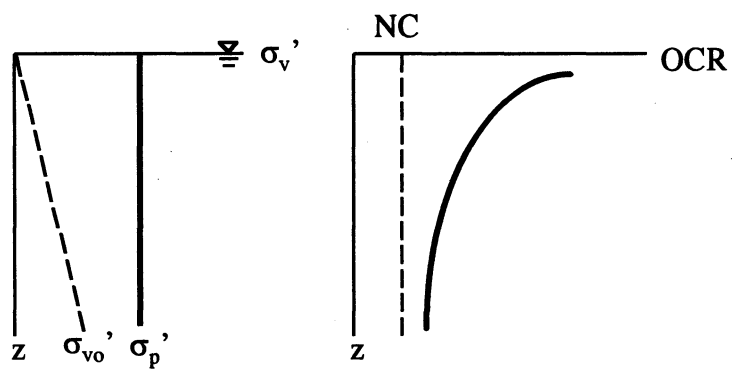

(f) Overconsolidated Deposits Caused by Desiccation

Figure 2.2. Profiles of Stress History Caused by Different Mechanisms. (Continued)

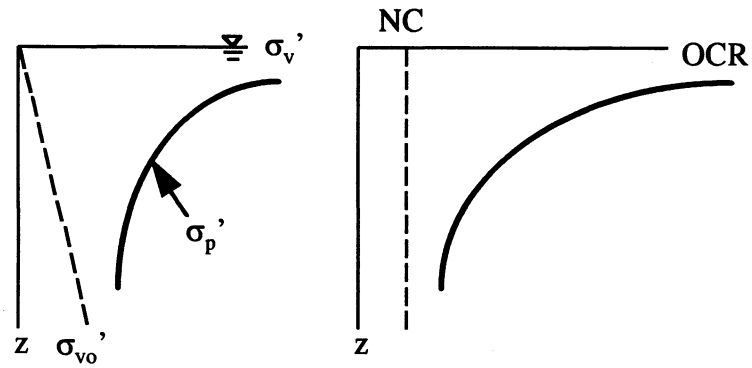

(g) Overconsolidated Deposits Caused by Cementation

Figure 2.2. Profiles of Stress History Caused by Different Mechanisms. (Continued)

Geochemical processes that cause cementation or bonding also impart a pseudo-preconsolidation effect. Examples of OCR profiles in structured cemented clays in Canada and Italy have been presented by Jamiolkowski et al. (1985) and measurements of calcium carbonate content can be useful to detect degree of cementation. Figure 2.2(g) illustrates a typical OCR profile of cemented soils in which the OCR decreases with depth at yet a faster rate and the resulting OCRs are higher than those due to desiccation.

If several of these mechanisms occurred during the sedimentation period and/or after an interim of environmental events for a given clay deposit, the final composite profile of preconsolidation stresses may indeed be rather complex. The best approach for obtaining detailed analysis of the true OCR profile would therefore be afforded by a comprehensive sampling and testing program using high quality piston samples and incremental-load oedometer tests taken at approximately 1-meter vertical intervals. These could be supplemented by constant-rate-of-strain consolidation tests to reduce laboratory testing times, however, expensive budgets for sampling and testing would be necessary. Examples of

complex profiles of σ_p' in clays are illustrated by Martin and Drahos (1986) for the Calvert clay in Richmond, Virginia. Here, alternating successive intervals of marine depositional and erosional events resulted in layered zones and irregular stress history profiles. Examples and discussion of other combined mechanisms of overconsolidation are given in Jamiolkowski et al. (1985).

The use of in-situ tests for profiling the apparent σ_p' profile in clay is attractive since it may be possible to discern a rather complicated and varied stress history that includes multiple effects (For example: erosion, reloading, aging, plus cementation). Also, the in-situ tests are conducted rather quickly and inexpensively, thus allowing an immediate assessment of the state of overconsolidation and its variation across the site of study. Therefore, a primary interest of this research program was to evaluate the ability and potential for using piezocone data to delineate profiles of OCR in supplementing reference values obtained from laboratory oedometer tests.

2.2. Methods of Interpreting σ_p' from Oedometer Tests

Traditionally, the preconsolidation stress (σ_p') of clays is determined from the laboratory oedometer or one-dimensional consolidation test. The oedometer test can be performed in several different fashions such as incremental-loading (IL), constant rate of strain (CRS), and controlled gradient test (CGT). In addition to σ_p', other soil properties can also be obtained from this test, such as soil compressibility (compression index, C_c; swelling index, C_s; recompression index, C_r; and constrained modulus, $D = 1/m_v$) as well as the time-dependent behavioral parameters (coefficient of consolidation, c_v, and coefficient of secondary compression, $C_{\alpha e}$). In addition, the magnitude of permeability or hydraulic conductivity (k) may be assessed.

The maximum past vertical stress or effective preconsolidation pressure from one-dimensional tests has been designated by different nomenclature over the years (P_c', σ_{vmax}', and σ_p'). As noted earlier, σ_p' is an important parameter defining the state of stress of clay deposits and separating the elastic (OC) region from the plastic (NC) region.

Conventionally, standard oedometer tests are conducted on small specimens taken from the field and the characteristic e-logσ_v' graphs show a change in slope at the yield

stress. Figure 2.3 shows results from a consolidation test on an overconsolidated marine clay from Surry, Virginia, and the interpreted yield stress is 900 kN/m^2 at the reported depth of 27 meters. It is important to impart sufficiently high enough stress levels during consolidation loading to fully define the normally consolidated region and magnitude of yield stress. Unfortunately, many commercial laboratories simply run oedometer tests using a standard set of stress increments, regardless of the consistency and hardness of the clay, and therefore, the tests do not completely reach the virgin compression line. In addition, sampling disturbance effects typically lower the overall e-logσ_v' curve from field conditions. Consequently, the value of σ_p' is often underestimated in routine testing and interpretation (Holtz, Jamiolkowski, and Lancellotta, 1986).

If the current state of vertical effective stress (σ_{vo}') is known, then the difference between the yield stress and current stress is referred to as the prestress (σ_p'-σ_{vo}'). Olsen et al. (1986) termed this value as the overconsolidation difference (OCD). More commonly, the degree of preconsolidation is expressed in normalized form, known as the overconsolidation ratio, OCR = σ_p'/σ_{vo}'. The advantages of this format are that no units are specified and the scaling laws of continuum mechanics can be utilized (Wroth, 1988). For the data shown in Figure 2.3, the current σ_{vo}' = 295 kN/m^2, and therefore, the in-situ OCR is about 3 for this marine clay.

The yield stress from oedometer tests is routinely interpreted using a graphical technique proposed by Casagrande (1936). In many soft clays, this approach is adequate and offers a reasonable value of σ_p' for engineering purposes. Other graphical techniques have been developed, however, and these are more applicable for stiff to hard clays that have been affected by sample disturbance, swelling, and the traumatic release of the ambient stress state. Table 2.1 lists a number of methods for interpreting the magnitude of yield stress from consolidation test results. Figure 2.4 illustrates the application of the conventional Casagrande (1936) approach to 4 specimens of the sandy clays of the Yorktown Formation from Newport News, Virginia (Mayne, 1989) and values of the interpreted σ_p' fall between 860 and 920 kPa. The method proposed by Butterfield (1979) using the natural logarithm of specific volume (v= 1+e) versus $\log_e(\sigma_v')$ has also been applied to these data, showing comparable results (Fig. 2.5). An approach by Jamiolkowksi and Marchetti (1969) was

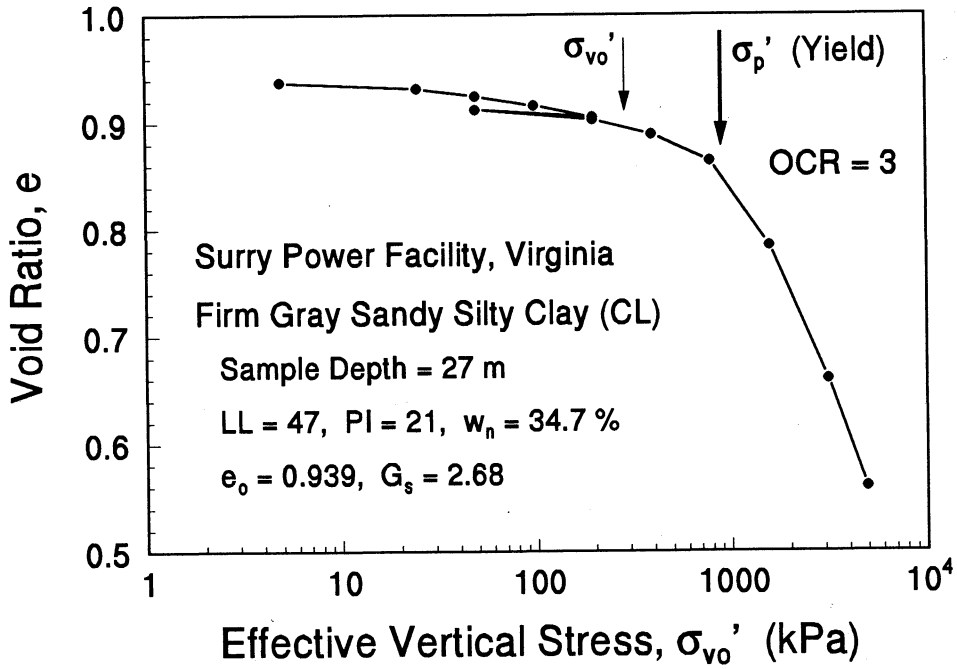

Figure 2.3. Yield Stress Observed in One-Dimensional Consolidation Test.

developed for controlled gradient tests utilizing a log-log plot of constrained modulus ($D = 1/m_v$) vs. average vertical stress (σ_{vAVE}') and the application is presented in Figure 2.6. Finally, a work-energy method proposed by Becker et al. (1987) is shown in Figure 2.7 for the Yorktown data. Comparable values of σ_p' are obtained for all four methods.

As noted previously, the stress state of soil is not merely a one-dimensional phenomenon. The utilization of routine consolidation tests with rigid lateral constraint and incremental application of vertical loads has proliferated because of the simplicity of equipment and test procedures. In reality, the stress history of natural materials is controlled, as a minimum, by a four-dimensional condition involving σ_x', σ_y', σ_z', and time (t). Series of extensive triaxial testing programs have found yield stresses associated with all types of stress paths. Consequently, recent developments in understanding soil behavior have evolved the concept of a yield surface. That is, the stress history of natural materials is best characterized by a three-dimensional yield envelope that is rheological and changes as a function of time (age, creep, and strain rate).

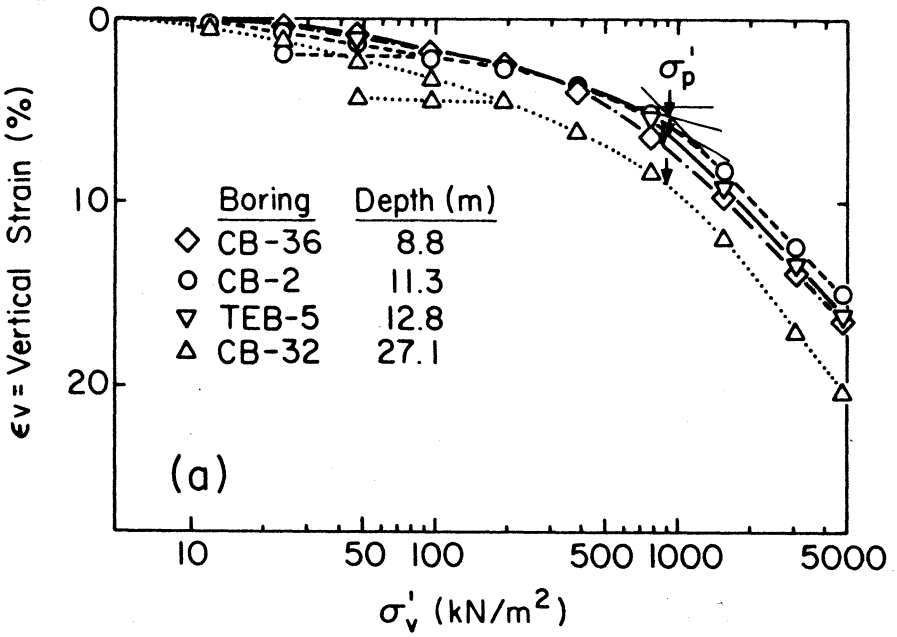

Figure 2.4. Interpretation of Yorktown Data Using Casagrande (1936) Method.

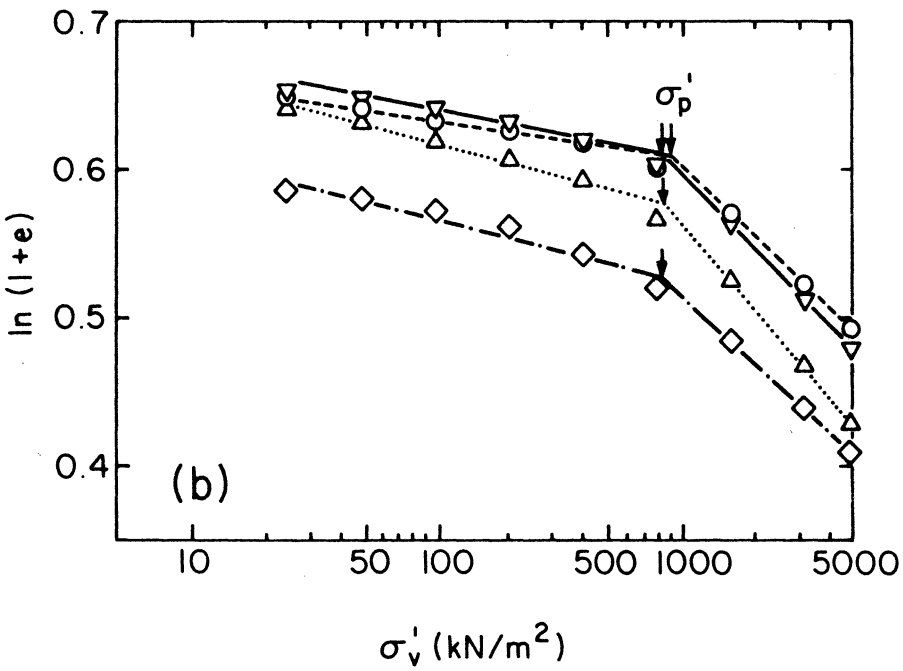

Figure 2.5. Interpretation of Yorktown Data Using Butterfield (1979) Method.

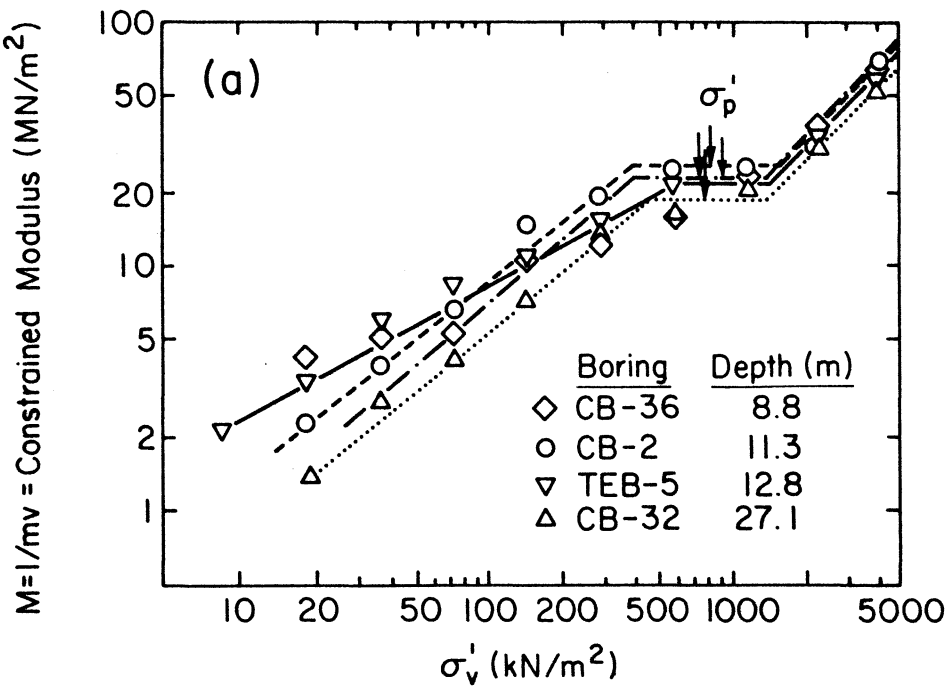

Figure 2.6. Interpretation of Yorktown Data Using Method by Jamiolkowski and Marchetti (1969).

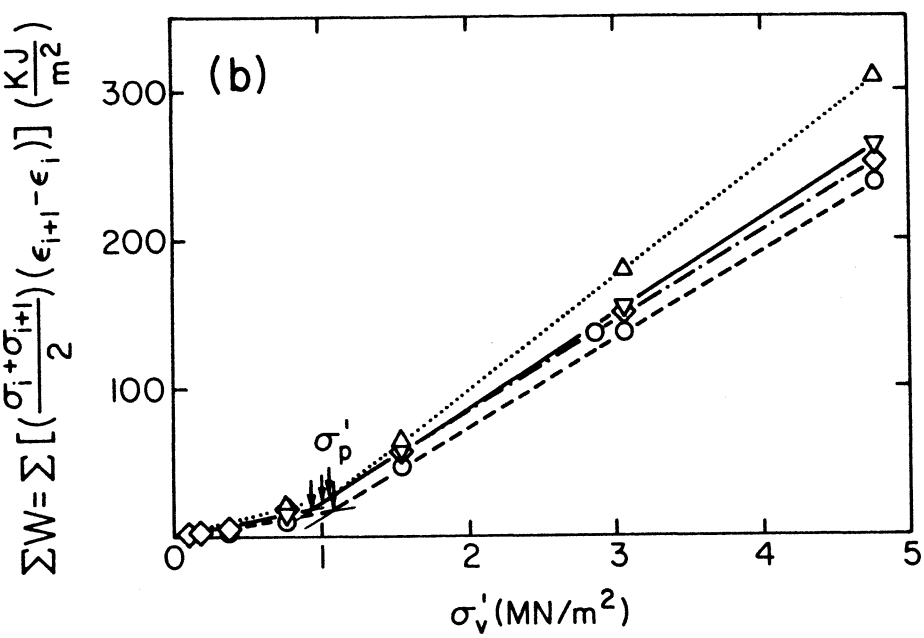

Figure 2.7. Interpretation of Yorktown Data Using Method of Becker et al. (1987).

Table 2.1. Methods for Interpreting Yield Stress σ_p' from Oedometer Tests.

Reference	Graphical Plot	Notes
Casagrande (1936)	e vs. log σ_v'	(1)
Schmertmann (1955)	Δe vs. log σ_v'	(2)
Janbu (1969)	$1/m_v$ vs. σ_{Av}'	(3)
Jamiolkowski & Marchetti (1969)	log $(1/m_v)$ vs. log σ_{Av}'	(3)
Sowers (1979)	e vs. log σ_v'	(1)
Butterfield (1979)	ln (v) vs. ln σ_v'	(4)
Becker et al. (1987)	$\sum W$ vs. σ_{Av}'	(5)
Ladd et al. (1977)	c_v vs. log σ_{Av}	(6)

Notes: (1) e = void ratio; σ_v' = vertical effective overburden stress.
(2) Δe = $e_{i+1} - e_i$.
(3) $1/m_v$ = $\Delta\sigma_v'/\Delta\epsilon_v'$ = constrained modulus; $\Delta\sigma_{Av}' = (\sigma_i'+\sigma_{i+1}')/2$.
(4) v = $1+e$ = specific volume.
(5) ΔW = $(\sigma_i'+\sigma_{i+1}')(\epsilon_{i+1}-\epsilon_i)/2$ = work per unit volume.
(6) c_v = coefficient of consolidation in vertical direction.
(7) m_v = coefficient of volumetric compressibility.

The complete yield surface for the sensitive natural Saint Alban Clay in Quebec (Leroueil, et al. 1979) is shown on the Cambridge q-p' stress space in Figure 2.8. Typical index properties of the clay are: LL = 45, PI = 20, w_n = 75, S_t = 18, and OCR = 2.2. A review of yield surfaces from clays worldwide suggests that the effective frictional properties (ϕ') of the clay primarily govern the actual shape of the envelope (Diaz-Rodriquez, Leroueil, and Aleman, 1992). The well-known preconsolidation pressure or yield stress (σ_p') is but one point on the yield surface where the locus crosses the K_{oNC}-line corresponding to normally-consolidated conditions. Available stress path data suggest the shape of the yield surface is best represented as a rotated ellipse in MIT q-p space. This concept is particularly useful in explaining the non-uniqueness in obtaining values of c'-ϕ'

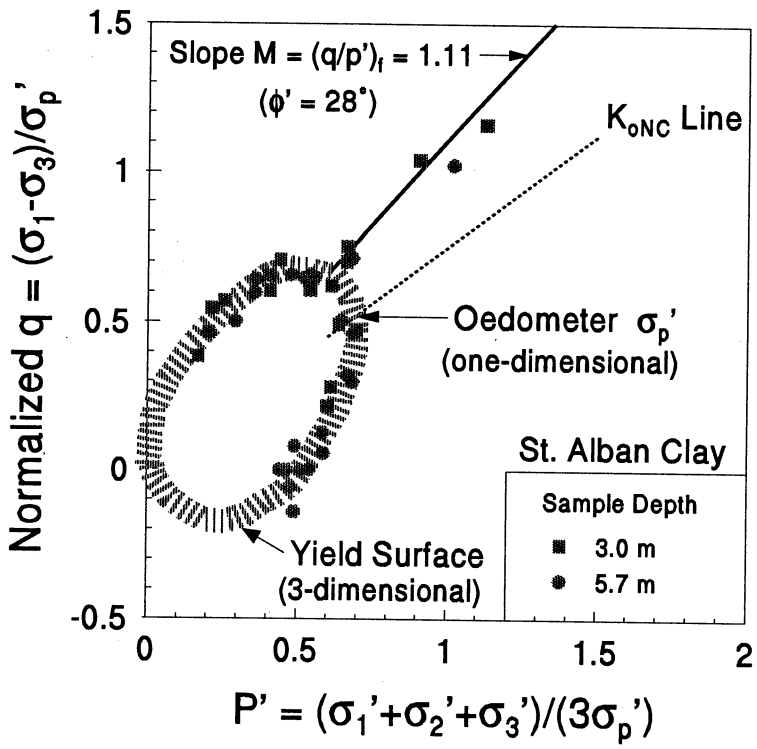

Figure 2.8. Three-Dimensional Yield Surface for St. Alban Clay, Quebec (after Leroueil, et al. 1979).

parameters from limited numbers of strength tests (Mesri and Abdel-Ghaffar, 1993), as well as the observed degradation of effective cohesion intercept (c') with time (Tavenas and Leroueil, 1977, 1987).

2.3. Piezocone Evaluation of Stress History in Clays

The interpretation of stress history from digital piezocone data is of great practical interest because results are immediate and continuous, whereas reference oedometer tests are expensive and require discrete sampling and long testing times for consolidation. Oedometer tests will always provide a means for obtaining a dependable reference value of σ_p', however, and piezocone tests should be calibrated accordingly.

Interpretative approaches ranging from empirical to sophisticated numerical techniques have been proposed for interrelating stress history (OCR or σ_p') with piezocone measurements (q_T, f_s, and u_m). Empirical approaches are often simple, yet undesirable

because they lack a rational engineering framework. More rigorous models are derived from analytical theories involving elasticity, plasticity, limit equilibrium, or cavity expansion, although most of them either require additional soil input parameters which are not commonly available in practice or else mandate the use of very sophisticated numerical procedures.

This section reviews, in chronological order, interpretation methods which use piezocone data for evaluating the stress history of clays. In most of the applications, the corrected cone tip resistance (q_T) or measured pore water pressure (u_m) are often normalized by the total or effective overburden stresses (σ_{vo} or σ_{vo}'), or equilibrium pore pressures (u_o). The third parameter, sleeve friction (f_s), is believed to be less reliable and less repeatable (Lunne et al. 1986a) and therefore will not be discussed henceforth. Pore pressures measured at different locations along the cone are generalized as those with the filter element located at cone tip such as midface or apex (u_1) and those with the filter element located immediately behind the cone base (u_2).

2.3.1. Empirical Approaches

Schmertmann (1978) presented a method of estimating the OCR of clay using static cone penetration test (CPT) data. The method requires the estimation of undrained shear strength (s_u) from q_c data and uses the normalized strength concept (SHANSEP) to correlate s_u/σ_{vo}' with OCR. Schmertmann also suggested a direct CPT method for estimating the overconsolidation of clays caused by mechanical removal of the overburden. The method is to approximate the increase of q_c with depth as a straight line and extrapolate the line to estimate the original ground elevation, therefore determining the original σ_p' profile with depth. This alternate approach does not account for overconsolidation caused by desiccation, groundwater fluctuations, and other factors other than mechanical overconsolidation.

Reporting some of the first piezocone records in the U.S., Baligh et al. (1980) observed that high values of u_1/q_c were associated with low OCR. Data from Boston Blue Clay and Atchafalaya Basin sites showed that u_1/q_c increased as the OCR decreased, as shown in Figure 2.9. It is noted that the parameter u_1/q_c is sensitive enough to distinguish zones in small OCR ranges ($1 \leq OCR \leq 2$) even with the filter element located on the tip.

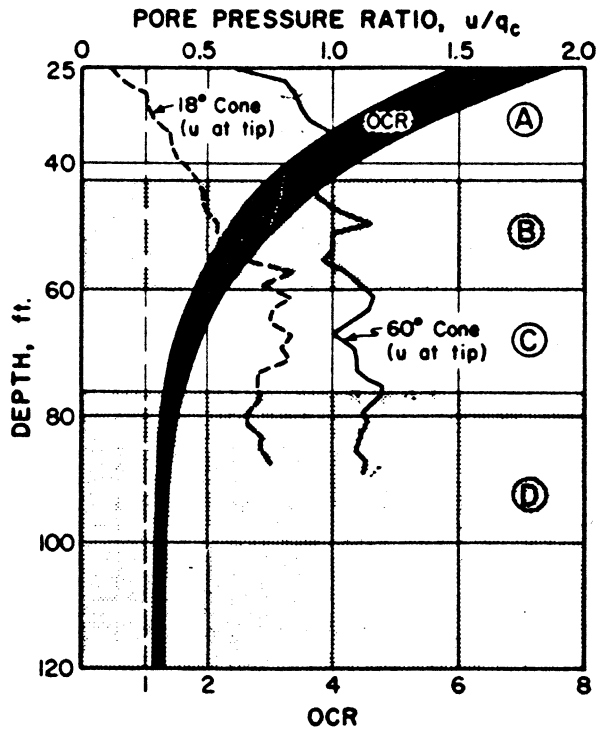

Figure 2.9. Trend of u_m/q_c with OCR for Boston Blue Clay (Baligh et al. 1980).

Campanella and Robertson (1981) proposed that the total pore pressure ratio (u_m/q_c) be replaced with the dynamic pore pressure ratio ($\Delta u_m/q_c$), in which $\Delta u_m = u_m - u_o$. Pore pressures were measured behind the tip (u_2) rather than at tip (u_1) due to the different type of cone used, consequently, shear-induced pore pressures played a more significant role. It appeared that for normally consolidated clays, the dynamic pore pressure (Δu_2) generated was linear with depth similar to the cone resistance. The $\Delta u_2/q_c$ ratio also appeared to be a constant value of approximately 0.7. For overconsolidated clays, Tumay et al. (1982) suggested the use of $\Delta u_m/q_c$ for indexing the profile of OCRs with depth, as shown in Figure 2.10. Here, $\Delta u_m/q_c$ decreases with increasing OCR.

Smits (1982) performed a series of piezocone penetration tests on kaolin in a laboratory calibration chamber. He concluded that a linear relationship existed between the normalized parameter $(u_m-u_o)/(q_c-u_o)$ and OCR, as shown in Figure 2.11. The piezocone penetrometers used had filter elements located behind the tip (u_2) and in a truncated cone tip (u_1). The pore pressure ratio decreased with increasing OCR and absolute

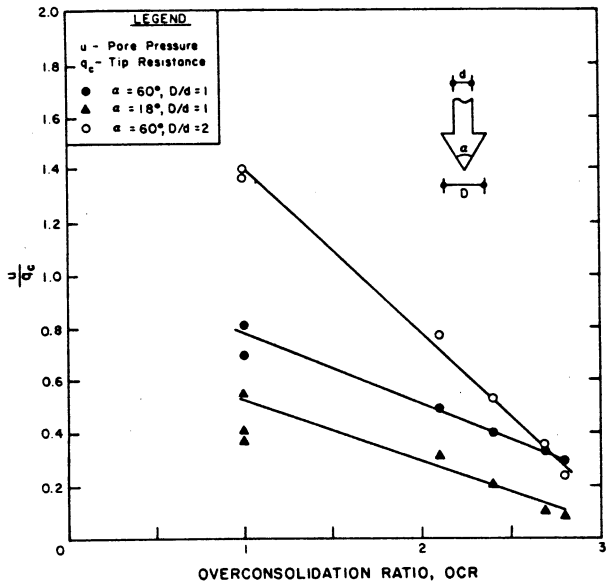

Figure 2.10. Variation of Pore Pressure Ratio $\Delta u_m/q_c$ with OCR for Louisiana Clays. (Tumay et al. 1982)

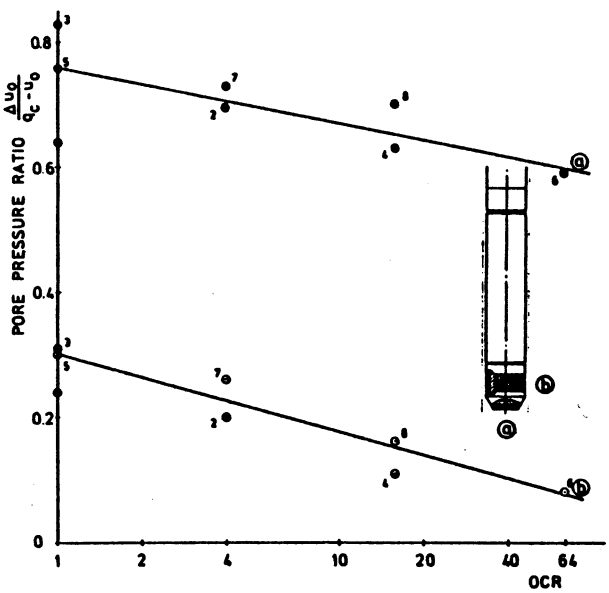

Figure 2.11. Pore Pressure Ratio $(u_m-u_o)/(q_c-u_o)$ versus OCR. (Smits 1982)

value of the decrease was roughly the same for pore pressure measurement at both locations.

Azzouz et al. (1982) used the normalized parameter $(u_1-u_o)/\sigma_{vo}'$ for correlating piezocone data and laboratory test results. The value of $(u_1-u_o)/\sigma_{vo}'$ was primarily used as an indicator for profiling a soft offshore marine clay with OCR = 1.15 $\pm$ 0.15, while no direct correlation between the parameter and OCR was reported.

Senneset et al. (1982) and Jefferies and Funegard (1983) suggested the use of a dynamic pore pressure ratio, $B_q = (u_m-u_o)/(q_c-\sigma_{vo})$, to eliminate the influence of water depth for offshore applications. This normalized parameter was later modified by replacing q_c with the corrected cone tip resistance (q_T), recommended by Wroth (1984) for the interpretation of OCR in clays. Wroth considered the prior parameters u_m/q_c , $(u_m-u_o)/q_c$, and $(u_m-u_o)/(q_c-u_o)$ unacceptable; the first because total (not the excess) pore pressure was contained in the numerator, and all three to be incorrect because the denominators are not a proper measure of shear stresses. In an undrained situation, the maximum shear stress can only be expressed in terms of principal stresses as a difference of two total stresses or a difference of two effective stresses. In fact, B_q was considered somewhat analogous to Skempton's pore pressure parameter $A = (\Delta u-\Delta\sigma_1)/(\Delta\sigma_1-\Delta\sigma_3)$ and Henkel's parameter $a' = (\Delta u-\Delta\sigma_{oct})/\Delta\tau_{oct}$, which correlate closely with OCR in conventional isotropic triaxial shear tests, as shown for Weald clay in Figure 2.12(a). Wroth utilized piezocone data from Onsoy and obtained a good site specific correlation between B_q and OCR that was very similar to the A_f versus OCR relationship in triaxial tests, as shown in Figure 2.12(b).

Jamiolkowski et al. (1985) investigated whether B_q should better reflect the in-situ OCR than piezocone parameters proposed earlier. After examining piezocone data from various types of clay ranging from soft NC Boston Blue Clay to heavily OC and microfissured Taranto clay, they concluded that no unique relationship between B_q and change in OCR should be expected. Lunne et al. (1985) also attempted a B_q-OCR correlations for several North Sea clays and the results appeared to be scattered, as indicated by Figure 2.13. Keaveny and Mitchell (1986) and Robertson et al. (1986) compiled additional piezocone data to investigate a relationship between OCR and B_q, again indicating the difficulty of reliably estimating the degree of overconsolidation in clays via a simple relationship with this parameter (see Figure 2.14).

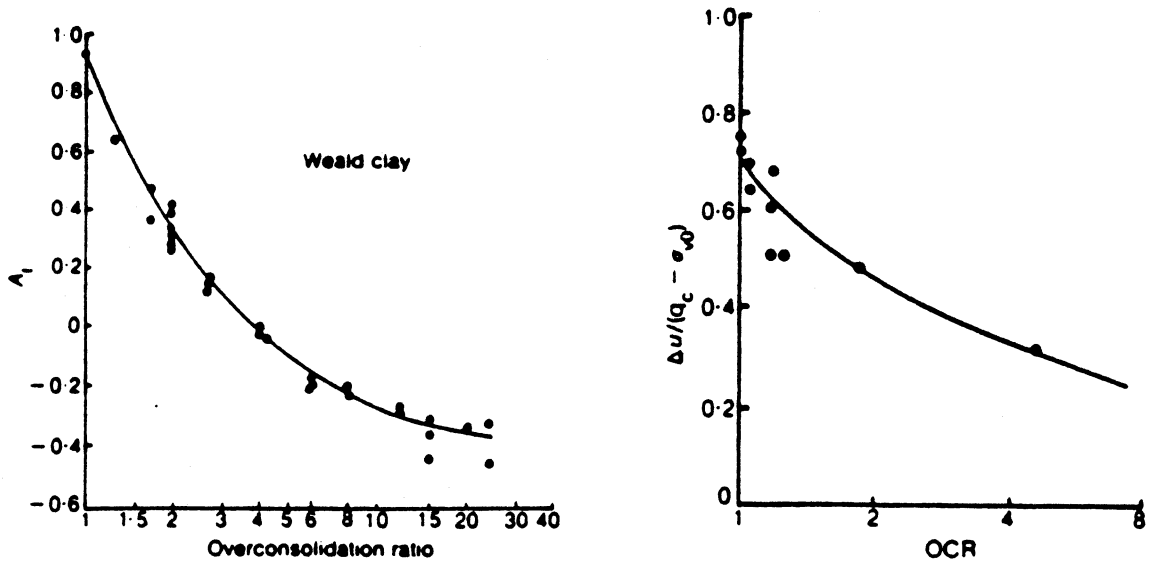

Figure 2.12. (a) Variation in A_f with OCR for Weald Clay. (Bishop and Henkel 1957)
(b) Variation in B_q with OCR for Onsoy Clay. (Wroth 1984)

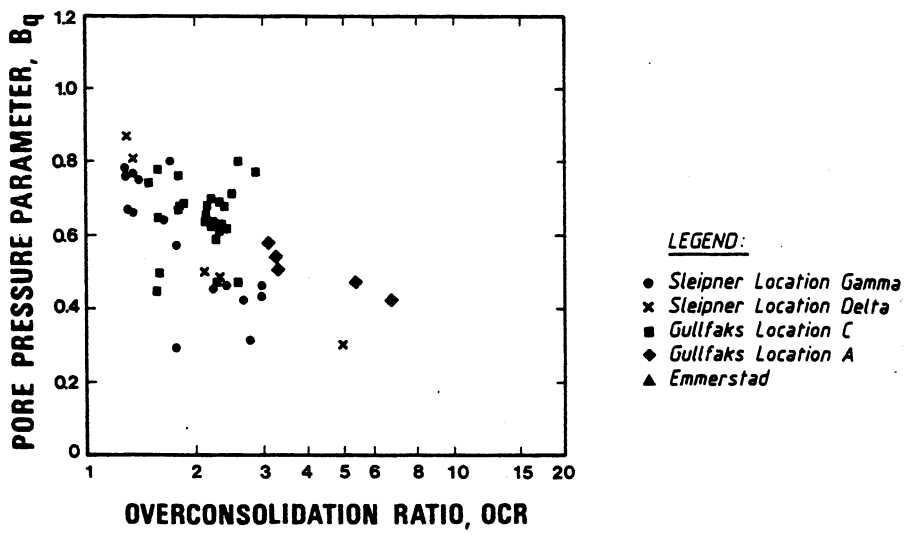

Figure 2.13. Parameter B_q versus OCR for North Sea Clays. (Lunne et al. 1985)

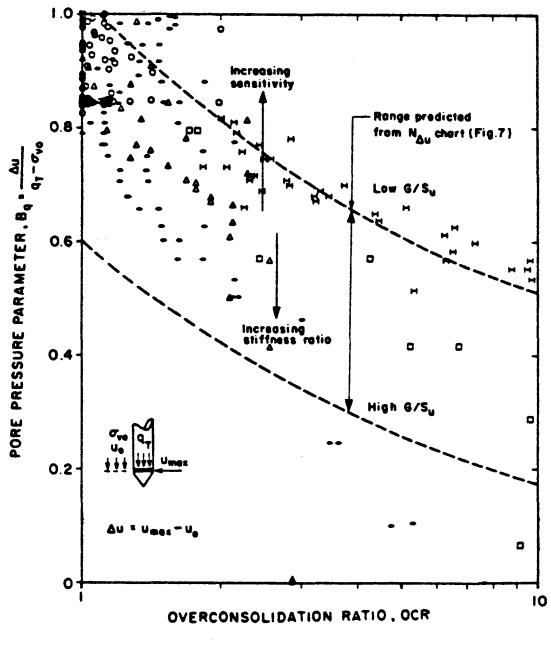

Figure 2.14. Parameter B_q versus OCR (Robertson, et al. 1986).

Battaglio et al. (1986) investigated the possibility of correlations between OCR and the pore pressure ratio parameter and $R_5 = (q_T-\sigma_{vo}-\Delta u_m)/\sigma_{vo}'$ using data from three Italian clays, as shown in Figure 2.15. A general trend was observed here, although not explored further with other available data.

Tavenas and Leroueil (1987) suggested $N_u = (u_m-u_o)/s_u$ to be a useful piezocone parameter for interpreting OCR of clays, although a prior knowledge of s_u is required. Data from sensitive Canadian Champlain clays and other clays from Quebec indicated that N_u decreases as OCR increases, as shown in Figure 2.16(a). However, data from heavily OC Saint Jean Vianney clay deviated from the observed trend. They also suggested a direct relationship between $(q_c-\sigma_{vo})$ and the preconsolidation pressure σ_p' using data from 11 Canadian clays, as presented in Figure 2.16(b). The normalized version of this parameter, $(q_T-\sigma_{vo})/\sigma_{vo}'$, is similar to that suggested by Schmertmann (1978), Mayne (1986, 1991), Wroth (1988), and Robertson (1990), as shown in Figure 2.17.

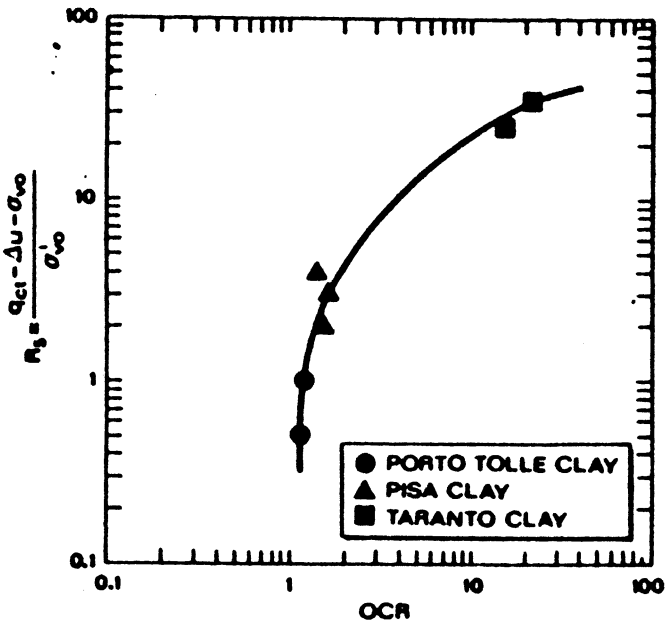

Figure 2.15. Piezocone Parameter R_5 versus OCR For Three Clays (Battaglio et al. 1986).

Crooks et al. (1988) proposed a correlation between the normalized cone parameter $(q_T-I_o)/I_o'$ and OCR_I, where $OCR_I = I'_y/I_o'$, I'_y = octahedral yield stress = $(I_{vy}'+2I_{hy}')/3$, and I'_o = mean effective in-situ stress = $(I_{vo}'+2I_{ho}')/3$. This relation implicitly includes the initial geostatic stress state (K_o) since both vertical and horizontal stresses are taken into account, though the range of K_o values may affect the correlation significantly. The results of applying this approach to piezocone interpretation for the Tarsuit site and Beaufort Sea clays in the Arctic are shown in Figure 2.18.

Rad and Lunne (1988) presented a series of direct correlations between the piezocone parameters (q_T, u_m, f_s) and undrained shear strength (s_u), such as q_T versus s_u, u_m versus s_u, f_s versus s_u, and the intercorrelations among q_T, u_m, and f_s. Each of these correlations also appeared to be functions of certain OCR ranges, and therefore could be used for estimating the approximate degree of overconsolidation.

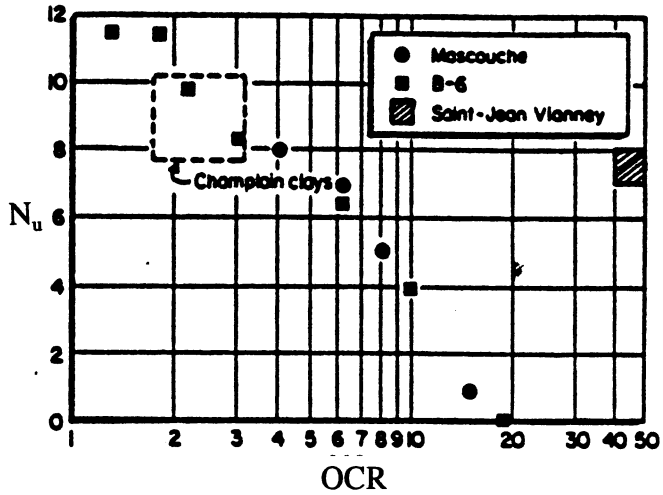

(a)

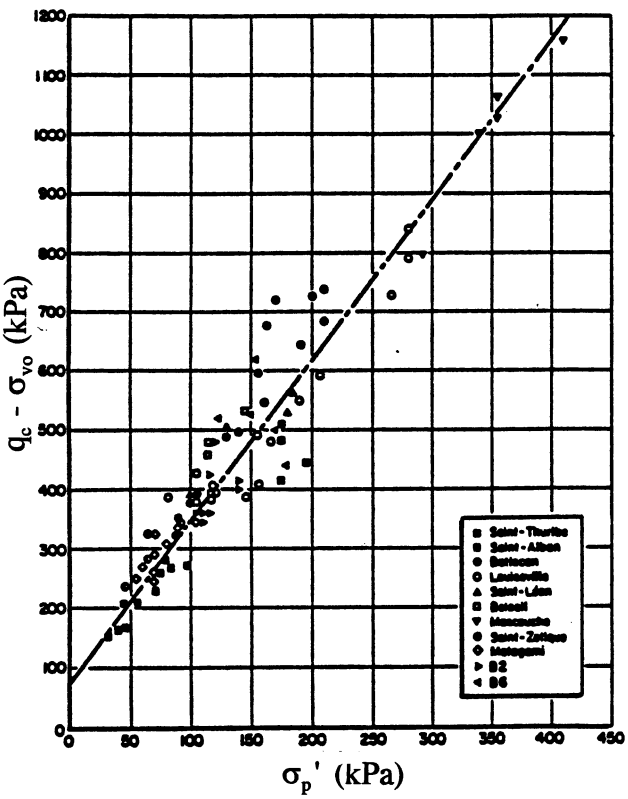

(b)

Figure 2.16. Relationships for (a) N_u versus OCR and (b) $(q_c-\sigma_{vo})$ versus σ_p' (Tavenas & Leroueil, 1987)

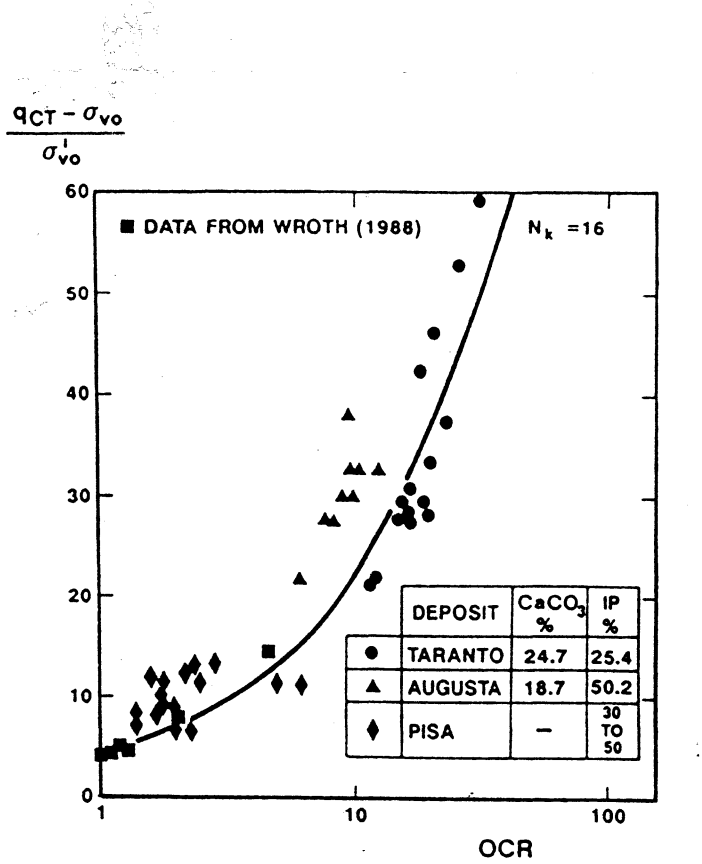

Figure 2.17. Normalized Cone Tip Resistance $(q_c-\sigma_{vo})/\sigma_{vo}'$ versus OCR (Robertson 1990).

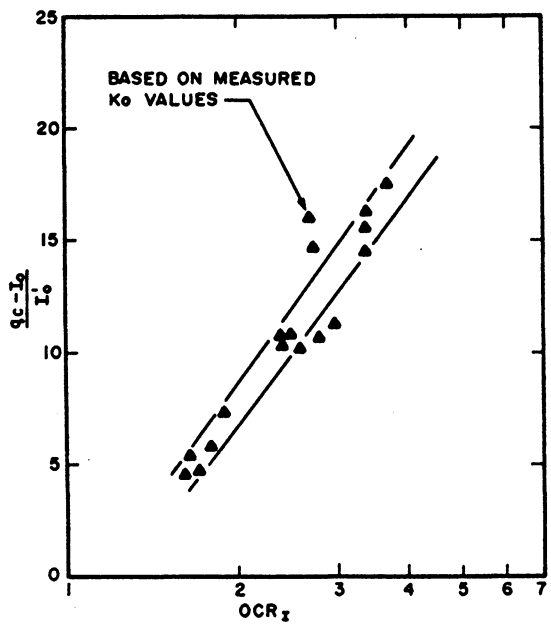

Figure 2.18. Normalized Cone Resistance Parameters Using Mean Effective Stresses $(q_c-I_o)/I_o'$ versus OCR. (Crooks et al. 1988)

Sully et al. (1988a,b) proposed three different piezocone parameters using pore pressure measurements: the ratio PPR1 = u_1/u_2; the ratio PPR = $(u_1-u_o)/(u_2-u_o)$, and the normalized pore pressure difference PPD = $(u_1-u_2)/u_o$, for correlating OCRs in clays. For example, using the minimum least squares method to compile data from several different sources, they suggested that OCR ≈ 0.66 + 1.43 PPD for the range: $1 < OCR < 10$, as shown by Figure 2.19. Several restrictions were given for the application of this expression, including having a phreatic level close to the ground surface, approximate hydrostatic water pressure distribution, different filter locations, and filter thickness (5 mm). For highly overconsolidated clays (OCR > 10), the relationship appeared to be inappropriate. Later, Sully and Campanella (1990) suggested use of another normalized pore pressure parameter, $(u_1-u_2)/\sigma_{vo}'$, for profiling K_o in clays.

Sills et al. (1988) used a quad-element piezocone to investigate the correlations between OCR and three different piezocone parameters in four clays: $B_q=(u_2-u_o)/(q_T-\sigma_{vo})$, $\beta=(u_2-u_o)/(u_1-u_o)$, and $Q=(q_T-\sigma_{vo})/\sigma_{vo}'$. They concluded that β gave a somewhat better indication of OCR, while both B_q and Q are very site specific. The derived ß-OCR relationship is shown in Figure 2.20.

Larsson and Mulabdić (1991) performed regression analyses for correlating existing piezocone parameters to σ_p' and OCR using data from Sweden, Norway, and U.K. Based on the available data, they indicated that the OCR may be estimated using the normalized piezocone parameters $(u_1-u_o)/\sigma_{vo}'$, $(u_1-u_2)/\sigma_{vo}'$, $(q_T-\sigma_{vo})/\sigma_{vo}'$, and $(q_T-u_2)/\sigma_{vo}'$. The relationships were also found to be slightly related to the index properties (liquid limits and plasticity indices) of the soils.

Mayne (1986, 1987), Mayne and Holtz (1988) and Mayne and Bachus (1988, 1989), suggested the use of the normalized piezocone parameters $\Delta u_m/\sigma_{vo}'$ for evaluating the OCR profiles in natural clay deposits. For Type 1 and 2 piezocones the empirical trends between OCR and $\Delta u_1/\sigma_{vo}'$ and $\Delta u_2/\sigma_{vo}'$ are shown in Figures 2.21a and b, respectively. Direct trends between the yield stress (σ_p') and excess pore pressure are shown for Δu_1 and Δu_2 were also observed by Mayne and Holtz (1988), Mayne and Bachus (1989), and Larsson and Mulabdic (1990), and these relationships will be explored later in this report.

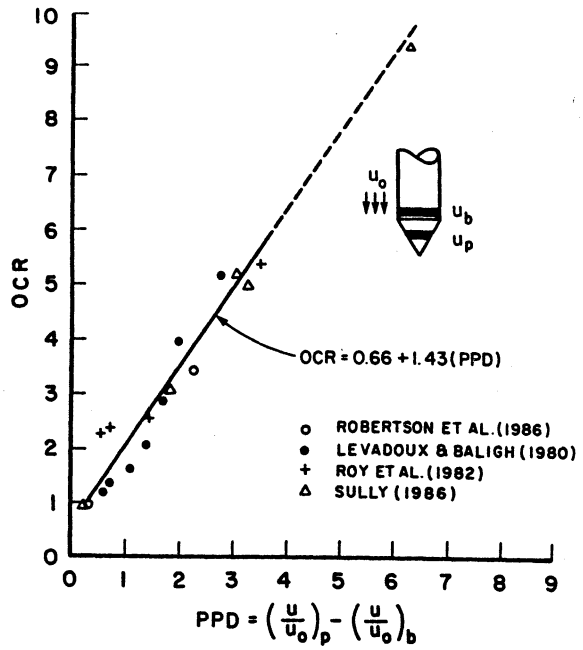

Figure 2.19. OCR Versus Pore Pressure Parameter PPD. (Sully et al. 1988b)

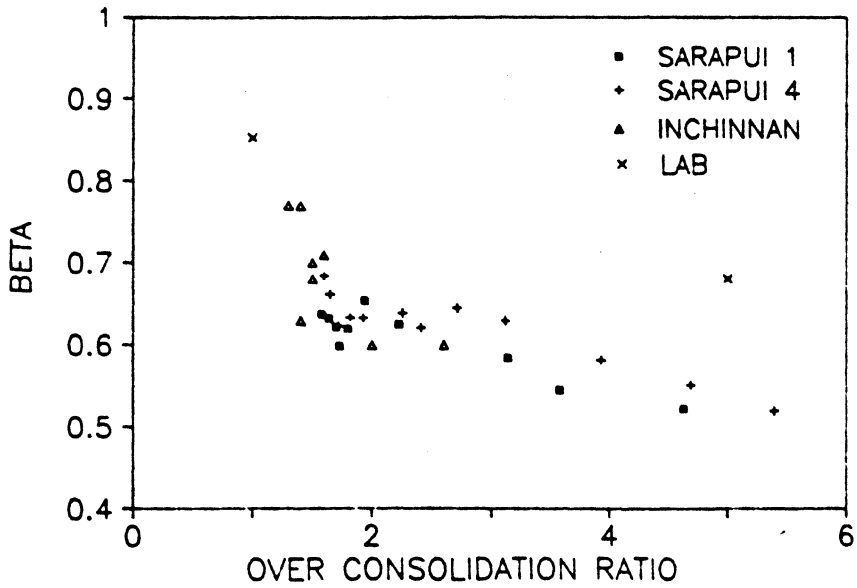

Figure 2.20. Piezocone Parameter $\beta = (u_2-u_o)/(u_1-u_o)$ Versus OCR. (Sills et al. 1988)

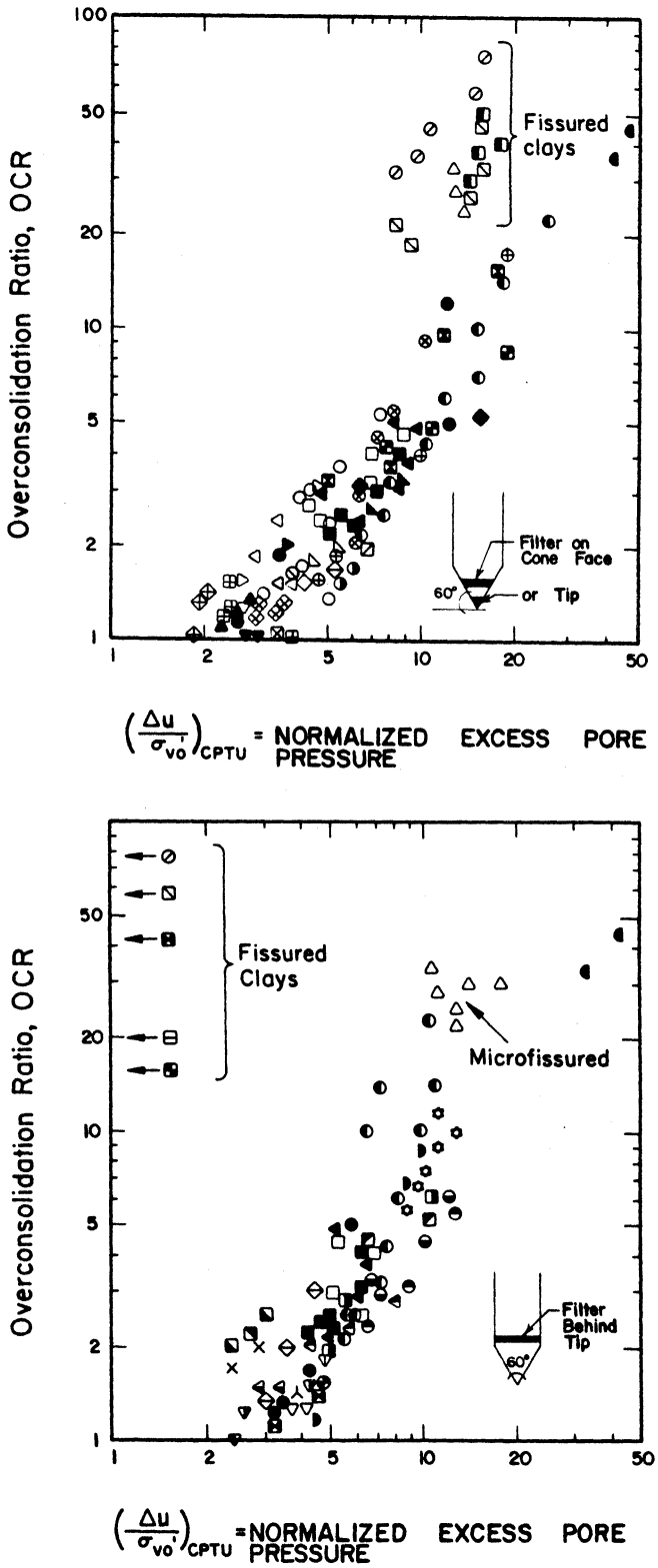

Figure 2.21. Relationships for: (a) OCR versus $\Delta u_1/\sigma_{vo}'$ and (b) OCR versus $\Delta u_2/\sigma_{vo}'$ (Mayne, 1991)

Table 2.2. Summary of Empirical Approaches for Predicting Stress History of Clays.

Stress History	Piezocone Parameters	References
σ_p'	q_c	Tavenas & Leroueil (1979)
	q_c	Mayne (1986)
	$(q_c-\sigma_{vo})$	Tavenas & Leroueil (1987)
	(u_m-u_o)	Mayne & Holtz (1988)
OCR	$(q_c-\sigma_{vo})/\sigma_{vo}'$	Schmertmann (1978)
	u_1/q_c	Baligh et al. (1980)
	$(u_2-u_o)/q_c$	Campanella & Robertson (1981)
	$(u_m-u_o)/(q_c-u_o)$	Smits (1982)
	$(u_1-u_o)/\sigma_{vo}'$	Azzouz et al. (1982)
	$B_q = (u_m-u_o)/(q_c-\sigma_{vo})$	Senneset et al. (1982)
	$B_q = (u_m-u_o)/(q_T-\sigma_{vo})$	Wroth (1984)
		Jamiolkowski et al. (1985)
		Robertson et al. (1986)
	$R_5 = (q_T-\sigma_{vo}-\Delta u_m)/\sigma_{vo}'$	Battaglio et al. (1986)
	$(u_m-u_o)/\sigma_{vo}'$	Mayne (1986); Mayne & Holtz (1988)
	$(u_m-u_o)/s_u$	Tavenas & Leroueil (1987)
	$(q_T-\sigma_{vo})/\sigma_{vo}'$	Wroth (1988)
	q_T, f_s, u_m	Rad & Lunne (1988)
	$PPD = (u_1-u_2)/u_o$	Sully et al. (1988)
	$PPR1 = u_1/u_2$	Sully et al. (1988)
	$PPR = (u_1-u_o)/(u_2-u_o)$	Sully et al. (1988)
	$\beta = (u_2-u_o)/(u_1-u_o)$	Sills et al. (1988)
	$(u_1-u_2)/\sigma_{vo}'$	Larsson & Mulabdić (1991)
	$(q_T-\sigma_{vo})/\sigma_{vo}'$	Larsson & Mulabdić (1991)
	(f_T/σ_{vo})	Larsson & Mulabdic (1991)
OCR_I	$(q_T-\sigma_o)/\sigma_o'$	Crooks et al. (1988)

Notes: σ_p' = effective yield stress or preconsolidation stress
OCR = $\sigma_{vo}'/\sigma_{vo}'$ = overconsolidation ratio in terms of vertical stresses
OCR_I = stress history in terms of mean effective stresses

2.3.2 Analytical Models

Konrad and Law (1987a) evaluated several existing methods for estimating OCR using piezocone data from five Canadian sites. They concluded: (1) there is no systematic correspondence between OCRs obtained from laboratory oedometer tests and those predicted by Schmertmann's extrapolation method (1978), probably due to the fact that the different processes leading to overconsolidation are not adequately considered in this method; (2) additional soil characteristics are required to link the parameter q_c/σ_p' (Tavenas and Leroueil 1979) to OCR; and (3) B_q is not sufficiently sensitive to correlate with OCR even within a given clay deposit.

By studying the stress path and induced pore pressures of soil element beneath the cone during penetration, Konrad and Law (1987a) derived an expression to evaluate the yield stress of clays. The vertical effective yield stress mobilized during cone penetration was expressed equal to the difference between the induced total vertical stress and the total pore pressure. The induced total vertical stress can be derived from the measured cone resistance, assuming that the unit shear stress at the cone-soil interface is computed using effective stress parameters combined with the measured pore pressures generated during penetration. The model requires a knowledge of the friction factor for the soil acting on the cone surface (δ), the effective friction angle of soil (ϕ'), and the apex angle (2θ) of the cone. The yield stress (σ_{yc}') is expressed by:

$$\sigma'_{yc} = \frac{q_T - \alpha u_2}{1 + \delta \tan\phi' \cot\theta} \qquad [2.1]$$

where α is a factor to convert the measured pore pressure to the pore pressure induced in the failure zone ($\alpha = u_1/u_2$). Konrad and Law recommended that $\alpha = 1.0$ to 1.1 for sensitive Canadian clays, $\delta = 0.5$ to 0.75 for smooth steel, and $\delta = 1.0$ for normal roughness. It is interesting to note that a simplification by substituting $\alpha = 1.0$, $\delta = 1.0$, $\theta = 30^o$, and $\phi' = 30^o$ into the above equation and normalization by σ_{vo}' by Robertson et al. (1988) leads to:

$$OCR \approx 0.5 \left(\frac{q_T - u_2}{\sigma'_{vo}} \right) \qquad [2.2]$$

Konrad and Law also examined factors affecting the relationships between the predicted and laboratory oedometer yield stress profiles, such as strain rate, stress path, and the strain softening effect. They suggested an empirical correction to include these effects, which indicates that the ratio of the predicted yield stress to the measured preconsolidation pressure (σ_{yc}'/σ_p') decreases with increasing OCR.

Sandven et al. (1988) provided a simple method to distinguish NC and OC clays. By assuming typical ranges of the cone bearing capacity factor N_c, the undrained shear strength factor α_u ($= s_u/\sigma_{vo}'$), and the unit weight ratio γ_w/γ, they propose a "theoretical" line in a q_T versus depth (z) plot of $q_T = 2\gamma z$. If the q_T line is close to the $2\gamma z$ line, the clay is most likely NC; if the q_T line is significantly larger than the $2\gamma z$ line, the clay is probably in an overconsolidated state. Sandven et al. (1988) and Senneset at al. (1989) also proposed the following expression to estimate the in-situ preconsolidation pressure:

$$\sigma'_p = \frac{q'_T + a'}{N_{qc}} - a' \qquad [2.3]$$

where $q_T' = q_T - u_2$ = effective cone resistance, $a' = c'/\tan\phi'$ =attraction, and N_{qc} = a bearing capacity coefficient as a function of ϕ' and B_q (See Figure 2.22a).

In addition to this effective stress approach, Sandven (1990) also suggested a total stress approach for predicting the preconsolidation pressure. The method is based on classical bearing capacity concepts, such that $q_T - \sigma_{vo} = N_c \cdot s_u$, and assumes the undrained strength is related to the preconsolidation pressure by the form: $s_u = \alpha'(\sigma_p' + a)$, resulting in the expression:

$$\sigma_p' = \frac{q_T - \sigma_{vo}}{N_c \ \alpha'} - a' \qquad [2.4]$$

where $\alpha' = \sin\phi'/2$ and N_c = bearing capacity factor. In Figure 2.22(b), a combined bearing capacity factor, $N_{c\alpha}$, is defined as $N_{c\alpha} = N_c \cdot \alpha'$.

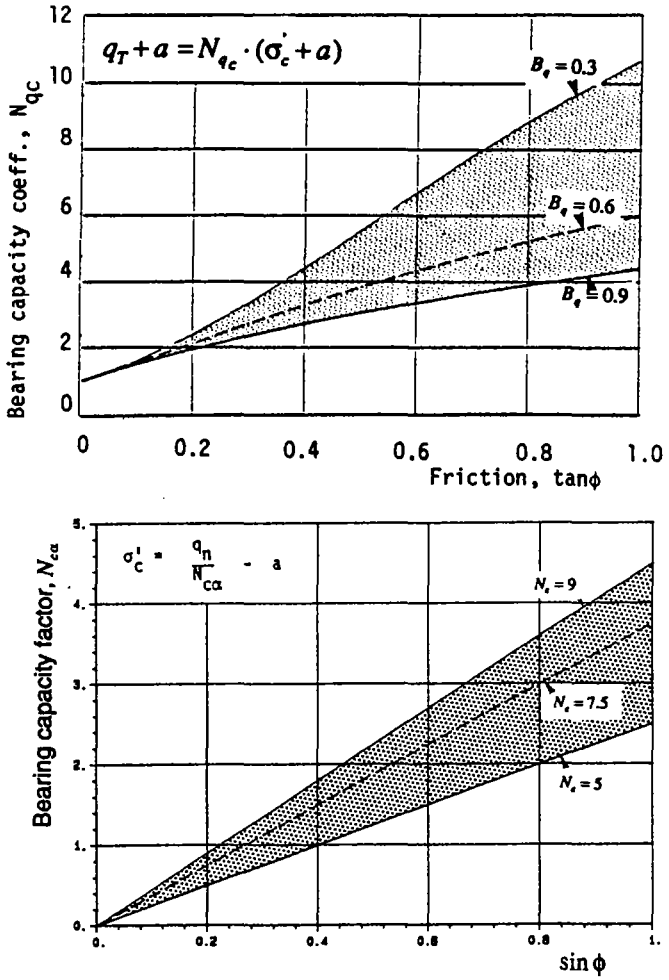

Figure 2.22. Cone Bearing Factors (a) N_{qc} and (b) $N_{c\alpha}$ (Sandven, 1988, 1990).

Wroth (1988) suggested out that the shear-induced component of the excess pore pressure generated during piezocone penetration plays an important role in describing the nature of the soil behavior, in particular the stress history. The proposed mechanism of the

piezocone penetration suggests that the pore water pressures measured behind the cone tip are significantly influenced by the shear stresses. However, Wroth provided no analytical method to uncouple the complicated octahedral normal and shear components of the excess pore pressures. He suggested that the normalized parameter $(q_T-\sigma_{vo})/\sigma_{vo}'$ be used for correlating piezocone test data with OCR in clays. Wroth also pointed out that the horizontal stress, σ_{ho}, or the mean principal stress, $p = \frac{1}{3}(\sigma_{vo}+2\sigma_{ho})$, are possibly better parameters than σ_{vo} for correlative purposes.

Houlsby (1988) used dimensional analysis to derive several piezocone parameters, $(u_m-u_o)/(q_T-\sigma_{vo}')$, $(q_T-\sigma_{vo}')/\sigma_{vo}'$, $(u_m-u_o)/s_u$, and $(u_m-u_o)/\sigma_{vo}'$. He also suggested that the parameter $(q_T-u_m)/\sigma_{vo}'$ may be a useful indicator of both soil type and OCR since it is analogous to σ_1'/σ_3' in the triaxial test, although (q_T-u_m) is often a small difference between two large quantities for Type 1 cones (u_1). For pore pressures measured at more than one location along the cone, Houlsby encouraged the use of $(u_2-u_o)/(u_1-u_o)$ or $(u_2-u_1)/(u_1-u_o)$.

Mayne (1987) and Mayne and Holtz (1988) utilized cylindrical cavity expansion theory and SHANSEP concepts to derive an expression for estimating OCR:

$$OCR = \left[\frac{\Delta u_m / \sigma'_{vo}}{(s_u / \sigma'_{vo})_{NC} \ln(G/s_u)} \right]^{1/\Lambda} \qquad [2.5]$$

where Λ = plastic volumetric strain ratio = $1 - \kappa/\lambda$, κ = swelling index, and λ = compression index. The range of undrained rigidity index ($I_r = G/s_u$) may vary from 20 to 1000 in clay, while the natural logarithm of the values change only from 3 to 7. By adopting typical values of $I_r = 400$, $\Lambda = 0.7$, and $(s_u/\sigma_{vo}')_{NC} = 0.35$, the above equation becomes:

$$OCR = 0.48[(\Delta u_m / \sigma'_{vo})]^{1.43} \qquad [2.6]$$

which compared well with data compiled from 36 clays.

Mayne and Bachus (1988) utilized both cylindrical and spherical cavity expansion with Modified Cam Clay for deriving expressions to relate OCR with excess pore pressure measurements. The concept of uncoupling the shear and normal components of the excess pore pressures is similar to that considered by Battaglio et al. (1981), except that this procedure extended the application to overconsolidated clays. An approach for pile installation effects by Randolph, Carter, and Wroth (1979) also bears resemblance to this method. The model expressed OCR in terms of either effective (ϕ') or total stress parameters (s_u) and required a value of the rigidity index (I_r). These convenient closed-form expressions are as follows:

$$OCR = 2\left[\frac{(\Delta u_m / \sigma'_{vo} - 1)}{(M/2)\ \ln(G/s_u) - 1}\right]^{1/\Lambda} \qquad [2.7]$$

$$OCR = \left[\frac{(\Delta u_m / \sigma'_{vo} - 1)}{(s_u / \sigma'_{vo})\ \ln(G/s_u) - (1/2)^{\Lambda}}\right]^{1/\Lambda} \qquad [2.8]$$

where $M = 6\sin\phi'/(3-\sin\phi')$. The appropriate value of rigidity index ($I_r = G/s_u$) was noted to be difficult to assess because of its dependancy on stress-level or strain-level.

The model was later improved by the following: (1) eliminating the rigidity index from the equations and (2) distinguishing between piezocones which measure u_1 and u_2 (Mayne 1991; Mayne and Chen 1994). In this regard, the inclusion of both cone resistance (q_T) and pore water pressure measurements (u_1 or u_2) made possible the removal of the reliance of the model on rigidity index. Chapter 5 describes the development and application of the methodology in detail. Two closed-form expressions are listed as follows for evaluating the OCR profiles of clays from Type 1 and Type 2 piezocone data:

$$OCR = \left[\frac{1}{1.95M}\left(\frac{q_T-u_1}{\sigma'_{vo}}+1\right)\right]^{1.33} \qquad [2.9]$$

$$OCR = \left[\frac{1}{(1.95M+1)}\left(\frac{q_T-u_2}{\sigma'_{vo}}\right)\right]^{1.33} \qquad [2.10]$$

Larsson and Mulabdić (1991) also justified the use of the parameter $(q_T-u_m)/\sigma_{vo}'$ by deriving a simplified model for the generation of pore pressures upon loading. Their study showed that the value of $(q_T-u_1)/\sigma_{vo}'$ is exactly equivalent to OCR for normally and lightly overconsolidated clays (OCR $\leq$ 15 to 20), while the value of $(q_T-u_1)/\sigma_{vo}'$ is smaller than OCR for heavily OC clays (OCR $>$ 15 to 20).

Based on a series of miniature piezocone tests in kaolinitic clays pressurized in calibration chambers, Kurup (1993) extended Eq. [2.10] to account for an anisotropic initial state of stress (K_o) by using the octahedral normal stress ($\sigma_o=\sigma_{oct}$), which resulted in:

$$OCR = \left[\frac{3}{(1.95M+1)(1+2K_o)}\left(\frac{q_T-u_2}{\sigma'_{vo}}\right)\right]^{1.33} \qquad [2.11]$$

Kurup removed K_o from above equation by using an empirical correlation between K_o and $(u_1-u_2)/\sigma_{vo}'$ proposed by Sully and Campanella (1991), giving:

$$OCR = \left[\frac{3}{(1.95M+1)}\left(\frac{q_T-u_2}{\sigma'_{vo}(1+2a^*)+2b^*(u_1-u_2)}\right)\right]^{1.33} \qquad [2.12]$$

where a* and b* are constants. The coefficient a* is always less than the normally consolidated value of K_o since the minimum value of $(u_1-u_2)/\sigma_{vo}'$ is between 0.25 and 0.75 depending upon the clay characteristics. The value of a* is typically about 0.5 and the second coefficient b* averages 0.11. Kurup (1993) replaced σ_{vo}' by $p'=(\sigma_{vo}'+2\sigma_{ho}')/3$ without actually rederiving the equation from an anisotropic initial state of stresses (i.e. does not follow the corresponding stress path for a soil element with anisotropic initial stress state). The equation was only calibrated against limited data from laboratory calibration chamber tests.

A summary of the aforementioned analytical approaches for evaluating the stress history of clays is given in Table 2.3.

Table 2.3. Summary of Analytical Models for Predicting Stress History of Clays.

Yield Parameter	Piezocone Parameters	References
σ_p'	$(q_T - u_2)$	Konrad & Law (1987)
	$(q_T - u_2)$	Sandven et al. (1988)
	$(q_T - \sigma_{vo})$	Sandven (1990)
	$(q_T - u_m)$	Larsson & Mulabdic (1991)
OCR	$(q_T - \sigma_{vo})/\sigma_{vo}'$	Wroth (1988)
	$(q_T - u_m)/\sigma_{vo}'$	Houlsby (1988); Mayne (1989)
	$(u_m - u_o)/\sigma_{vo}'$	Mayne & Bachus (1988)
	$(q_T - u_m)/\sigma_{vo}'$	Mayne (1991)
	(q_T, u_1, u_2)	Kurup (1993)
	$(u_1 - u_2)/\sigma_{vo}'$	Mayne & Chen (1994)

2.3.3 Numerical Simulations

A number of different approaches can be pursued for a numerical analysis of the cone penetration problem in clays. These include: finite elements, finite differences, discrete element method, strain path, and dislocation-based theory.

Baligh (1985) postulated that the strain path of deformed soil elements is more suitable for describing deep penetration problems. The strain path method (SPM) estimates the velocity fields and determines the resulting soil deformations by integrating the velocity along streamlines. Strain rates are determined by differentiating the velocities with respect to the spatial coordinates, and the strain paths of different soil elements can be determined by integrating the strain rates. Once the strains are known, a constitutive soil model is selected to calculate the stress regime by means of an effective stress approach, or the deviatoric stresses and the shear-induced pore pressures can be computed by a total stress approach. Subsequently, the stress conditions including total stresses and total pore pressures can be computed at every soil element.

Examples of the shear deformation fields from the strain path method are shown in Figure 2.23. Baligh considered the strain path method more appropriate for deep penetration problems than the solutions offered by cavity expansion theory, because the former accounted for: (1) all locations in vertical direction (i.e. two-dimensional cavity expansion), (2) deformation history or strain paths during penetration, and (3) strain rates by using the appropriate flow function. However, the strain path method is sensitive to the constitutive soil relations selected and requires detailed numerical iterations. Baligh (1986a, 1986b) studied the stress and strain fields around a penetrating object using SPM. Simple soil models such as bilinearly and hyperbolically elastic-plastic models were used for the determination of stresses.

The distributions of octahedral stresses and sheared-induced pore pressures during simple pile penetration is shown in Figure 2.24. The octahedral stresses not only control the penetration resistance but also contribute principally to the excess pore pressures (Δu) at the tip. The contribution of shear-induced pore pressures (Δu_s) to the tip pore pressure is generally small and typically less than 20% for Boston Blue Clay in the range $1 \leq OCR \leq 10$. For the evaluation of stress history (OCR) from piezocone tests, the octahedral stresses are related to the net cone resistance thus the undrained shear strength of clays. The OCR of clay can then be determined using SHANSEP procedures if the clay exhibits normalized strength behavior. Excess pore pressures are also good indicators of OCR in clays, although Baligh commented that attempts to utilize the Δu measurements for estimating

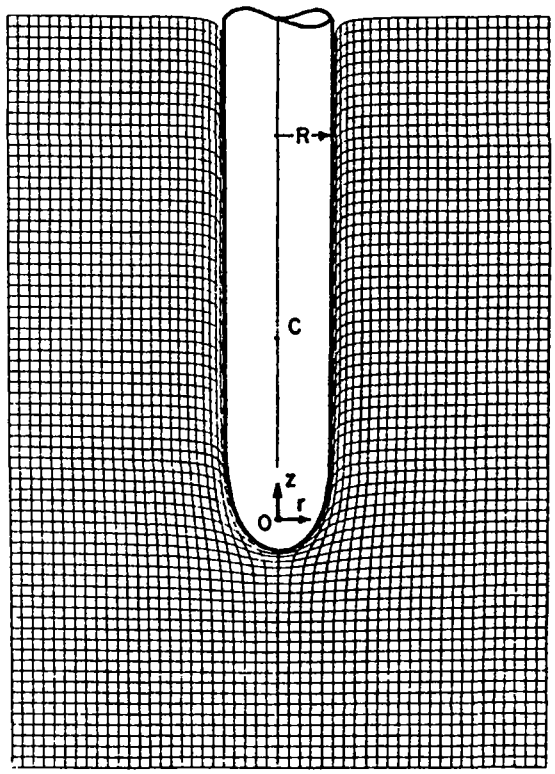

Figure 2.23. Shear Deformations in Saturated Clays Due to Simple Pile Penetration. (Baligh, 1975)

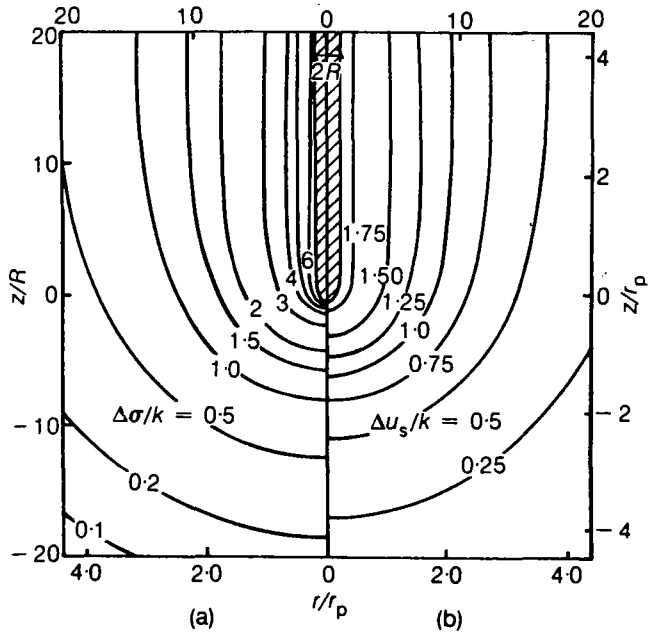

Figure 2.24. Simple Pile Penetration in Hyperbolic Soil: (a) Octahedral Stress Increments and (b) Shear-induced Pore Pressures (Baligh, 1986b).

the OCR of clays are not likely to succeed without a thorough understanding of various factors affecting the octahedral stresses.

Whittle and Aubeny (1993) utilized the Strain Path Method and a generalized effective stress soil model (MIT-E3) to predict the undrained shear strength from both the cone tip resistance (q_T) and tip pore pressures (u_1). The MIT-E3 model (Whittle, 1993) requires 15 soil parameters which are determined from a series of laboratory tests such as oedometer tests, anisotropically-consolidated triaxial shear tests (CK_0UC and CK_0UE), and resonant column (or in-situ cross-hole shear wave velocity tests). For data obtained at the South Boston site, Figure 2.25 shows the SPM predictions of the net tip resistance and excess pore pressures using the MIT-E3 model and Modified Cam Clay (MCC). The magnitudes of excess pore pressures, predicted at all locations around the penetrometer using the MIT-E3 model, increase very significantly with OCR, as shown in Figure 2.26.

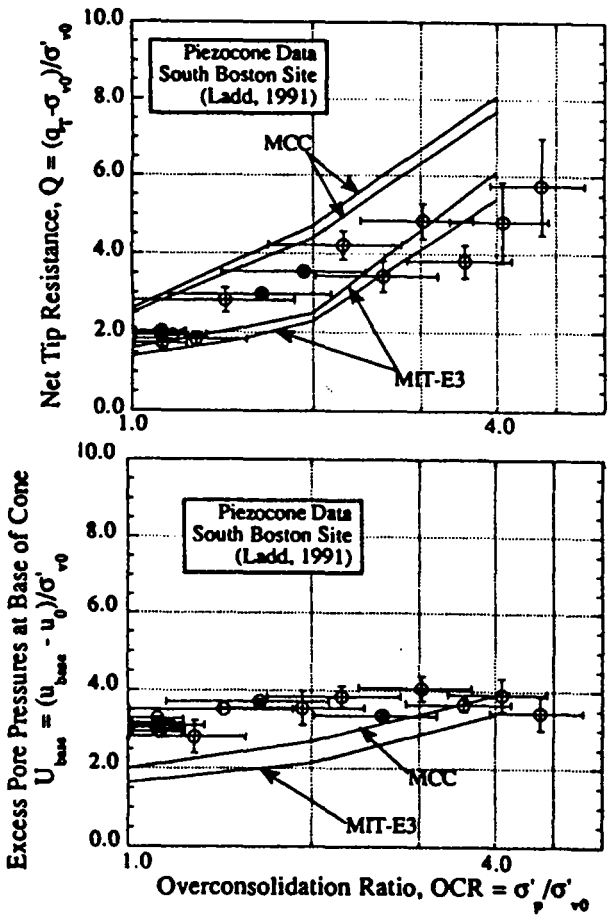

Figure 2.25. Comparison of SPM/MIT-E3 Prediction with Piezocone Measurements in Boston Blue Clay (Whittle and Aubeny, 1993).

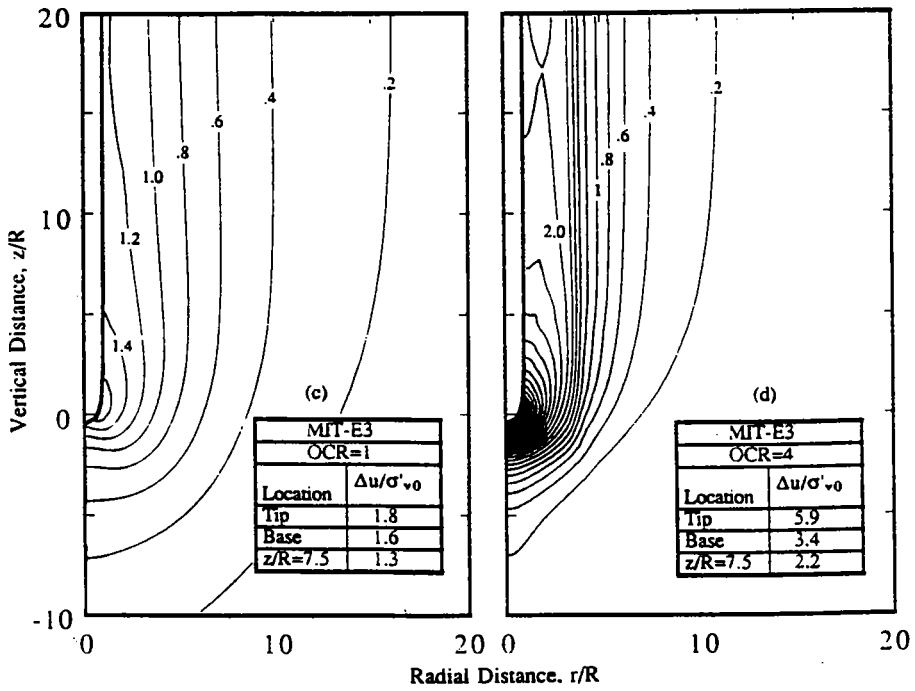

Figure 2.26. Predicted Excess Pore Pressure Around the Simple Pile (Whittle and Aubeny, 1993)

Tumay et al. (1985) and Acar and Tumay (1986) developed an approach similar to the Strain Path Method that studied the flow field around cones penetrating an inviscid fluid. The method evaluates stream function, velocity field, and strain rates around cones in steady penetration. In soft clays, the flow field gives the first approximations to the strains induced around the cone.

Sandven (1990) analyzed the stress conditions around a cone using the finite element method (FEM). Quadrilateral elements were used in the analysis and the initial states of stress were assumed to be isotropic. In terms of total stress, the cone bearing factor was calculated from the net cone tip resistance (q_T) which was determined from the computed normal and shear stresses. While the primary goal of this study was to evaluate the undrained shear strength of clays, the OCR can be interpreted using the normalized strength concept. Sandven concluded that FEM simulation of the cone penetration is of limited applicability for practical interpretation of piezocone data, however, it may help in picturing

delicate aspects of the penetration problem, such as pore pressure distribution, extension of failure zone, and the influence of cone geometry.

Problems of cone penetration analyzed by FEM often ignore the high vertical and lateral stresses developed adjacent to the shaft of the cone during penetration. The assumed "pre-bored" hole before the cone is in place leads to the underestimation of penetration pressures. Houlsby and Teh (1988) attempted to overcome this problem by using the SPM to obtain the initial stress state, followed by a large strain FEM analysis to determine the stress state of deformed soil elements. Cone bearing factors were derived from the computed stresses (Teh and Houlsby, 1988, 1991).

Table 2.4 summarizes the types of numerical simulation methods used for evaluating cone penetration problems in clays.

Table 2.4. Summary of Numerical Simulation Techniques for Piezocone Penetration.

Method	Soil Model	References
SPM	Bilinear & Hyperbolic	Baligh (1985, 1986a, 1986b)
Flow Field Method	Plasticity	Tumay et al. (1985)
SPM + FEM	Elastic-Plastic	Houlsby and Teh (1988)
FEM	Elastic-Plastic	Sandven (1990)
Dislocation Analysis	Elastic	Elsworth (1991,1993)
SPM	MIT-E3	Whittle and Aubeny (1993)
SPM	MCC	Whittle and Aubeny (1993)

Notes: SPM - Strain Path Method;
FEM - Finite Element Method;
MCC - Modified Cam Clay;
MIT-E3 - Mass. Inst. of Tech. Effective Stress Model 3.

2.4 Conclusions

The stress history of clays is normally evaluated by defining a yield point or preconsolidation stress from a conventional laboratory oedometer test. The use of in-situ tests for profiling the apparent σ_p' profile in clay is attractive since it may be possible to discern a rather complicated and varied stress history that includes multiple effects (For examples: erosion, reloading, aging, plus cementation). Also, the in-situ tests are conducted rather quickly and inexpensively, thus allowing an immediate assessment of the state of overconsolidation upon the completion of field testing, as well as a mapping of its variation across the site of study.

A primary interest of this research program was to evaluate the ability and potential for using piezocone data to delineate profiles of OCR in supplementing reference values obtained from laboratory oedometer tests using either face (u_1) or shoulder (u_2) measurements of penetration pore pressure, or both. Methods of evaluating the stress history in clays from the results of piezocone tests have been reviewed in this chapter. The approaches have been separated into the categories of: empirical, analytical, and numerical simulation. Direct relationships have been proposed between the yield stress (σ_p') and various piezocone parameters, as well as relationships between the OCR and normalized piezocone parameters.

CHAPTER 3

PIEZOCONE DATABASE AND STATISTICAL RELATIONSHIPS

3.0. Piezocone Database

A piezocone database is compiled for calibrating PCPT-OCR models in clay deposits. The data can also be used for evaluating various piezocone parameters and generating statistical correlations between the piezocone parameters and the OCR. The database contains over 600 piezocone soundings obtained from 205 clay sites around the world. In Figure 3.1, a world map shows that most of the piezocone data have been collected from the eastern and western United States, southern Canada, western Europe, and southeastern Asia, where piezocone penetration tests have been used more frequently than in other parts of the world.

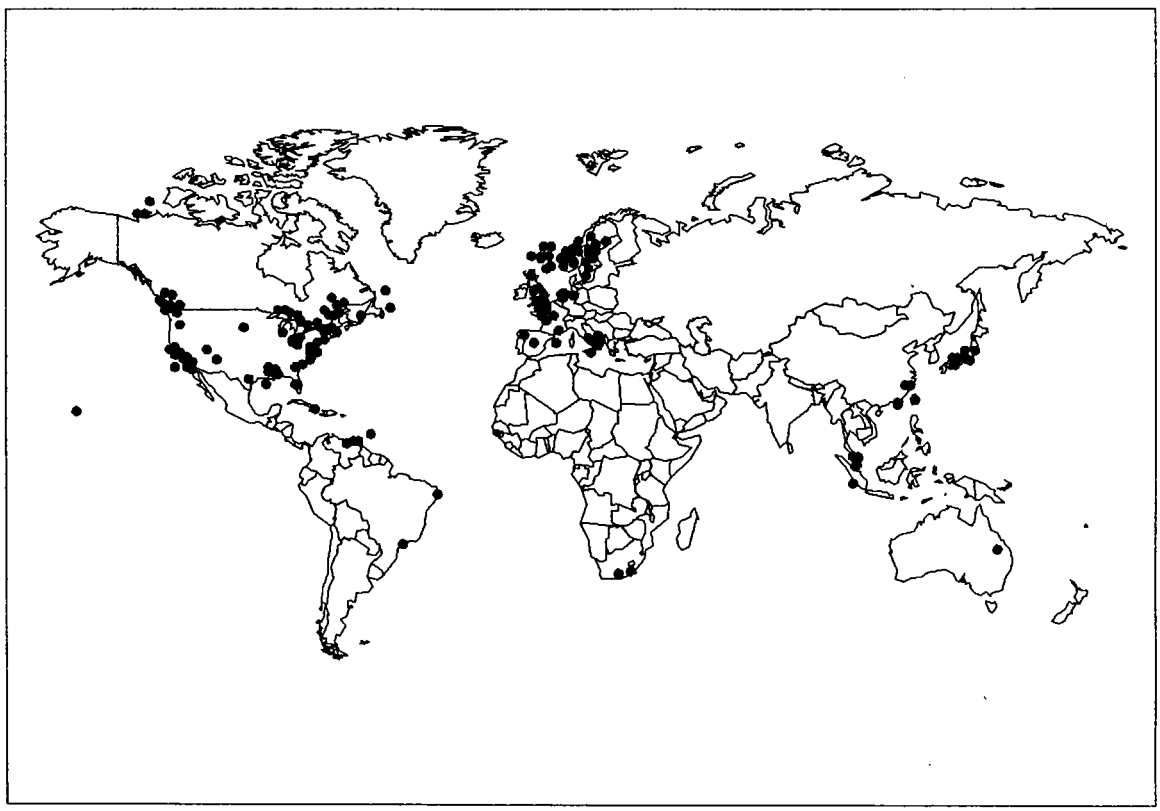

Figure 3.1. Locations of Piezocone Clay Sites in Database.

A summary table which lists some relevant information in the database is presented in Appendix B. The information includes: (1) site name in alphabetical order, (2) data completeness rating, (3) site location, (4) country, (5) soil description, (6) natural water content, (7) liquid limit, (8) plasticity index, (9) sensitivity, (10) oedometric overconsolidation ratio, (11) undrained shear strength, (12) effective friction angle, (13) cone tip area, (14) porous filter location, and (15) reference source. Based upon the availability of the piezocone details and specific soil property information at each site, the completeness of the data are evaluated and assigned a rating. The rating is designed to assist in selecting data for calibrating the piezocone models in evaluating the OCR profile of clays, therefore, only key parameters such as those listed in Table 3.1 are taken into consideration. It is important to note that the class categories are not intended to reflect the quality of the data.

In Table 3.1, Class I sites contain the most complete information available for evaluation and Class VI sites correspond to sites where incomplete data existed. For the purposes of calibrating the PCPT-OCR model, data from Class I sites can be used for evaluating Type 1, Type 2, and dual-type models, while data from Class II sites can only be used for either the Type 1 or Type 2 models. By assuming a value for the effective friction angle (ϕ'), data from Class III sites may be used for all three models as an approximation, while data from Class IV sites may be used only for approximating either the Type 1 or Type 2 model. Class V sites contain little or no backup OCR information, and therefore, can only be used for statistical correlations among piezocone parameters (such as q_T versus u_m and u_1 versus u_2). Class VI sites include those where either the piezocone data are incomplete or uncertainties exist as to specific important variables (depth to groundwater table, porous element position, etc.).

It should also be noted that while the authors made every attempt to obtain fully complete sets of data and as many contributions to the database as possible, many omissions of data were incurred because special reports and unpublished documents were difficult, if not impossible, to obtain. Not all firms or agencies contacted were willing to share information, details, or correspondence, and in some instances, data could only be obtained if a "blind" site was assured because of potential legal difficulties or classified status.

Table 3.1. Classification Criteria for the Completeness of Piezocone Data.

Class	q_T	u_m	σ_{vo}'	u_o	OCR	ϕ'
I	Y	B	Y	Y	Y	Y
II	Y	E	Y	Y	Y	Y
III	Y	B	Y	Y	Y	N
IV	Y	E	Y	Y	Y	N
V	Y	E	Y	Y	N	N
VI	N	N	Y/N	Y/N	Y/N	Y/N

Notes: Y - information available
N - information not available
B - both u_1 and u_2 are available
E - only either u_1 or u_2 is available
Y/N - information may or may not be available

The piezocone data compiled included the cone tip resistance (q_T) and the pore pressures measured at various locations, such as the tip apex (u_{1t}), the tip face (u_{1f}), behind the tip (u_2), and at a distance on the shaft behind the friction sleeve (u_3). For the cone tip resistance, corrected q_T data were obtained, where available. Except at a few sites where piezocone tests were performed by Georgia Tech personnel (see Chapter IV and Appendix A), most data were collected from the published geotechnical literature or unpublished reports and private files that were either obtained in digital form or transferred into digital format using an HP Sketch Pro digitizing tablet. The piezocone data were then stored as a tabulated form in the spreadsheet (such as QPRO and EXCEL) and tracked using a database management software program (FOXPRO).

The soil information was collected with an emphasis on the index properties (w_n = natural water content, LL = liquid limit, PI = plasticity index, and S_t = sensitivity), stress history (OCR or σ_p'), effective frictional characteristics (ϕ'), and undrained shear strength (s_u). Geologic origins of the clay deposits considered include glacial, fluvial, alluvial, deltaic, diluvial, lacustrine, and marine deposits. The database contains many well-known formations such as Boston Blue clay, Leda clay, London clay, Beaumont clay, Champlain

Sea clay, Norwegian quick clay, and San Francisco Bay Mud. The natural clay deposits in the database range from soft, intact, normally consolidated materials to very stiff to hard, fissured, heavily overconsolidated soils. The complete range in undrained shear strengths obtained from various laboratory and in-situ tests for all clays considered is 5 kN/m^2 $\leq s_u \leq$ 850 kN/m^2, while the OCR varies from 1 to 100+. The database contains some highly plastic clays as well as low plasticity silty materials with the plasticity index (PI) ranging from 4 to 100. The natural water content (w_n) of the clay deposits in the database extends from 10% to 200% and the range in liquid limit is $15 \leq LL \leq 170$. The natural clay deposits include insensitive materials (S_t = 1 to 2) to moderate sensitive (S_t = 5 to 20), as well as very sensitive quick clay ($50 \leq S_t \leq 500+$).

To evaluate the possible correlative trends between the piezocone parameters and stress history, a spreadsheet which contains discrete data points of preconsolidation stress (σ_p') from the laboratory oedometer tests and piezocone measurements (q_T, u_1, u_2, and u_3) corresponding to the same depths, was prepared, as presented in Appendix C. Other pertinent soil information, such as soil type, effective overburden stress (σ_{vo}'), hydrostatic pore pressure (u_o), and average plasticity index are also included. The spreadsheet contains as many as 1,450 data points selected from the database. It was necessary in certain instances that a few data points be filtered from the spreadsheet when measured anomalies occurred either in the desiccated crust or in silty/sandy layers. Other data points excluded from the analysis included unreasonable pore pressure measurements (e.g. $u_m > q_T$) or uncertain q_T corrections (either the value of net area ratio "a" or penetration pore pressure u_2 were unknown). In other cases, a random stone or gravel was encountered or the pore pressure filter became de-saturated. In these cases, a judgement call was made by the authors to remove spurious points.

Since most of the data were collected from the literature, the quality of the data relies heavily on how well-documented the sources of information were. In the event that the tests were not performed properly or the results were not reported precisely, the reliability of the data becomes uncertain. This is especially true for the piezocone test since it requires extra caution in operation and interpretation. Problems such as inadequate filter saturation, clogged filters, electronic noise, crosstalk, electronic drift, temperature variations, and

uncorrected q_c measurements are crucial, while in some cases these difficulties were not fully discussed by the sources of the data. Besides, the processed piezocone data were subject to incurred errors in the redigitizing sequence, particularly if they were not presented on proper scales or if plotted on distorted axes in their original formats. Therefore, it is important to realize that the statistical evaluations derived from the database, while revealing some general trends, should be considered only approximate and used judiciously.

3.1. Cross-Correlations Among Piezocone Measurements

The piezocone penetration test normally provides three separate and distinct measurements: cone tip resistance (q_T), sleeve friction (f_s), and induced pore water pressure (u_m). The sleeve friction is considered less reliable in comparison with the other two measurements (Lunne et al. 1986a), and therefore will not be discussed herein because of significant variations obtained in f_s values using different commercial cones. Also, corrections for pore pressure effects on f_s are difficult to obtain and apply properly.

The pore water pressures are measured with porous filters located at three of the more common positions: the cone face/tip apex (u_1), immediately behind the cone base (u_2), and behind the friction sleeve (u_3). In the following sections, the cross-relationships among piezocone parameters q_T, u_1, and u_2 are examined. By far, u_1 and u_2 are the most predominant readings taken and these are the focus aspects studied herein. Relationships for the u_3 position have not been explored here because they are abundant.

3.1.1. Type 1 Pore Pressures

Robertson et al. (1986) and Powell et al. (1988) noted that penetration pore pressures vary across the cone face in clays, and in particular, increase from the apex to the shoulder. However, it is common to designate any and all pore pressures on the cone face by u_1 (Sully et al. 1988; Robertson et al 1988; Rad and Lunne, 1988; Mayne et al, 1990). Brown (1993) distinguished the approximate magnitudes of u_1 for pore pressures measured at cone midface (u_{1f}) from those measured at the apex (u_{1t}), and concluded a relationship of $u_{1t}/u_{1f} = 0.895$ using data from 4 intact clays ($1 \leq OCR \leq 2$). Figure 3.2 combines results from 7 clays in the database ($1 \leq OCR \leq 80$) and indicates an average relationship of $u_{1t}/u_{1f} = 0.861$. The

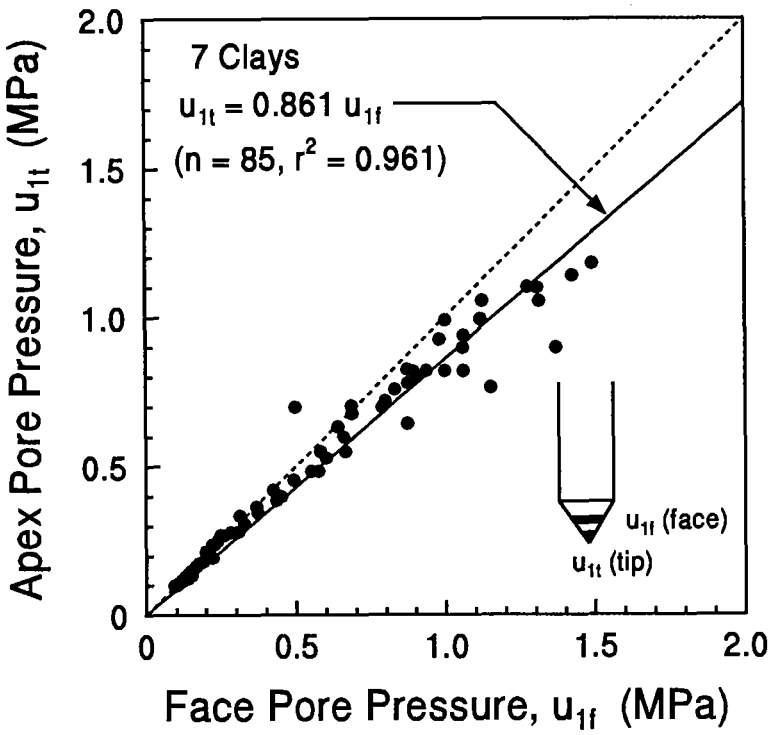

Figure 3.2. Comparison of Type 1 Pore Water Pressures at Apex Versus Midface.

results indicate that the pore pressure measured at mid-face of the cone is indeed higher than that measured at the cone apex in natural clay deposits. In fact, the ratio u_{1t}/u_{1f} appears to vary with OCR, according to data presented by Powell et al (1988). Although it is desirable to distinguish between these two different filter locations, sources of data did not often distinguish the exact position of the u_1 element. Therefore, a generic Type 1 pore pressure ($u_1 = u_{1t}$ or $u_1 = u_{1f}$, whichever is available or larger) has been adopted in the subsequent analyses. It appears that the more recent cones favor a mid-tip element, however, because it is less vulnerable to damage than an apex position, and therefore, more data have been collected at midface.

3.1.2. Type 2 Pore Pressures

The porous filter location of most commercial Type 2 piezocones varies from immediately behind the cone tip base to positions of up to 5 mm from the base. To

distinguish this difference in the database is difficult since many sources of information do not provide the precise details of their cone geometry. In the small zone of Type 2 filter locations, the difference in pore pressure response is not believed to be significant, as concluded by Larsson and Mulabdić (1991) and Brown (1993). In some cases involving fissured clays, however, the width of the filter element has an effect (Campanella and Robertson 1988) that deserves further study. In this report, the filter location label u_{bt} or u_2 refers to all elements located directly behind the tip at the shoulder.

3.1.3. Cone Tip Resistance and Type 1 Pore Pressures

Baligh et al. (1981) indicated the ratio u_1/q_c averaged about 0.85 for NC Boston Blue clay and that the ratio appeared inversely proportional to OCR. Assessing data from several sites, Mayne et al. (1990) reported that $u_1/q_T \approx 0.639$ for intact Leda clays and $u_1/q_T \approx 0.728$ for other intact clays. Brown (1993) further summarized results of pore pressures measured with the porous element located from the apex to upper mid-face and indicated that $0.593 \leq u_1/q_T \leq 0.631$ for the Leda clays and $0.684 \leq u_1/q_T \leq 0.763$ for other intact clays.

Data from 78 clay sites in this study indicate that u_1/q_T averages 0.722 for all intact clays and $u_1/q_T \approx 0.499$ for fissured clays, as shown in Figure 3.3. The coefficient of determination (r^2) for intact clays is 0.918, while the fissured data are much more scattered ($r^2 = 0.659$).

3.1.4. Cone Tip Resistance and Type 2 Pore Pressures

Mayne et al. (1990) determined average values of $u_2/q_T \approx 0.537$ and 0.534 for intact Leda clays and other intact clays, respectively. Brown (1993) reported that $u_2/q_T \approx 0.592$ and 0.575 for the Leda and intact clays, respectively. Thus, pore pressures for the shoulder position in many types of intact clays respond similarly.

Data from 100 clay sites in this study indicate that the ratio u_2/q_T averages about 0.528 ($r^2 = 0.862$) for all intact clays, while no statistically significant relationship can be concluded for the fissured clay data since u_2 can be positive, zero or negative, as shown in Figure 3.4. The degree of fissuring must thus play an important role in determining the magnitude of penetration pore pressures.

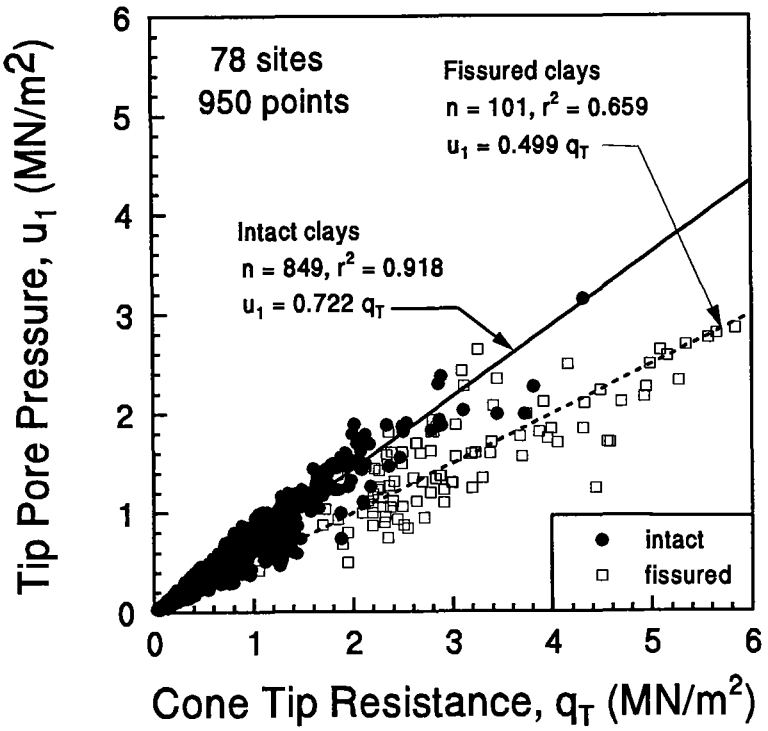

Figure 3.3. General Relationship Between Type 1 Pore Pressures and Cone Tip Resistance.

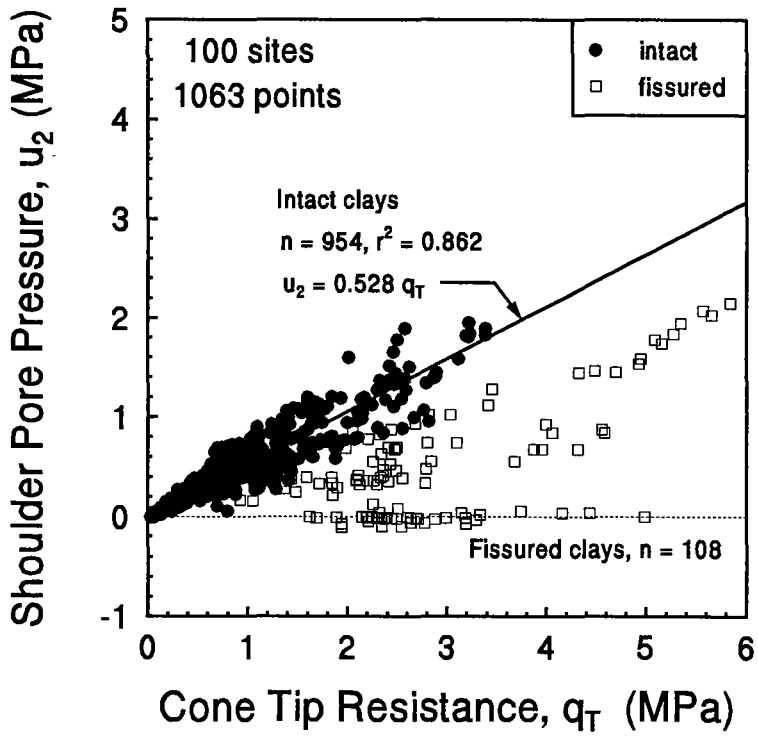

Figure 3.4. General Relationship Between Type 2 Pore Pressures and Cone Tip Resistance.

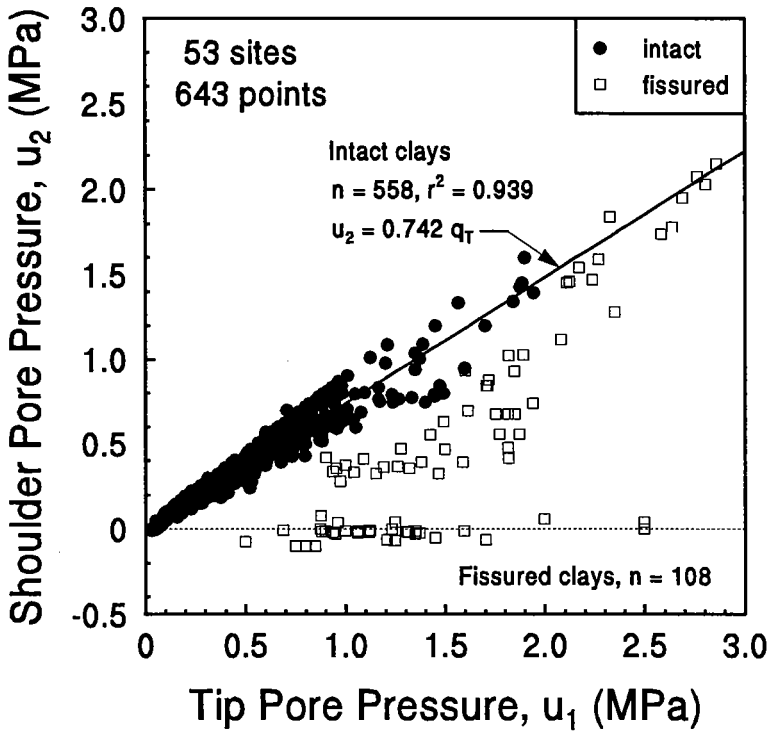

Figure 3.5. General Comparision of Type 1 and 2 Penetration Pore Pressures.

3.1.5. Type 1 and Type 2 Pore Pressures

It is common to assume a conversion ratio $u_2/u_1 \approx 0.8$ in correcting raw q_c measurements from Type 1 piezocones (Lunne et al, 1985; Campanella and Robertson, 1988). For intact clays, this assumption is only approximate, however, and the actual ratio u_2/u_1 depends on OCR, degree of fissuring, sensitivity, and fabric. Mayne et al. (1990) reported that the ratio u_2/u_1 averaged about 0.901 for intact Leda clays and $u_2/u_1 \approx 0.701$ for other intact clays. Data from 53 different clay sites herein show a well-defined correlation ($r^2 = 0.939$) between u_2 and u_1 for intact clays ($u_2/u_1 \approx 0.742$), while data are scattered for fissured clays, as indicated in Figure 3.5. Again, degree of fissuring plays an issue here but has not been quantified.

Table 3.2 summarizes results of linear regression analyses from previous and current studies. Comparing with results from Mayne et al. (1990) and Brown (1993), Figures 3.2 to 3.5 show similar trends of relationships among the parameters u_1, u_2, and q_T, although

the size of the database herein is significantly larger. This provides a consistent foundation for examining further various normalized piezocone parameters in interpreting the preconsolidation stresses of natural clay deposits.

Table 3.2. Summary of Statistics in Cross-Correlations Among q_T, u_1, and u_2.

Ratio	Soil Type	Mayne et al. (1990) n	r^2	Ratio	Brown (1993) n	r^2	Ratio	This Study* n	r^2	Ratio
u_{1t}/u_{1f}	intact	NA	NA	NA	61	0.953	0.895	85	0.961	0.861
u_1/q_T	intact	166	0.955	0.728	289	0.963	0.713	849	0.918	0.722
	Leda	24	0.977	0.639	16	0.976	0.612	-	-	-
u_2/q_T	intact	166	0.897	0.534	337	0.905	0.575	954	0.862	0.528
	Leda	70	0.912	0.537	72	0.923	0.592	-	-	-
u_2/u_1	intact	106	0.940	0.701	NA	NA	NA	558	0.939	0.742
	Leda	25	0.999	0.901	NA	NA	NA	-	-	-

Notes: n = number of data points in regression analysis
r^2 = coefficient of determination
u_{1t} = pore pressure measured at tip apex
u_{1f} = pore pressure measured on cone face (mid-face)
u_1 = u_{1t} or u_{1f}, whichever is available or larger
u_2 = pore pressure measured behind the tip
q_T = corrected cone tip resistance
NA = not available
(*) = intact clays in this study include Leda clays

3.2. Simple Regression Analyses of Piezocone Data

3.2.1. Overconsolidation Ratio Relationships

Least squares regression analyses have been performed between the OCR and selected piezocone parameters. Statistical relationships are reported where the trends are significant, although scattered results occur for certain of the parameters. A summary of the results

from simple linear regression analyses between the OCR and piezocone parameters is presented in Table 3.3. In the cases where arithmetic scales have been assumed, the adopted form of the regression is: OCR = $\alpha_1 + \beta_1 X$, where X = independent profiling variable and overconsolidation ratio is the dependent variable. In the cases where logarithmic scales are utilized, the adopted form of the regression is taken as: OCR = $\alpha_2 X^{\beta 2}$. In the latter case between log OCR and log X, the regression slope (m) becomes the exponent β_2 in the power function and the intercept (b) is used to obtain the coefficient $\alpha_2 = 10^b$. The number of data points is given by the parameter n and the statistical measure of goodness of fit is reported in terms of the coefficient of determination (r^2).

Applicable to all types of cone penetration tests, the normalized net cone tip resistance $(q_T-\sigma_{vo})/\sigma_{vo}'$ has been used for interpreting the undrained strength ratio (s_u/σ_{vo}') in clays (Schmertmann 1978). Although the parameter does not utilize pore pressure data, the u_2 value is essential for correcting the cone tip resistance from q_c to q_T. In cases where u_1 is measured instead of u_2, an uncertainty is involved in obtaining q_T. In any event, Mayne (1986) and Larsson and Mulabdic (1991) used $(q_T-\sigma_{vo})/\sigma_{vo}'$ for indexing OCR profiles directly and Robertson (1990) employed the same parameter for evaluating soil classification.

In a critical appraisal of in-situ test interpretation, Wroth (1988) reasoned that the parameter $(q_T-\sigma_{vo})/\sigma_{vo}'$ would be an appropriate one for evaluating OCR in natural clay materials. However, Mayne (1991) indicated that the relationship between the OCR and $(q_T-\sigma_{vo})/\sigma_{vo}'$ is more complicated than just a direct comparison between the two parameters. Other soil parameters, such as soil frictional characteristics (ϕ') and rigidity index ($I_r = G/s_u$) should be involved if a rational relationship was desired.

The results of regression analyses between OCR and $(q_T-\sigma_{vo})/\sigma_{vo}'$ are presented in Figure 3.6 and Table 3.3, indicating a fair to good statistical trend, depending upon the data subset and assumed format. The data have been sorted into two categories: intact clays and fissured clays. Results from the regression analyses indicate that the behavior is different between these two subsets.

Table 3.3. Summary of Simple Regression Analyses Between Overconsolidation Ratio (OCR) and Various Normalized Piezocone Parameters for Clays.

Cone Type	Parameter (X)	Soil Group	Arithmetic Scale n	r^2	α_1	β_1	Logarithmic Scale n	r^2	α_2	β_2
All Data	$(q_T-\sigma_{vo})/\sigma_{vo}'$	all	1256	0.467	-0.607	0.479	1256	0.685	0.311	0.011
		intact	1167	0.668	0.068	0.320	1167	0.664	0.419	0.883
Type 1(1)	$(q_T-\sigma_{vo})/\sigma_{vo}'$	all	611	0.701	-4.458	1.041	611	0.749	0.192	1.273
		intact	526	0.630	-0.099	0.308	526	0.560	0.448	0.745
	$\Delta u_1/(q_T-\sigma_{vo})$	all	611	0.155	18.41	-18.97	611	0.181	1.356	-1.379
		intact	526	0.015	2.670	-0.979	526	0.012	1.566	-0.185
	$\Delta u_1/\sigma_{vo}'$	all	611	0.416	-4.293	1.580	611	0.519	0.385	1.135
		intact	526	0.466	0.249	0.350	526	0.390	0.741	0.565
	$(q_T-u_1)/\sigma_{vo}'$	all	611	0.771	-2.972	1.879	611	0.647	0.789	0.992
		intact	526	0.408	0.349	0.570	526	0.298	1.123	0.457
Type 2(2)	$(q_T-\sigma_{vo})/\sigma_{vo}'$	all	884	0.645	-4.332	0.992	884	0.635	0.259	1.107
		intact	811	0.596	0.131	0.278	811	0.472	0.521	0.681
	$\Delta u_2/(q_T-\sigma_{vo})$	all	884	0.206	13.47	-17.72	884	0.377	1.026	-1.077
		intact	811	0.009	2.484	-0.742	811	0.013	1.614	-0.185
	$\Delta u_2/\sigma_{vo}'$	all	884	0.099	0.156	0.046	884	0.028	2.612	-0.170
		intact	811	0.514	0.372	0.435	811	0.364	0.875	0.586
	$(q_T-u_2)/\sigma_{vo}'$	all	884	0.830	-3.123	1.287	884	0.628	0.545	0.969
		intact	811	0.413	0.303	0.432	811	0.304	0.900	0.537
Both(3)										
	$(u_1-u_2)/u_o$	all	582	0.446	2.148	0.873	582	0.485	2.024	0.566
		intact	516	0.668	1.278	0.650	516	0.299	1.881	0.357
	$(u_1-u_2)/\sigma_{vo}'$	all	606	0.342	2.797	0.747	606	0.477	1.903	0.625
		intact	540	0.688	1.475	0.533	540	0.352	1.805	0.414

Notes: Arithmetic scale: $OCR = \alpha_1 + \beta_1 X$
Logarithmic scale: $OCR = \alpha_2 X^{\beta 2}$
n = number of data points in regression analysis
r^2 = coefficient of determination
(1) = subset database where Type 1 piezocones available
(2) = subset database where Type 2 piezocones available
(3) = subset database where both types of piezocone available

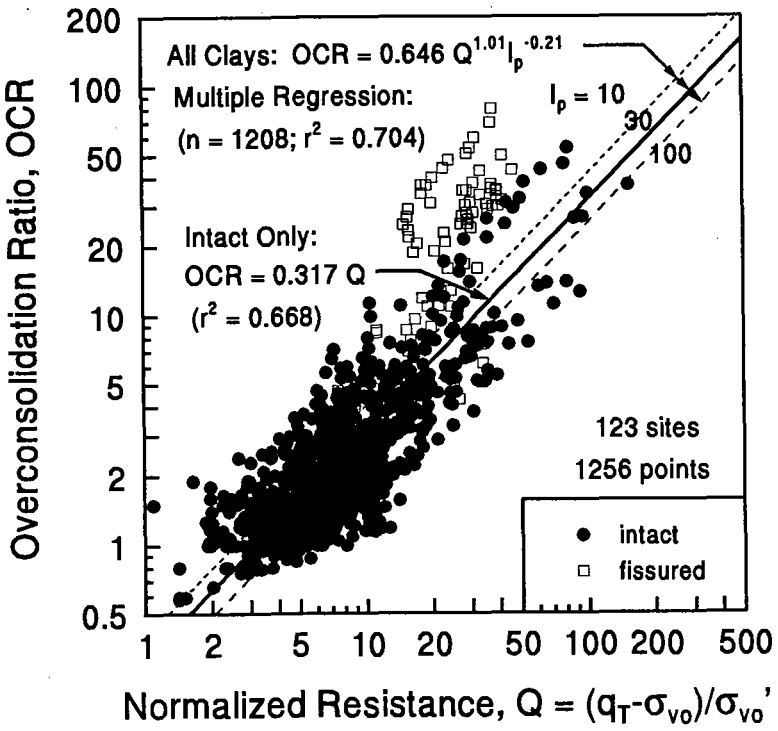

Figure 3.6. Relationship Between OCR and Normalized Cone Resistance, Q.

The parameter $B_q = \Delta u/(q_T-\sigma_{vo})$ has been proposed by many researchers for indexing OCR, including Wroth (1984) and Robertson et al. (1986). Semi-logarithmic plots are presented in Figures 3.7(a) and 3.7(b) for both types of piezocones, indicating only a marginal trend of OCR decreasing with B_q increasing. The notion that B_q is analogous to Skempton's triaxial pore pressure parameter A_f due to shear-induced pore pressures is misleading because of the very large octahedral normal stress component affecting Δu, and thus B_q. It may be concluded that the correlation between the OCR and B_q is indeed very site specific (Jamiolkowski et al. 1985; Konrad and Law 1987) and that other variables are important in the relationship (Mayne and Bachus, 1988). Values of the coefficient of determination ($0.01 < r^2 < 0.38$) in Table 3.3 indicate that direct correlations are rather poor when applied to a large number of data from clay sites worldwide.

The normalized excess pore pressure, $\Delta u/\sigma_{vo}'$, indicates different pore pressure responses for normally-consolidated and overconsolidated clays and should be useful as an

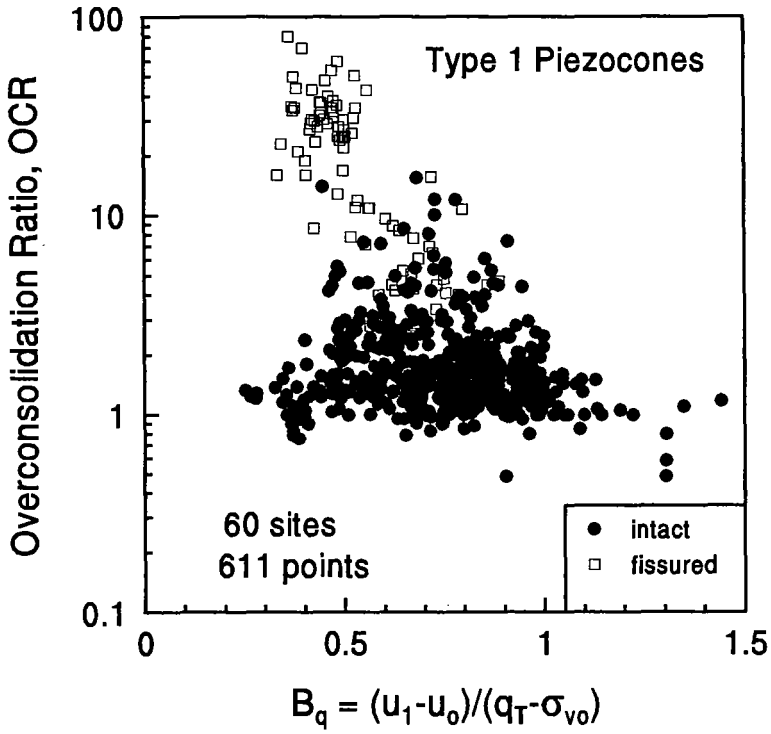

Figure 3.7a. Relationship Between OCR and Parameter B_q for Type 1 Piezocones.

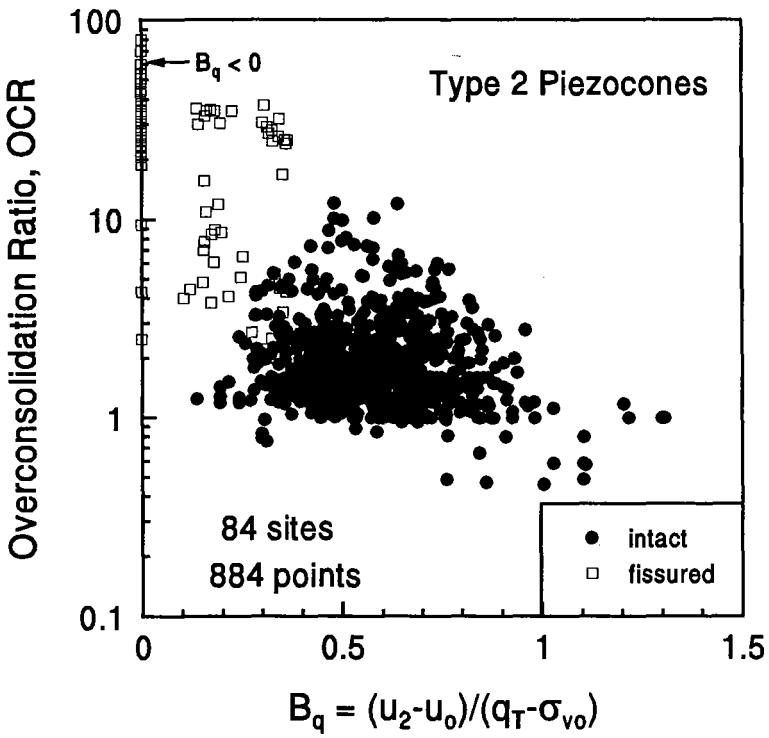

Figure 3.7b. Relationship Between OCR and Parameter B_q for Type 2 Piezocones.

indicator of stress history (Mayne 1986; Houlsby 1988; Campanella and Robertson 1988). Both the arithmetic and logarithmic plots indicate only fair statistical trends between OCR and $\Delta u/\sigma_{vo}'$ for both the Type 1 and Type 2 piezocones in intact clays. The values of coefficient of determination (r^2) range from $0.47 < r^2 < 0.51$, except for the Type 2 piezocones when fissured clays are included ($r^2 < 0.1$) since $\Delta u_2/\sigma_{vo}'$ could be near zero or even negative for fissured clay materials.

For piezocones with dual pore pressure measurements, different responses in u_1 and u_2 should be good indicators of the stress history in clays. Sully et al. (1988) proposed the pore pressure parameter PPD = $(u_1-u_2)/u_o$ when the OCR is smaller than 10. Sully and Campanella (1991) further developed the normalized parameter PPSV = $(u_1-u_2)/\sigma_{vo}'$ for empirically evaluating K_o in clays. Larsson and Mulabdic (1991) and Mayne and Chen (1994) used the parameter PPSV for evaluating the OCR profiles of specific clay deposits. When applied to a large number of data from 50 intact clay sites, the results of this study show only fair statistical relationships between the OCR and either PPD ($r^2 = 0.668$) or PPSV ($r^2 = 0.688$).

The normalized piezocone parameter, $(q_T-u_m)/\sigma_{vo}'$, has been suggested by many researchers based upon theoretical derivations (Battaglio, et al. 1986; Konrad and Law 1987; Sandven et al. 1988; Houlsby 1988; Robertson et al, 1988; Mayne 1989, 1991; and Larsson and Mulabdić 1991). A direct trend of OCR increasing with $(q_T-u_m)/\sigma_{vo}'$ is observed and verified. However, according to several independent theories, the relationship also should be a function of other soil parameters such as frictional characteristics (ϕ'), plastic volumetric strain ratio ($\Lambda = 1-\kappa/\lambda$), and other factors. The significance of these soil parameters will be discussed later in the derivation of some analytical models for piezocone evaluation of stress history in clays. Unlike what has been observed for the parameters Q, B_q, and $\Delta u/\sigma_{vo}'$, the statistical significance of the direct correlations between the OCR and $(q_T-u_m)/\sigma_{vo}'$ for the combined total of all intact and fissured clays ($0.77 < r^2 < 0.83$), are stronger than those for intact clays alone ($r^2 = 0.41$).

3.2.2. Preconsolidation Stress Relationships

A direct correlation between the cone tip resistance (q_c) and the preconsolidation

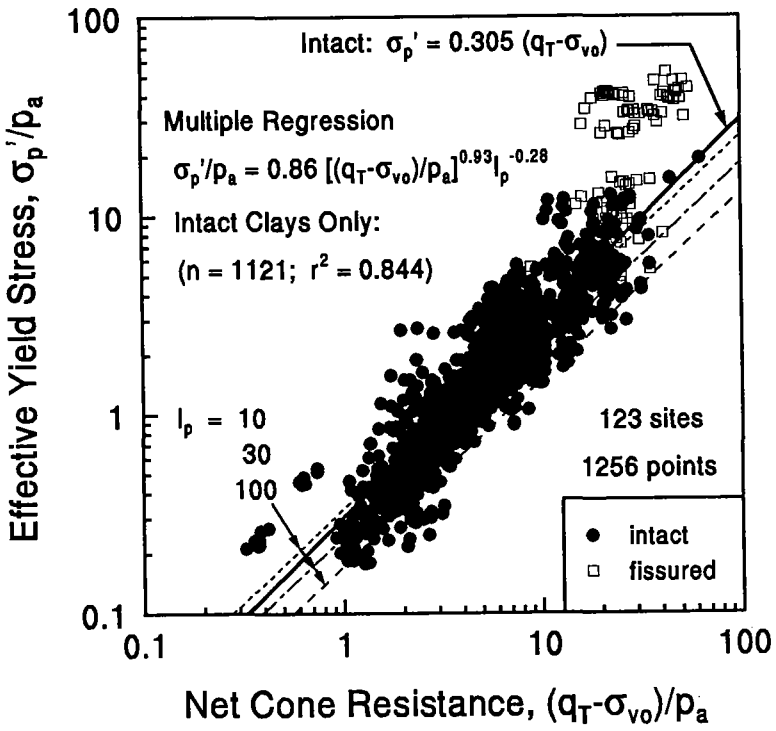

Figure 3.8. Relationship Between Yield Stress and Net Cone Resistance.

pressure (σ_p') was proposed by Tavenas and Leroueil (1979) and later verified by Mayne (1986). Later, σ_p' was better related to net corrected cone tip resistance ($q_T-\sigma_{vo}$). It was noted that σ_p' increased with excess pore water pressure (Δu). In this study, direct correlations between σ_p' and various piezocone parameters were examined using a large database. A summary of the results of simple linear regression analyses is presented in Table 3.4. In the cases involving arithmetic scales, the adopted form of the regression is: $\sigma_p' = \alpha_1 + \beta_1 X$, where X = independent profiling variable. All stresses have been made dimensionless using a reference stress p_a = 1 atm ~ 100 kPa ~ 1 kg/cm^2 ~ 1 tsf, so that no units are introduced. In the cases involving logarithmic scales, the adopted form of the regression is: $\sigma_p' = \alpha_2 X^{\beta 2}$; again, with dimensionless parameters utilized.

The parameters ($q_T-\sigma_{vo}$), Δu, and (q_T-u) show strong statistical trends. Figure 3.8 illustrates the relationship between the preconsolidation stress (σ_p'/p_a) and net cone tip

Table 3.4. Summary of Simple Regression Analyses Between Yield Stress (σ_p'/p_a) and Various Piezocone Parameters for Clays.

Cone Type	Parameter (X)	Soil Group	Arithmetic Scale n	r^2	α_1	β_1	Logarithmic Scale n	r^2	α_2	β_2
All Data	$(q_T-\sigma_{vo})/p_a$	all	1256	0.588	-1.764	0.659	1256	0.821	0.265	1.104
		intact	1167	0.693	0.181	0.289	1167	0.800	0.308	0.978
Type 1(1)	$(q_T-\sigma_{vo})/p_a$	all	611	0.717	-2.591	0.860	611	0.882	0.196	1.295
		intact	526	0.766	0.021	0.308	526	0.841	0.252	1.083
	$\Delta u_1/p_a$	all	611	0.457	-2.184	1.269	611	0.749	0.339	1.249
		intact	526	0.675	0.224	0.368	526	0.729	0.419	0.954
	$(q_T-u_1)/p_a$	all	611	0.780	-1.818	1.600	611	0.800	0.744	1.059
		intact	526	0.542	0.456	0.522	526	0.671	0.785	0.813
Type 2(2)	$(q_T-\sigma_{vo})/p_a$	all	884	0.694	-2.598	0.830	884	0.829	0.227	1.200
		intact	811	0.743	-0.034	0.320	811	0.790	0.286	1.104
	$\Delta u_2/p_a$	all	884	0.084	1.274	0.761	NA	NA	NA	NA
		intact	811	0.722	0.004	0.563	811	0.729	0.551	0.952
	$(q_T-u_2)/p_a$	all	884	0.797	-1.864	1.069	884	0.804	0.490	1.053
		intact	811	0.564	0.358	0.419	811	0.696	0.553	0.895
Both(3)	$(q_T-\sigma_{vo})/p_a$	all	606	0.750	-2.149	0.914	606	0.805	0.235	1.233
		intact	540	0.551	-0.114	0.389	540	0.697	0.281	1.038
	$(u_1-u_2)/p_a$	all	606	0.644	-0.808	2.618	606	0.648	1.545	0.866
		intact	540	0.368	0.564	1.015	540	0.458	1.302	0.649

Notes: Arithmetic scale: $\sigma_p'/p_a = \alpha_1 + \beta_1 X$, where p_a = atmospheric pressure ≈ 100 kPa

Logarithmic scale: $\sigma_p'/p_a = \alpha_2 X^{\beta 2}$

n = number of data points in regression analysis
r^2 = coefficient of determination
NA = Not applicable
(1) = subset database where Type 1 piezocones available
(2) = subset database where Type 2 piezocones available
(3) = subset database where both types of piezocone available

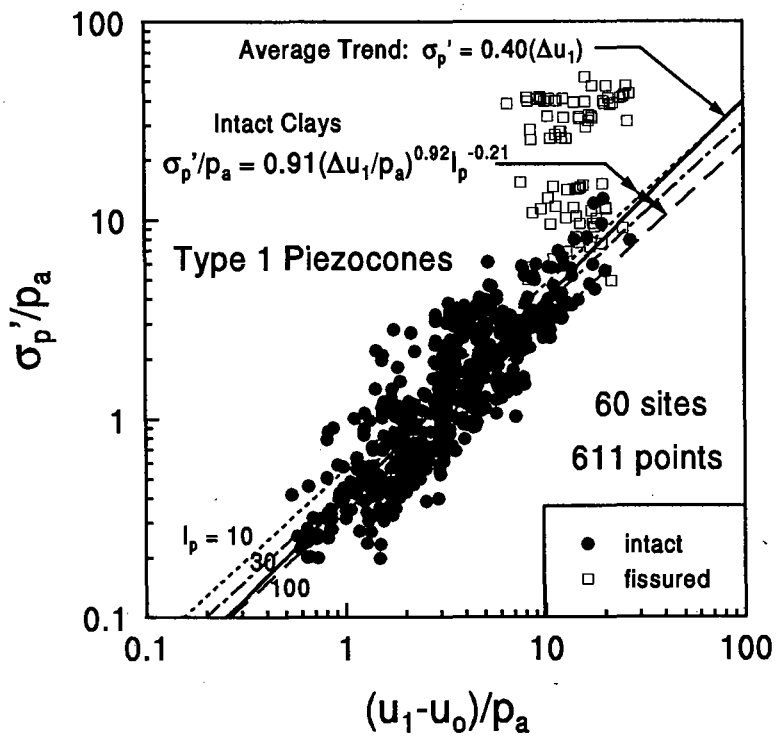

Figure 3.9.a. Relationship Between Yield Stress and Type 1 Excess Pore Pressures.

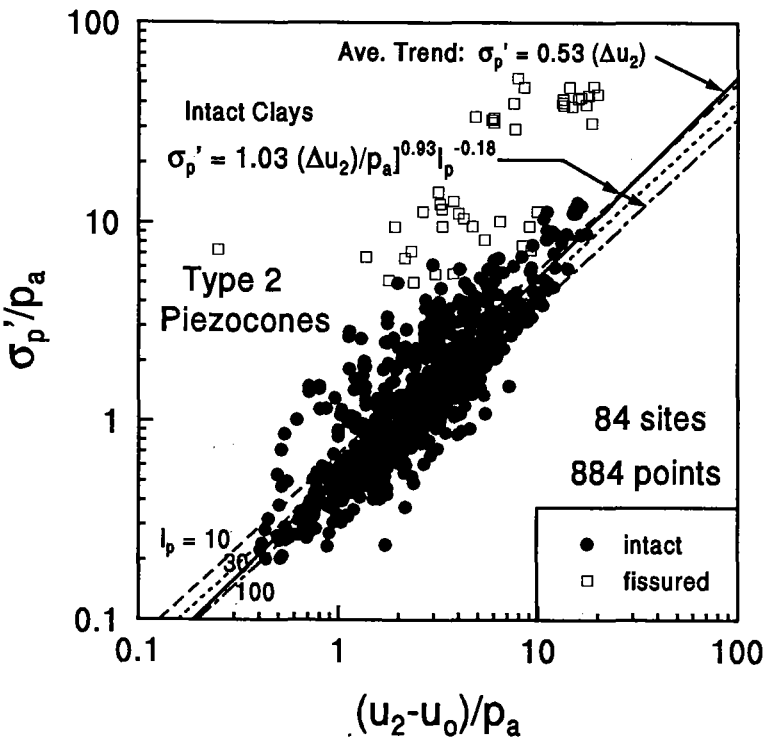

Figure 3.9.b. Relationship Between Yield Stress and Type 2 Excess Pore Pressures.

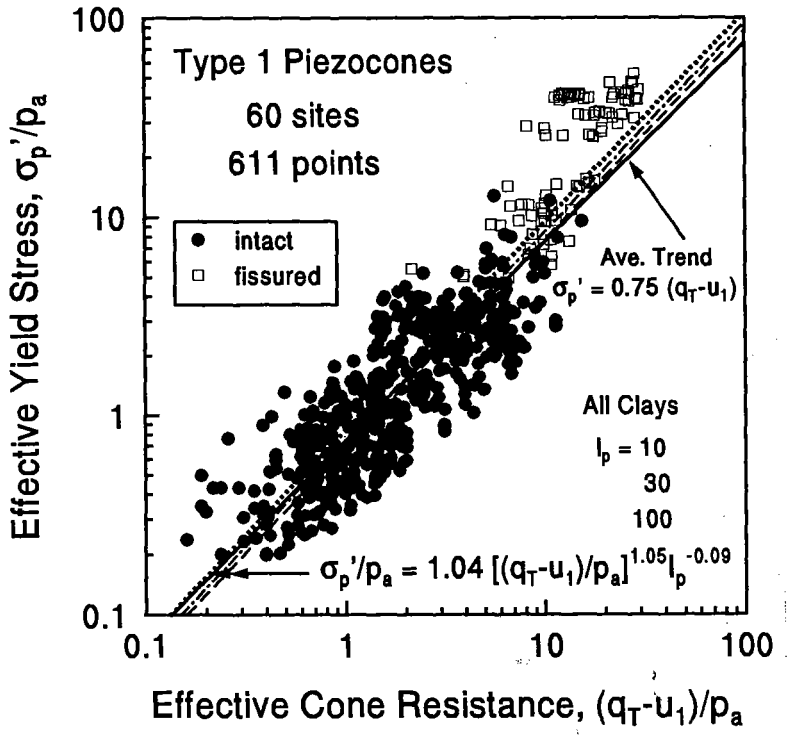

Figure 3.10.a. Relationship Between Yield Stress and Type 1 Effective Cone Resistance.

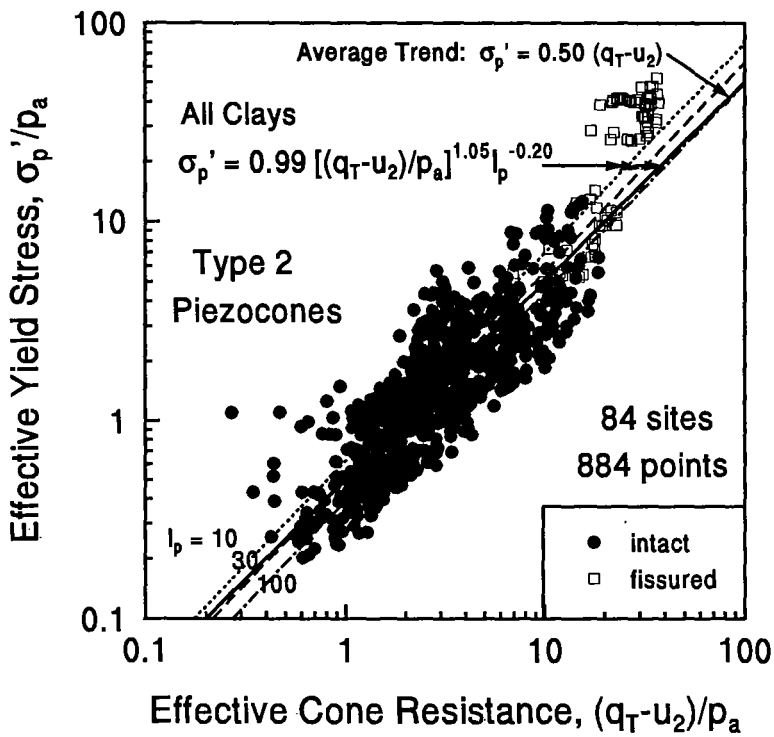

Figure 3.10.b. Relationship Between Yield Stress and Type 2 Effective Cone Resistance.

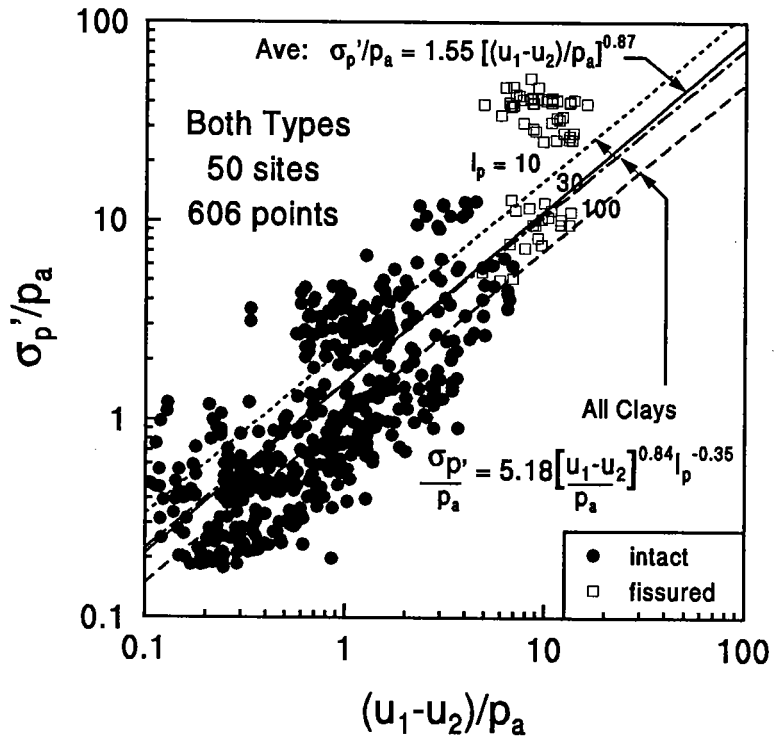

Figure 3.11. Relationship Between Yield Stress and Penetration Pore Pressure Difference.

resistance $(q_T-\sigma_{vo})/p_a$. Similar trends were reported by Tavenas and Leroueil (1987), Mayne and Holtz (1988), and Larsson and Mulabdic (1991). Correlations between the preconsolidation pressure σ_p'/p_a and excess pore pressures $\Delta u/p_a$ for both Type 1 and Type 2 piezocone are shown in Figure 3.9(a) and 3.9(b), respectively. It is clear that the $\Delta u/p_a$ relationships are more statistically significant for intact clays only. In contrast, the relationships between σ_p' and (q_T-u) have higher values of r^2 when both intact and fissured clays included together. Figures 3.10(a) and 3.10(b) illustrate the direct relationships between yield stress and effective cone resistance $(q_T-u)/p_a$. For piezocones with dual pore pressure measurements or where both types of pore pressure measurements are available from paired soundings, Figure 3.11 shows the statistical relationship between yield stress and $(u_1-u_2)/p_a$ for all clays including intact and fissured.

A review of Table 3.4 indicates that the coefficient of determination (r^2) for each of the correlations for σ_p' are generally higher than that of the corresponding OCR relationship

given for normalized parameters in Table 3.3. This is likely because of errors incurred in estimating the magnitude of σ_{vo}' from the total overburden (σ_{vo}) or the unit weight and the hydrostatic pore pressure (u_o), and/or depth to the groundwater table.

3.2.3. Summary of Simple Regression Analyses

A number of the most frequently used piezocone parameters were examined using the compiled database. Among these parameters, $(q_T-u_m)/\sigma_{vo}'$ generally provides a rather reliable direct correlation with the OCR for all clays (intact and fissured) while σ_p' correlates well with Δu for intact clays only. The parameter $(q_T-\sigma_{vo})$ also shows strong statistical trends for intact clays when correlated with σ_p'. For those, the exponential components are close to 1.0 in the logarithmic scale and the best-fit line fit is obtained by forcing the intercept to zero in the arithmetic scale.

Thus, for practical use, a number of simple statistical relationships can be adopted. Based on the aforementioned, the following empirical relationships are suggested for providing a first-order estimate of OCR in either intact and/or fissured clays:

$$\text{Type 1 : } \quad OCR = 0.78 \left(\frac{q_T-u_1}{\sigma_{vo}'} \right) \quad n=611 \quad r^2=0.719 \qquad [3.1a]$$

$$\text{Type 2 : } \quad OCR = 0.53 \left(\frac{q_T-u_2}{\sigma_{vo}'} \right) \quad n=884 \quad r^2=0.746 \qquad [3.1b]$$

For empirically evaluating the magnitude of σ_p' in intact clays only, the following expressions are presented:

$$\text{Type 1 : } \sigma_p' = 0.40\ (u_1-u_o) \quad n=526 \quad r^2=0.667 \qquad [3.2a]$$

$$\text{Type 2 : } \sigma_p' = 0.53\ (u_2-u_o) \quad n=811 \quad r^2=0.722 \qquad [3.2b]$$

$$\text{All : } \sigma_p' = 0.31\ (q_T-\sigma_{vo}) \quad n=1355 \quad r^2=0.745 \qquad [3.2c]$$

3.3. Multiple Regression Studies of Piezocone Data

3.3.1. OCR Relationships

One of the most common index properties used to characterize clay materials is the plasticity index (PI or I_p). For almost all clays, a determination of I_p offers the geotechnical engineer a quick glimpse of the potential problems associated with lean or fat clays. Consequently, multiple linear regression analyses have been performed to express OCR (and σ_p') in terms of the aforementioned piezocone parameters and the plasticity index. Table 3.5 shows the results of analyses between OCR, plasticity index, and the normalized parameters $(q_T-\sigma_{vo})/\sigma_{vo}'$, B_q, $\Delta u/\sigma_{vo}'$, $(q_T-u_m)/\sigma_{vo}'$, $(u_1-u_2)/u_o$, and $(u_1-u_2)/\sigma_{vo}'$. In all cases, the adopted form of the regression is: $OCR = \alpha\ X^{\beta 1}\ I_p^{\beta 2}$, where X = independent profiling variable.

3.3.2. Yield Stress Relationships

Results of the analyses between σ_p', plasticity index, and the parameters $(q_T-\sigma_{vo})$, Δu, (q_T-u_m), and (u_1-u_2) are summarized in Table 3.6. In all cases, the adopted form of the regression is: $\sigma_p'/p_a = \alpha\ X^{\beta 1}\ I_p^{\beta 2}$, where X = independent profiling variable. Again, the coefficient of determination (r^2) of the correlation between each parameter and σ_p' is generally higher than that of the corresponding OCR relationship. In comparison with the

Table 3.5. Summary of Multiple Regression Analyses Between OCR and Various Normalized Piezocone Parameters.

Cone Type	Parameter (X)	Soil Group	n	r^2	α	β_1	β_2
All Data	$(q_T-\sigma_{vo})/\sigma_{vo}'$	all	1208	0.704	0.646	1.008	-0.214
		intact	1121	0.733	1.135	0.804	-0.284
Type 1(1)	$(q_T-\sigma_{vo})/\sigma_{vo}'$	all	562	0.733	0.193	1.258	0.005
		intact	484	0.611	1.233	0.663	-0.249
	$\Delta u_1/(q_T-\sigma_{vo})$	all	562	0.181	3.955	-1.280	-0.298
		intact	484	0.201	7.529	-0.155	-0.444
	$\Delta u_1/\sigma_{vo}'$	all	562	0.497	0.480	1.079	-0.038
		intact	484	0.467	2.540	0.477	-0.314
	$(q_T-u_1)/\sigma_{vo}'$	all	562	0.640	1.172	0.982	-0.113
		intact	484	0.418	3.899	0.404	-0.343
Type 2(2)	$(q_T-\sigma_{vo})/\sigma_{vo}'$	all	820	0.649	0.366	1.117	-0.108
		intact	747	0.555	1.179	0.654	-0.226
	$\Delta u_2/(q_T-\sigma_{vo})$	all	820	NA	NA	NA	NA
		intact	747	0.145	4.568	-0.238	-0.313
	$\Delta u_2/\sigma_{vo}'$	all	820	NA	NA	NA	NA
		intact	747	0.457	1.864	0.578	-0.220
	$(q_T-u_2)/\sigma_{vo}'$	all	820	0.657	1.092	0.983	-0.210
		intact	747	0.417	2.373	0.525	-0.280
Both(3)	$(q_T-\sigma_{vo})/\sigma_{vo}'$	all	583	0.669	0.919	1.102	-0.356
		intact	519	0.664	1.787	0.799	-0.413
	$(u_1-u_2)/u_o$	all	559	0.491	2.525	0.571	-0.062
		intact	495	0.329	3.768	0.331	-0.201
	$(u_1-u_2)/\sigma_{vo}'$	all	583	0.646	0.435	0.818	0.233
		intact	519	0.538	0.588	0.627	0.144

Notes: $OCR = \alpha X^{\beta 1} I_p^{\beta 2}$

n = number of data points in regression analysis

r^2 = coefficient of determination

NA = Not applicable

(1) = subset database where Type 1 piezocones available

(2) = subset database where Type 2 piezocones available

(3) = subset database where both types of piezocone available

Table 3.6. Summary of Multiple Regression Analyses Between Yield Stress and Various Piezocone Parameters.

Cone Type	Parameter (X)	Soil Group	n	r^2	α	β_1	β_2
All Data	$(q_T-\sigma_{vo})/p_a$	all	1208	0.832	1.529	0.088	-0.196
		intact	1121	0.844	1.862	0.937	-0.285
Type 1(1)	$(q_T-\sigma_{vo})/p_a$	all	562	0.883	0.154	1.303	0.069
		intact	484	0.844	0.397	1.065	-0.118
	$\Delta u_1/p_a$	all	562	0.752	0.289	1.256	0.050
		intact	484	0.727	0.913	0.919	-0.205
	$(q_T-u_1)/p_a$	all	562	0.804	1.036	1.052	-0.091
		intact	484	0.705	2.205	0.773	-0.288
Type 2(2)	$(q_T-\sigma_{vo})/p_a$	all	820	0.836	0.286	1.201	-0.062
		intact	747	0.812	0.585	0.978	-0.191
	$\Delta u_2/p_a$	all	820	NA	NA	NA	NA
		intact	747	0.763	1.051	0.932	-0.181
	$(q_T-u_2)/p_a$	all	820	0.823	0.991	1.052	-0.201
		intact	747	0.741	1.554	0.863	-0.291
Both(3)	$(q_T-\sigma_{vo})/p_a$	all	583	0.844	0.656	1.219	-0.289
		intact	519	0.807	1.429	0.949	-0.444
	$(u_1-u_2)/p_a$	all	583	0.684	5.179	0.843	-0.352
		intact	519	0.582	7.634	0.548	-0.533

Notes: $\sigma_p'/p_a = \alpha\, X^{\beta 1}\, I_p^{\beta 2}$, where p_a = atmospheric pressure $\approx$ 100 kPa

n = number of data points in regression analysis
r^2 = coefficient of determination
NA = Not Applicable
(1) = subset database where Type 1 piezocones available
(2) = subset database where Type 2 piezocones available
(3) = subset database where both types of piezocone available

results from simple linear regression analyses in Tables 3.3 and 3.4, the inclusion of plasticity index statistically improves the relationships. The effects of varying I_p in the correlations between σ_p' and the piezocone parameters considered are shown in Figures 3.8 to 3.11. It appears that the parameters $(q_T-\sigma_{vo})$, Δu, and (q_T-u) show stronger statistical significances than other parameters considered. Showing as examples, the alternate versions of Eq. [3.2] are:

$$\text{Type 1 :} \quad \frac{\sigma_p'}{p_a} = 0.91 \left(\frac{u_1-u_o}{p_a}\right)^{0.92} I_p^{-0.21} \quad , \; n=484 \quad r^2=0.727 \qquad [3.3a]$$

$$\text{Type 2 :} \quad \frac{\sigma_p'}{p_a} = 1.03 \left(\frac{u_2-u_o}{p_a}\right)^{0.93} I_p^{-0.18} \quad , \; n=747 \quad r^2=0.763 \qquad [3.3b]$$

$$\text{All :} \quad \frac{\sigma_p'}{p_a} = 0.16 \left(\frac{q_T-\sigma_{vo}}{p_a}\right)^{0.72} I_p^{-0.24} \quad , \; n=1310 \quad r^2=0.717 \qquad [3.3c]$$

It is interesting to note relationships between σ_p' and vane strength (s_{uv}) also depend upon plasticity index (Chandler, 1988). In this regard, the cone does not appear as significantly influenced by index properties since the relationships in Eqn [3.3] are proportional to $(I_p)^{-0.2}$, whereas for the vane, the trend between σ_p' and s_{uv} is proportional to $(I_p)^{-0.5}$, as noted by Mayne and Mitchell (1988). Perhaps this reflects differences in the amount of strength anisotropy affecting the two tests. Note that undrained strengths measured in the triaxial compression mode are little affected by plasticity index, while extension strengths are related somewhat to I_p (Larsson, 1980; Jamiolkowski, et al. 1985). Therefore, the vane may more reflect extension-type loading, while the cone may be more influenced by compression-type loading.

3.4. Summary and Conclusions

A large database containing over 600 piezocone soundings from 205 clay sites around the world has been compiled for evaluating various piezocone parameters in interpreting the stress history of clays. Cross-correlations among piezocone measurements q_T, u_1, and u_2 show trends similar to results from previous studies. Correlations between the stress history (measured in terms of preconsolidation pressure, σ_p', and the overconsolidation ratio, OCR $= \sigma_p'/\sigma_{vo}'$), and several of the most frequently used piezocone parameters were examined and their statistical significances were discussed.

Direct correlations for σ_p' in terms of stress difference (q_T-σ_{vo}, Δu_m, and q_T-u_m) generally indicated slightly better statistical trends than those obtained with normalized piezocone parameters and OCR. This likely occurs because of errors incurred in evaluating σ_{vo}' from the unit weights of soils and hydrostatic pore pressures or level of the groundwater table. Although it may be desirable to incorporate other soil properties such as rigidity index ($I_r = G/s_u$), frictional characteristics (ϕ') and plastic volumetric strain ratio (Λ) into the correlations, the parameters (q_T-σ_{vo}), Δu, and (q_T-u_m) provide reasonable direct correlations with σ_p', considering the diversity and variety of data. Results of multiple regression analyses indicated slight improvements in the statistical correlations when plasticity index was also incorporated.

CHAPTER 4

EXPERIMENTAL FIELD TESTING PROGRAM IN OVERCONSOLIDATED CLAYS

Special series of piezocone soundings were conducted at two clay test sites for obtaining cone resistances and penetration pore water pressure measurements for both u_1 and u_2 filter elements. One test site was located in Port Huron, Michigan, and consisted of up to 30 meters of soft to firm, lean glacial lake silty clays that were lightly overconsolidated. Separate paired sets of Type 1 and 2 piezocones were conducted by Georgia Tech (GT) personnel using a conventional drill rig and complementary laboratory test data were provided by a commercial laboratory.

The second test site was located in Baton Rouge, Louisiana, and was comprised of more than 40 meters of very stiff desiccated, plastic deltaic clays that were moderately overconsolidated. Here, piezocone testing was accomplished using special dual- and triple-element porous element penetrometers and cone truck operated by the Louisiana Transportation Research Center (LTRC) under contract to Georgia Tech. At Baton Rouge, multiple measurements of cone tip resistance and pore water pressures at three different positions along the cone (u_1, u_2, and u_3) were obtained. Thin-walled tube samples were obtained in adjacent borings and transported to GT for reference laboratory testing.

4.1 PORT HURON SITE, MICHIGAN

The geology of the Port Huron area mainly consists of glacial and lacustrine sediment formed during the late Pleistocene. The uppermost soils consist of silty sands and sandy silts to shallow depths of 1 to 3 meters. These are underlain by deep deposits of soft grey silty clays to clayey silts of low to moderate plasticity that extend to depths of up to 30 meters. The clay is underlain by a thin layer of clayey sand and weathered shale bedrock. The groundwater level at the time of our testing program was located 1.5 to 2 meters below the ground surface.

The test site reported herein was actually a portion of the expansion project of the Blue Water Bridge Plaza, which serves as a customs facility on the border between the U.S. and Canada. Prior to construction of the toll plaza at the site, a program of borings and samples were made to delineate the general geotechnical properties of the clay unit (Schleede 1985). Field testing included standard penetration tests (SPT), split-barrel samples, and thin-walled tube samples obtained for laboratory testing. The lab program included index tests, one-dimensional consolidation, and unconfined compression tests.

In November 1992, a series of seven piezocone soundings and six dilatometer tests were performed at the project site in Port Huron, Michigan. Two separate areas were tested: (1) a region located beneath the intersection of the bridge plaza and Pine Grove Avenue, and (2) an area near the intersection of the bridge plaza and the west ramp, as shown on the site plan presented as Figure 4.1. Each test area included 3 to 4 piezocones and 3 dilatometer soundings. Prior to this field testing program, the site had been subjected to a soil improvement program by the stone column method. This included the area under the bridge abutments which were also constructed with reinforced earth walls. Both testing

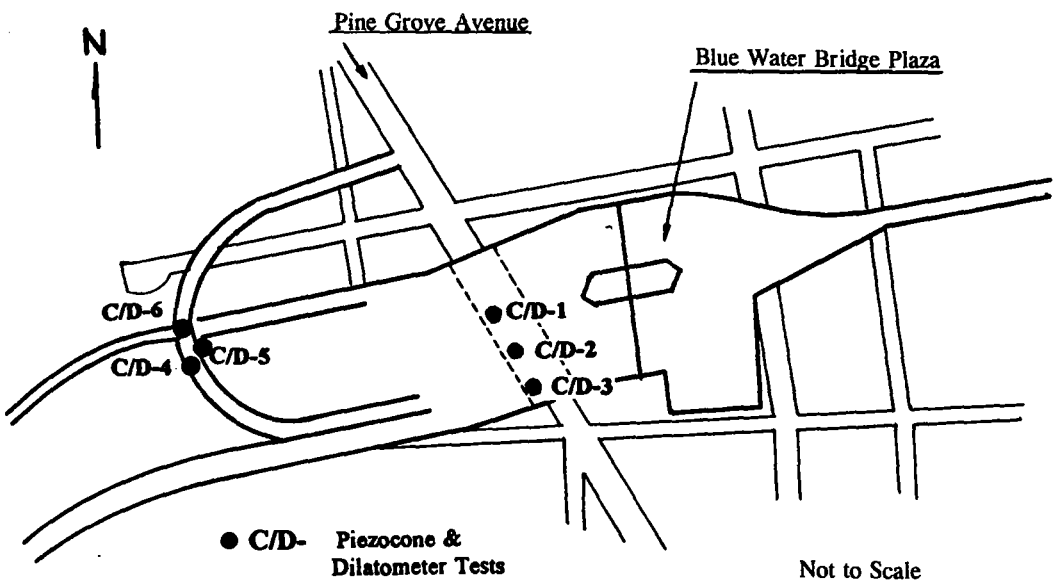

Figure 4.1. Site Plan and Field Test Locations at Port Huron, Michigan.

Figure 4.2. Piezocone Testing Operations at Port Huron, Michigan.

locations are fairly close to the walls (within 2 to 5 meters), and thus influenced by the additional vertical stresses imposed by the 5-m high walls.

4.1.1. Piezocone Penetration Tests

The GT piezocone system was utilized at the Port Huron with a CME-75 drill rig to advance the penetrometers. The electronic signals were transmitted via a 10-line cable up the EW rods to the data acquisition system inside a cargo van (Figure 4.2). The GT equipment and operational procedures are described in detail in Appendix A. A total of seven piezocone tests were performed at the site, including two Type 1 PCPTs (Test Nos. C-4A and C-5), where penetration pore water pressures were measured midface (u_1), and five Type 2 PCPTs (Nos. C-1, 2, 3, 4, and 6), where pore pressures were measured at the shoulder position (u_2).

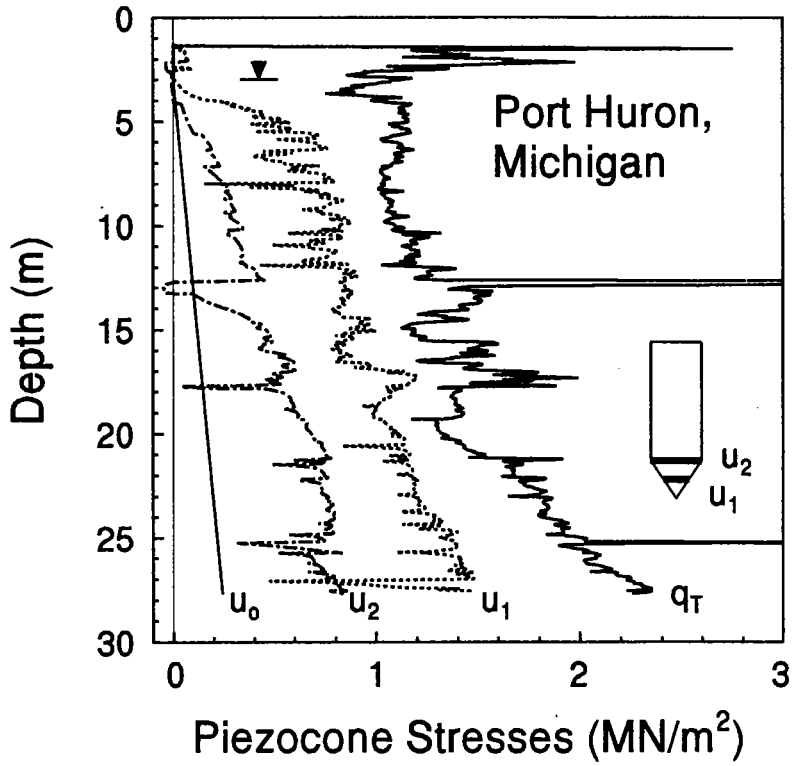

Figure 4.3. Results from a Paired Set of Piezocone Soundings at Port Huron Site.

A composite piezocone profile from paired Type 1 and 2 soundings (Nos. C-4 and C-4A) is presented in Figure 4.3. Both soundings showed similar profiles of measured cone tip resistance (q_c). In Figure 4.3, only the corrected cone tip resistance (q_T) from the Type 2 sounding is presented for clarity. In all cases, $q_T > u_1 > u_2$. Beneath a layer of fill, the composite sounding indicates a thick lacustrine deposit of clay that can be separated into three major substrata: (1) stiff homogeneous clay from 3 to 13 meters; (2) variable clayey silt from 13 to 19 meters; and (3) firm uniform silty clay from 19 to 28 meters. The record in Figure 4.3 illustrates the excellent stratigraphic detailing capabilities of the piezocones, particularly the matched spikes in the profiles of q_T, u_1, and u_2 that show the existence of thin interbedded sand layers at depths of approximately 12, 17, and 25 meters. Below a depth of 20 m, the ratio of u_2/u_1 is fairly constant at 0.6, which is quite typical for normally-consolidated to lightly overconsolidated clays. Soil classification using the chart by Robertson (1990) indicated sensitive fine-grained clayey silts and silty clay materials.

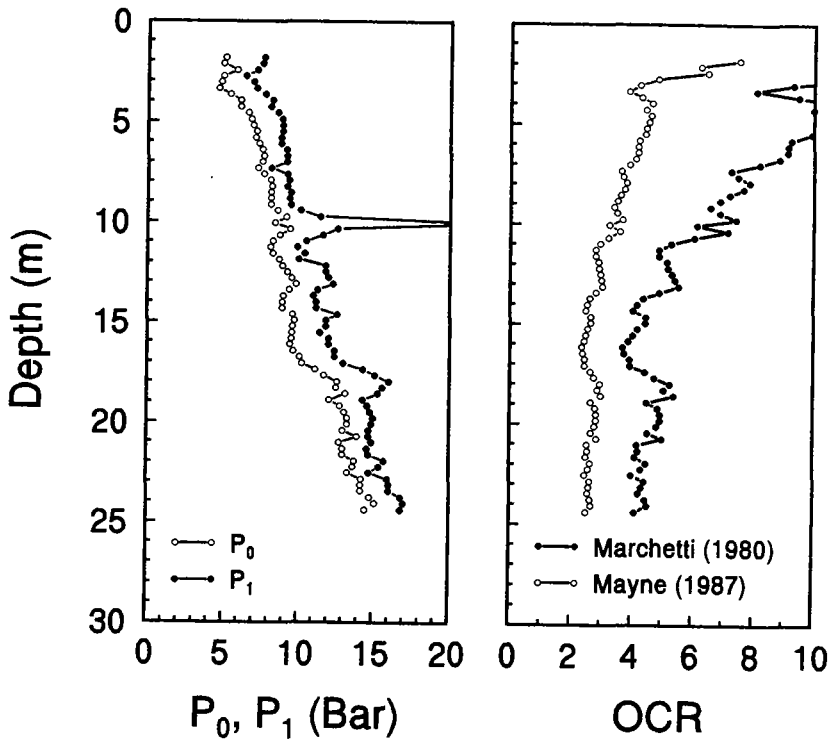

Figure 4.4. Results from a Dilatometer Sounding at Port Huron Site.

4.1.2. Dilatometer Tests

In addition to the piezocone tests, six dilatometer tests (DMT) were conducted to depths of up to 30 meters at intervals of 0.30 meters. A typical result and the interpreted profiles of overconsolidation ratio are shown in Figure 4.4. The OCR profile predicted using the method proposed by Mayne (1987) indicated the clays were lightly overconsolidated, while the Marchetti (1980) method showed the materials were more overconsolidated.

4.1.3. Laboratory Test Data

Laboratory tests were performed on thin-walled tube samples retrieved from borings advanced for the Blue Water Bridge Plaza project. These borings were drilled by Robert Stevens & Associates of Stafford, Virginia, under contract to John S. Jones & Associates of Purcellville, Virginia. Samples were transported for testing to the commercial laboratory

of Law Engineering, Chantilly, Virginia. These tests included index, consolidation, and CIUC triaxial shear on representative specimens.

The clays classify as lean (CL), according the Unified Soil Classification System. The natural water content of the clays ranges from 15% to 30% and the liquid limits vary from 25 to 40. The range of plasticity index extends from 10 to 20. A summary plot of the index properties using data from Schleede (1985) and the recent investigation is presented in Figure 4.5.

One-dimensional consolidation tests (ASTM D-2435) were performed by a commercial laboratory using a Hogentogler-type dead-weight oedometer apparatus. Results of 19 oedometer tests are summarized and reported in Table 4.1. The in-place void ratios of the clay substrata range from 0.45 to 1.04, with an average value of $e_o = 0.65 \pm 0.20$. Values of the virgin compression index (C_c) from the normally-consolidated region of the compression curve indicate values between 0.09 to 0.35, with an average value of $C_c = 0.17 \pm 0.08$. The value of the swelling index averaged $C_s = 0.04 \pm 0.02$ for these clays. The value of the effective preconsolidation stress (σ_p') was also evaluated from each of the consolidation curves using the Casagrande method of construction. These are reported in

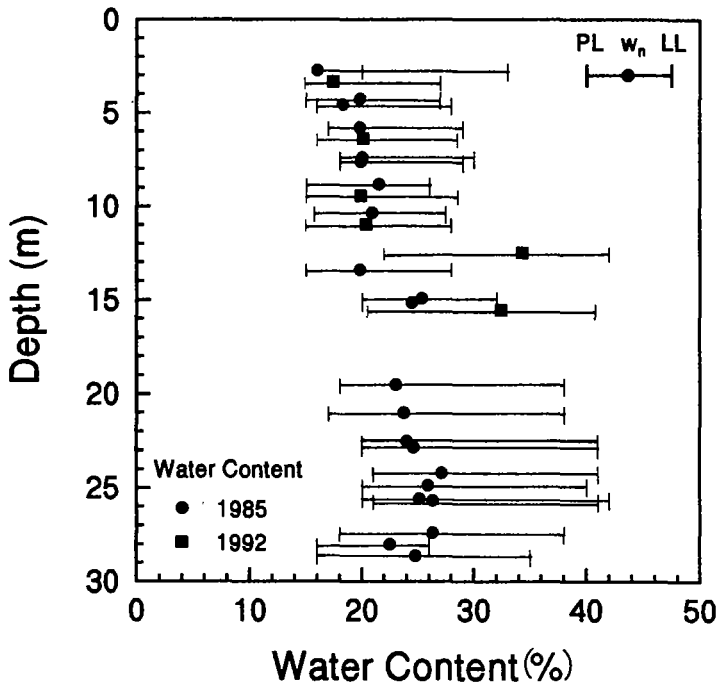

Figure 4.5. Summary Profile of Index Properties at Port Huron Site.

Table 4.1 and indicate corresponding overconsolidation ratios (OCR = σ_p'/σ_{vo}') that range from about 4 at shallow depths to around 1.2 at deeper depths. In a few instances, underconsolidated values (OCRs < 1) were obtained. It is believed, however, that these reflect difficulties associated with sample disturbance effects or destructuring of the clay, and consequently, have not been included in the final analysis.

Table 4.1. Summary of Consolidation Test Results (1992) for Port Huron Site.

Borehole Number	Depth (m)	e_o --	w_n (%)	σ_{vo}' (kPa)	σ_p' (kPa)	OCR	C_c	C_s
102	3.4	0.51	18.3	67	78	1.17	0.09	0.03
	9.4	0.55	20.0	133	232	1.75	0.13	0.03
	15.5	0.71	26.3	191	122	0.64	0.13	0.04
105	3.4	0.51	17.8	67	86	1.28	0.09	0.02
	9.4	0.50	18.1	133	103	0.77	0.10	0.02
	15.5	0.72	26.1	191	137	0.72	0.17	0.02
202	3.4	0.52	19.0	67	152	2.27	0.12	0.04
	6.4	0.59	21.0	100	235	2.35	0.15	0.03
	9.4	0.58	20.3	133	210	1.58	0.19	0.03
	12.5	1.04	38.6	166	220	1.33	0.33	0.04
	15.5	0.66	24.2	191	191	1.00	0.15	0.04
204	3.4	0.47	17.2	67	254	3.80	0.11	0.02
	6.4	0.64	19.2	100	440	4.40	0.16	0.03
	11.0	0.56	20.4	149	284	1.90	0.15	0.03
	12.5	0.95	34.3	166	196	1.18	0.29	0.07
	15.5	1.02	36.7	191	254	1.33	0.35	0.06
206	3.4	0.45	15.8	67	269	4.02	0.10	0.04
	9.4	0.58	21.0	133	269	2.02	0.15	0.03
	15.5	0.75	27.0	191	279	1.46	0.19	0.04

Note: σ_p' determined by Casagrande's method.

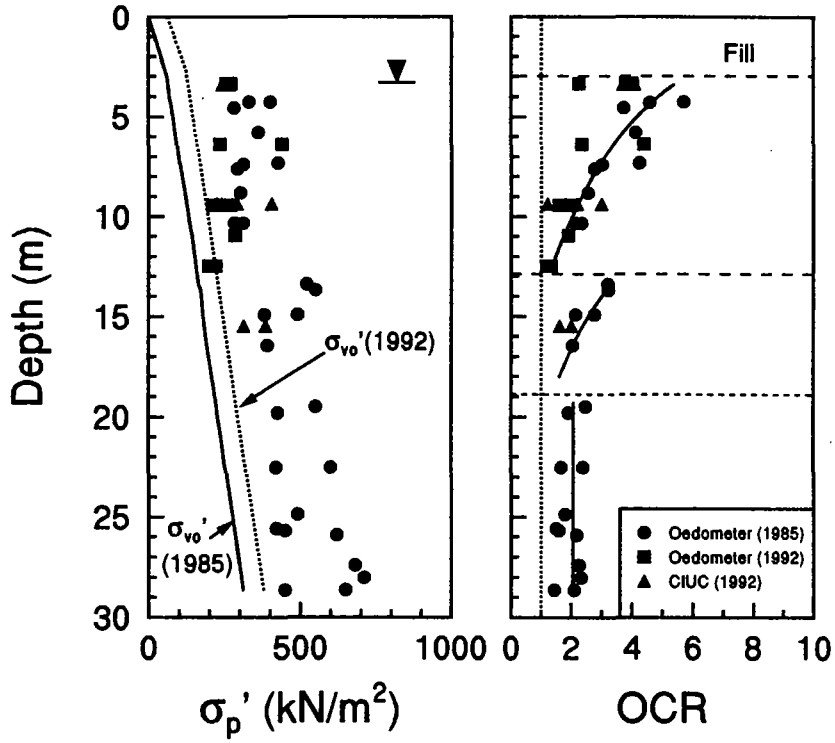

Figure 4.6. Profiles of Yield Stress and OCR with Depth at Port Huron Site.

Summary profiles of the preconsolidation stress and overconsolidation ratio with depth are presented in Figure 4.6. The effective overburden profile increased during the period from 1985 to 1992 due to the placement of fill and a reinforced earth wall at the site. It can be seen that the stress history profile the Port Huron site is quite complex and may be divided into several sublayers. The layered profile matches the interpreted profile from piezocone test results, which includes: (1) stiff homogeneous clay from 3 to 13 meters (1 < OCR < 6); (2) variable clayey silt from 13 to 19 meters (1.5 < OCR < 3.5); and (3) firm uniform silty clay from 19 to 28 meters (OCR $\approx$ 2).

Series of isotropically-consolidated undrained triaxial compression (CIUC) tests were also performed on specimens of the clays from Port Huron by the commercial lab. These tests were useful in providing assessments of the undrained shear strength (s_u) and effective stress friction angle (ϕ') of the materials. Table 4.2 presents a summary of the individual CIUC tests and measured properties.

Table 4.2. Summary of CIUC Triaxial Test Results for Port Huron Site.

Borehole Number	Depth (m)	σ_{vo}' (kPa)	σ_c' (kPa)	ϕ' (deg.)	s_u (kPa)	ϵ_f (%)	s_u/σ_c' ---
102	3.4	67	165	27.4	109	22.0	0.66
	9.4	133	147	27.7	84	19.6	0.57
	9.4	133	294	27.0	129	15.2	0.44
105	3.4	67	29	34.4	49	16.8	1.69
	3.4	67	176	33.0	120	16.6	0.68
	15.5	191	171	28.4	93	14.5	0.54
	15.5	191	318	25.4	127	12.7	0.40
202	3.4	67	28	34.1	53	21.9	1.89
	3.4	67	165	34.8	138	16.6	0.84
	9.4	133	147	26.8	73	21.2	0.50
206	3.4	67	29	33.4	54	20.5	1.86
	3.4	67	176	32.3	124	13.3	0.70
	15.5	191	171	27.7	71	9.0	0.42
	15.5	191	318	26.5	94	11.2	0.30

Notes:

1. Effective friction angle ϕ' determined at maximum $(\sigma_1'-\sigma_3')_f$.
2. Undrained shear strength $s_u = (\sigma_1'-\sigma_3')_f/2$.
3. σ_c' = effective confining stress.
4. ϵ_f = strain at failure (percent).

A summary Cambridge q-p' diagram is shown in Figure 4.7, where $q = (\sigma_1-\sigma_3)$ and $p' = \frac{1}{3}(\sigma_1'+\sigma_2'+\sigma_3')$. Assuming $c' = 0$, the effective frictional envelope may be described by the parameter $M = (q/p')_f = 1.11$, corresponding to an effective stress friction angle, $\phi' = \sin^{-1}[3M/(6+M)]$, or $\phi' = 28.0°$. If the tension zone is considered at low stress levels, an apparent cohesion intercept can be obtained from regression analyses of the data, which results in $\phi' = 24.4°$ and $c' = 14$ kPa.

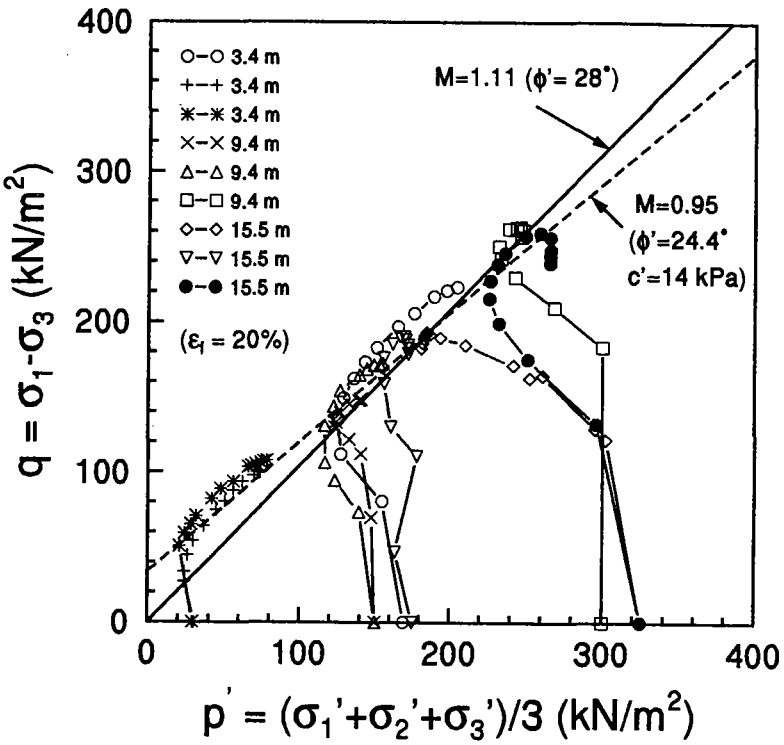

Figure 4.7. Summary Cambridge q-p' Stress Paths from Triaxial Tests on Specimens from Port Huron Site.

4.2. BATON ROUGE SITE, LOUISIANA

A second test site was established in a deep desiccated deposit of overconsolidated and fissured clay in Baton Rouge, Louisiana. The test site is located at the north corner of the intersection of interstate highway I-10 and Highland Road (State Route 42), southeast of the city of Baton Rouge, as shown in the site plan in Figure 4.8. The soundings were conducted about 2 m apart. The field testing program was conducted in late June of 1993 and utilized a Van den Berg cone truck to push Fugro piezocones to depths of 37 meters. In-situ testing included one standard electric cone, seven piezocones, and one dilatometer sounding. In addition, thin-walled Shelby tube samples were obtained at the site in early September of 1993 using a conventional drill rig. These samples were carefully transported to the Geotechnical Laboratory at GT for index, consolidation, and triaxial shear testing.

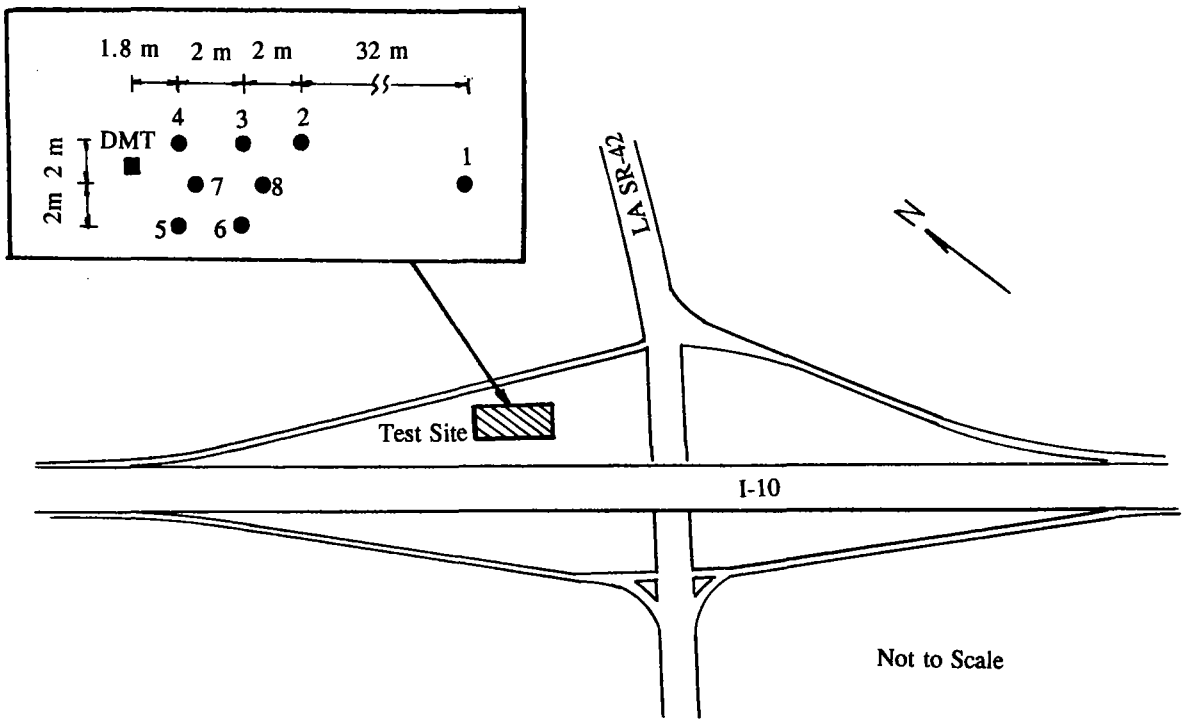

Figure 4.8. Site Plan and Field Test Locations at Baton Rouge Site, Louisiana.

The purpose of the test program was to obtain high quality piezocone data with multiple pore pressure measurements at different positions. Two different dual-element piezocones and a triple-element piezocone that provided separate and simultaneous pore pressure measurements were used at this site. The results are believed to include the first set of triple-element piezocone tests performed in the United States.

4.2.1. Geologic Setting

The overconsolidated clays at the Baton Rouge site are Pleistocene Age terrace deposits that were originally deposited in a deltaic environment and subsequently subjected to high desiccation. These stiff clays are known to be expansive and cover extensive regions of Louisiana and Texas. They are indeed related to the famous Beaumont clays in Houston (Mahar and O'Neill, 1983). Arman and McManis (1977) describe the soil formation in the Baton Rouge area as having a very stiff consistency, low moisture content,

commonly oxidized (typically reddish-brown or yellow in color), and containing calcareous concretions or iron oxide bands. They reported that these stiff clays are generally weakened by a network of fissures and slickensides.

Records of prior soil borings conducted by the Louisiana State Department of Transportation and Development (LDOTD) during the construction of I-10 circa 1970 indicated that the soils at the test site were comprised of tan to grey, stiff to very stiff, silty clays with slickensides and occasional sand pockets. These observations were later confirmed from samples retrieved from depths of 5 to 35 meters for this study. At the test site, the groundwater lies 4.5 meters below the ground surface.

4.2.2. Piezocone Penetration Tests

Three different versions of 15-cm^2 Fugro-type cones were used in this study, including a standard electric cone, two identical dual-element piezocones (with simultaneous measurements of u_1 and u_3), and a special triple-element piezocone (u_1, u_2, and u_3), as shown in Figure 4.9. A single-element seismic piezocone (u_2) also shown in the figure was planned but not used in this testing program due to electronic difficulties.

Porous elements of these piezocones were located at three different positions: mid-face (u_1), behind the tip (u_2), and behind the friction sleeve (u_3). All porous filters were made from high density polyethylene material. An acrylic cell equipped with a magnetic agitator and deaired by a vacuum pump was used to saturate the cones and porous elements. This device was on loan from the Department of Civil Engineering of Louisiana State University. In order to maintain saturation, a plastic bag filled with deaired water was attached and duct-taped to the cone. No friction reducer was used since the diameter of the 15-cm^2 (43.7 mm) cone is larger than the diameter of the cone rods (35 mm) used.

The assembled cone was hydraulically advanced into the ground using the reaction provided by a 178 kN (20-tonne) Van den Berg cone rig, as shown in Figure 4.10, that was operated and provided under subcontract by the Louisiana Transportation Research Center (LTRC). The interior of the rig was air-conditioned and featured a hydraulic actuator, cone rods, and a computerized data acquisition system (Figure 4.11). An underground-use cable with one end connected to the data acquisition system was threaded through the rods in

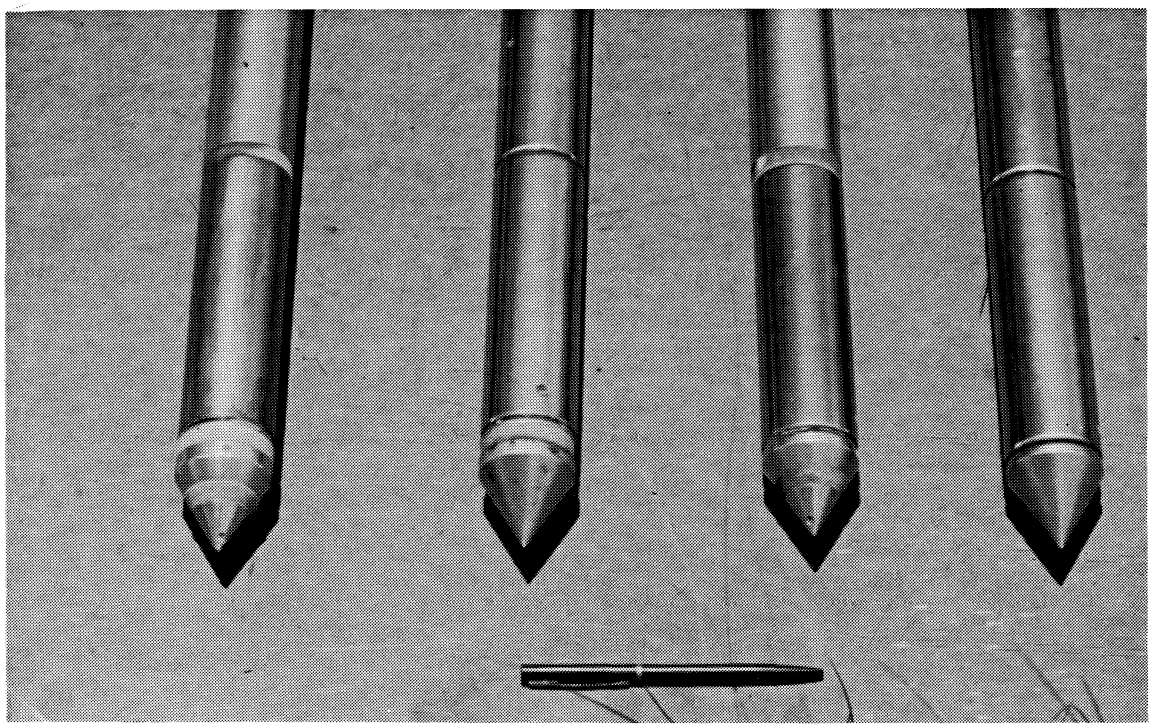

Figure 4.9. Multiple-Element Fugro-Type Cone Penetrometers Used At Baton Rouge Site.

Figure 4.10. Van den Berg Type Cone Truck at Louisiana Transportaton Research Center.

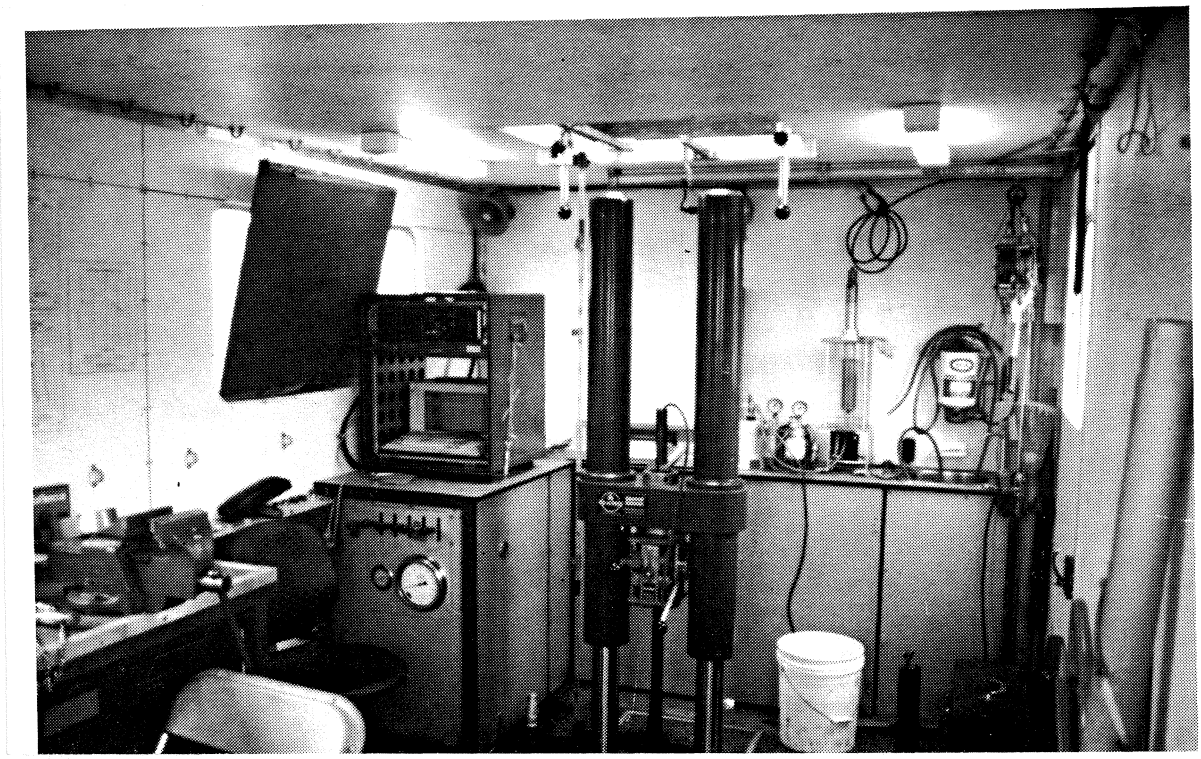

Figure 4.11. Interior View of the LTRC Cone Truck Operations.

advance. A potentiometer was used to monitor the changes in depth over one-meter intervals. The data acquisition system consisted of an analog-digital signal convertor, an electronic signal conditioner, a Compaq personal computer, and HP color plotter. The data acquisition software is capable of showing the actual results graphically on the screen at the same time the cone is being pushed into the ground. All tests were performed at a rate of 20 mm/sec continuously, and only stopped intermittently while the next rod was added.

A summary of the cone/piezocone penetration tests performed for this research program is listed in Table 4.3. The electric cone penetration test was carried out by LTRC initially to assess the feasibility of the site. The seven piezocone penetration tests were performed under the supervision of Georgia Tech personnel. It is important to point out that the first three piezocone tests were conducted without complete and proper saturation of the porous elements. Consequently, almost no pore water pressures were measured for those tests until the filters became saturated under the high hydrostatic pressures at depths

greater than 30 m. The poor results obtained from these tests clearly demonstrated the importance of proper saturation techniques. After the first three tests, strict saturation procedures were enforced to ensure proper pore pressure response. An additionally implemented step was to prepunch the holes with a larger dummy cone to the depth of groundwater table, whereby the well-saturated piezocone was lowered into the hole. The episode confirms the well-recognized fact that saturation of the cone and the filter elements is an extremely important aspect of piezocone testing.

The special triple-element piezocone, equipped with three pore pressure transducers, was lent in kind to the GT research program by Kaare Senneset from the Norwegian Institute of Technology, Trondheim. The data acquisition system of the LTRC cone truck was programmed to read only two pore pressure measurements at any given time, therefore, readings from the transducer located above the friction sleeve (u_3) were not recorded during the triple-element piezocone soundings. The u_3 data were obtained from the adjacent dual-element piezocone soundings which measured u_1 and u_3.

Table 4.3. Summary of Piezocone Tests at Baton Rouge Site.

Test No.	Test ID	Cone No.	Type Filter	Penetration Depth (m)	Remarks
1	06039301	V601	none	31	standard CPT
2	06079301	2W/V207	u_1, u_3	33	without pre-saturation
3	06079302	2W/V207	u_1, u_3	38	without pre-saturation
4	06079303	2W/V207	u_1, u_3	35	without pre-saturation
5	06089301	3W/V263	u_1, u_2, u_3	36	saturation/no prepunch
6	06089302	2W/V207	u_1, u_3	37	saturation/prepunch
7	06099301	3W/V263	u_1, u_2, u_3	36	saturation/prepunch
8	06109301	3W/V263	u_1, u_2, u_3	37	saturation/prepunch

Notes:
1. u_1 measured at midface position.
2. u_2 measured at shoulder position.
3. u_3 measured on cone shaft behind friction sleeve.

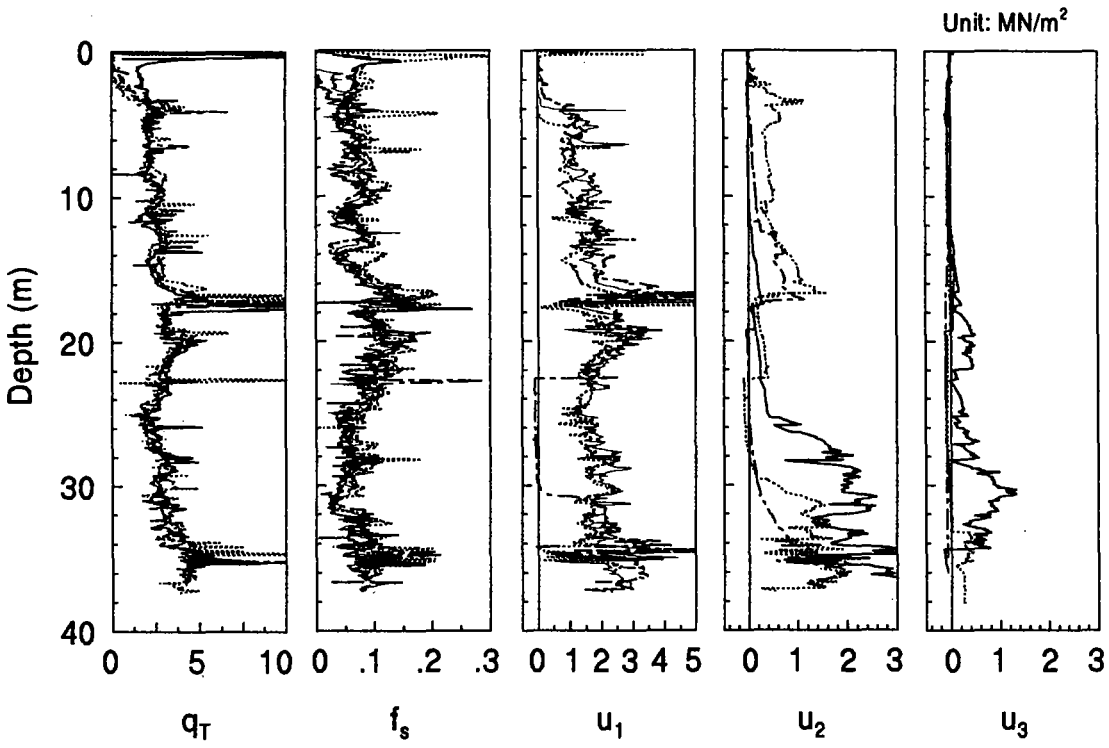

Figure 4.12. Summary Measurements from Four Piezocone Records at Baton Rouge Site.

A summary plot of the data from 4 piezocone records is presented in Figure 4.12. This figure clearly demonstrates the excellent repeatability of the measurements of q_T, f_s, and u_1. However, significant scatter and variability is evident for the u_2 and u_3 readings obtained in separate soundings. A comparison of detailed pore pressure responses are illustrated by the combined record presented in Figure 4.13.

Occasional spikes in the q_T readings and the corresponding pore pressure decays in Figures 4.12 and 4.13 indicate that sand lenses or sandy pockets exist embedded in the clay strata. In particular, measured pore pressures in one of the u_1 channels and all of the u_2 and u_3 channels dropped significantly at depths of about 17 and 23 meters. The magnitudes of penetration pore pressures were not fully recovered until the cone advanced another 8 to 10 meters deeper. It is believed that the loss of pore pressures in these intervals was caused by the existence of dense dilatant sand layers at the specific depths (i.e., 17 and 23 m) and the subsequent pore pressure responses may therefore be incomplete.

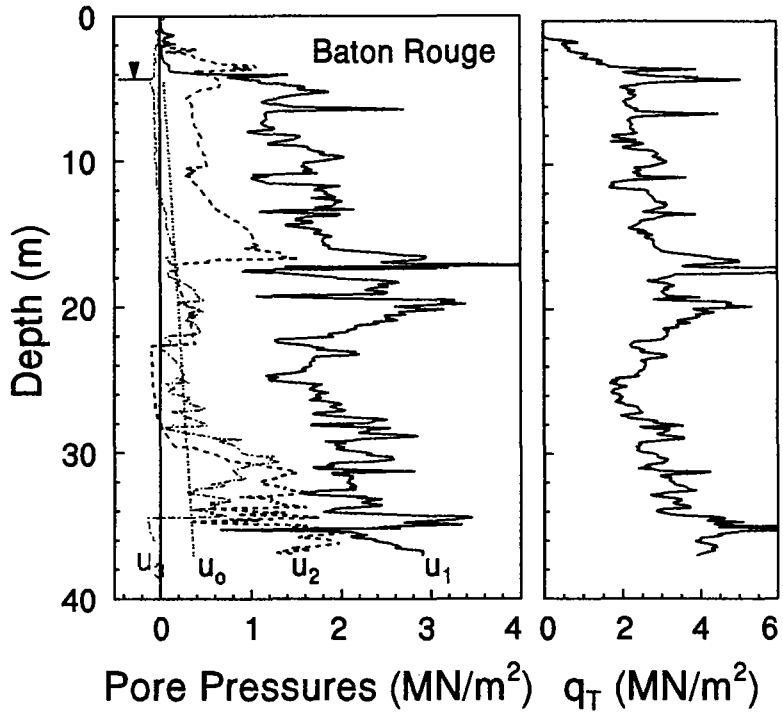

Figure 4.13. Composite Triple-Element Piezocone Sounding at Baton Rouge Site.

Dissipation test were conducted at selected depths during test soundings Nos. 6, 7, and 8. The results of the recorded decays of penetration pore pressure are presented in Figure 4.14. Although not pursued in this study, results from piezocone dissipation tests are useful in evaluating the time-dependent behavior of clays, such as the hydraulic conductivity (k) and (horizontal) coefficient of consolidation (c_h).

4.2.3. Dilatometer Test

Utilizing the LTRC cone rig, a dilatometer test (DMT) sounding was conducted to a depth of 31 meters at intervals of 0.20 meters. The corrected A and B readings are designated p_o and p_1, respectively, and shown in Figure 4.15. Also shown is the OCR predicted using Marchetti (1980) indicating the clays to be moderately overconsolidated and a method by Mayne (1987) showing the materials to be less overconsolidated. However, the latter approach is specifically appropriate for intact clays and not really applicable to the desiccated fissured clays at Baton Rouge.

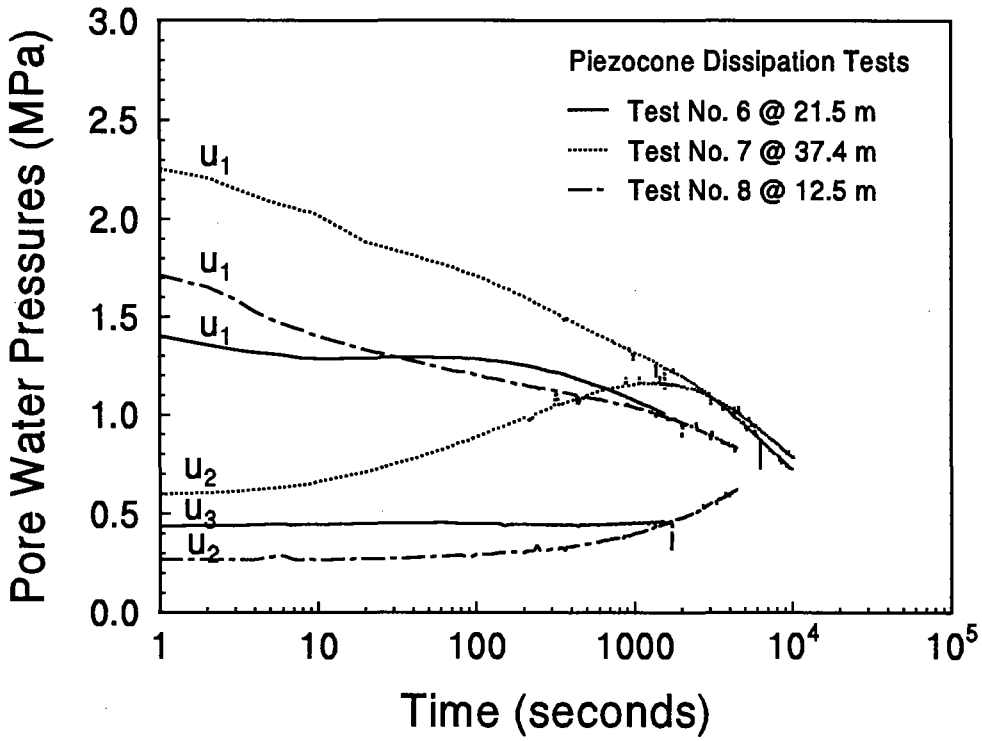

Figure 4.14. Results of Piezocone Dissipation Tests at Baton Rouge Site.

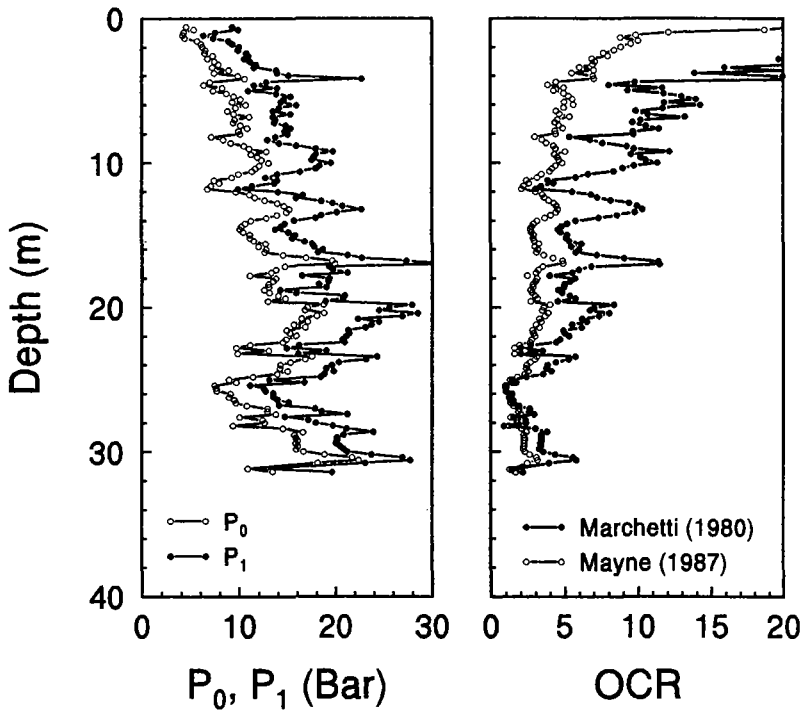

Figure 4.15. Results of Flat Dilatometer Testing at Baton Rouge Site.

4.2.4. Field Sampling and Laboratory Testing

Sixteen 76-mm diameter Shelby tube samples were retrieved at 1.5 and 3.0 m intervals during rotary drilling operations provided by LDOTD. All tubes were carefully sealed and transported to the GT laboratory in Atlanta within 48 hours. Tube samples were stored vertically in a near 100% humidity moisture room to minimize any moisture losses. The number and types of laboratory tests conducted on the samples are listed in Table 4.4. In general, all tests were completed within 60 days from the time of sampling. It was well understood that excessive moisture loss and long storage time may affect the test results, especially for very stiff, fissured, desiccated materials. Further complicating the task was the fact that the samples exhibited high swell potential.

Table 4.4. Summary of Laboratory Tests on Tube Samples From Baton Rouge Site.

Test Type	Specification	Quantity	Purpose
Water Content	ASTM D-2216	13	w_n
Liquid Limit	ASTM D-4318	2	LL
Fall Cone	BS-1377	13	LL, s_{ufc}
Plastic Limit	ASTM D-4318	13	PL
Lab Vane Shear	ASTM D-4648	15	s_{uv}
Consolidation	ASTM D-2435	22*	σ_p', C_c, C_s, γ_T, e_o
Triaxial (CIUC)	ASTM D-4767	8	ϕ', s_{utc}, e_o, γ_T
$CaCO_3$ Content	ASTM-4373	12	Cementation

Notes:
1. *Automated Geocomp consolidometer used for 18 tests and Wykeham-Farrance deadweight oedometer used for 4 tests.
2. w_n = natural water content; LL = liquid limit; PL = plastic limit.
3. s_{ufc} = undrained shear strength from fall cone test.
4. s_{uv} = undrained shear strength from miniature vane shear test.
5. σ_p' = preconsolidation pressure.
6. C_c = compression index; C_s = swelling index.
7. γ_T = total unit weight; e_o = initial void ratio.
8. ϕ' = effective stress friction angle.
9. s_{utc} = undrained shear strength from CIUC test.

The series of laboratory tests conducted in the GT geotechnical laboratory included: water contents, Atterberg limits, fall cone, laboratory vane shear, one-dimensional consolidation, and triaxial shear. In addition, determinations of calcium carbonate content were made on small bulk specimens supplied to Dr. Alan Lutenegger of University of Massachusetts, Amherst. The total calcite and dolomite contents of the clay samples average 2.9% $\pm$ 0.9%, indicating that the clays at Baton Rouge site are not cemented.

4.2.5. Index and Classification Tests

In general, the fall cone test was used to determine the liquid limit (LL) of the clays from Baton Rouge. These were supplemented by a limited number of Casagrande cup tests which gave similar values. Results of the index testing are summarized in Table 4.5. The brown to grey stiff fissured clays have 39 < LL < 76 with an average value of LL = 60 $\pm$ 20 percent. The plastic limits range from 19 to 43 and average 28 $\pm$ 12 percent. This

Table 4.5. Summary of Laboratory Index Testing at Baton Rouge Site.

Sample No.	Depth (m)	Soil Type	PL (%)	w_n (%)	LL (%)	PI (%)	LI (--)
2	5.49	CH	26	30	52	26	0.154
3	6.10	MH	36	42	76	40	0.150
4	7.62	MH	34	39	69	35	-0.142
5	10.67	CH	19	32	55	36	0.361
6	12.19	CH	28	32	70	42	0.095
7	13.72	CH	29	46	70	41	0.415
8	15.24	CL	16	23	48	32	0.218
9	18.29	CH	23	35	58	35	0.343
10	22.25	MH	34	35	60	26	0.038
11	24.38	CH	27	30	63	36	0.083
12	28.35	CL	22	27	39	17	0.294
13	30.48	CH	43	80	102	59	0.627
14	33.53	CH	27	34	67	40	0.175

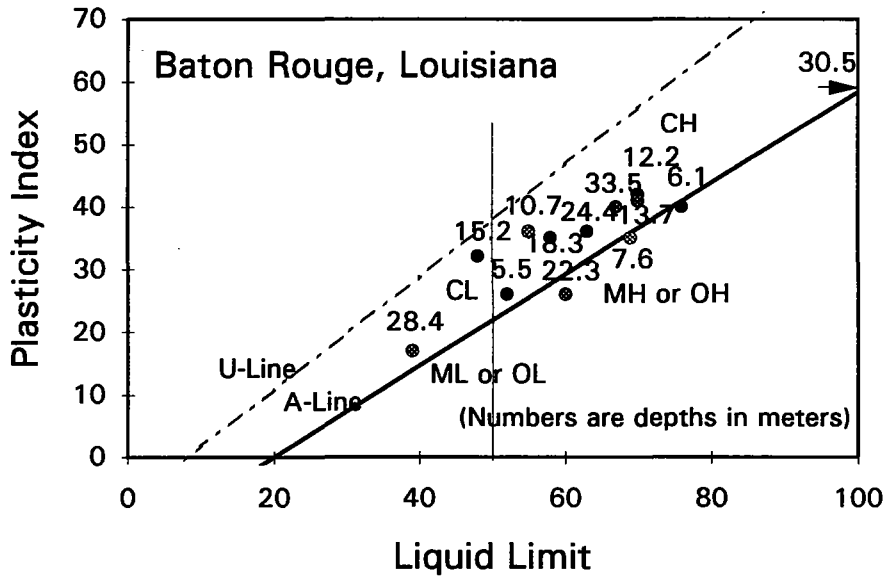

Figure 4.16. Plasticity Chart for USCS Classification at Baton Rouge.

provides a range of plasticity index of 17 < PI < 42 and a mean value of PI = 33 ± 13 percent. The associated values of PI versus LL are plotted on the plasticity chart from the Unified Soil Classification System in Figure 4.16, indicating that the soils primarily consist of CH materials.

Natural water contents at the site vary from 23 to 46% (Mean w_n = 34 ± 12%) and are only slightly higher than the plastic limit, as shown by Figure 4.17. Exception to this included the sample at a depth of 30.5 meters contained organics that indicated a very high natural water content (w_n = 80%) and high plasticity index (PI = 59). Initially, laboratory miniature vane shear tests were carried out to evaluate the order of magnitude of the undrained shear strength (s_u) of the clay materials. It is believed that the fall cone test sheared a much smaller portion of the sample than the vane shear test, therefore it is more likely to be affected by localized variations on the intact portions of the soil specimens.

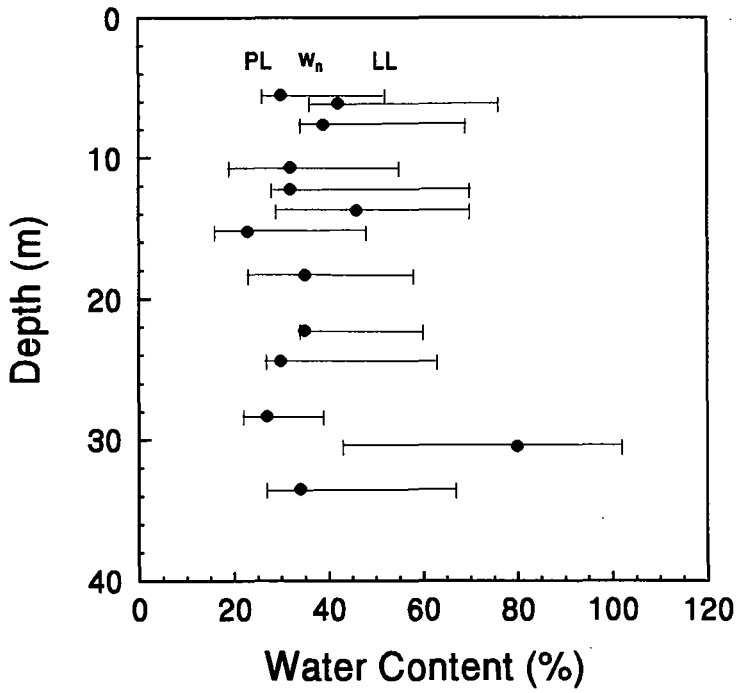

Figure 4.17. Summary Profile of Index Properties at Baton Rouge Site.

For the Baton Rouge clay, the effects of fissures and slickensides are obviously important here on the overall and operational strength. Scattered results in undrained shear strength also indicate that neither the fall cone nor the laboratory vane shear test are suitable for evaluating the s_u of stiff fissured clay materials where $s_u > 100$ kN/m^2.

4.2.6. Consolidation Tests

Two types of consolidation devices were used to perform one-dimensional incremental-load tests: two Wykeham Farrance (WF) dead-weight oedometers and five Geocomp (GC) computer-controlled consolidometers. These apparatuses are shown in Figures 4.18 and 4.19, respectively. All specimens were 19.1 mm thick, while the specimens used for the dead-weight oedometer were 63.5 mm in diameter and the specimens used for the automated consolidometer were 50.8 mm in diameter. Some disturbance and

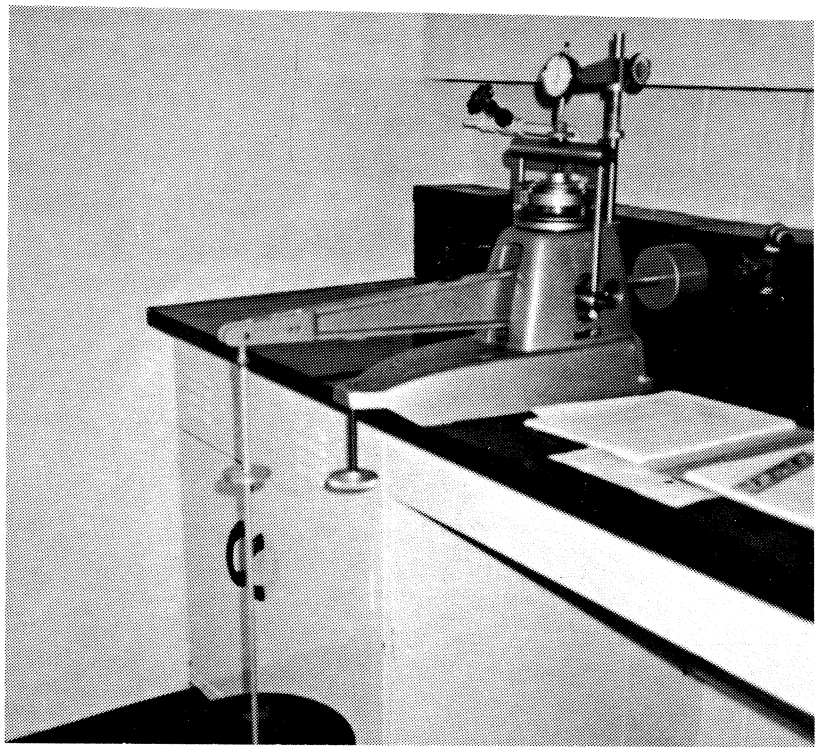

Figure 4.18. Wykeham-Farrance Incremental Load Oedometer.

handling difficulties were observed during specimen preparation due to the dry and fissured nature of the clay. Specimens were loaded in increments up to maximum applied vertical stresses of 4.8 MN/m^2, and then unloaded stepwise at the end of the test. The applied load increment ratio was one (LIR = 1), except at load sequences greater than 1.5 MN/m^2, where LIR = 0.8 were used. The square root time method was used to estimate the end-of-primary consolidation ($t_p = t_{100}$) during each load increment. A few load increments were performed with each load cycle being extended over a longer period of time (generally less than 24 hours) to investigate the effects of secondary consolidation. A comparison of these different procedures for test GC-17 is shown in Figure 4.20, indicating that the effect of secondary consolidation on the determination of preconsolidation stress is not particularly significant for the stiff, fissured clays from the Baton Rouge site. Note the very high swelling response during incremental unloading at the end of the tests.

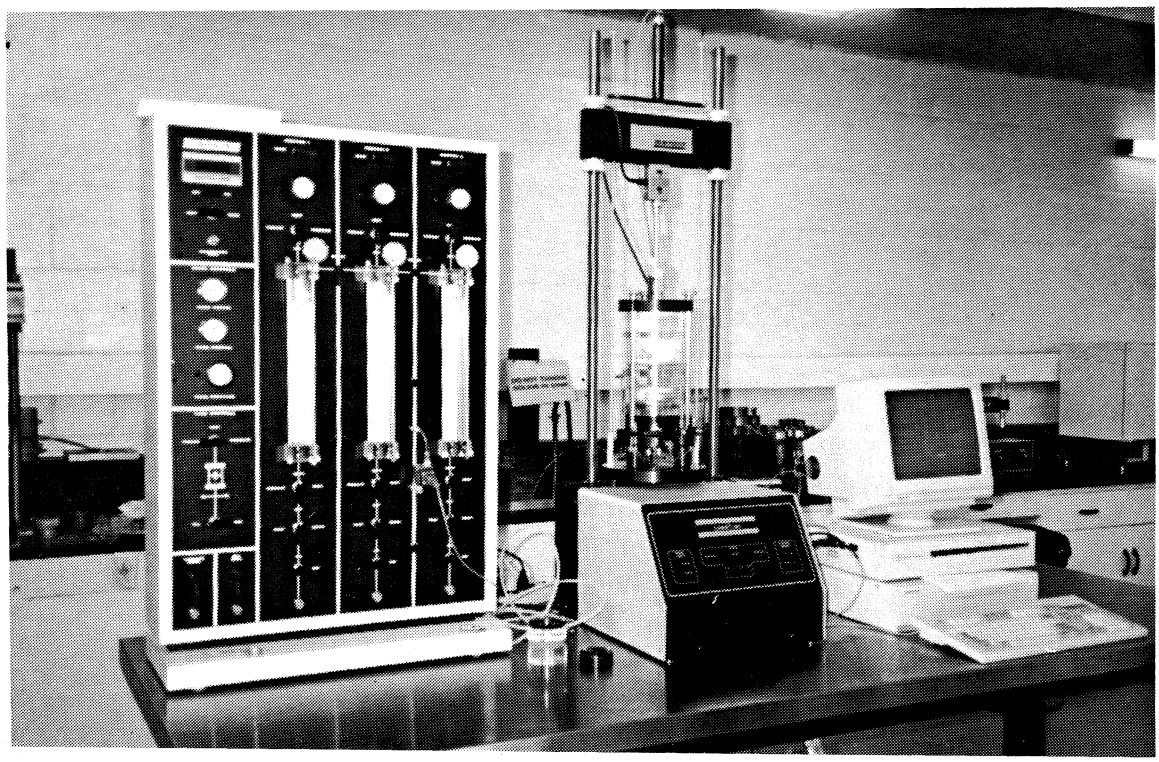

Figure 4.19. GeoComp Computer-Automated Consolidometers.

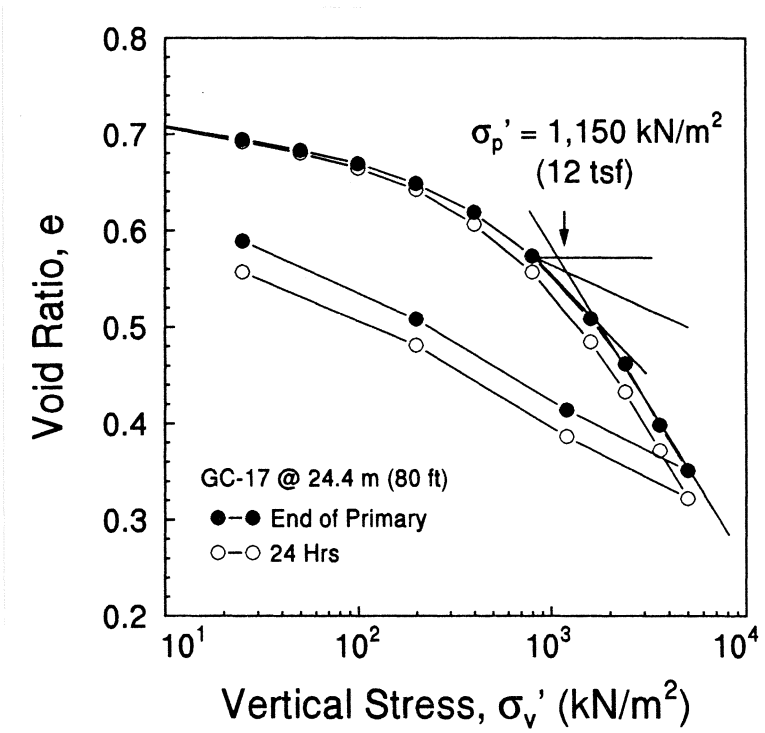

Figure. 4.20. Comparison Between End-of-Primary and 24-Hour Consolidation Tests.

Table 4.6. Summary of Consolidation Test Results for Baton Rouge Site.

Test No.	Depth (m)	w_n (%)	γ_t (kN/m^3)	e_o -	σ_{vo}' (kPa)	σ_p' (kPa)	OCR -	C_c -	C_s -
GC-5	5.5	29	18.4	0.77	92	1437	15.6	0.50	0.14
WF-1	6.1	45	17.6	1.21	97	1054	10.9	0.47	0.20
GC-6	7.0	40	18.2	1.09	105	1245	11.9	0.53	0.22
GC-1	7.6	42	17.9	1.07	110	1198	10.9	0.62	0.15
GC-14	7.9	35	18.3	0.99	113	1341	11.9	0.52	0.19
GC-9	8.5*	23	17.9	0.72	118	1054	8.9	0.26	0.05
GC-2	10.7*	30	19.2	0.85	137	958	7.0	0.26	0.06
GC-13	11.3	27	19.1	0.81	142	1198	8.4	0.34	0.10
GC-7	11.6	26	19.6	0.76	145	1245	8.6	0.42	0.06
WF-2	12.2	34	18.4	0.96	150	1150	7.7	0.42	0.15
GC-8	13.1	32	18.5	0.95	158	958	6.1	0.58	0.16
GC-3	13.7*	25	20.0	0.70	163	1054	6.5	0.31	0.06
GC-10	14.6	39	17.7	1.15	171	766	4.5	0.68	0.14
GC-4	15.2	24	20.7	0.58	177	766	4.3	0.33	0.08
WF-4	15.9	25	20.0	0.68	182	958	5.3	0.26	0.09
GC-11	16.2	26	19.4	0.77	185	766	4.2	0.39	0.18
WF-3	18.3	30	17.3	1.02	203	910	4.5	0.34	0.12
GC-16	22.3	40	17.6	1.13	238	958	4.0	0.45	0.17
GC-17	24.4	27	19.7	0.72	256	1150	4.5	0.31	0.11
GC-18	28.4	29	19.3	0.79	290	1150	4.0	0.31	0.09
GC-19	30.5	33	17.9	1.09	309	479	1.6	0.41	0.07
GC-20	33.5	39	19.3	0.86	336	1150	3.4	0.41	0.14

Notes: * - sand content 10 to 15%.

The curves of void ratio versus log(σ_v') for all 24 consolidation tests are shown in Figure 4.21. A complete summary of the consolidation test results is presented in Table 4.6. The magnitudes of the compression index (C_c) range from 0.26 to 0.68, with a mean value of $C_c = 0.42 \pm 0.16$. The swelling index (C_s) determined from the unload cycle at end of each test varies from 0.05 to 0.19 and an average value $C_s = 0.12 \pm 0.07$. The effective preconsolidation stress (σ_p') was interpreted using several different methods and these are summarized in Table 4.7. The results using methodologies suggested by Casagrande (1963) and Becker et al. (1987) gave the most consistent and reasonable estimates. Due to the strong desiccation phenomenon that caused much of the observed

Table 4.7. Interpretation of Preconsolidation Pressure from Oedometer Test Results on Specimens from Baton Rouge Site.

Specimen No.	Depth (m)	Effective Preconsolidation Stress, σ_p' (kN/m^2) (1)	(2)	(3)	(4)	(5)	(6)
GC-5	5.5	958	1437	1198	1437	NA	NA
WF-1	6.1	671	1054	766	1102	958	766
GC-6	7.0	766	1245	1054	1533	1916	1533
GC-1	7.6	958	1198	1150	1485	NA	NA
GC-14	8.2	862	1389	862	1341	NA	NA
GC-9	8.5	383	1054	479	1102	NA	NA
GC-2	10.7	383	958	431	958	96	57
GC-13	11.3	671	1198	862	1150	77	57
GC-7	11.6	719	1245	910	1341	NA	NA
WF-2	12.2	814	1150	1102	1198	1916	1054
GC-8	13.1	527	958	766	1006	1150	1150
GC-3	13.7	527	1054	623	1054	NA	NA
GC-10	14.6	383	766	575	575	575	479
GC-4	15.2	479	766	575	814	NA	NA
WF-4	15.9	527	958	766	958	1150	814
GC-11	16.2	575	766	575	766	NA	NA
WF-3	18.3	766	910	766	910	NA	NA
GC-16	22.3	575	958	719	1293	96	77
GC-17	24.4	766	1150	766	1198	NA	NA
GC-18	28.4	671	1150	814	1150	NA	NA
GC-19	30.5	335	479	383	527	287	192
GC-20	33.5	814	1150	766	1054	575	NA

Notes: Interpretative Method:

(1) Sowers (1979)
(2) Casagrande (1936)
(3) Butterfield (1979)
(4) Becker et al. (1987)
(5) Janbu (1969)
(6) Jamiolkowski and Marchetti (1969)

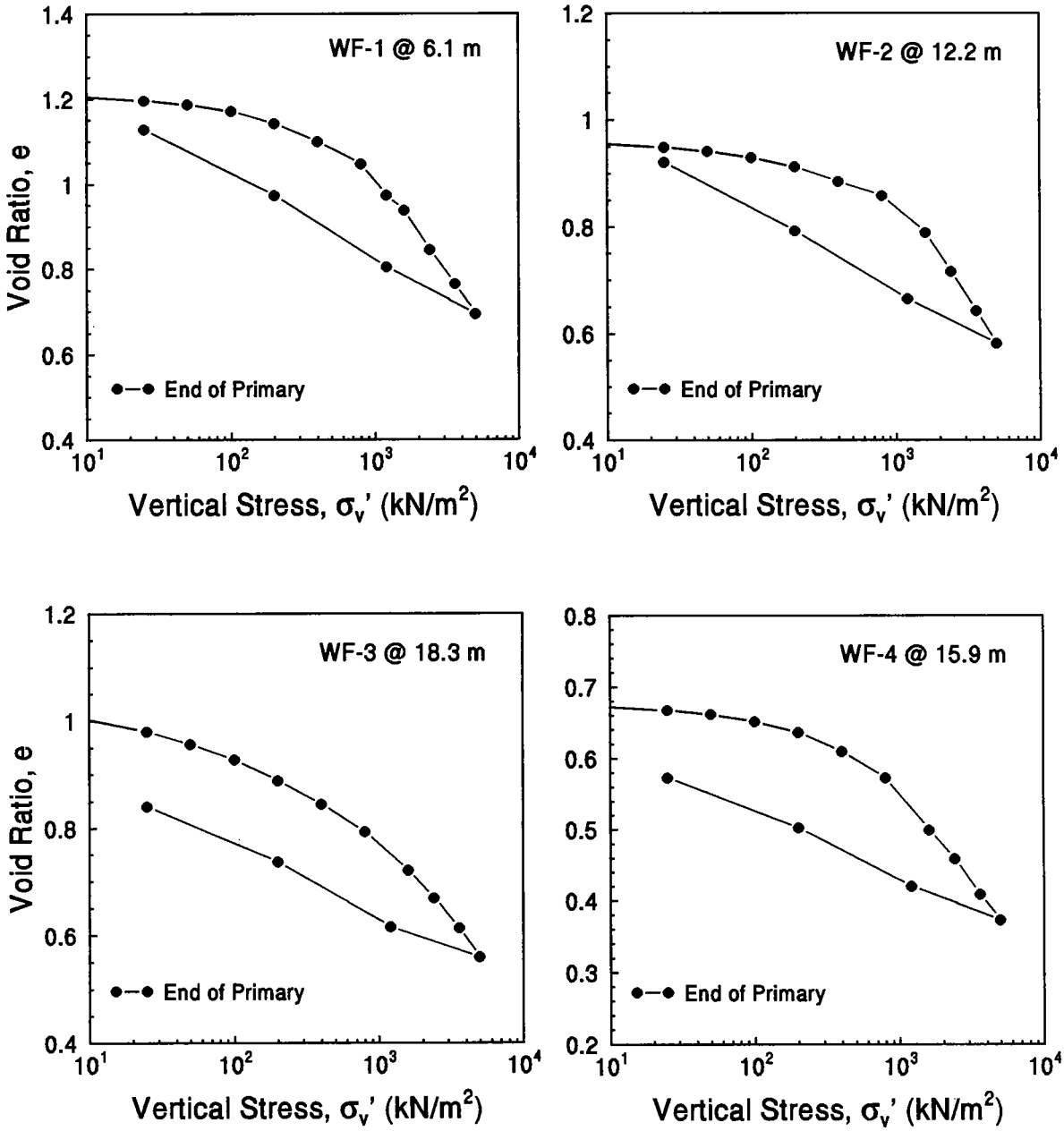

Figure 4.21 Results of Laboratory Consolidation Tests for Soil Samples Retrieved from Baton Rouge Site.

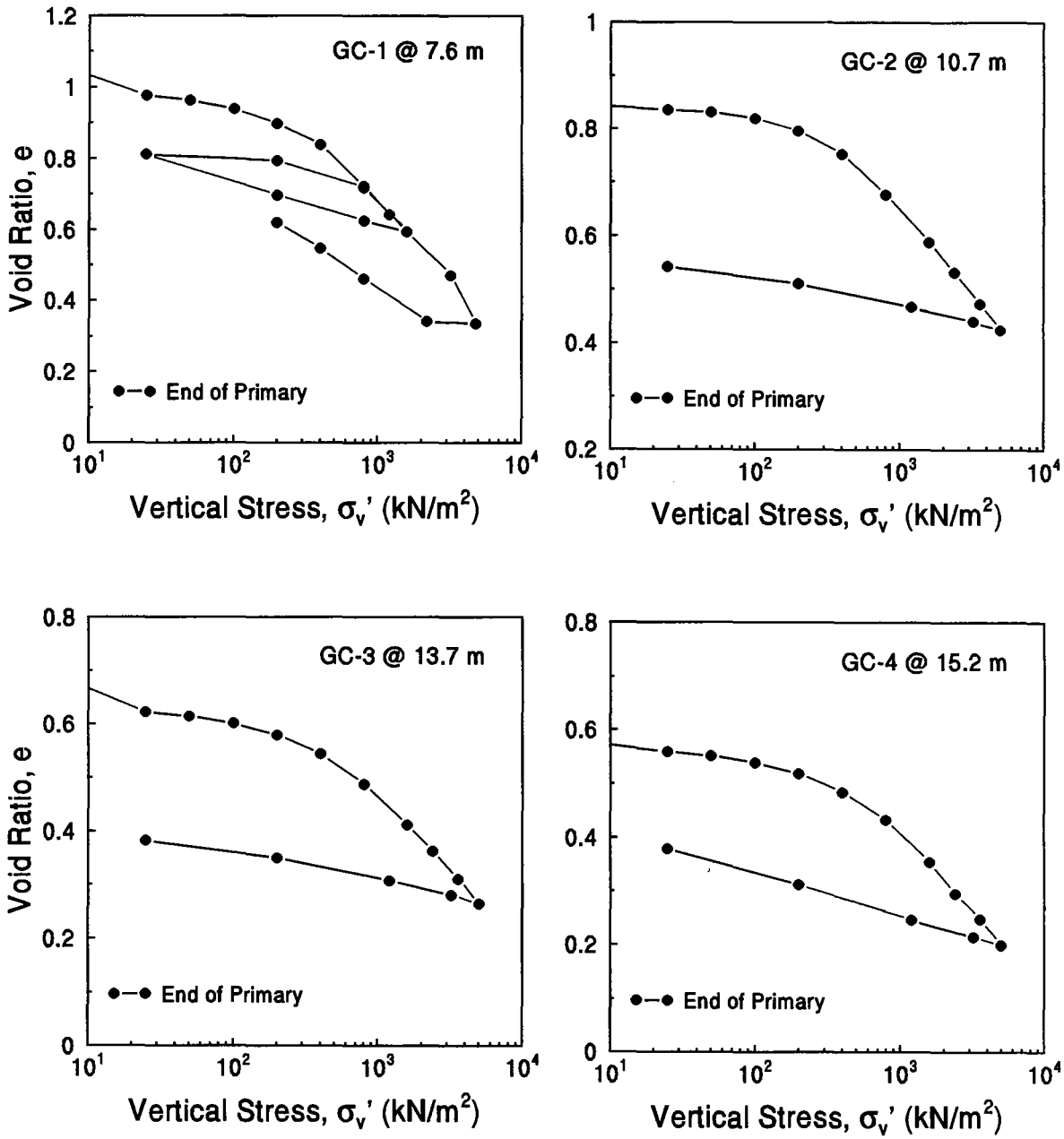

Figure 4.21 Results of Laboratory Consolidation Tests for Soil Samples Retrieved from Baton Rouge Site. (Continued)

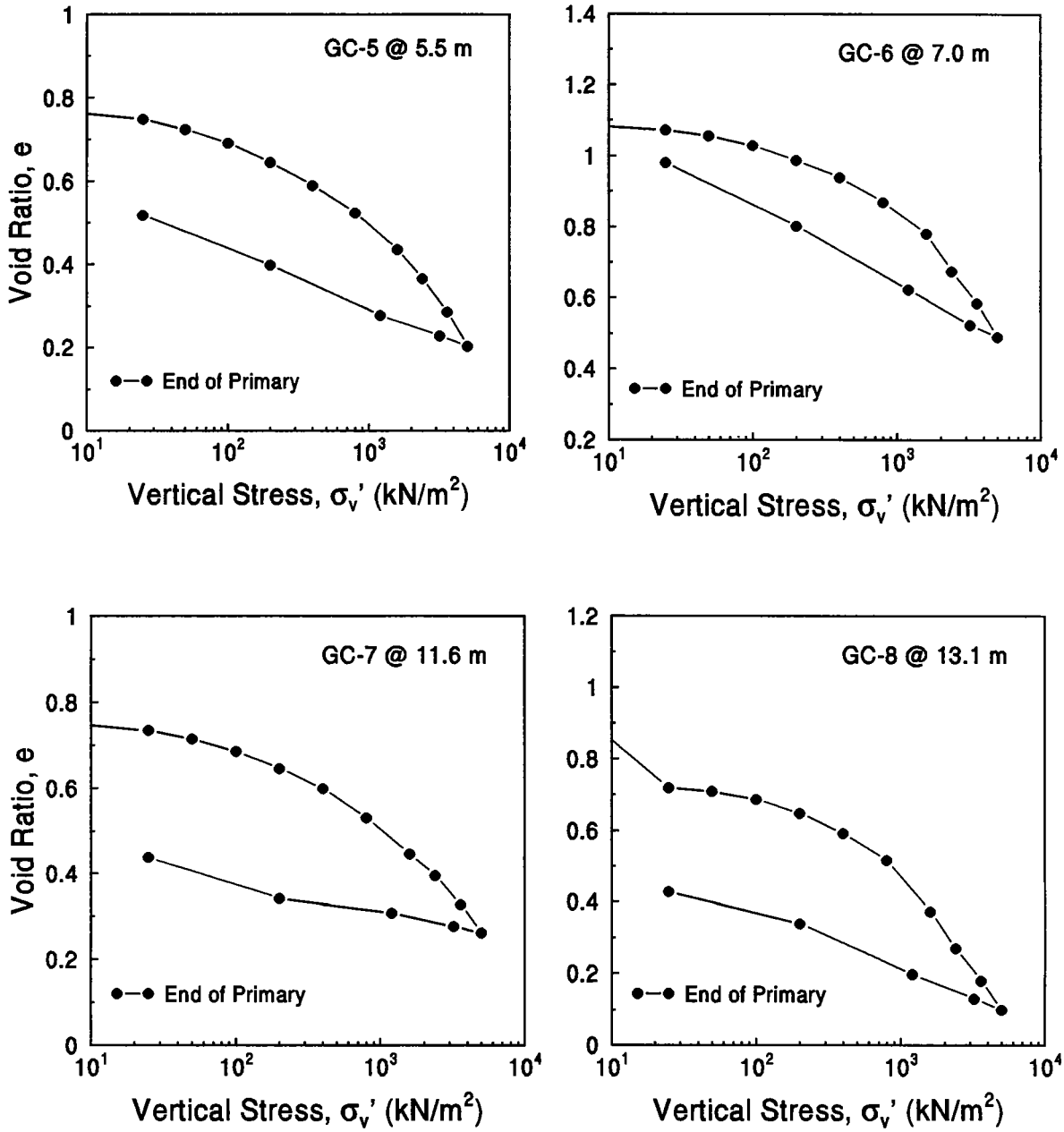

Figure 4.21 Results of Laboratory Consolidation Tests for Soil Samples Retrieved from Baton Rouge Site. (Continued)

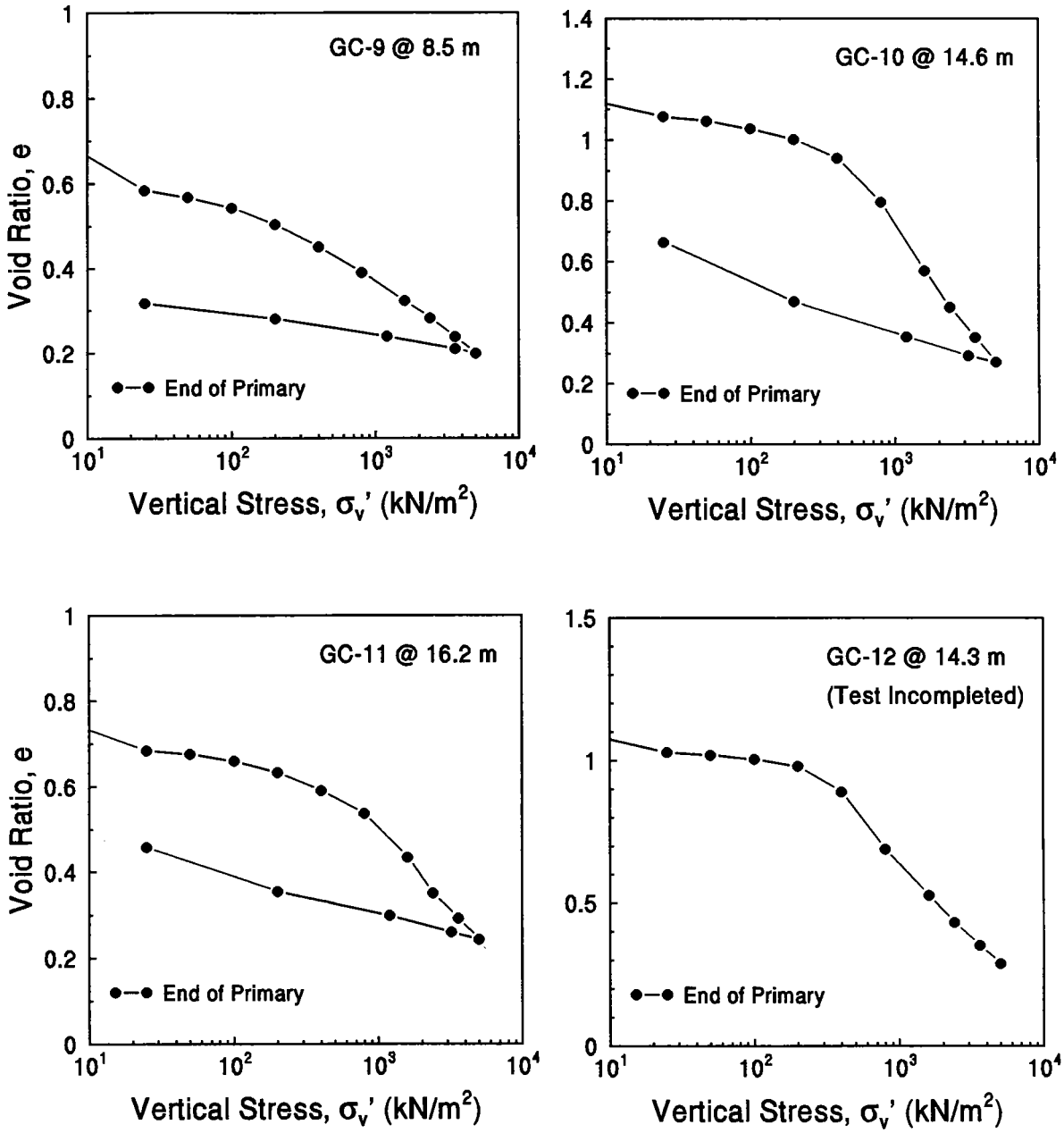

Figure 4.21 Results of Laboratory Consolidation Tests for Soil Samples Retrieved from Baton Rouge Site. (Continued)

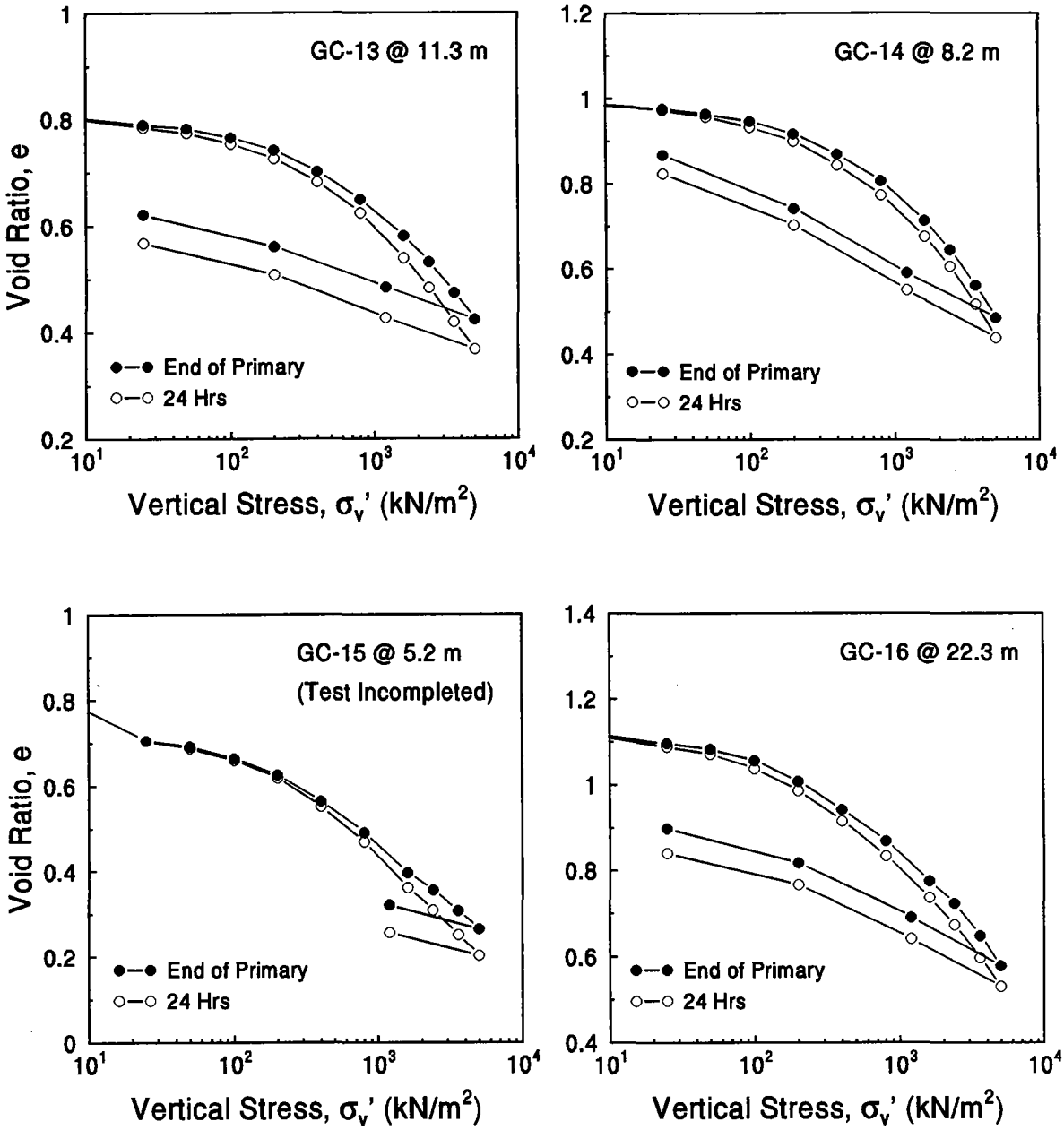

Figure 4.21 Results of Laboratory Consolidation Tests for Soil Samples Retrieved from Baton Rouge Site. (Continued)

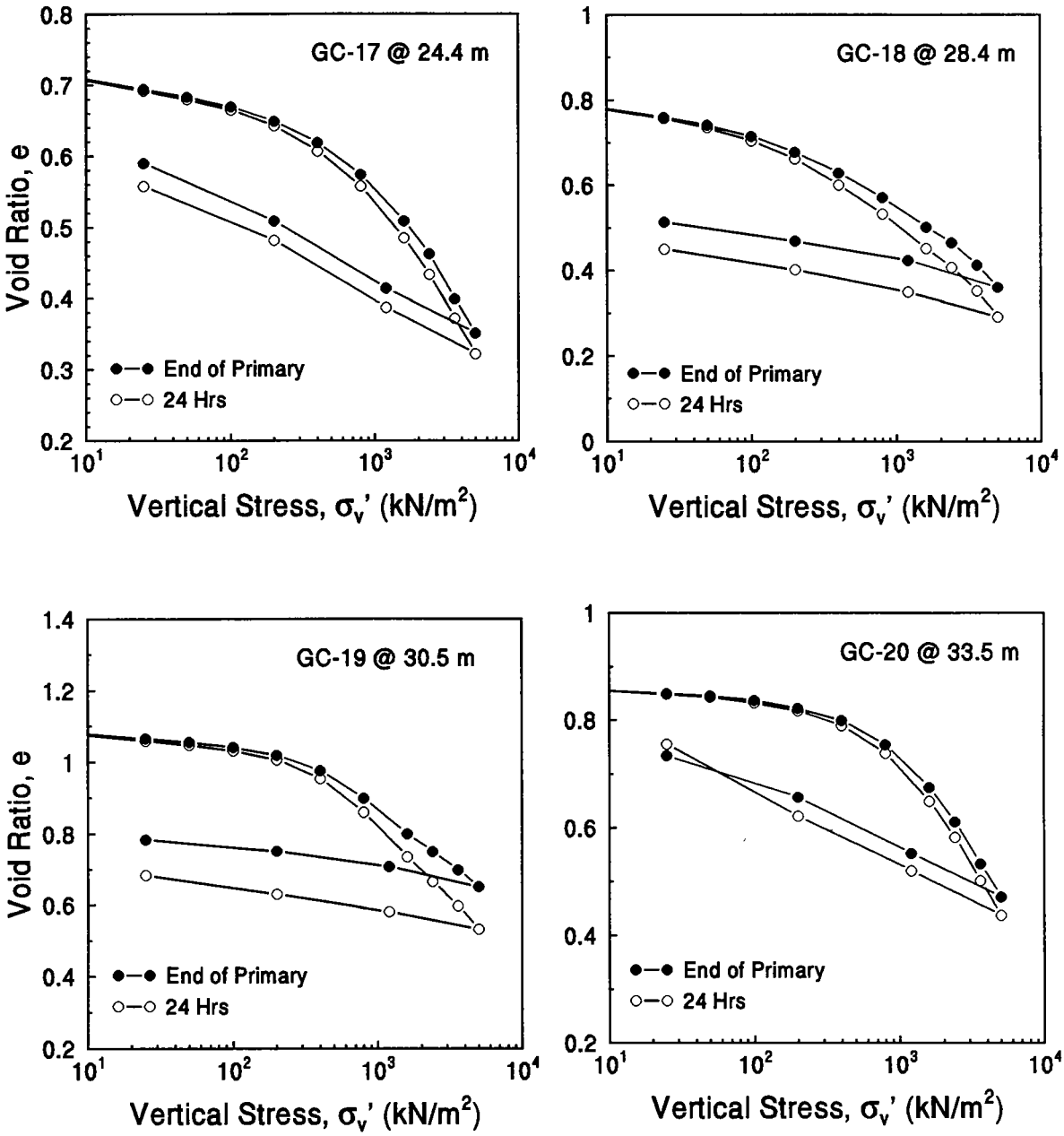

Figure 4.21 Results of Laboratory Consolidation Tests for Soil Samples Retrieved from Baton Rouge Site. (Continued)

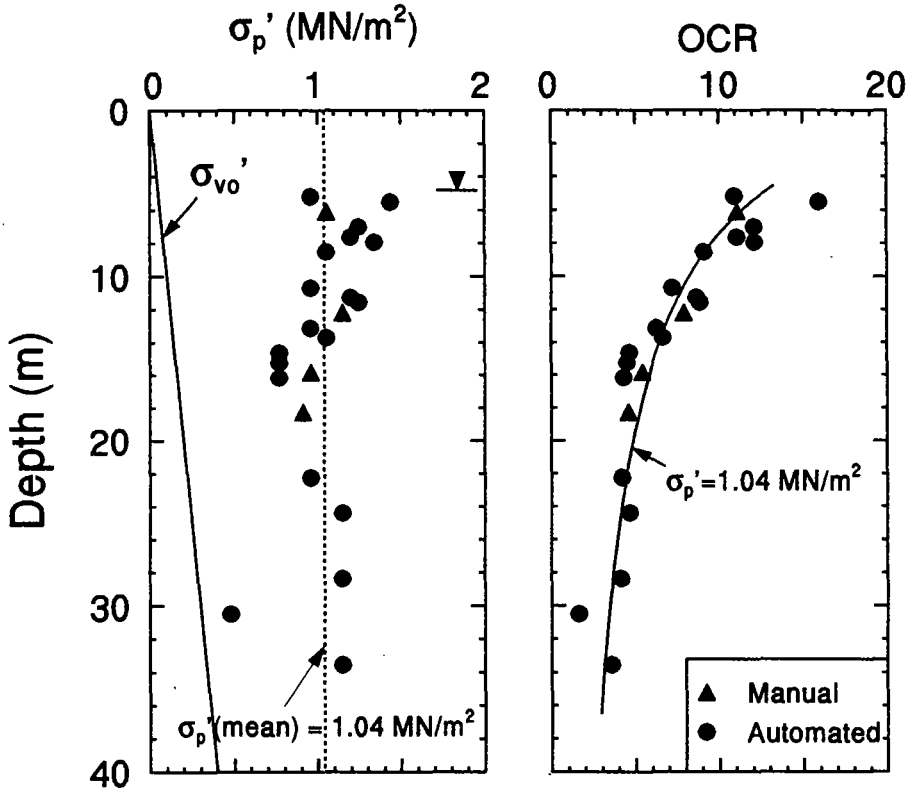

Figure 4.22. Interpreted Profiles of Yield Stress and OCR at Baton Rouge Site.

overconsolidation of the Baton Rouge clay, it is noted that the preconsolidation pressures of the deposit can be approximated by a constant value of $\sigma_p' = 1.04$ MN/m^2, as illustrated by Figure 4.22. The corresponding profiles of OCR are also shown in Figure 4.22 and indicate the OCR decreases from OCR = 15 at 4 meters depth to about OCR = 5 at the depth of 36 meters.

4.2.7. Triaxial Compression Tests

A C.K. Chan-Type automated triaxial testing device was used to perform a series of isotropically-consolidated undrained triaxial compression (CIUC) tests on specimens of Baton Rouge clay. These tests were performed in accordance with ASTM D-4767 standards. The setup of the device used is shown in Figure 4.23. Specimens (71 mm in diameter and 142 mm in height) trimmed from samples taken from various depths were

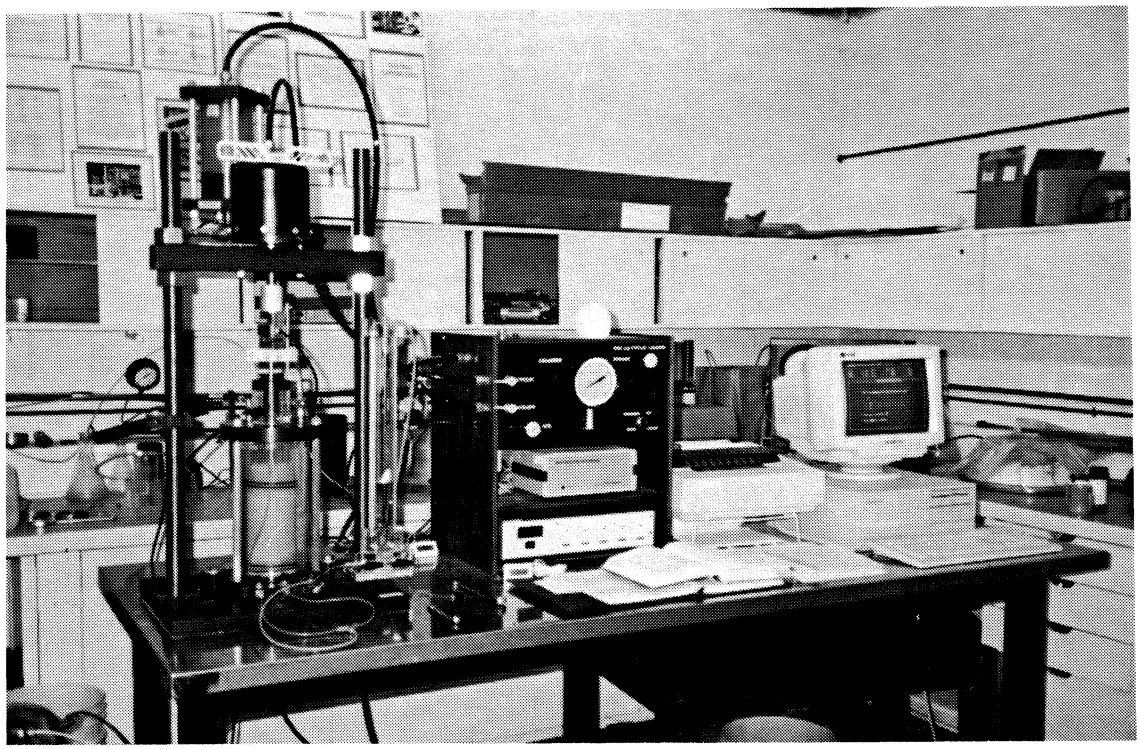

Figure 4.23. View of the C.K. Chan Automated Triaxial System.

isotropically-consolidated to 1.1 and 2.0 times their effective vertical overburden stresses and sheared to at least 20% strain. One specimen was consolidated to higher stress levels for studying the stress paths nearer to the true yield surface. Strain rates varying from 1.5% per hour to 10% per hour were used. It is believed that the faster strain rates helped to reduce the weakening effect caused by swelling along the pre-existing fissures.

A summary Cambridge q-p' diagram is shown in Figure 4.24, where $q = (\sigma_1-\sigma_3)$ and $p' = \frac{1}{3}(\sigma_1'+\sigma_2'+\sigma_3')$. The effective frictional envelope may be described by the parameter $M = (q/p')_f = 1.13$, corresponding to an effective $\phi' = \sin^{-1}[3M/(6+M)]$, or $\phi' = 28.5°$ at large strains ($\epsilon_f \approx 20\%$). The stress-strain curves and corresponding pore pressure measurements for each test are presented in Figure 4.25. The undrained shear strength determined from CIUC tests ranges from 60 to 120 kN/m^2, which is typically lower than those determined by the miniature vane shear tests due to the fissured nature of the

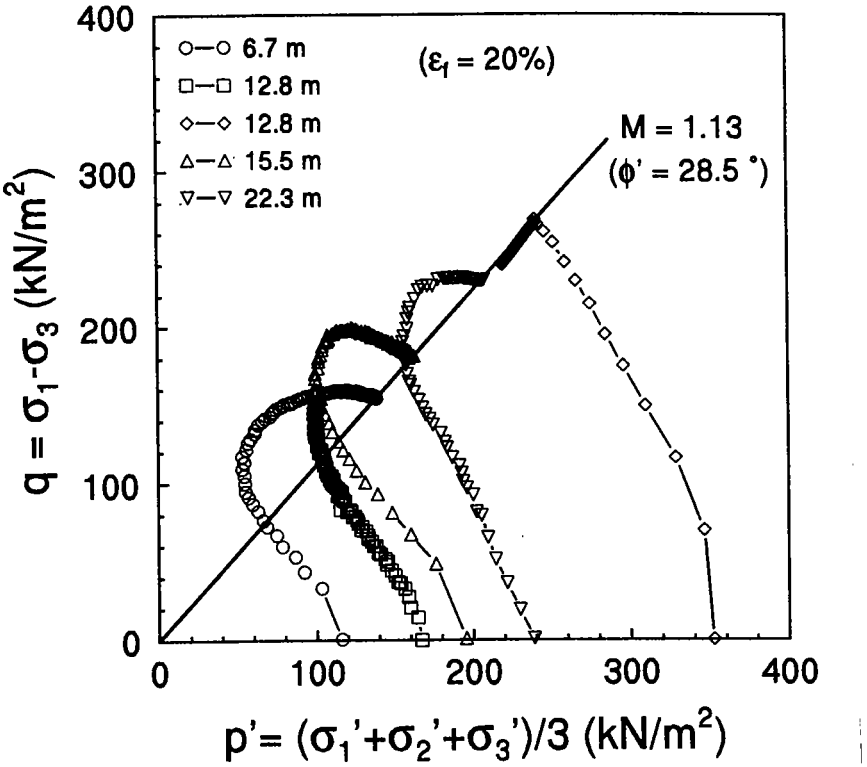

Figure 4.24. Summary Cambridge q-p' Stress Paths for Baton Rouge Site.

desiccated clay. McManis and Arman (1986) reported that the consolidated triaxial test tends to result in higher shear strengths than the unconsolidated triaxial test (UU) due to the decrease of void ratio during consolidation. This might not be true in this case since the preconsolidation pressures were so high that the applied consolidation stresses might not be adequate in closing up the cracks and fissures opened by swelling.

4.3. EVALUATION OF IN-SITU MEASUREMENT VARIABILITY

All measurements obtained from in-situ tests include variability and uncertainty that may be due to either natural or artificial sources, or both. The component of natural variability is caused by geologic features such as soil fabric, the presence of sand seams in the clay matrix, fissures, varves, and inclusions. The component that is artificially-induced includes those due to measurement errors, such as electronic noise, crosstalk between channels, electrical drift, inadequate saturation of the porous filter element, clogging of the

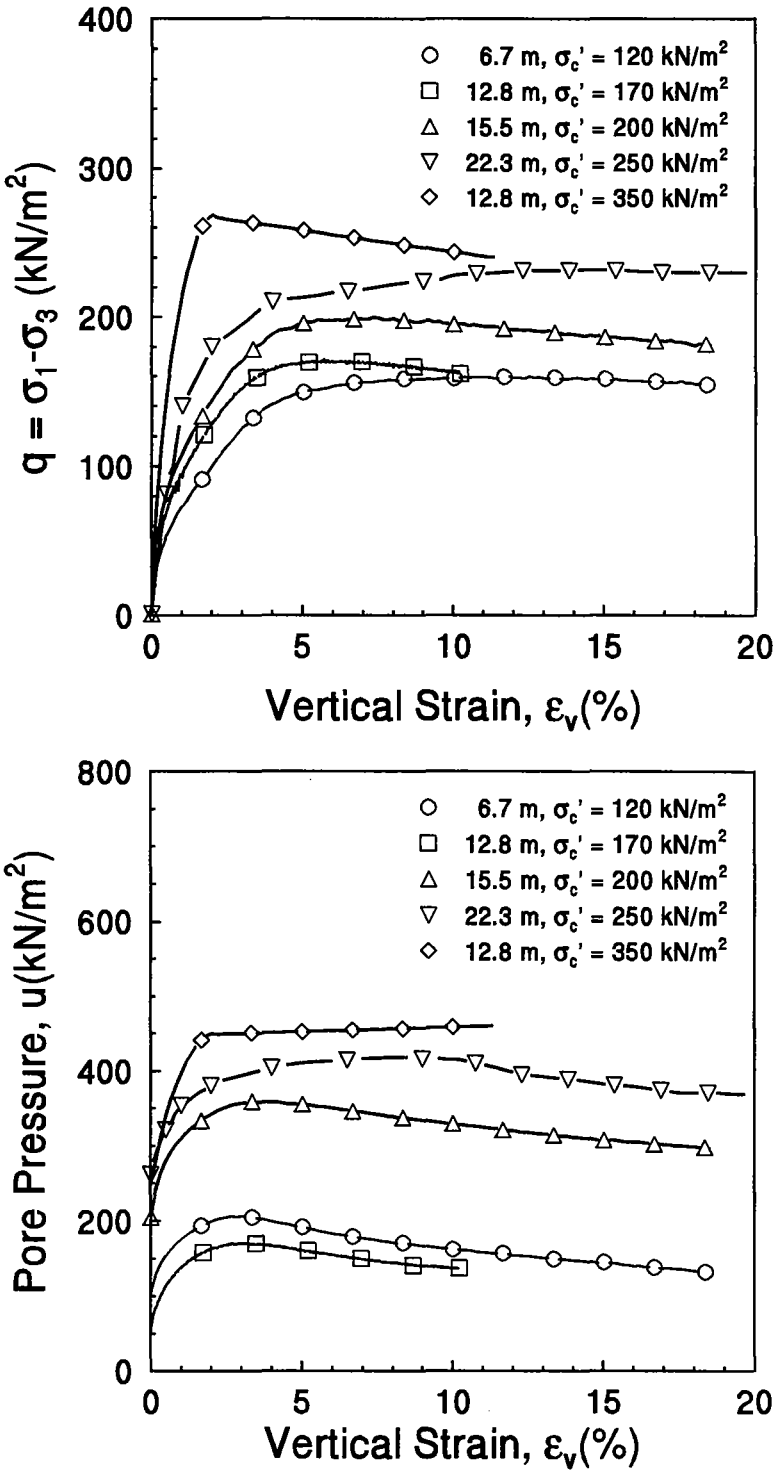

Figure 4.25. Stress-Strain Curves and Excess Pore Water Pressure Versus Strain Relationships for CIUC Triaxial Tests on Specimens from Baton Rouge Site.

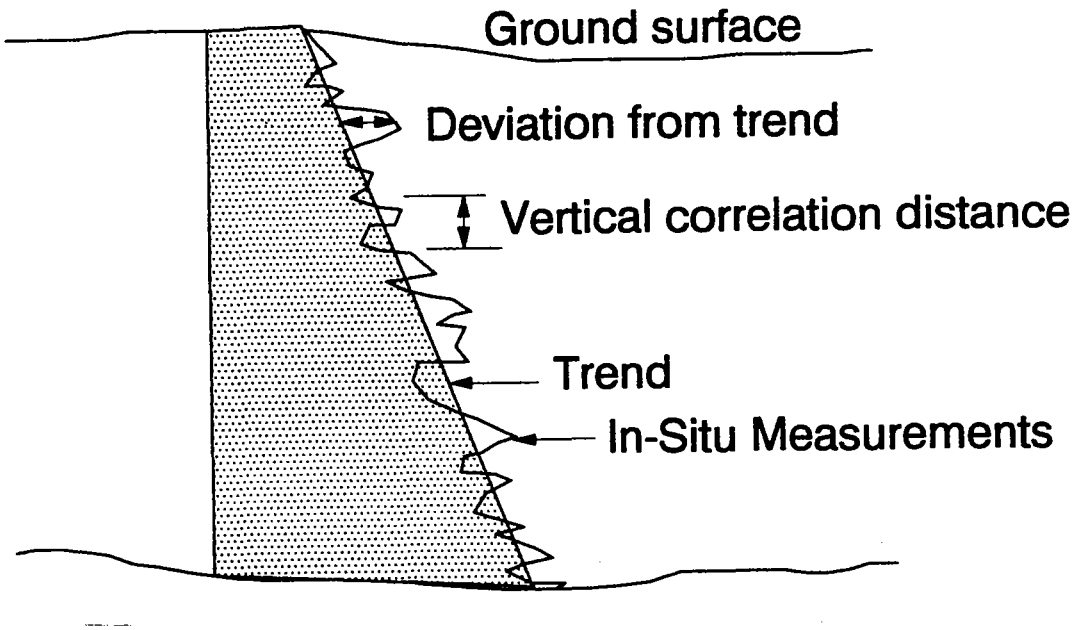

Figure 4.26. In-Situ Measurement Profile Showing Trend and Inherent Variability.

filter, sensitivity of the load cell, and other electro-mechanical factors. Before attempting an assessment of any given soil property from the results of in-situ tests, it is therefore necessary to sort out the irrelevant variations from the actual trend of the results. In the specific approach discussed herein, the raw piezocone data have subsequently been filtered to produce interpreted profiles of OCR that are free from the effects of local variability and measurement errors.

Figure 4.26 shows a hypothetical soil profile with property variations incurred because of the aforementioned causes. In a probabilistic soil profile, an engineering property can be characterized by two components. The first is a smoothly varying deterministic trend, representing changes in the average value of the soil property with depth. The second represents the local deviations about this trend, representing the natural geologic variability of the soil. Alternatively, the variability of a soil profile can be

described by the correlation distance of the soil property (Kulhawy et al. 1992). The correlation distance (δ_v) is the distance within which the local deviations from the trend show a strong correlation from point to point. Usually, soil properties are assumed to be perfectly correlated within the correlation distance and uncorrelated outside the correlation distance. The correlation distance can be determined from the autocorrelation function. In a highly variable profile, the autocorrelation function dissipates quickly, resulting in a small correlation distance. Conversely, in a relatively homogeneous profile, the dissipation is slow, resulting in a large correlation distance.

Kulhawy et al. (1992) determined the best estimates for the downhole trend of corrected cone tip resistances in a reliability-based evaluation of clay strength from the cone penetration test. The smoothing technique was based on the vertical correlation distance (δ_v) resulting from the study of autocorrelation functions. For the natural clay deposits considered, δ_v ranged from 0.19 m to 0.49 m. The relatively homogeneous clays (Glava, Anacostia, and San Francisco) had the largest correlation distances, ranging from 0.40 m to 0.49 m. The very heterogeneous, very sandy, and fissured clays (Yorktown and Brent Cross) had the smallest correlation distances, ranging from 0.19 m to 0.23 m. For sensitive clays (Arnprior and Ottawa), δ_v ranged from 0.26 m to 0.30 m. Overall, the average vertical correlation distance was 0.31 m.

In this study, raw piezocone measurements (q_T, u_1, and u_2) were processed in several different manners depending upon the degree of variability in the test results. For homogeneous clay deposits that exhibit little variations in raw measurements, no smoothing and filtering processes were required. Example of this is shown in Figure 4.27 for the data from soft clay at Backböl, Sweden.

For a complex and structured material that presents significant variability with the depth, a "moving average" technique was employed. This averaging approach is based upon the representative vertical correlation distance of 0.31 meters determined by Kulhawy et al. (1992). Using data from the structured St. Jean Vianney clay site in Quebec, an example of this smoothing trend is depicted in Figure 4.28.

In some cases the raw piezocone measurements display a general trend with depth but show occasional spikes in q_T (usually with associated decays in pore pressures) because

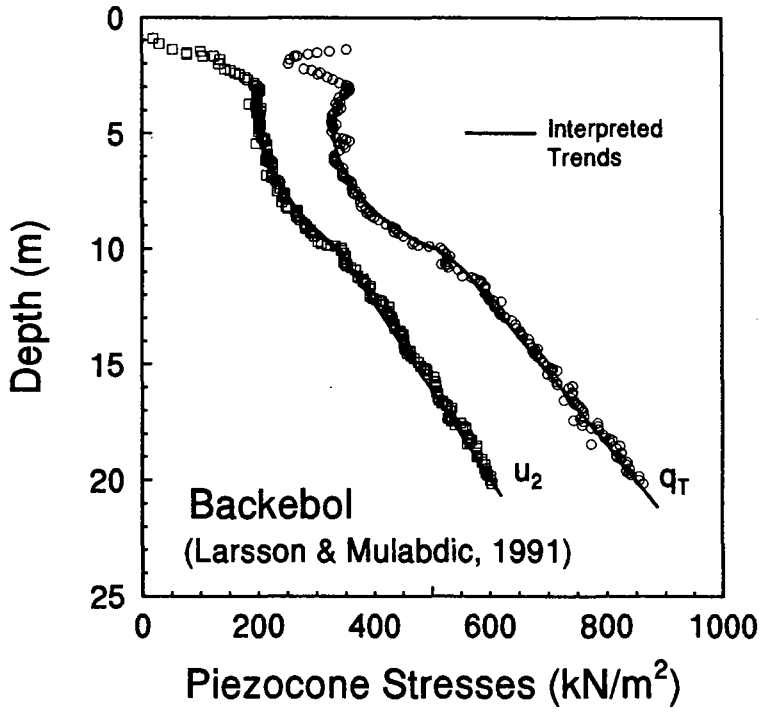

Figure 4.27. Example Piezocone Measurements in a Homogeneous Clay Deposit.

of interbedded silts and sand layers or seams. In this case, the "moving average" technique is not appropriate since it tends to distort the trend and result in misleading interpretations of given soil properties. A rational approach is to filter out the spikes in q_T (and/or penetration in pore pressures) and retain the remaining data which represent the actual trend of the measurements. Here, an example is illustrated using data from the Keelung River site in Taiwan in Figure 4.29.

In the cases where the "moving average" technique has been employed, raw piezocone data within the depth interval of 0.31 m were averaged and plotted for indicating the trends. For the cases shown, a curve-fitting method was then imposed on the interpreted profile to obtain a trend of OCR, since the actual OCR profiles are more likely to have a gradual trend than an erratic profile reflecting other factors causing variability of the piezocone measurements. In some instances, it was necessary to use combined functions,

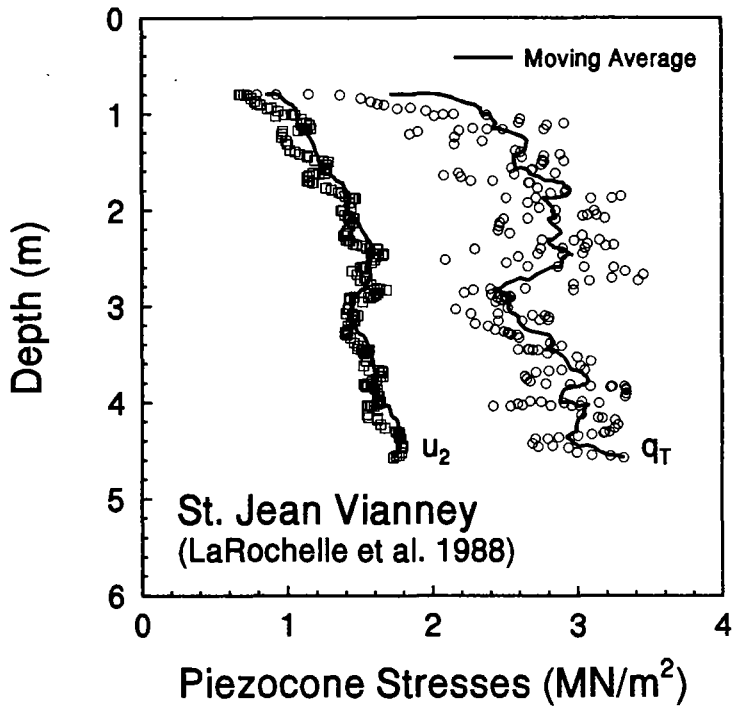

Figure 4.28. Example of Variable Piezocone Measurements in a Complex, Structured Clay.

or separate layered interpretations due to the actual complexities in the stress history profile of the site. These methodologies described in this section will be used in subsequent chapters for the interpretation of OCR profiles from piezocone data and comparison with others from reference oedometer tests.

4.4. Summary of Field Testing Programs

Piezocone penetration tests were conducted at two test sites: (1) a lightly overconsolidated lean glacial lacustrine clay in Port Huron, Michigan, and (2) a moderately overconsolidated plastic deltaic clay in Baton Rouge, Louisiana.

At Port Huron, paired sets of both types of piezocone penetrometers were used to obtain different pore pressure responses. A complex OCR profile indicated a layered

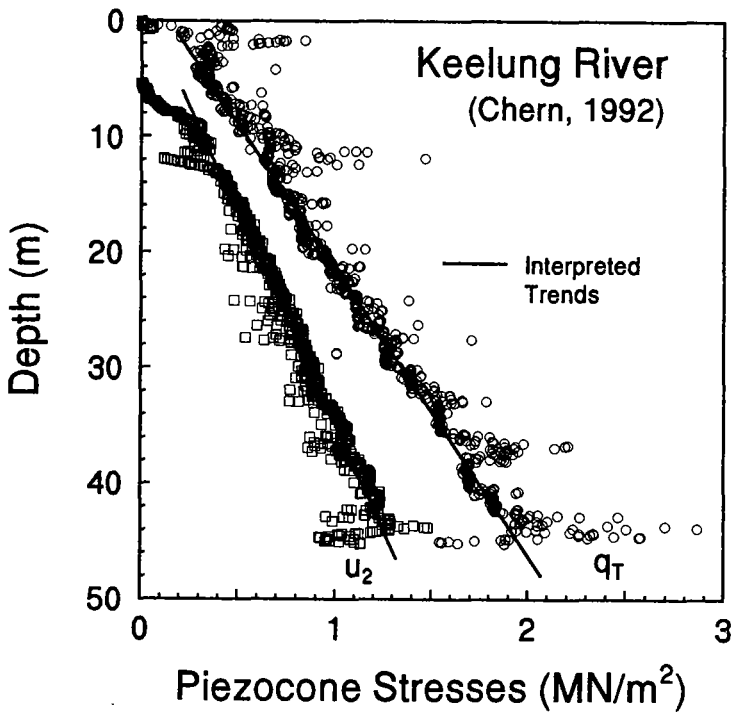

Figure 4.29. Example of Variable Piezocone Measurements in a Clay Matrix with Interbedded Macrofabric of Silt and Sand Layers or Seams.

deposit, possibly due to various stages of loading and unloading sequences during deposition. The range of OCRs varied from 1 to about 5 at this site.

At Baton Rouge, dual- and triple-element piezocones were used to obtain penetration pore pressures u_1, u_2, and u_3. Soil samples were retrieved from the site for laboratory testing at Georgia Tech. A relatively constant value of preconsolidation pressure was obtained from the laboratory consolidation testing on samples taken from a range of depths of up to 34 meters. Desiccation caused much of the observed overconsolidation of the Baton Rouge clay resulting in $5 < \text{OCRs} < 15$.

CHAPTER 5

AN INITIAL PIEZOCONE MODEL FOR PREDICTING OCR IN CLAYS

The practical problem of determining the in-situ stress history of soils requires an approach based upon physical reasoning, theoretical soil mechanics principles, and normalized engineering parameters (Wroth 1988). The method should also be calibrated for a variety of known conditions to examine its merits and possible shortcomings. The procedures for data reduction should be stated simply, if possible, so that a minimal number of soil constants are required for implementation and thus encouraging its routine use by practicing engineers.

As noted previously, several theoretical models have been proposed for profiling the yield stress (σ_p') of clays by piezocone penetration tests (PCPT). Konrad and Law (1987) developed an effective stress analysis for Type 1 cones that was calibrated with data from 5 sensitive Canadian clays. Senneset et al. (1989) utilized plasticity theory for deriving a Type 2 cone interpretation, which was evaluated with data from 7 Norwegian soils (Sandven 1990). Whittle and Aubeny (1993) used a sophisticated constitutive soil model (MIT-E3) coupled with numerical strain path analyses to evaluate OCR from PCPT data in Boston Blue Clay. Empirical methodologies have also been developed from PCPT data compiled from a limited selection of sites and sources (Sully et al. 1988a, 1988b; Rad and Lunne 1988; Larsson and Mulabdic 1990). This chapter describes a simple piezocone model that has been derived from an approximate theoretical basis, has been more extensively calibrated than any other model to date, and addresses both Type 1 and 2 pore pressure measurements. It is the intent of this chapter to review its primary features and applications.

5.1 Model Development

The piezocone model utilizes both cavity expansion theory (Vesić 1972, 1977) and Modified Cam Clay (Wroth 1984; Wroth and Houlsby 1985) to interrelate stress history with cone tip resistance (q_T) and penetration pore water pressure (u_1 or u_2) in clay. The basic

assumptions taken and evolutionary chart of the model development are summarized in Figure 5.1. An iterative approach to the problem has been adopted to attempt to balance theory and experimental field test results (Mayne 1991, 1992, 1993; Mayne and Chen 1994). In the version of the model described in this chapter, no attempt has been made to account for the effects of initial stress state ($K_o = \sigma_{ho}'/\sigma_{vo}'$), strength anisotropy, stress rotation, or strain rate, although each of these is recognized to be important in clay behavior. An improved version of the model will be introduced later in Chapter 7, in which some of these effects will be investigated. A more rigorous approach could be developed to accommodate strain fields (Acar and Tumay 1986) or strain paths (Baligh 1986), as well as more generalized constitutive soil models that better address anisotropy and rotation effects (Whittle and Aubeny 1993). However, these added complexities would also undoubtably result in more encumbered expressions than the simple approaches discussed herein.

For clay under an initial isotropic state of stress, spherical cavity expansion (SCE) theory combined with considerations of the conservation of energy law (Vesić 1977) states that:

$$q_T - p_o = s_u \left[\frac{4}{3}(\ln I_r + 1) + \frac{\pi}{2} + 1\right] \qquad [5.1]$$

where q_T = corrected cone tip resistance, p_o = total overburden stress, s_u = undrained shear strength, $I_r = G/s_u$ = rigidity index, and G = shear modulus of the clay. The excess pore pressures induced solely by changes in the octahedral normal stress are also obtained from spherical cavity expansion (Vesić 1972):

$$\Delta u_{oct} = \frac{4}{3} s_u (\ln I_r + 1) \qquad [5.2]$$

To relate s_u to OCR, Modified Cam Clay (MCC) concepts are invoked (Wroth, 1984):

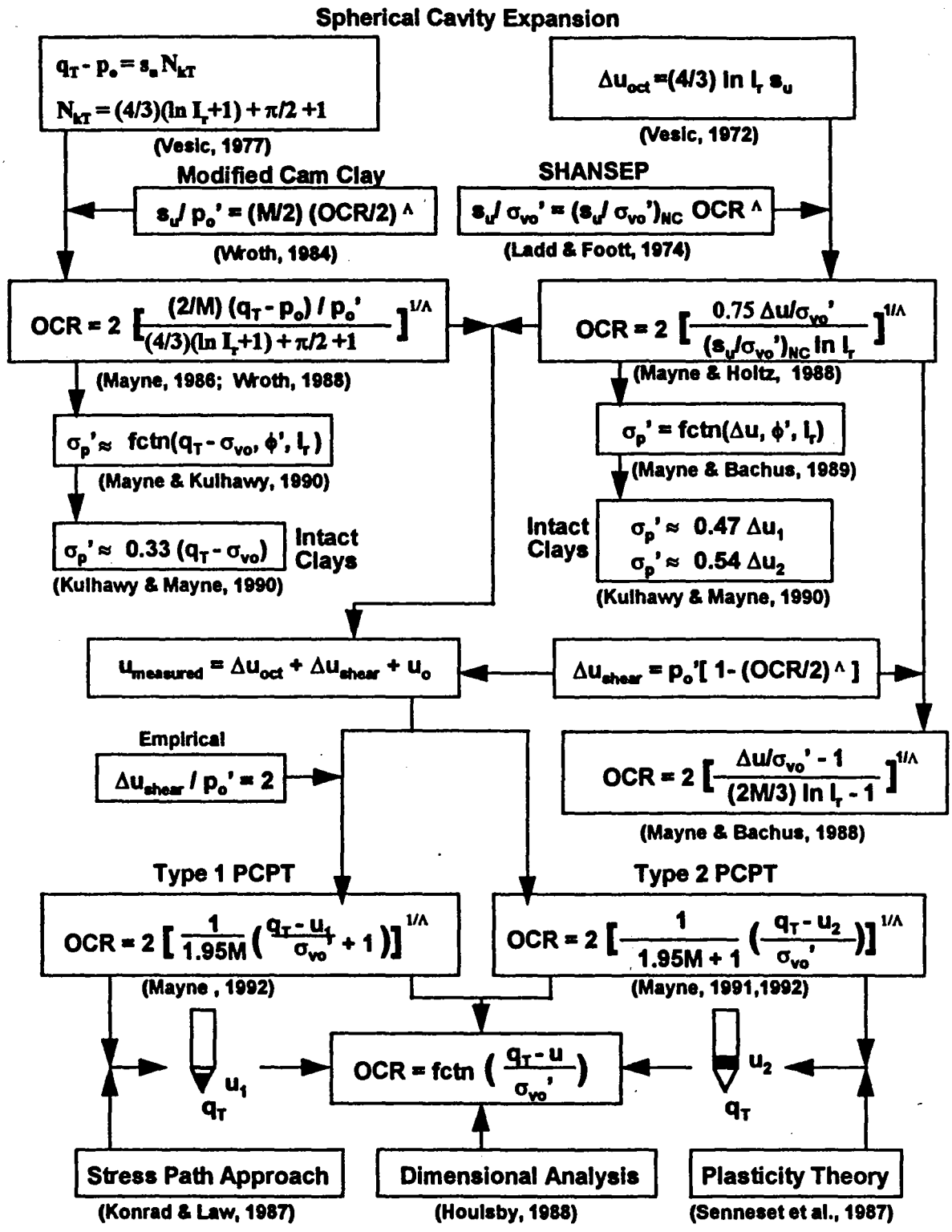

Figure 5.1 Chronology and Evaluation of Cavity Expansion/Critical State Piezocone Model.

$$\frac{s_u}{\sigma'_{vo}} = \frac{M}{2}\left(\frac{OCR}{2}\right)^{\Lambda} \qquad [5.3]$$

where $M = 6\sin\phi'/(3-\sin\phi')$, ϕ' = effective stress friction angle, Λ = plastic volumetric strain ratio = $1-\kappa/\lambda$, κ = isotropic swelling index, and λ = isotropic virgin compression index.

The measured excess pore water pressures (Δu_m) induced by an advancing probe are due to a combination of changes in octahedral normal and shear stresses:

$$\Delta u_m = \Delta u_{oct} + \Delta u_{shear} \qquad [5.4]$$

While it is not possible to decouple field measurements of Δu into these components, a theoretical separation is possible. One premise of the original SCE/MCC model was that shear-induced pore pressures were negligible, so that $\Delta u_m \approx \Delta u_{oct}$ (Mayne, 1991). This made for an easy formulation, such that:

$$OCR = 2\left[\frac{1}{1.95M}\left(\frac{q_T - u_m}{p'_o} - 1\right)\right]^{1/\Lambda} \qquad [5.5]$$

The parameter Λ is essentially constant for natural intact and uncemented clays and averages about 0.75, 0.80, and 0.85 for compression, simple shear, and extension modes, respectively (Mayne 1988; Wroth 1984; Kulhawy and Mayne 1990). A value $\Lambda = 0.75$ has been adopted herein, corresponding to triaxial compression test results on insensitive and unstructured sedimentary clays. In certain structured and cemented materials, however, the

value of Λ may be as high as 1.0, as indicated by Table 5.1 (Brown and Mayne 1993).

An interesting feature of Eq. [5.5] is that the derived piezocone parameter, $(q_T-u_m)/p_o'$, is also compatible with a normalized formulation of the Konrad and Law (1987) model, as shown by Robertson et al. (1988), as well as a suitable parameter obtained from dimensional analysis (Houlsby, 1988). Database calibration efforts using Type 1

Table 5.1 Applicable Values of Λ for Different Types of Clay in Triaxial Compression.

Clay Type	Example	Parameter Λ	Reference
Laboratory Remolded	Weald Clay, U.K.	0.624	Wroth and Houlsby (1985)
Natural, Intact	Boston Blue Clay, Massachusetts	0.777	Ladd and Foott (1974)
Laboratory, Slurry (or Resedimented)	Kaolinitic Clay	0.782	Mayne (1993)
Structured, Sensitive, Marine	Saint Alban, Quebec	0.972	Tavenas, et al. (1978)

cones with Eq. [5.5] indicated that reasonable predictions of OCR were afforded in heavily overconsolidated clays, but in soft normally-consolidated deposits the profiles of OCR were severely underestimated. For a general predictive capability, the inclusion of a shear-induced pore pressure term was deemed necessary, resulting in the adoption of the following:

$$\text{Type 1:} \qquad \Delta u_{shear} = 2p_o' \qquad [5.6a]$$

$$\text{Type 2:} \qquad \Delta u_{shear} = p_o'[1 - (OCR/2)]^{\Lambda} \qquad [5.6b]$$

where Modified Cam Clay provides the expression for Type 2 cones (Wroth 1984) and the approximate relationship given for Type 1 cones is empirical but similar to that obtained for a total stress path derived from elastic theory under a rigid circular loading.

By adopting a value of $\Lambda = 0.75$ and allowing $p_o' \approx \sigma_{vo}'$, the forms of the predictive model become:

$$\text{Type 1:} \quad OCR = 2\left[\frac{1}{1.95M}\left(\frac{q_T - u_1}{\sigma'_{vo}} + 1\right)\right]^{1.33} \qquad [5.7a]$$

$$\text{Type 2:} \quad OCR = 2\left[\frac{1}{1.95M+1}\left(\frac{q_T - u_2}{\sigma'_{vo}}\right)\right]^{1.33} \qquad [5.7b]$$

For values of $\phi' = 20°$, 30°, and 40°, the corresponding values of M are 0.77, 1.20, and 1.63, respectively. The full observed range of ϕ' for natural clays appears to be $17° \leq \phi' \leq 43°$ (Diaz-Rodriquez et al. 1992) and the relevant ϕ' should be ideally determined from consolidated triaxial tests conducted on high quality samples, or possibly, from slow drained direct shear box tests. It should further be noted that, for Type 1 piezocones, there exists some uncertainty in the actual magnitudes of q_T resistances since the u_2 measurement is required for proper correction. This is particularly true in soft clays, since the difference between point resistance and pore water pressure (q_T-u_1) is often rather small. Unfortunately, a conversion from u_1 to u_2 is not particularly straightforward (Powell et al. 1988 and Mayne et al. 1990).

The parametric influence of ϕ' on the predicted stress history profile is illustrated in Figure 5.2(a) for Type 2 piezocone data in soft clay at the Lower 232nd Street site (Campanella et al. 1988). The deposit consists of a sensitive glacial marine clay (PI = 19, $S_t \approx 12$). At this site, reference values of yield stress (σ_p') from oedometer tests were supplemented by results from flat dilatometer tests.

The parametric effect of Λ on the predictions is presented in Figure 5.2(b) using Type piezocone data at the St. Hilaire site in Quebec (LaFleur et al. 1988). The estimated profile of σ_p' shows no more uncertainty than the oedometer results on high quality samples of the sensitive clay (PI = 40, $S_t \approx 14$). For this marine deposit which is likely structured, a value

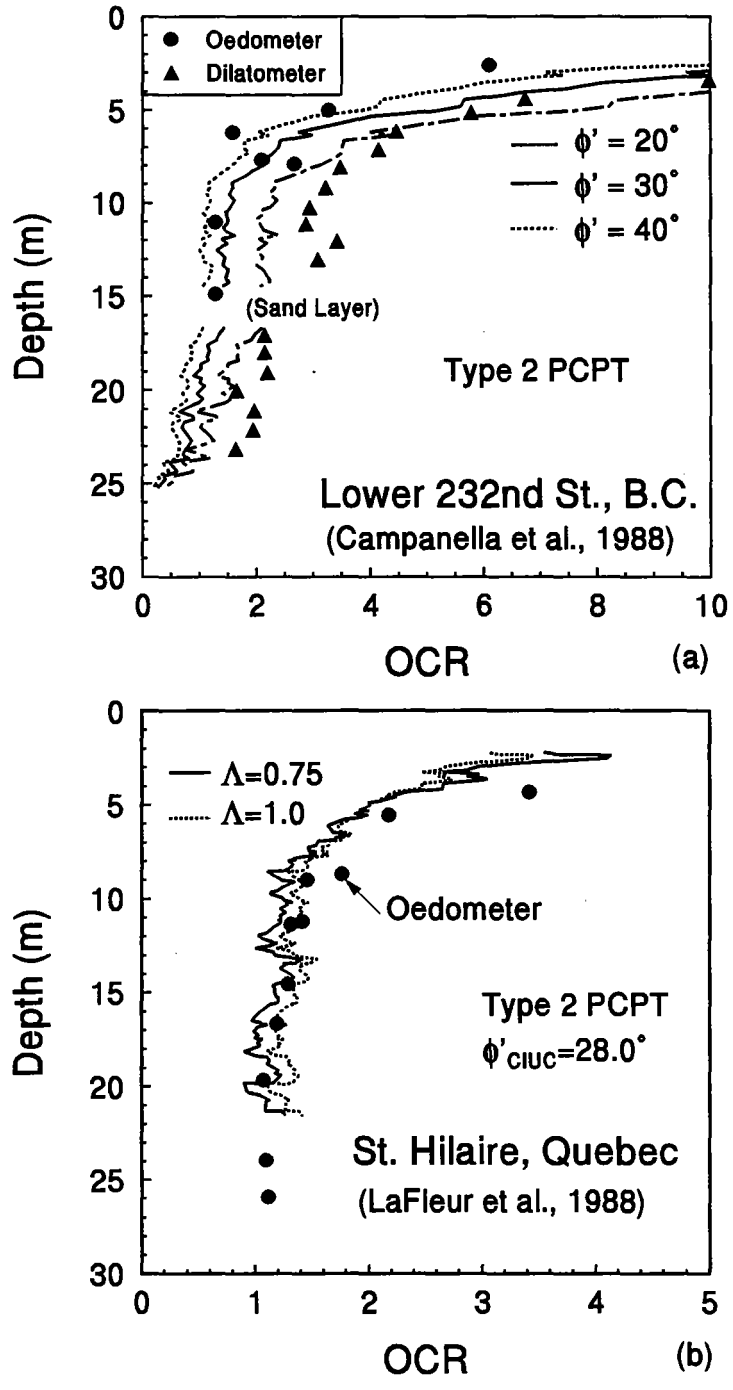

Figure 5.2. Parametric Effect of (a) Effective Stress Friction Angle (ϕ') and (b) Plastic Volumetric Strain Ratio (Λ).

of $\Lambda = 1$ may be more appropriate, particularly for predictions at depths exceeding 16 meters. In fact, for structured clays having $\Lambda = 1$, the versions of Eqs. [5.7] become:

$$\text{Type 1:} \quad \sigma_p' = \frac{6 - 2\sin\phi'}{11.7\sin\phi'} (q_T - u_1 + \sigma_{vo}') \qquad [5.8a]$$

$$\text{Type 2:} \quad \sigma_p' = \frac{6 - 2\sin\phi'}{3 + 10.7\sin\phi'} (q_T - u_2) \qquad [5.8b]$$

Furthermore, Eq. [5.8b] reduces to the form: $\sigma_p' = 0.6(q_T - u_2)$ for the case where $\phi' = 30°$. This format is quite similar to that derived by Senneset, et al. (1989) from plasticity theory considerations. Since the MCC formulation is actually an effective stress method that encompasses total stress behavior, the model can alternatively be represented by:

$$\text{Type 1:} \quad OCR = 2 \left[\frac{1}{6.56(s_u / \sigma_{vnc}')} \left(\frac{q_T - u_1}{\sigma_{vo}'} + 1 \right) \right]^{1.33} \qquad [5.9a]$$

$$\text{Type 2:} \quad OCR = 2 \left[\frac{1}{6.56(s_u / \sigma_{vnc}')+1} \left(\frac{q_T - u_2}{\sigma_{vo}'} \right) \right]^{1.33} \qquad [5.9b]$$

where (s_u/σ_{vnc}') is the normalized undrained shear strength to effective overburden ratio for

normally consolidated clay (OCR = 1) corresponding to triaxial compression loading. Eq. [5.9] is offered as a total stress solution to the problem, in lieu of inputting ϕ' as a parameter.

As dual-element and triple-element piezocones become more popular, the development of a model incorporating several simultaneous measurements (q_T, u_1, u_2, u_3) for profiling the stress history of clay deposits appears attractive, especially if ϕ' is not needed. In this regard, an attempt to combine the preliminary Eqs. [5.7a] and [5.7b] to remove ϕ' (or M), resulted in:

$$OCR = 2 \left[\left(\frac{u_1 - u_2}{\sigma'_{vo}} \right) - 1 \right]^{1.33} \qquad [5.10]$$

It is noted that q_t also vanishes (unfortunately) and the prediction becomes solely a function of the parameter $(u_1-u_2)/\sigma_{vo}'$. Also interesting is that this parameter has been independently suggested by Sully and Campanella (1990) and Larsson and Mulabdić (1991), but only from an empirical basis. It appears prudent to retain q_t in the theoretical derivation, however, because a more stable profile of OCR is obtained.

5.2 Applications to Laboratory Data

The initial SCE/MCC method has been applied with reasonable success to cone penetration data from laboratory chamber tests, using both fixed- and flexible-walled systems, as discussed subsequently.

5.2.1. Fixed-Wall Chamber Tests

Measurements from a laboratory series of miniature electric cone (23 mm diameter) and piezoprobe (19 mm diameter) soundings have been carried out in deposits of kaolinitic clay prepared in a large fixed-wall steel chamber (Mayne 1993). The lean clay was initially

prestressed under one-dimensional conditions at $\Delta\sigma_v$ = 48 kPa using pneumatic pressure and a rigid piston system. Consolidation tests verified that the intended preconsolidation stresses were obtained. After primary consolidation, the deposit was rebounded to atmospheric pressure to form an overconsolidated profile. Index parameters for the clay included: w_n = 34.4%, LL = 33, PI = 11, CF = 33, G_s = 2.65, and D_{50} = 6μ. Isotropically-consolidated undrained triaxial compression tests with pore pressure measurements indicated ϕ' = 33.5° (or M = 1.35) and plastic volumetric strain ratio Λ = 0.78.

Results of the miniature cone and penetration pore pressure measurements form the equivalent of a composite Type 2 piezocone sounding. The predicted OCR profile is presented in Figure 5.3(a) and indicates rather good agreement with the known stress history.

5.2.3. Flexible-Wall Chamber Tests

Kurup (1993) and Kurup, et al. (1994) reported the results of miniature (11 mm diameter) piezocone tests on laboratory kaolin in a pressurized chamber with independent control of vertical and horizontal stresses. Figure 5.3(b) shows the PCPT predictions for an overconsolidated specimen (OCR = 5) subjected to an effective vertical confining stress σ_{vc}' = 41.4 kPa, backpressure of 138 kPa, and final applied consolidation ratio, K_c = $\sigma_{hc}'/\sigma_{vc}'$ = 1 prior to penetration. In these tests, the chamber pressures are maintained constant during penetration. The results indicate the Type 2 model prediction agrees fairly well with the induced OCR profile in these pressured chamber tests on K50 kaolin.

5.3 Applications to Field Test Data

A significant number of clay sites worldwide exist already with reference oedometric profiles of OCR and piezocone test data for model verification. The database has been described previously in Chapter 3. A total of 16 sites have been selected for verification and relevant information on these sites is available in Table 5.2.

5.3.1. Type 1 Piezocone Sites

Measured and predicted profiles of OCR for four clay sites tested by Type 1 PCPTs

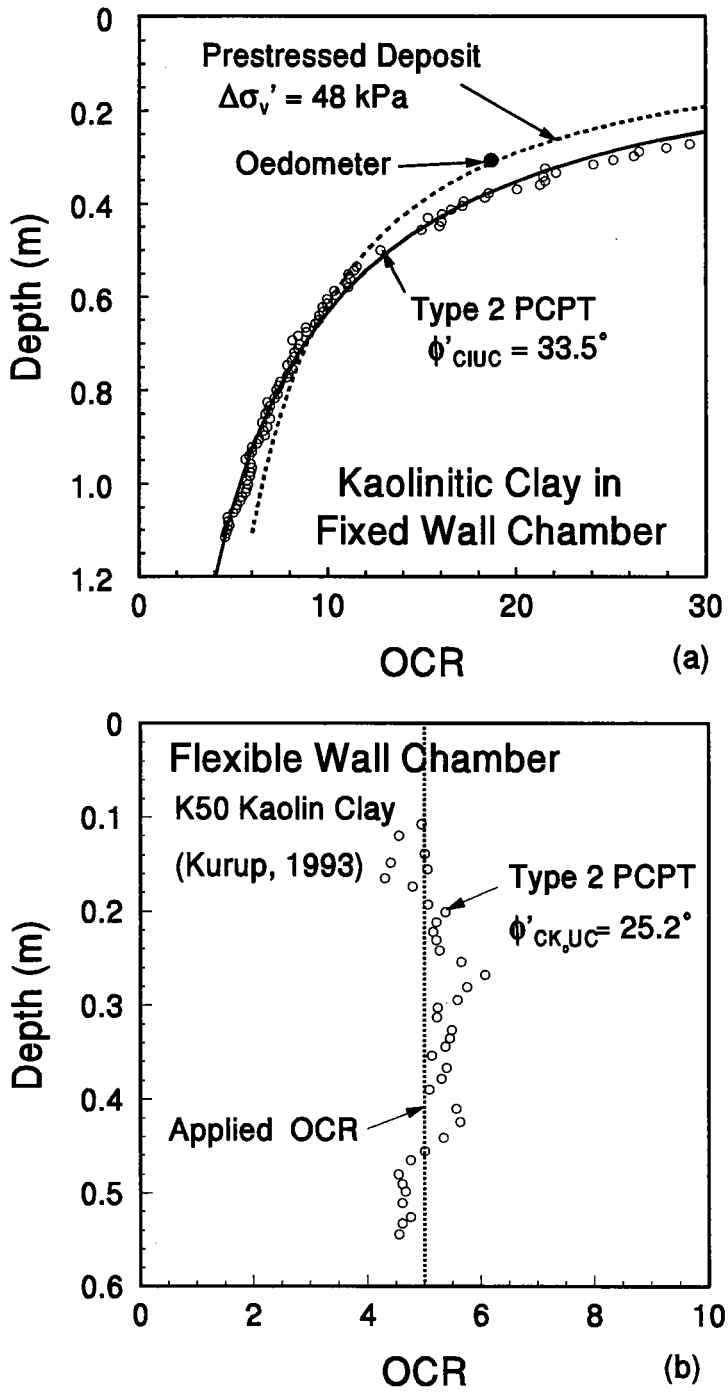

Figure 5.3. PCPT-OCR Model Predictions for (a) Depressurized Fixed-Walled Chamber Tests and (b) Pressurized Flexible-Walled Chamber Tests.

Table 5.2. Summary of Piezocone Clay Sites and Relevant Information.

Site	Description	w_n	LL	PI	S_t	OCR	ϕ'	Reference
Baton Rouge, Louisiana	stiff, fissured	35	58	30	NA	3-15	28°	Chen (1994)
Bowie, Maryland	hard, fissured	23	47	25	NA	2-9	25°	Franz & Hull (1993)
Brent Cross, U.K.	London, fissured	29	75	50	NA	25-80	20°	Lunne et al. (1986)
Chek Lap Kok, H. K.	soft, marine	70	70	40	4-15	1-12	28°	Koutsoftas et al. (1987)
Evanston, Illinois	soft, glacial	23	37	18	2	1-2	26.9°	Finno (1989)
Site GC, North Sea	marine, offshore	46	39	22	-	1.5-3	36°	Skomedal & Bayne (1988)
Haga, Norway	stiff, sensitive	35	41	15	4-7	2-15	30.2°	Lunne et al. (1986)
Kringalik Plateau, Arctic	stiff, offshore	30	42	23	-	3-9	32°	Hughes et al. (1984)
Lower 232nd St, B.C.	silty, glacial	45	40	19	11	1-2	-	Campanella et al. (1988)
Muni Metro, California	recent Bay Mud	55	65	30	2-7	1-1.5	29°	Koutsoftas (1989)
NRCC, Ontario	sensitive, Leda	80	66	35	200	1.5-4	30°	Konrad & Law (1987)
Port Huron, Michigan	glacial/lacustrine	22	35	15	-	1-4	27°	Chen (1994)
Ska Edeby, Sweden	organic, varved	80	85	50	15	1-1.3	30°	Larsson & Mulabdic (1991)
St. Hilaire, Quebec	sensitive, Leda	60	60	35	12-16	1-2	28°	LaFleur et al. (1988)
St. Jean Vianney, Quebec	sensitive, Leda	47	31	8	500+	25-50	40°	LaRochelle et al. (1988)
Taranto, Italy	hard, cemented	23	60	27	NA	20-40	28°	Battaglio et al. (1986)
Fixed Wall Chamber	kaolinitic clay	34	33	11	1.5	6-30	33.5°	Mayne (1993)
Flexible Wall Chamber	kaolinitic clay	24	30	14	-	5	25.2°	Kurup (1993)

Notes: NA - Not Applicable

are presented in Figure 5.4 including: (a) soft Chicago glacial clay bed along the western shores of Lake Michigan serving as part of a deep foundation experimental test site (Finno 1989); (b) recent Bay Mud in downtown San Francisco for the Muni subway station (Koutsoftas 1989); (c) upper and lower marine clays for the new Hong Kong airport (Koutsoftas et al. 1987); and (d) a desiccated and fissured deposit of Pleistocene clay off I-10 in Baton Rouge recently tested by the authors. In each case, some degree of variability is observed for the reference OCR profile obtained from consolidation tests. Overall, the general trends and approximate magnitudes of the PCPT-predicted OCRs are in agreement with the oedometer results.

5.3.2. Type 2 Piezocone Sites

Results of the model application for clays tested by Type 2 PCPTs are presented in Figure 5.5 for the following: (a) very soft slightly organic sensitive glacial clay at the

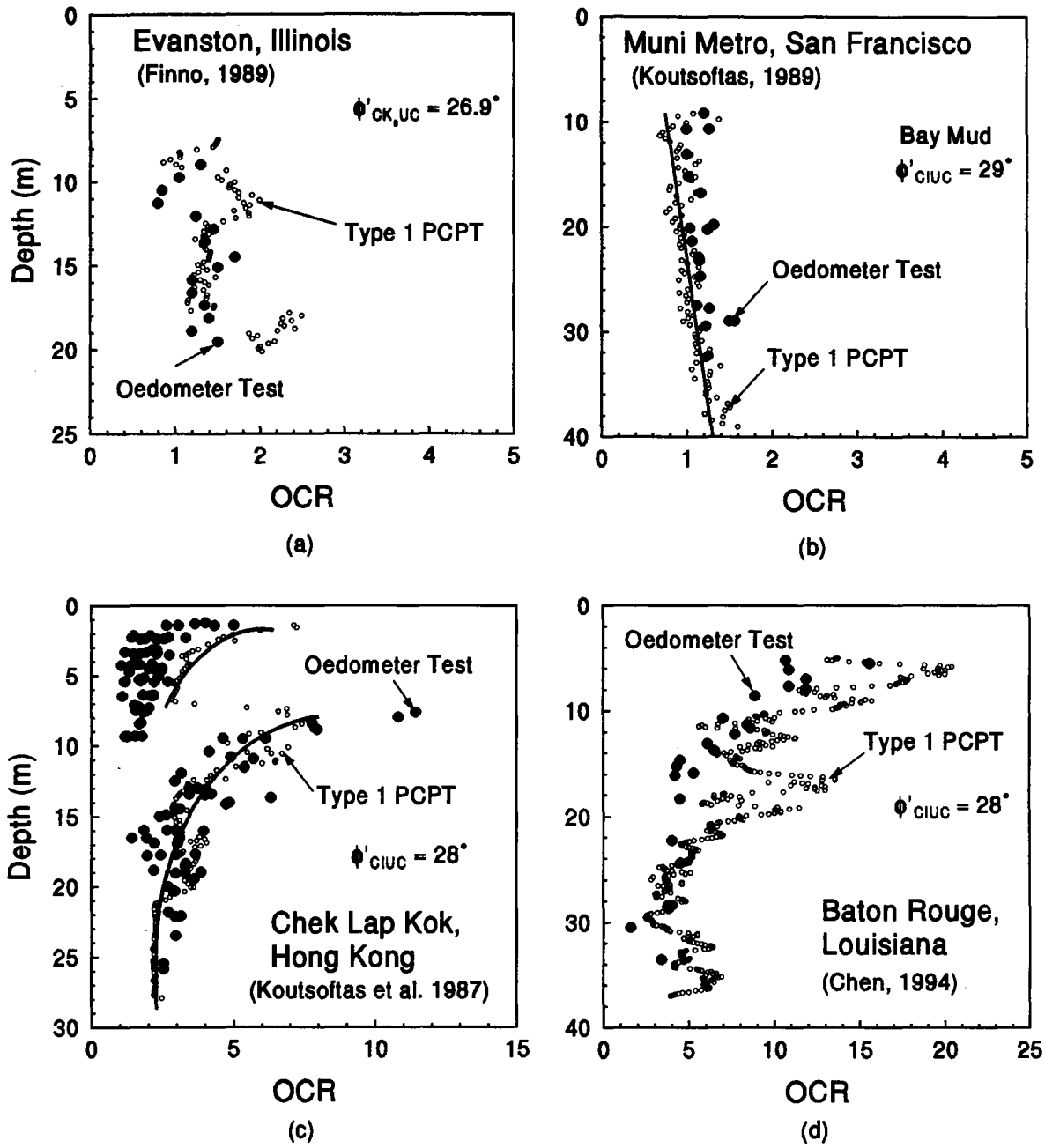

Figure 5.4. Measured and Estimated OCRs for Type 1 Piezocone Sites.

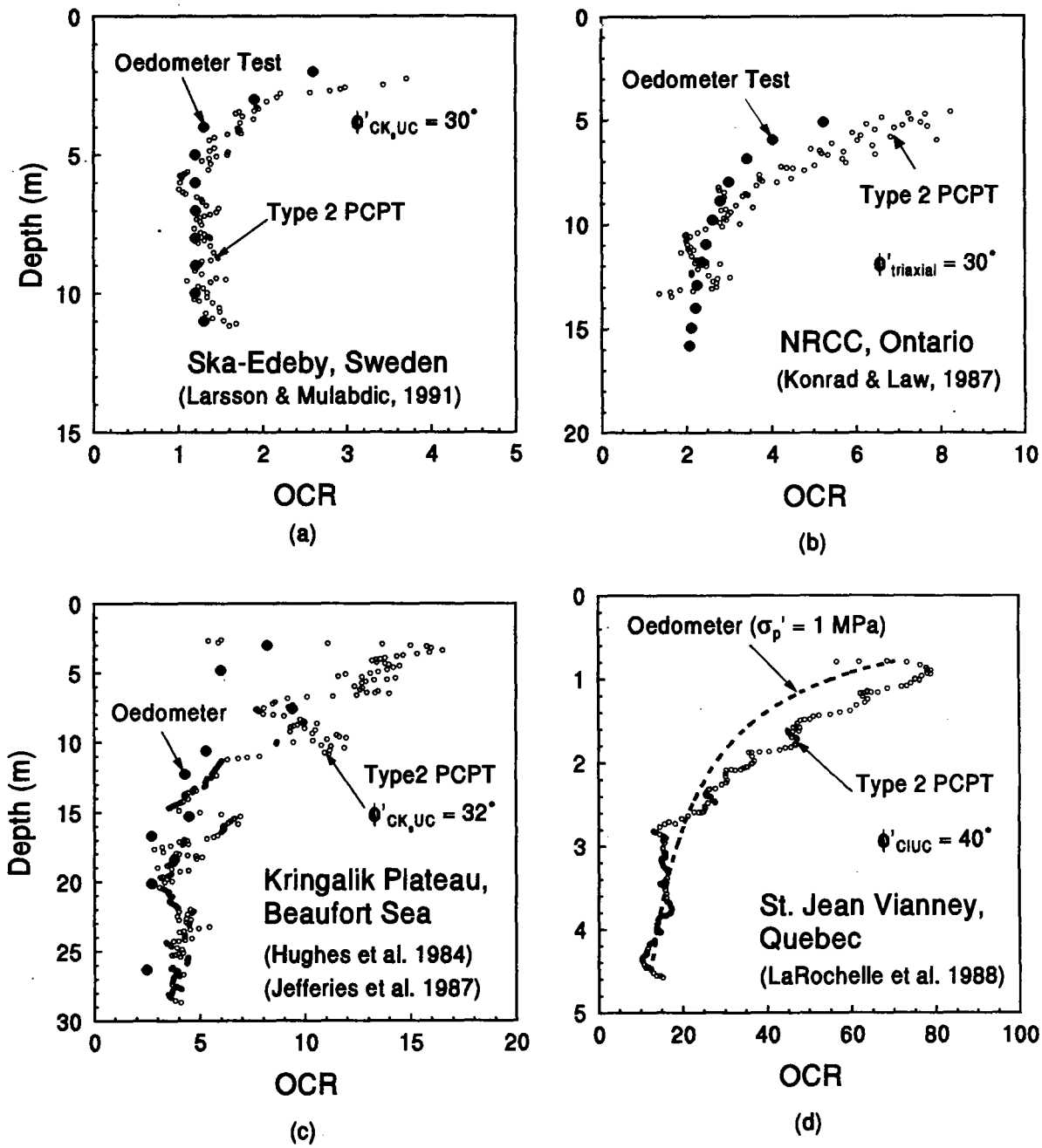

Figure 5.5. Measured and Estimated OCRs for Type 2 Piezocone Sites.

Skå-Edeby site (Larsson and Mulabdić 1991); (b) a highly sensitive Champlain Sea clay at the site of the National Research Council of Canada (NRCC) in Ottawa (Konrad and Law 1987); (c) stiff silty clay from the Kringalik Plateau in the Arctic Beaufort Sea (Hughes et al. 1984; Jefferies et al. 1987); and (d) a highly overconsolidated deposit of very sensitive clay in Quebec (LaRochelle et al. 1988). Quantitative estimates of OCRs for each of these deposits are not exact, but reasonable and comparable.

5.3.3. Sites Tested by Both Piezocone Types

Predictions of OCR using data from both types of piezometric elements are presented for four additional sites in Figure 5.6 including: (a) lightly overconsolidated sandy silty clay in the North Sea (Skomedal and Bayne 1988); (b) medium stiff moderately overconsolidated deposit of lean sensitive clay at Haga, Norway (Gillespie et al. 1984; Lunne et al. 1986a); (c) hard microfissured and cemented clay at Taranto, Italy (Jamiolkowski et al. 1985; Battaglio et al. 1986); and (d) heavily overconsolidated and fissured London clay at Brent Cross (Lunne et al. 1986b). In these cases, relatively good predictions are evident for both Type 1 and 2 piezocones in a variety of clays and covering a wide range of OCRs from about 1 to over 60.

5.3.4. Sites Tested by Both Piezocone Types Using Dual Model

The dual-type piezocone model using Eq. [5.10] has been applied to four additional field cases involving clay deposits where both u_1 and u_2 measurements have been made available, either from parallel soundings of Type 1 and 2 piezocones or by special multiple-element cones.

Figure 5.7(a) shows the results of Eq. [5.10] using data from dual soundings in the soft homogeneous clay (PI = 37, $S_t \sim 8$, $\phi' = 34^o$) at Onsoy, Norway. The PCPT profile are seen to slightly overpredict OCRs in the shallow crustal layer. The interpreted OCRs from a quad-element PCPT sounding in the soft and plastic Guanabara Bay clay (PI = 60, $S_t \sim 4$, $\phi' = 25^o$) in Rio de Janeiro, Brazil are presented in Figure 5.7(b). The application to the stiff and slightly sensitive OC clay at Haga, Norway (PI = 15, $S_t \sim 4$ to 7, $\phi' = 30.2^o$) is shown in Figure 5.7(c). Figure 5.7(d) illustrates the general successful results

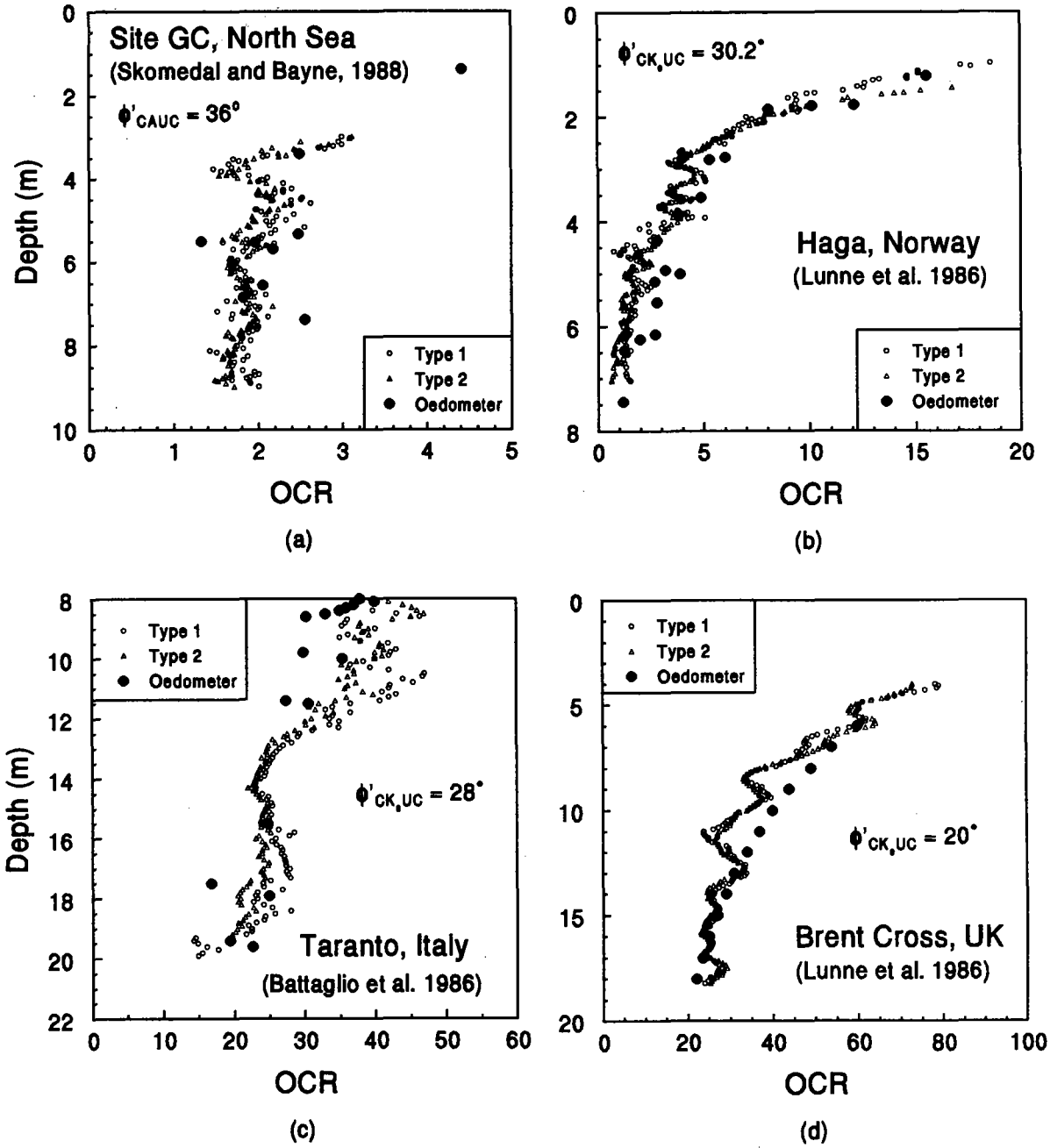

Figure 5.6. Measured and Estimated OCRs for Clay Sites by Both Type 1 and 2 Piezocones.

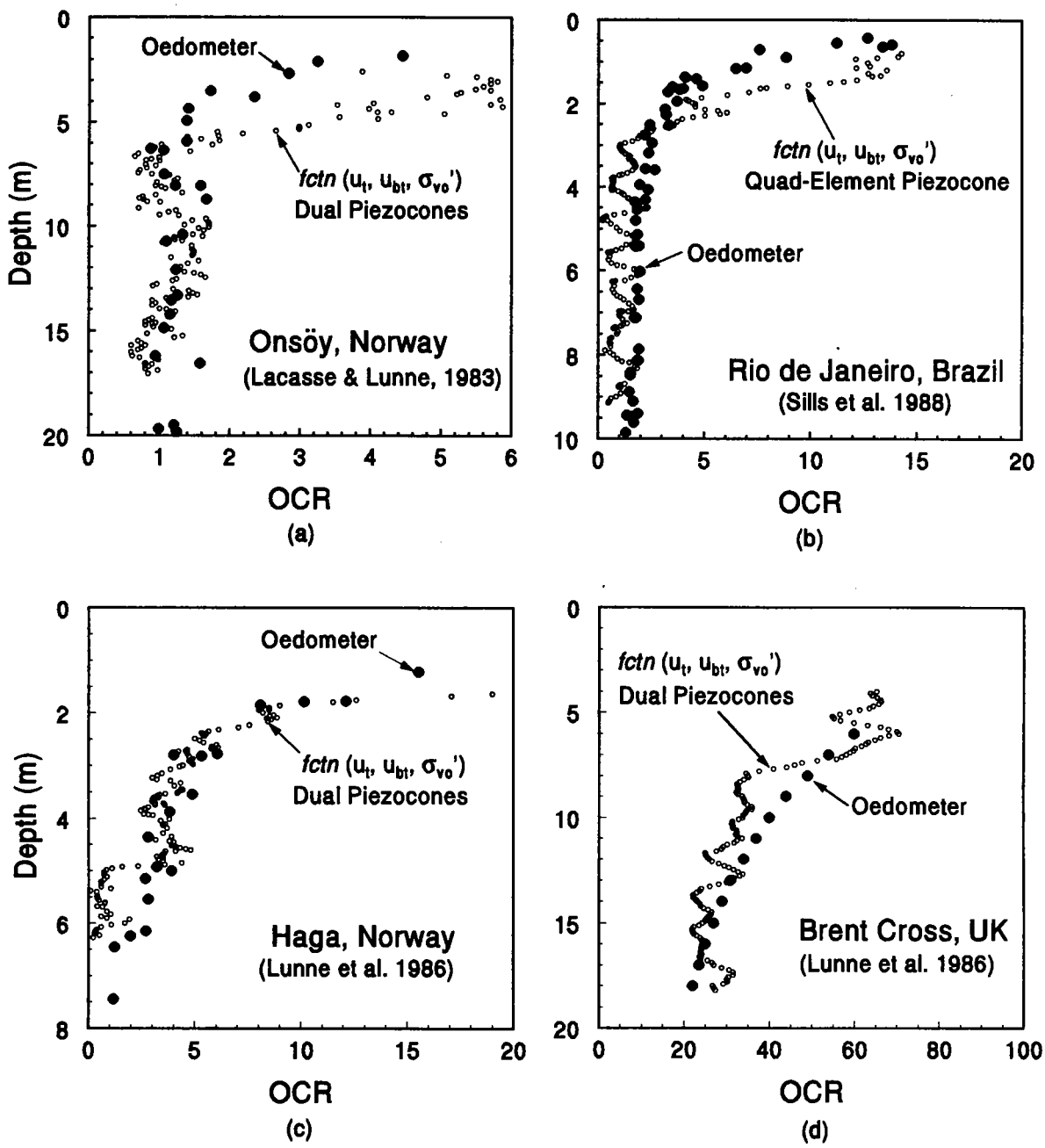

Figure 5.7. Measured and Estimated OCRs for Clay Sites by Both Types of Piezocones Using the Dual Model.

for the heavily OC fissured London clay at Brent Cross, UK (PI = 50, $\phi' = 20^o$). The applicability of Eq. [5.10] to some very sensitive, structural, and cemented clays as northern Quebec (Roy et al 1982; LaRochelle et al. 1988), appears limited, however, since both u_1 and u_2 are relatively close in magnitude and the methodology neglects important factors such as sensitivity, macrofabric, age, etc.

5.4 Conclusions

A simple analytical model for evaluating stress history of clays from piezocone results has been developed for general use by either Type 1 (u_1 on cone face) or Type 2 (u_2 behind cone tip) piezocones. The method is based on a hybrid spherical cavity expansion theory coupled with isotropic Modified Cam Clay and intended as an approximate indicator of in-situ OCR. The SCE/MCC model relates the OCR to the effective friction angle of the clay (ϕ') and normalized cone parameters, $(q_T-u_1)/\sigma_{vo}'$ or $(q_T-u_2)/\sigma_{vo}'$, for Type 1 and Type 2 piezocone, respectively. Combining the formulations for both piezocone types, the reliance on ϕ' vanishes and dual piezocone data is related to OCR via the parameter $(u_1-u_2)/\sigma_{vo}'$. Using a compiled database, piezocone data from many natural and diverse clays worldwide, as well as controlled laboratory deposits of kaolin in fixed- and flexible-walled chambers, have been used to evaluate the predictive quality of OCR in comparisons with values from reference oedometer tests.

CHAPTER 6

PIEZOCONE EVALUATION OF UNDRAINED STRENGTH IN CLAYS

6.1 Traditional Interpretations

The interpretation of undrained shear strength (s_u) using cone penetration test parameters has been investigated since the advent of cone penetrometers. Konrad and Law (1987) provide a review of the primary approaches in this regard. For the conventional mechanical and electric cones, the earliest theoretical derivations assumed a perfectly plastic medium in accordance with classical limit plasticity approaches to interpret s_u from q_c. Later, simple cavity expansion (CE) theories were adopted for determining the cone bearing factor (N_{kT}). Cavity expansion assumes an elastic-plastic medium in either spherical or cylindrical formulations (Vesić 1972). For CE assessment of PCPT data, s_u may be determined from the conventional approach using net cone resistance:

$$s_u = \frac{q_T - \sigma_{vo}}{N_{KT}} \qquad [6.1]$$

or, alternatively, via the excess pore water pressure measurements:

$$s_u = \frac{\Delta u}{N_{\Delta u}} \qquad [6.2]$$

where N_{kT} and $N_{\Delta u}$ are cone bearing factors (Robertson and Campanella, 1983). Both N_{kT} and $N_{\Delta u}$ are functions of the rigidity index, defined as the ratio of shear modulus to shear strength ($I_r=G/s_u$). The magnitude of I_r depends upon the stress level of loading (or strain level), therefore, adding difficulty to the direct interpretation of s_u. For example, Konrad and Law (1987) incorporated spherical cavity expansion theory into an effective frictional model for assessing s_u. In this approach, additional parameters such as soil-steel friction angle (δ), pore water pressure ratio ($\alpha=u_1/u_2$), effective friction angle (ϕ'), and relevant I_r are required, but these parameters are not normally known aprior in routine practice.

In addition to the aforementioned analytical approaches, numerical methods have also been used for determining s_u from cone data. Baligh (1986) and Houlsby and Wroth (1989) considered streamlines of soil flow around the cone utilizing the strain path method. Sandven (1990) used finite elements for the problem. In each of these cases, an appropriate value of N_{kT} must be assigned before s_u can be determined from data. In practice, the value of N_{kT} is estimated from past experience, empirical correlations, as well as from theoretical considerations, and the results are somewhat scattered. Ranges of N_{kT} have been reported in the literature and backcalculated values between 7 and 32 have been noted for a variety of reference s_u tests (Powell and Quarterman 1988; Wroth 1988). Often, a representative value of $N_{kT} = 15$ is adopted for obtaining the average s_u in intact clays.

The actual mechanism for soil failure around a penetrating cone is very complex and offers a great challenge to sophisticated numerical simulation techniques. Nevertheless, solving the problem with a simple closed-form approach is desirable for practical reasons. A new interpretation method is derived herein for determining s_u by combining spherical cavity expansion theory and Modified Cam Clay.

In the proposed model discussed herein, s_u is expressed in terms of the PCPT parameter (q_T-u_2), effective stress friction angle (ϕ'), and plastic volumetric strain ratio (Λ). The model approximately accounts for differences in s_u caused by the initial state of stress (CIUC vs. CAUC). Parametric studies are conducted for evaluating the sensitivity of the parameters ϕ' and Λ within normal ranges, resulting in a simple expression for general use. Predictions are compared with those evaluated by traditional N_{kT} reference values, as well as laboratory test results determined from isotropically and anisotropically-consolidated undrained triaxial compression tests. An approach for extending the model predictions to vane strengths is also proposed and evaluated.

6.2 Model Development

The cone tip resistance (q_T) is conventionally expressed in terms of the undrained shear strength (s_u):

$$q_T = N_{KT}\, s_u + p_o \qquad [6.3]$$

where p_o = in-situ total normal stress and N_{kT} = cone bearing factor. If the spherical cavity expansion theory of Vesić (1977) is invoked, N_{kT} is given by:

$$N_{KT} = \frac{4}{3}(\ln I_r + 1) + \frac{\pi}{2} + 1 \qquad [6.4]$$

where $I_r = G/s_u$ = rigidity index. Combining Eqs. [6.3] and [6.4], the expression for the net cone tip resistance becomes:

$$q_T - p_o = (\frac{4}{3}\ln I_r + 3.90)\, s_u \qquad [6.5]$$

Alternatively, for later use, Eq. [6.5] can be rearranged in the form:

$$\frac{4}{3}\ln I_r = (q_T - p_o)/s_u - 3.90 \qquad [6.6]$$

The excess pore water pressures ($\Delta u = u_2 - u_o$) generated during piezocone penetration may also be expressed in terms of cavity expansion and critical-state concepts (Mayne and Bachus 1988). As a first approximation these excess pressures are due to a combination of changes in octahedral normal and shear stresses, whereby:

$$\Delta u_m = \Delta u_{oct} + \Delta u_{shear} \qquad [6.7]$$

Later, in Chapter 7, a more rigorous assessment of excess pore water pressures will be conducted. Using spherical cavity expansion theory (Vesic, 1972) to describe the octahedral component leads to:

$$\Delta u_{oct} = \frac{4}{3} (\ln I_r)\, s_u \qquad [6.8]$$

Substituting Eq. [6.6] into [6.8] the dependence on I_r is removed and the octahedral component of excess pore water pressures becomes:

$$\Delta u_{oct} = q_T - p_o - 3.9 s_u \qquad [6.9]$$

Referencing a constant p stress path for an initially isotropically-consolidated clay as shown in Figure 6.1, the shear-induced component of excess pore water pressures becomes (Wroth 1984):

$$\Delta u_{shear} = p_o' - p_f' \qquad [6.10]$$

where p_o' is the initial effective normal stress, and p_f' is the mean effective stress at failure such that $p_f' = 2s_u/M$, where $M = 6\sin\phi'/(3-\sin\phi')$ and equals the value of (q/p') at failure. Note that a conventional triaxial compression test induces a second component of Δu that is caused by increases in octahedral stress (due to the applied total stress path of $\Delta q/\Delta p = 3$). Additional details are given in Wroth (1984). By substituting Eqs. [6.9] and [6.10] into Eq. [6.7], the following is obtained:

$$u_2 - u_o = (q_T - p_o - 3.9 s_u) + (p_o' - 2s_u/M) \qquad [6.11]$$

This expression results in a piezocone evaluation of s_u corresponding to CIUC triaxial results:

$$(s_u)_{CIUC} = \frac{q_T - u_2}{(2/M + 3.9)} \qquad [6.12]$$

This preliminary model is based on the isotropic version of Modified Cam Clay. The

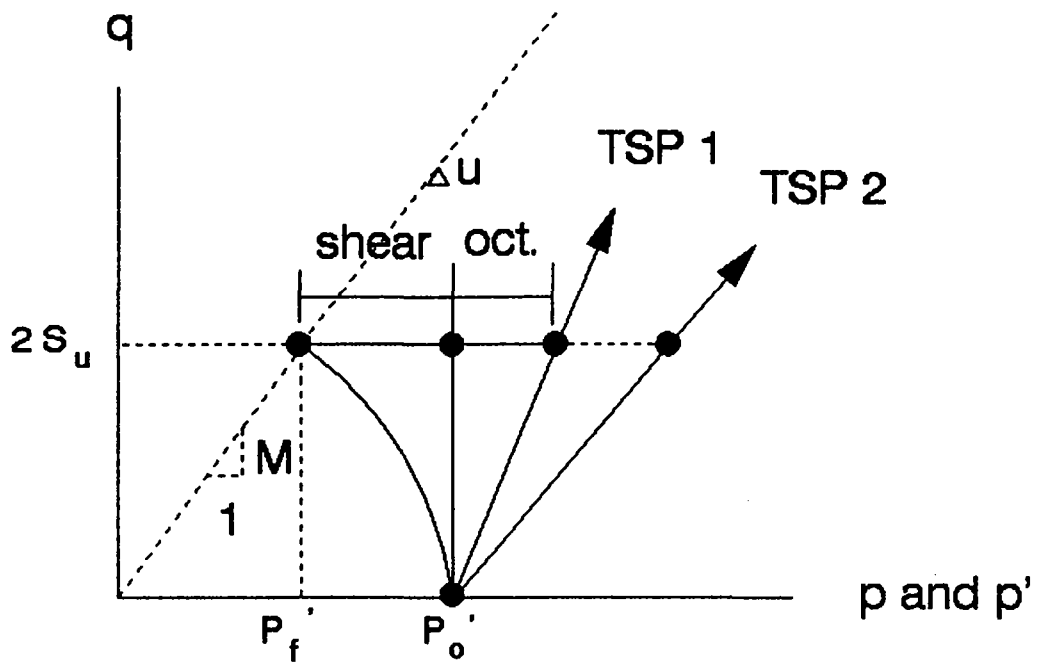

$$p' = \frac{1}{3} (\sigma_1' + \sigma_2' + \sigma_3')$$

$$q = \sigma_1 - \sigma_3$$

TSP = Total Stress Path

Figure 6.1. Interpretation of Excess Pore Water Pressures Observed in Triaxial Compression Tests (Wroth 1984).

corresponding normalized undrained shear strength ratio that accounts for stress history is given by:

$$\left(\frac{s_u}{\sigma'_{vo}}\right)_{CIUC} = \frac{M}{2}\left(\frac{OCR}{2}\right)^{\Lambda} \qquad [6.13]$$

in which σ_{vo}' is the in-situ effective vertical stress and Λ is the plastic volumetric strain ratio. Note that for isotropic consolidation, $P_o' = \sigma_{vo}'$. From Modified Cam-Clay, the parameter Λ equals $(1 - \kappa/\lambda)$, where κ and λ are the isotropic swelling and compression indices, respectively.

Since the actual stress state in the field is rarely isotropic, an anisotropic model for predicting s_u is desirable. Wroth (1984) derived a more elaborate expression for the normalized undrained shear strength corresponding to anisotropically-consolidated compression (CAUC) that assumed the initial state of stress in the NC region is approximated by the Jaky (1944) equation: $K_{oNC} = 1 - \sin\phi'$. The form of this anisotropic MCC expression is:

$$\left(\frac{s_u}{\sigma'_{vo}}\right)_{CAUC} = \frac{\sin\phi'}{2a_k}\left(\frac{a_k^2+1}{2}\right)^{\Lambda} OCR^{\Lambda} \qquad [6.14]$$

where $a_k = (3-\sin\phi')/(6-4\sin\phi')$. By combining Eqs. [6.13] and [6.14], the ratio of anisotropic to isotropic strength becomes:

$$\frac{(s_u/\sigma'_{vo})_{CAUC}}{(s_u/\sigma'_{vo})_{CIUC}} = \frac{\sin\phi' \,(a_k^2 + 1)^{\Lambda}}{a_k \, M} \qquad [6.15]$$

The above expression is solely a function of ϕ' and Λ of the soil. For a typical value $\Lambda = 0.75$, the factor ranges from 0.96 at $\phi' = 20^o$ to 0.76 at $\phi' = 40^o$. Kulhawy and Mayne (1990) calibrated Eq. [6.15] against 48 intact clays, as shown in Figure 6.2. The theory and

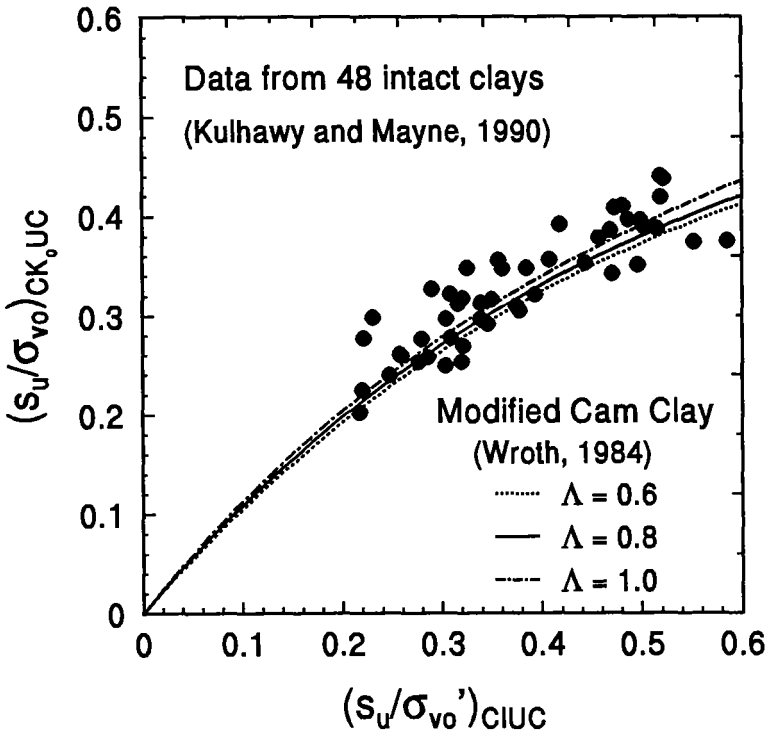

Figure 6.2. Comparison of Anisotropic and Isotropic Undrained Strength Ratios for Normally-Consolidated Clays (Kulhawy and Mayne 1990).

available data indicate that the normalized undrained strength ratio from CAUC tests is typically lower than the ratio for CIUC tests. Subsequently, the approximate value of s_u for the anisotropic compression mode can be expressed as:

$$(s_u)_{CAUC} = \frac{q_T - u_2}{(2/M + 3.9)} \frac{\sin\phi'(a_k^2+1)^{\Lambda}}{a_k M} \qquad [6.16]$$

This may be alternatively expressed in the more simplified form:

$$s_u = \frac{q_T - u_2}{N_{qu}} \qquad [6.17]$$

in which $N_{qu} = (2/M) + 3.9$ applies for CIUC tests

and $N_{qu} = a_k\,(2 + 3.9M)/[\sin\phi'(a_k^2+1)^{\Lambda}]$ for CAUC tests.

A flow chart outlining the development of the model is shown in Figure 6.3.

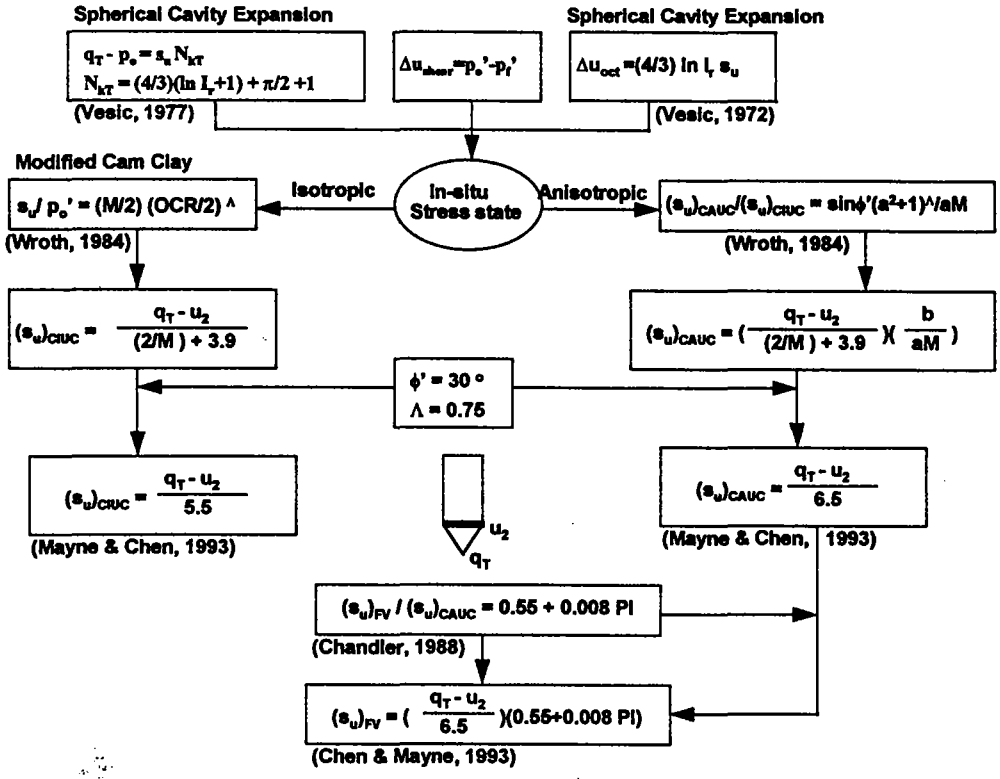

Figure 6.3. Evolution of SCE/MCC Piezocone Model for Undrained Strength. Evaluation.

6.3. Parametric Study

Among the parameters required for prediction, q_T and u_2 are obtained directly from Type 2 piezocone results, while N_{qu} is dependent on ϕ' and Λ of the soil. A parametric study was therefore performed to investigate the significance of ϕ' and Λ in the model. Diaz-Rodriguez et al. (1992) reported a full range of ϕ' for triaxial compression tests on natural clays worldwide from 17.5° to 43°. A review of 132 different sets of laboratory triaxial tests on clays compiled by Mayne (1980, 1988) indicates that $0.6 \leq \Lambda \leq 0.8$ for insensitive natural clays and $0.9 \leq \Lambda \leq 1.0$ for structured and cemented clays. These studies also confirmed that $18^o \leq \phi' \leq 41^o$ for natural clays.

Figure 6.4 shows the theoretical variation of N_{qu} over a wide range of ϕ' for both CIUC and CAUC conditions. For CIUC, the value of N_{qu} is independent of Λ and the value of N_{qu} varies from 5.0 to 6.5 for the aforementioned range of ϕ'. For CAUC, the values of N_{qu} are dependent upon both ϕ' and Λ. It appears that N_{qu} is only slightly sensitive to variations of ϕ' and Λ within normal ranges and N_{qu} varies from 6.1 to 7.1. Parametric

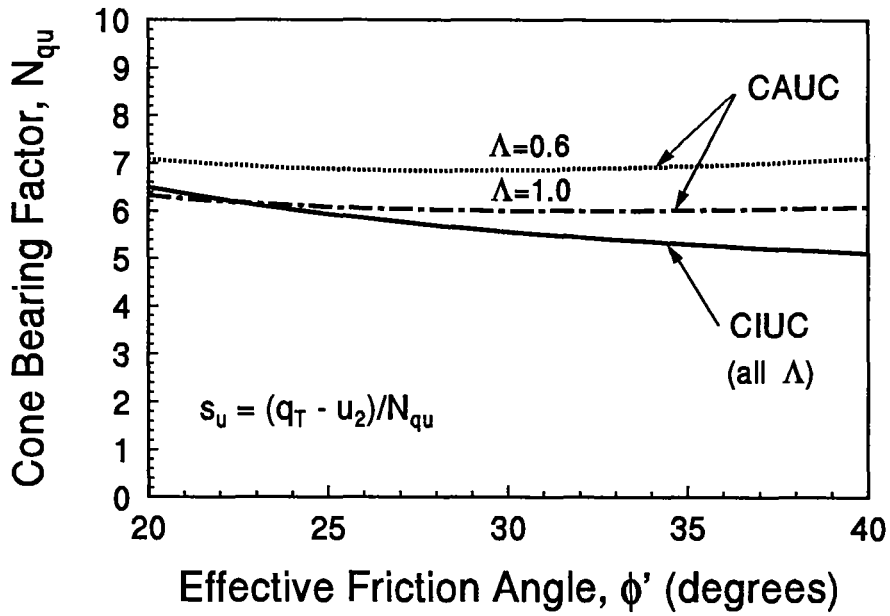

Figure 6.4. Cone Bearing Factor N_{qu} as a Function of ϕ', Λ, and Test Type for Isotropic SCE/MCC Model.

studies were performed using data from several sites where relevant information was available. Results from the studies, such as those for Lilla Mellösa and Gloucester sites shown in Figure 6.5, indicate that the CAUC model is not particularly sensitive to either ϕ' or Λ. If average values of $\phi' = 30°$ and $\Lambda = 0.75$ are adopted, the bearing factor N_{qu} equals 5.5 and 6.5 for CIUC and CAUC, respectively. For engineering use, the following expression is recommended:

$$(s_u)_{CIUC} = \frac{q_T - u_2}{5.5} \qquad [6.18a]$$

$$(s_u)_{CAUC} = \frac{q_T - u_2}{6.5} \qquad [6.18b]$$

Since clays in nature are consolidated under anisotropic states of stress, $(s_u)_{CAUC}$ is usually more applicable.

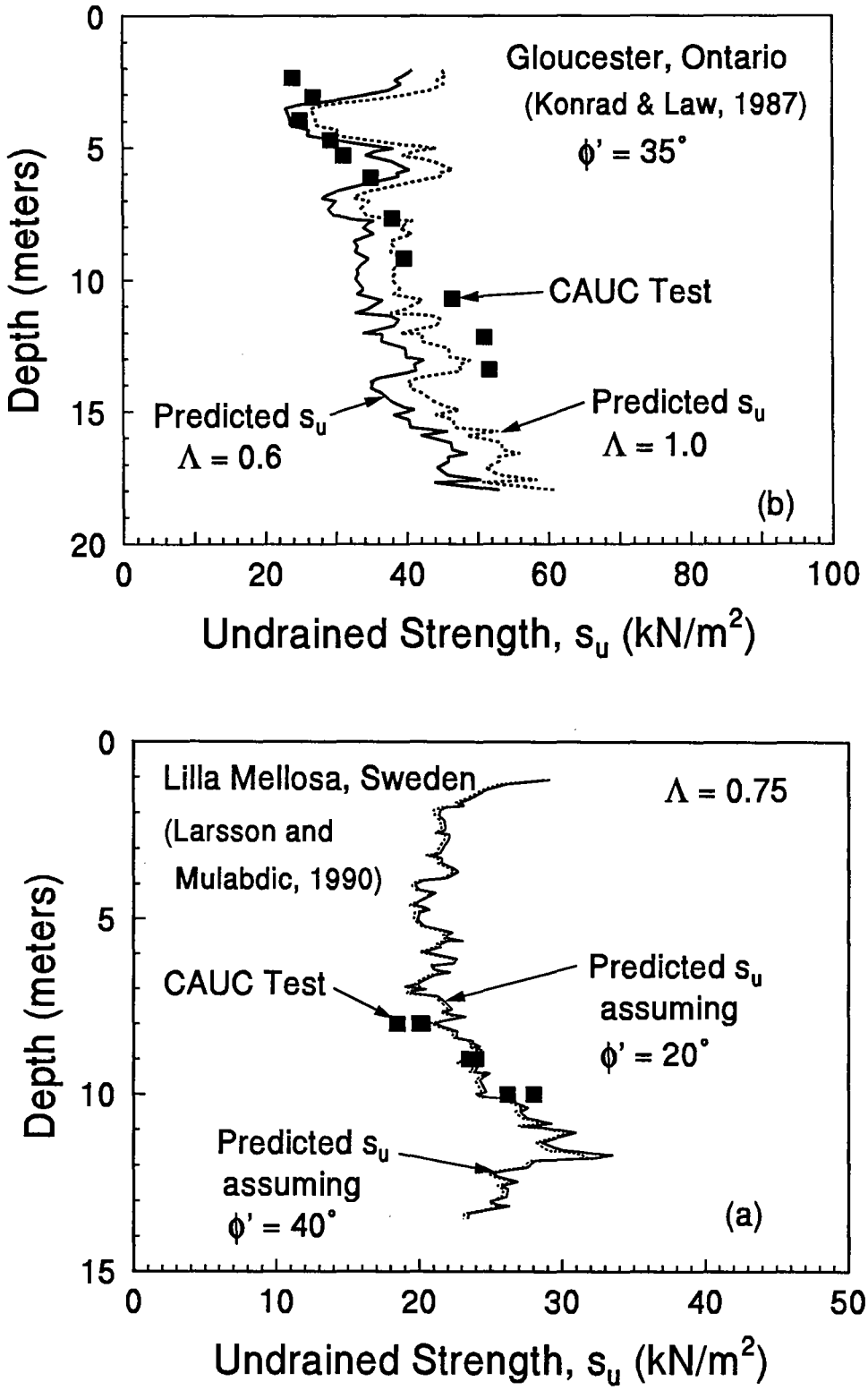

Figure 6.5. Parametric Effects of ϕ' and Λ on PCPT Predictions for CAUC Test.

6.4. Laboratory Chamber Tests

The newly proposed method for evaluating s_u from PCPT was applied to results from a laboratory-controlled testing program. In this event, a series of miniature in-situ tests were performed in prestressed kaolinitic clay during an experimental test program involving model foundation testing in a large fixed-wall calibration chamber as discussed previously in Chapter 5. The deposit of clay was formed from a lean kaolinitic-silica slurry that was comprised of a 50-50 mixture of Peerless Clay No. 2 and very fine SuperSil 125 at an initial water content w_n = 66%. Resulting index properties were: LL = 33, PI = 11, CF = 33%, G_s = 2.65, and D_{50} = 0.006 mm. Additional details may be found in Mayne, Kulhawy, and Trautmann (1992) and Mayne (1993).

The slurry was pumped into a large cylindrical steel chamber having an inside diameter of 1.37 m and height of 2.13 m. Pneumatic pressure was applied to the top of a rigid piston and the slurry was consolidated one-dimensionally at $\Delta\sigma_p'$ = 48 kN/m^2 with double drainage permitted. After completion of primary consolidation, the specimen was rebounded to atmospheric conditions, resulting in a mechanically-overconsolidated profile with OCR = $(\Delta\sigma_p'+\sigma_{vo}')/\sigma_{vo}'$. A water reservoir maintained the "groundwater" level contiguous with the surface of the clay. After prestressing, the clay had an average water content w_n = 34.5 percent, e_o = 0.914, and γ_T = 18.2 kN/m^3.

A complementary suite of laboratory testing included triaxial, direct simple shear, oedometer, creep, isotropic consolidation, K_o tests, and fall cone tests was conducted on the material. Some of these test results are reported in McManus and Kulhawy (1991). Figure 6.6 shows the effective stress paths for CIUC triaxial tests on the material at four levels of induced OCR. The triaxial data indicate an effective stress friction angle ϕ' = 33.5° (or critical state failure parameter M = 1.35).

The results of a conventional one-dimensional consolidation test on a retrieved sample of the clay is presented in Figure 6.7. The interpreted σ_p' = 50 kN/m^2 is consistent with the known applied stress history to the deposit. Consolidation parameters derived from the oedometer testing include: C_c = 0.214, C_s = 0.028, and $C_{\alpha e}$ = 0.0067.

Miniature in-situ tests were conducted to evaluate the uniformity and consistency of the prestressed clay deposit (Mayne 1993). These included vane shear, electric cone, two

types of piezoprobe, as well as water content determinations. A motorized Wykeham-Farrance vane apparatus was used to perform the vane shear tests with a rectangular blade (12.7 mm diameter by 25.4 mm height). Undrained strengths measured by the vane were essentially constant with depth at $s_{uv} = 8.51 \pm 0.73$ kPa. Consolidated water contents decreased from about 36% at the top to 34% at the bottom of the deposit. Electric cone penetration tests were performed using a 23.3-mm diameter miniature penetrometer (Fugro-type geometry) with 60° apex to provide measurements of q_c. The cone has a net area ratio $a = 0.88$. Piezoprobe soundings were conducted using 19.1-mm diameter 60° tipped brass cones that were fitted with miniature Druck transducers and sintered brass porous elements. Two types of piezoprobes were built so that penetration pore water pressures could be measured at the tip (u_1) and behind the tip (u_2). Figure 6.8 shows the records from one set of penetration tests in the prestressed clay deposit. The combined data from the cone and piezoprobes result in the equivalence of a piezocone sounding. The measured cone tip resistance (q_c) has been corrected to q_T to account for pore water pressure effects on equal areas of the cone geometry (Lunne et al. 1986).

A comparison of the measured triaxial compression strengths and predicted s_u profiles in the overconsolidated clay is shown in Figure 6.9. Measured values of s_u include the results from unconfined compression (UC) tests on retrieved samples at depths of 300, 600, and 900 mm, as well as a SHANSEP value taken at the oedometer test depth and normalized relationship determined from the CIUC tests:

$$\frac{s_u}{\sigma_{vo}'} = 0.336\ OCR^{0.79} \qquad [6.19]$$

Reasonable agreement is seen for the range predicted by PCPT for isotropic and anisotropic undrained shear strengths.

6.5. Field Case Studies

Twenty well-documented sites selected from the geotechnical literature have been studied for the calibration of the proposed model. Table 6.1 summarizes the soil information and sources of data for these sites. The soils at these sites range from soft, sensitive,

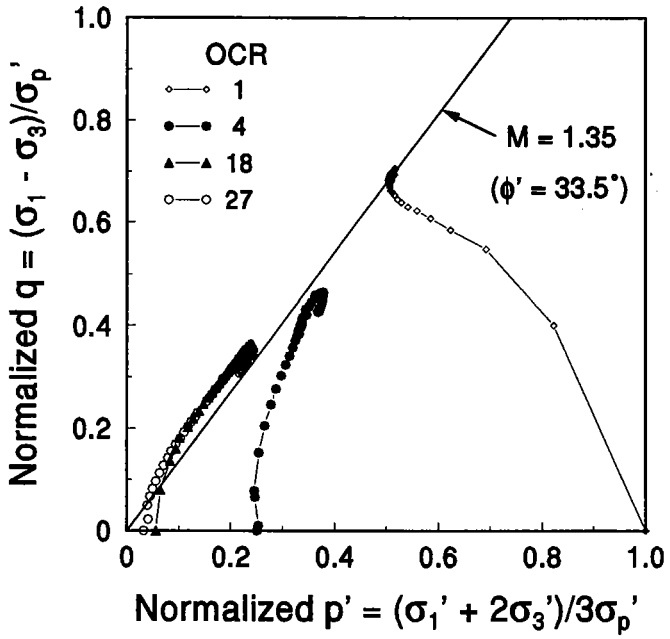

Figure 6.6. Effective Stress Paths for CIUC Tests on Kaolinitic Clay. (McManus and Kulhawy 1990).

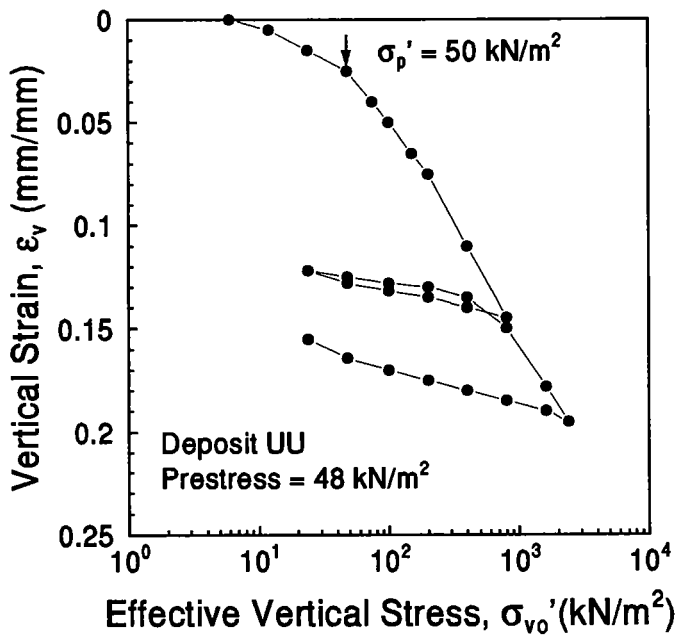

Figure 6.7. Oedometer Test Results on Prestressed Kaolinitic Clay. (Mayne, Kulhawy & Trautmann 1992).

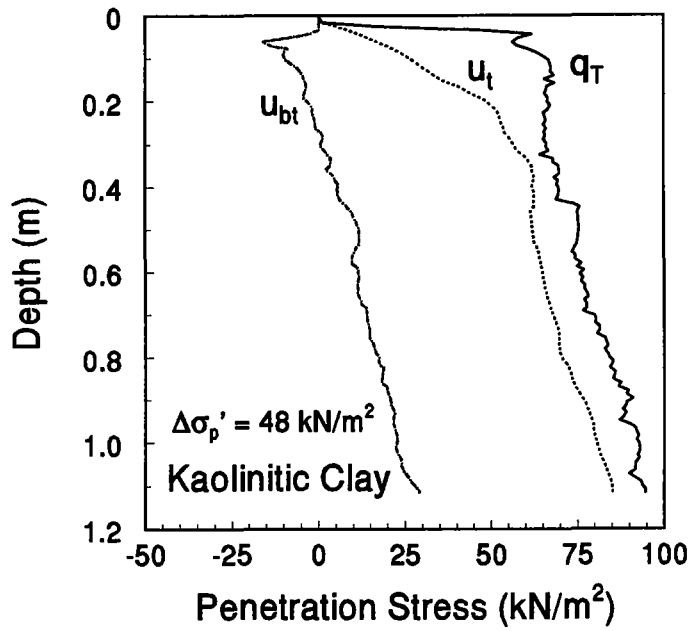

Figure 6.8. Results of Composite Piezocone Test from Miniature Electric Cone and Piezoprobe Soundings. (Mayne 1993)

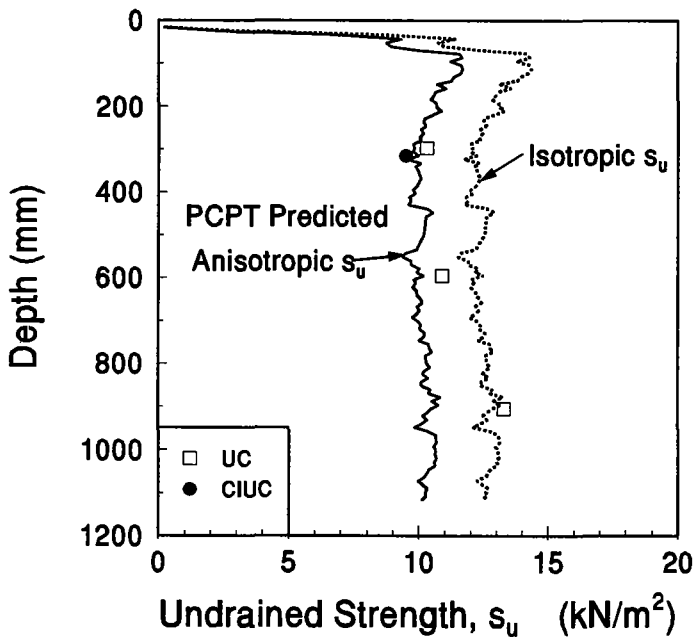

Figure 6.9. Measured-TC and PCPT Predicted Strengths of Kaolinitic Clay.

normally consolidated or lightly overconsolidated to very stiff, heavily overconsolidated clay deposits. The clays at St. Alban, Onsøy, and Chek Lap Kok are considered to be moderately sensitive, while the clays at Taranto are noted to be hard and cemented. Bothkennar is a national test site in the U.K. and is comprised of relatively homogeneous and low to moderately sensitive clay, while Yorktown consists of very sandy clays. Keelung River, Norfolk Road, Malaysian Marine clay, and McDonald Farm sites are normally consolidated to lightly overconsolidated and are considered as fairly low sensitivity soil deposits.

Table 6.1. List of Piezocone Clay Sites with Reference Strengths, Indices, and Sources of Data.

Site	Description	w_n	LL	PI	S_t	OCR	s_u	Reference
Bäckebol, Sweden	Soft, glacial	90	80	45	20±	1-3	FV	Larsson & Mulabdić (1991)
Bothkennar, Scotland	NC, soft	65	73	41	4-6	1-3	CAUC	Powell et al. (1988)
Chek Lap, Hong Kong	Soft, marine	70	70	40	4-15	1-12	CIUC	Koutsoftas et al. (1987)
Colebrook, B.C	NC, soft	45	36	11	UA	1±	FV	Crawford & Campanella
Gloucester, Ontario	NC, aged Leda	70	50	25	20-95	1-2	CAUC	Konrad & Law (1987)
Keelung River, Taiwan	LOC, soft	37	40	15	UA	1-3	CIUC	Chern (1992)
Lilla Mellösa, Sweden	NC, organic	100	95	65	15	1.2	CAUC	Larsson & Mulabdić (1991)
Lower 232nd St, B.C	NC, silty	45	40	19	11	1-2	FV	Greig et al. (1988)
Malaysian Marine Clay	NC, soft	65	70	45	4-5	1-3	FV	Chang (1991)
Massena IDA, New York	LOC, soft	55	34	14	8	1±	FV	Lutenegger & Kabir (1988)
Massena RRC, New York	LOC, soft, silty	43	54	30	6	1-10	FV	Lutenegger & Kabir (1988)
McDonald Farm, Canada	NC, clay silt	34	35	15	2-7	1-2	FV	Greig et al. (1988)
Mukendal, Sweden	Quick, firm	81	55	26	300	1-1.5	FV	Larsson & Mulabdić (1991)
Muni Metro, California	LOC Bay Mud	55	65	30	2-7	1-1.5	CIUC	Koutsoftas (1989)
Norfolk Rd, Singapore	LOC, soft	60	85	50	3	1-2	FV	Chang (1991)
Onsøy, Norway	NC, soft, aged	63	65	37	6-9	1-4	CAUC	Lunne et al. (1986)
St. Alban, Québec	Sensitive, aged	63	45	22	22	2-3	CIUC	Roy et al. (1982)
Taranto, Italy	HOC/cemented	23	60	27	NA	30±	UU	Jamiolkowski et al. (1982)
Valoya, Norway	HOC, very stiff	40	52	20	3-4	3-11	CIUC	Sandven (1990)
Yorktown, Virginia	MOC, sandy	31	31	4	4-8	4-12	CIUC	Mayne (1989)

Notes: NC - Normally Consolidated; LOC - Lightly Overconsolidated
MOC - Moderately Overconsolidated; HOC - Heavily Overconsolidated
NA - Not Available; UA - Unavailable

The selection of the reference test is crucial in this study since s_u can vary over a wide range depending upon the consolidation process, shearing mode, fabric, direction of loading, strain rate, stress rotation, and disturbance effects. For laboratory tests, CIUC and CAUC tests have been selected where available, except for the Taranto site, in which the

results from high quality unconsolidated undrained triaxial compression tests (UU) were available (Jamiolkowski et al. 1988). Field vane tests (FV) have also been included in this study since it has been widely used in determining s_u. Among these tests, CIUC or CAUC tests are superior to the UU test as major reference tests since (1) the soil behavior beneath the cone tip is similar to that exhibited in triaxial compression, and (2) the consolidated undrained test (CU) is considered to be more reliable than both the UU and unconfined compression (UC) tests regarding sampling disturbance and strain rate effects.

6.5.1 Triaxial Reference Strengths

A comparison of measured and predicted profiles of s_u for St. Alban clay using the triaxial and piezocone data is shown in Figure 6.10. The conventional interpretation using N_{kT} and the new approach using N_{qu} are both shown with the latter providing a slightly better fit.

Figure 6.11 shows predicted profiles of s_u (triaxial) for eight additional sites using the approach: $s_u = (q_t - u_2)/N_{qu}$. In general, this model provides fairly reasonable profiles of s_u are obtained for Keelung River, Chek Lap Kok, Yorktown, Muni Metro, and Taranto sites; while slight over-predictions are evident for the Bothkennar, Onsøy, and Valoya sites. It must be pointed out that the soils at each of these sites are essentially intact clays, therefore, this approach may require further verification before application to fissured clays. The over-predictions may be inevitable since the strain rate near cone tip is significantly higher than the shearing rates used for laboratory triaxial tests (Baligh 1986).

Values of N_{qu} were back-calculated for those sites where CU reference tests were available. The back-calculated N_{kT} from net cone resistances and undrained shear strengths were also obtained from PCPT data and CU tests. Results of this study indicate that values of N_{kT} for these particular sites reviewed ranged from 10 to 16, while backcalculated values of N_{qu} consistently varied in a much smaller range between 5.7 and 8.5 for these intact clays. For fissured clays, however, Powell and Quarterman (1988) observed that $20 \leq N_{kT} \leq 30$. Consequently, additional studies of N_{qu} for fissured clays should be investigated.

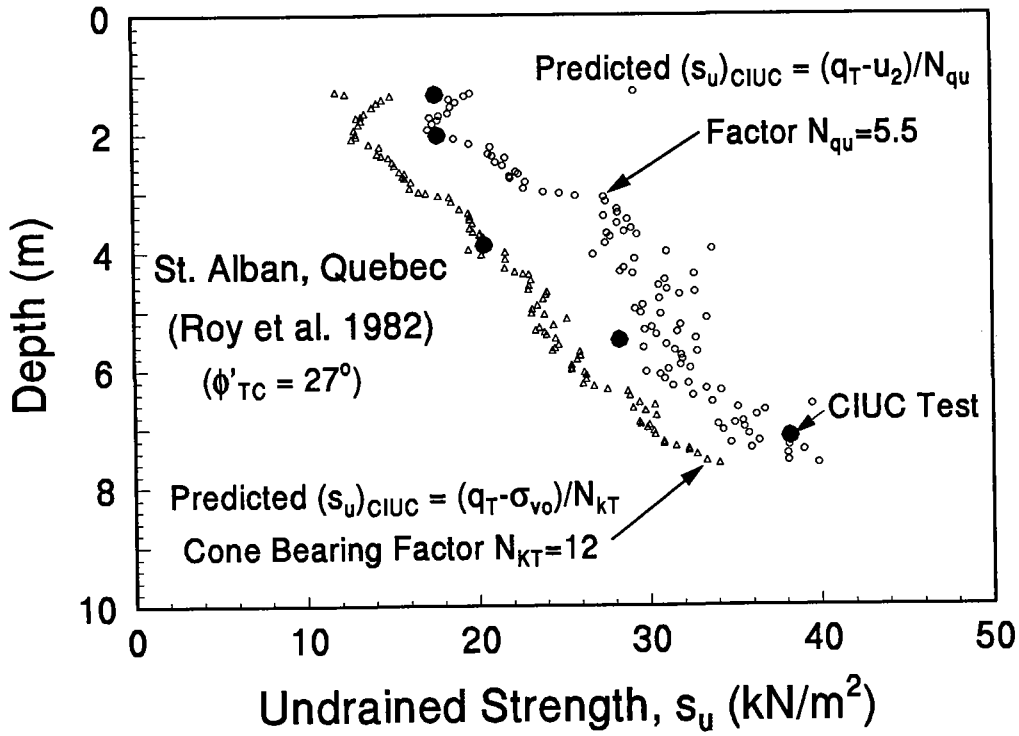

Figure 6.10. Comparison of N_{kT} and N_{qu} Predictions for PCPT-s_u Profiles at St. Alban Clay, Quebec.

6.5.2. Vane Reference Strengths

The field vane (FV) test can also be used as a reference test provided that the difference in s_u shearing mode is taken into account.

Wroth (1984) pointed out that the (s_u/σ_{vo}') ratio determined from FV tests is lower than s_u determined from CIUC and CAUC tests and is relatively insensitive to ϕ'. Furthermore, Chandler (1988) presented an empirical correlation in which the strength ratio $V_r = (s_u)/_{FV}$ to $(s_u)_{CAUC}$ is a function of plasticity index (I_P) of the soil, as shown in Figure 6.12. By introducing V_r into Eq. [6.18b], $(s_u)_{FV}$ may be estimated from the following expression:

$$(s_u)_{FV} = \frac{(q_T-u_2)(69 + I_p)}{812} \qquad [6.20]$$

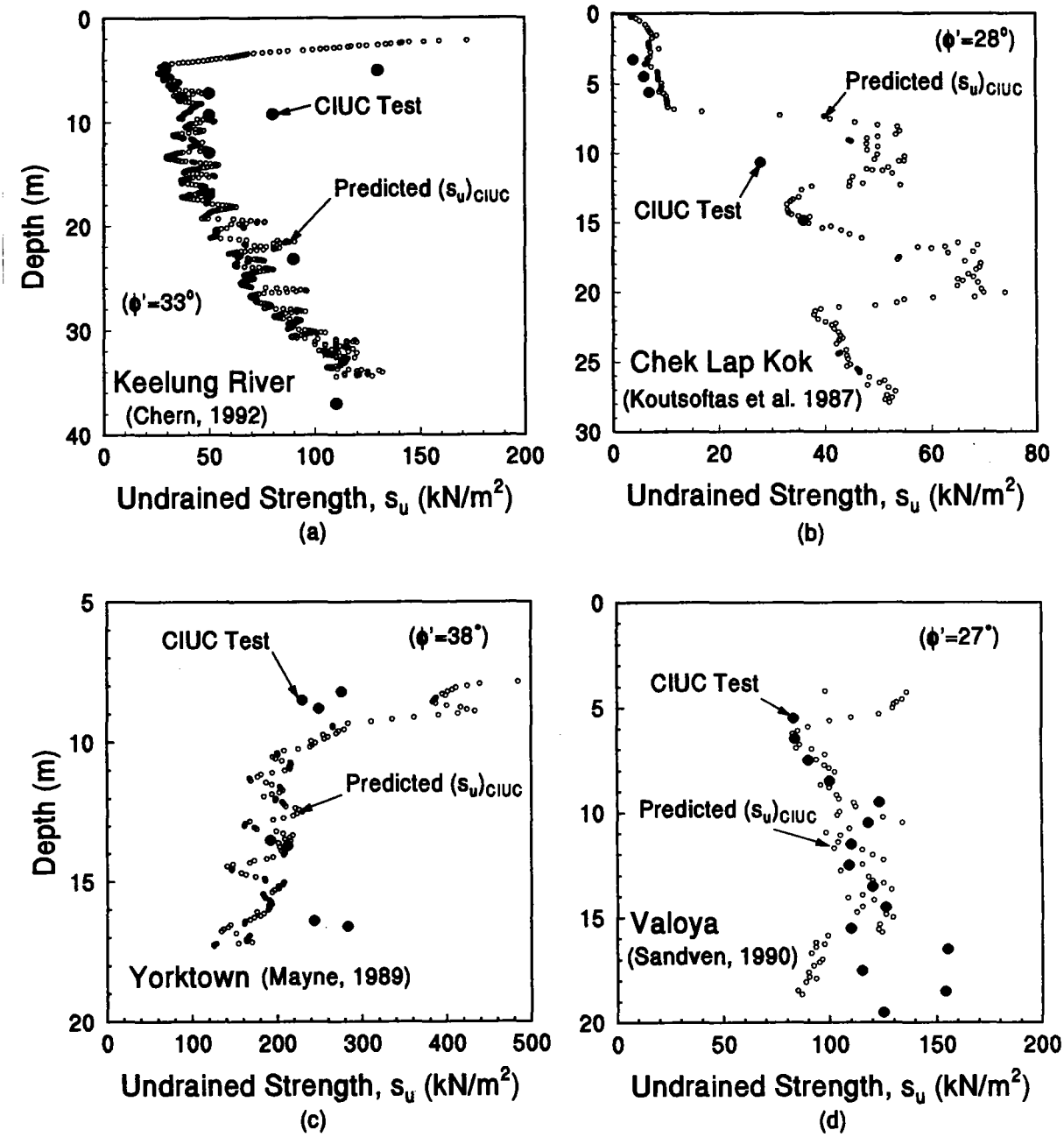

Figure 6.11a. PCPT-s_u Profiles at Clay Sites with Reference Triaxial Compression Tests.

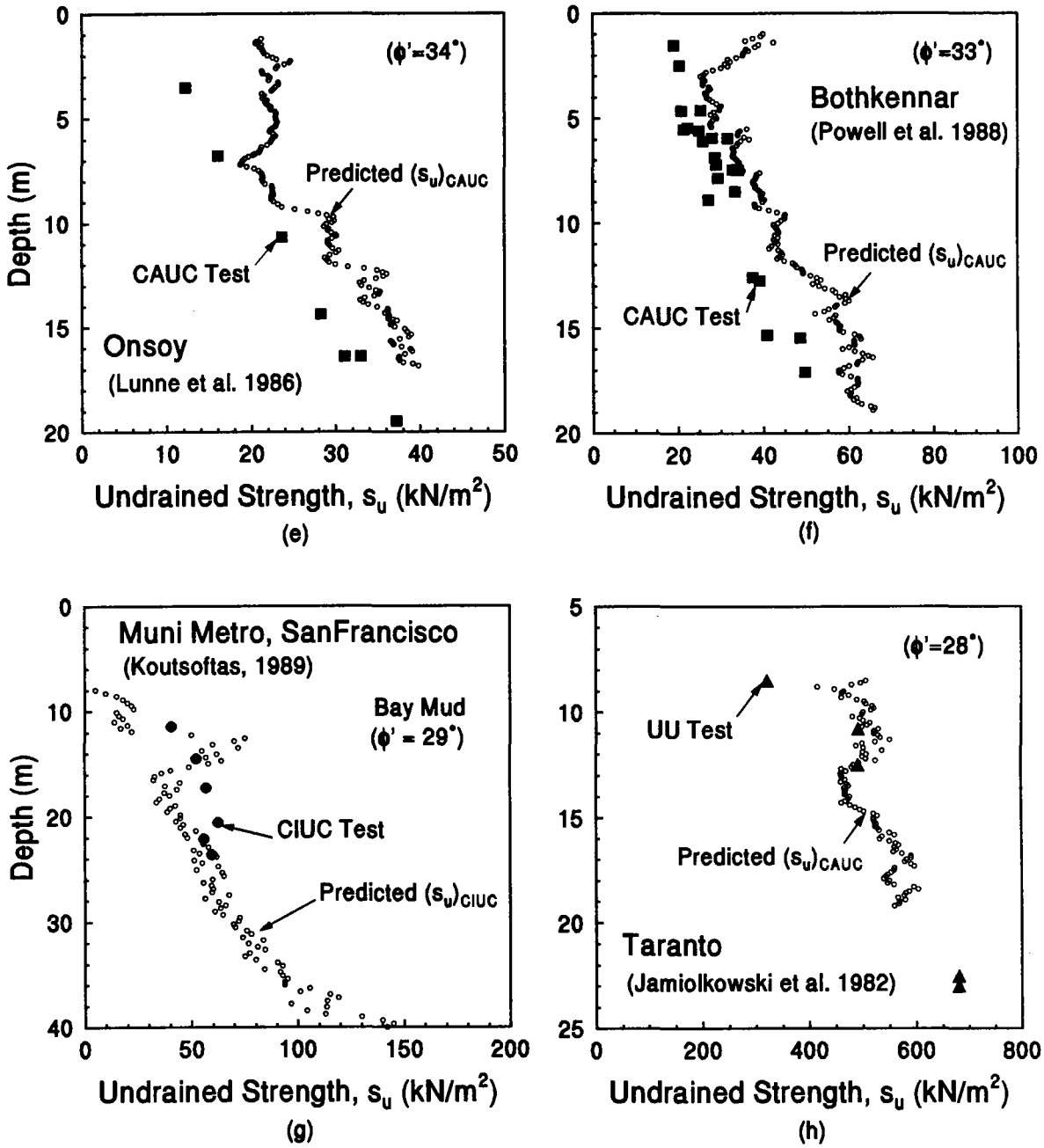

Figure 6.11b. PCPT-s_u Profiles at Clay Sites with Reference Triaxial Compression Tests. (Continued)

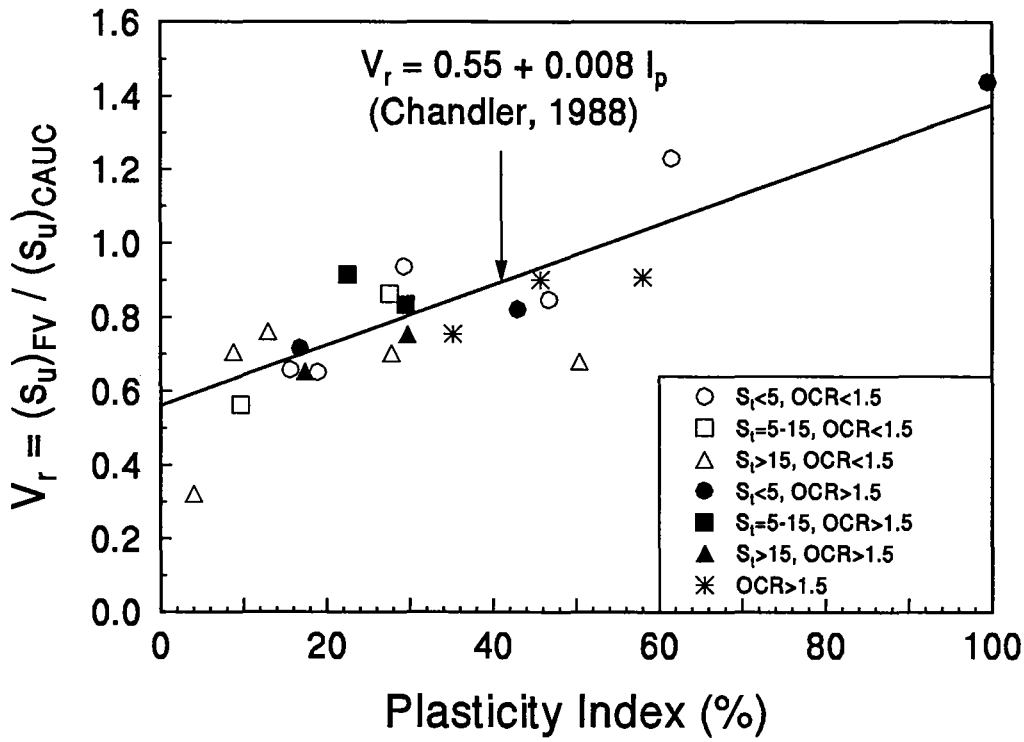

Figure 6.12. Relationship between the Strength Ratio of Vane to Triaxial (V_r) and Plasticity Index, I_p. (Chandler, 1988)

A comparison of measured and predicted profiles of vane s_u for the McDonald Farm site, is shown in Figure 6.13. The estimates of vane strength from piezocone data are seen to be lower than the actual reference values.

Predicted profiles for 8 additional sites where FV data are presented in Fig. 6.14. Results for Malaysian marine clay, Lower 232nd Street, Norfolk Road, Massena RRC, and Colebrook Road sites fit reasonably well, while slight over-predictions are observed for Bäckebol and Munkedal sites. The profile at Massena IDA is consistently underpredicted.

6.6. Conclusions

A hybrid theory approximately relates s_u to the effective cone resistance, $(q_T - u_2)$. In particular, the approach attempts to approximately distinguish between isotropic and anisotropic triaxial compression strengths, and has been extended empirically to the vane

reference mode. The predictions are somewhat insensitive to ϕ' and Λ resulting in $S_u = (q_T-u_2)/5.5$ for CIUC and $s_u = (q_T-u_2)/6.5$ for CAUC modes. Calibration of the model has been applied to 20 sites across the globe, where the full range of reference strengths includes $6 \leq s_u \leq 500$ kN/m^2. The results indicate a reasonable degree of success for intact clays.

A summary graph of the undrained shear strengths obtained from reference CIUC, CAUC and UU tests are plotted versus the piezocone parameter (q_T-u_2) in Figure 6.15. For the intact clays, the overall predictions using the proposed average values for the factor $N_{qu} = (q_T-u_2)/s_u$ for CIUC and CAUC tests (i.e. 5.5 and 6.5) appear satisfactory, although overpredictions are apparent for some clays (such as Onsoy, Bothkennar, and Gloucester) at low strengths ($s_u < 50$ kN/m^2).

Finally, the proposed $(q_T - u_2)$ model makes use of two piezocone measurements while still being simple and convenient for practicing engineers. However, further calibration of the model is necessary, particularly in fissured materials. Additional factors such as K_o-induced anisotropy, stress rotation effects, soil fabric, sensitivity, and strain rate should also be evaluated.

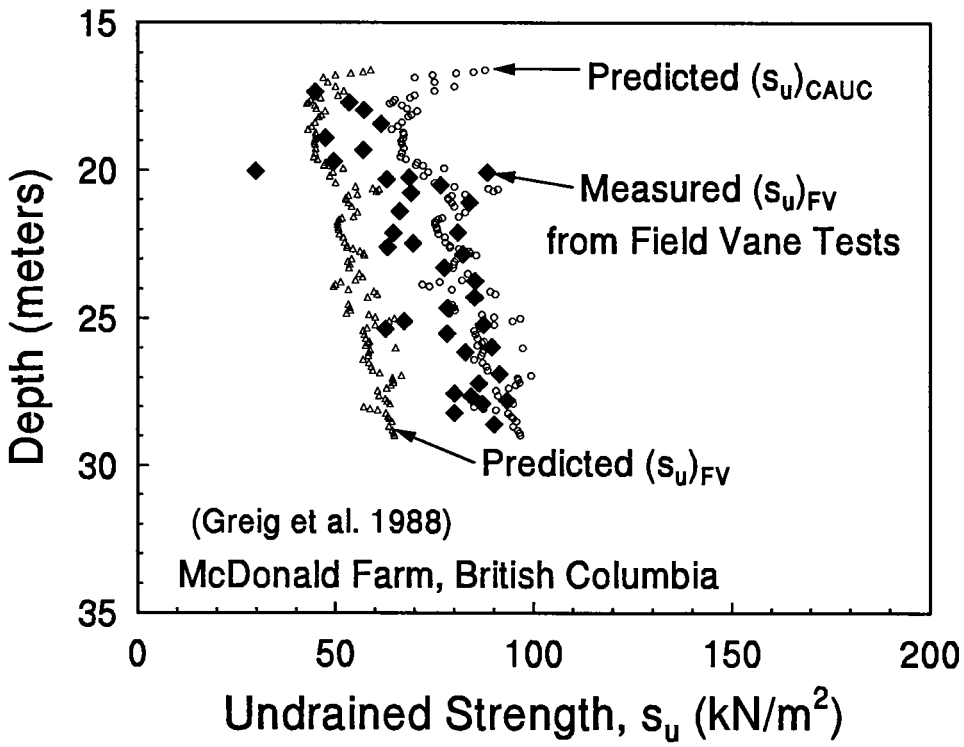

Figure 6.13. Comparison of Measured and Predicted Vane Strengths at McDonald Farm Site, British Columbia.

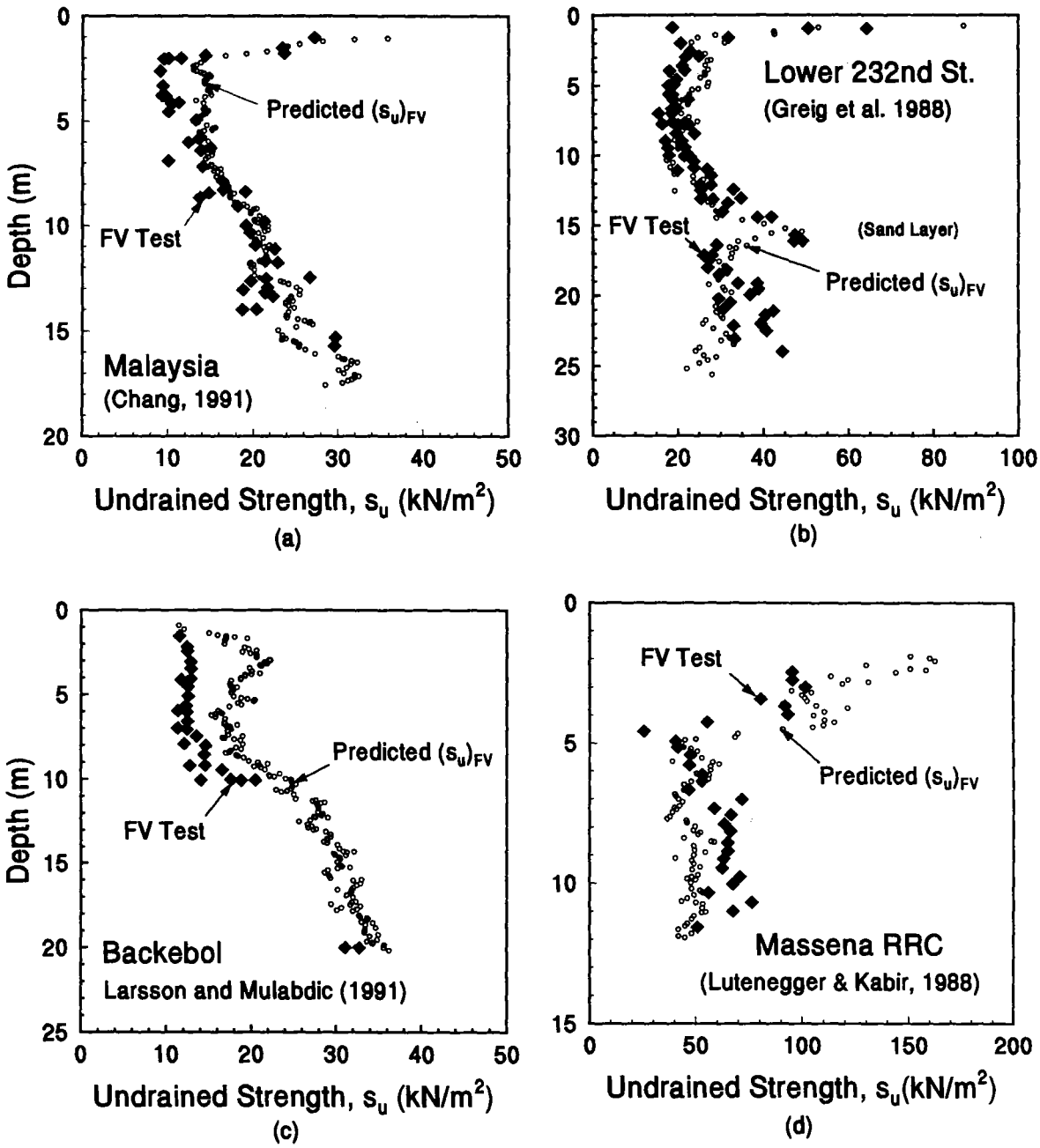

Figure 6.14a. PCPT-s_u Profiles at Clay Sites with Reference Field Vane Tests.

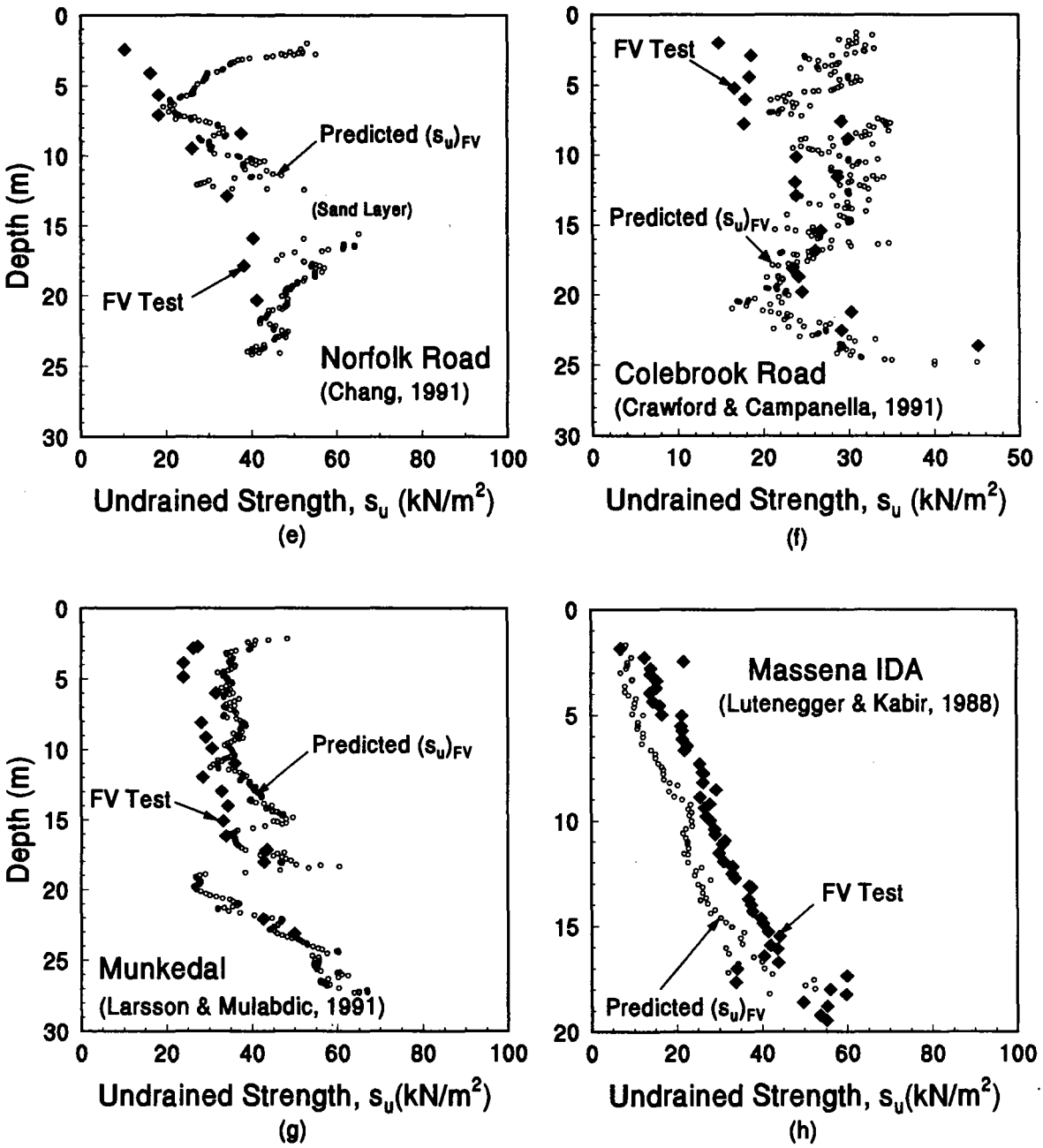

Figure 6.14b. PCPT-s_u Profiles at Clay Sites with Reference Field Vane Tests. (Continued)

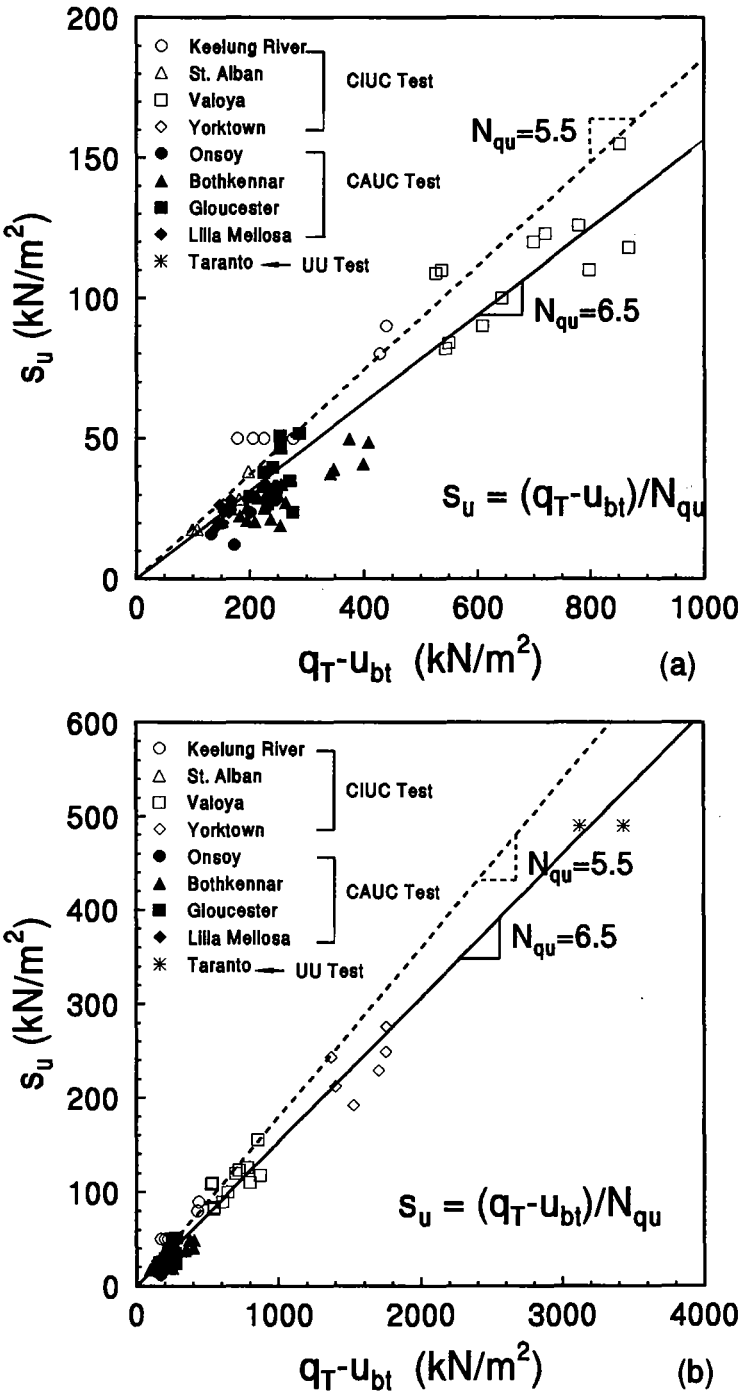

Figure 6.15. Summary of Triaxial Reference Strengths Versus Effective Cone Resistance.

CHAPTER 7

A SOIL BEHAVIORAL MODEL FOR PREDICTING OCR IN CLAYS

7.1 Preface

An analytical model has been developed for evaluating OCR profiles in natural clay deposits using a piezocone with either u_1 or u_2 pore pressure measurements or dual (u_1 and u_2) measurements. In order to fully address soil behavioral influences on the advancing cone, the model is derived in a consistent framework using spherical cavity expansion theory and constitutive soil models that incorporates several important considerations such as: (1) initial stress state, (2) strength anisotropy, (3) stress path analysis, and (4) strain rates. A combined dual-type model is obtained for interpreting the OCR from results of a special piezocone with dual pore pressure measurements, or where both u_1 and u_2 are available from paired soundings. An important consideration for keeping the method attractive to practicing engineers is to examine these effects within the domain of simple analytical solutions, without involving sophisticated numerical techniques. If the full set of input parameters (c', ϕ', K_o, K_{45}, Λ, and $d\epsilon/dt$) are utilized, an iterative solution form is required. Parametric studies indicate that approximate closed-form expressions can be obtained and used adequately in routine explorations.

The piezocone model predictions of OCR are reasonably validated by a series of calibration comparisons against actual test data. Nevertheless, it is unrealistic to expect the model performs to the same degree of success for all clay sites universally since many facets of the test can be accounted for only by crude approximations. True soil behavior is far more complicated than most existing constitutive soil models can fully simulate. For instance, the micro-structure and soil fabric are difficult to quantify as input values, although they may have a decisive influence on soil behavior. Baligh (1985) postulated that the stress path analysis of soil elements is inadequate for describing deep penetration problems and proposed that the strain path method be examined. The cavity expansion theory is, in fact, a one-dimensional simplification of the strain path approach and indeed has its limitations in explaining the complete details surrounding penetration problems (Baligh 1985).

Nevertheless, the proposed model provides an adequate interpretation of the stress history in many clays, considering all of the simplifications, constraints, and limitations. More sophisticated approaches often require cumbersome and detailed numerical procedures, but the results are not necessarily superior than the simpler analytical method.

7.2. Model Development

7.2.1. Cone Tip Resistance

Although spherical cavity expansion (SCE) theory assumes an initial isotropic state of stress, its simplicity makes it very attractive in studying cone penetration problems. For the net cone tip resistance, spherical cavity expansion theory states (Vesić 1977):

$$q_T - p_o = s_u \left[\frac{4}{3}(\ln I_r + 1) + \frac{\pi}{2} + 1\right] \qquad [7.1]$$

where s_u = undrained shear strength, q_T = corrected cone tip resistance, p_o = mean total overburden stress = $\frac{1}{3}(\sigma_{vo}+2\sigma_{ho})$, $I_r = G/s_u$ = rigidity index, and G = shear modulus of the clay. A study by Keaveny and Mitchell (1986) concluded that the relevant s_u for the cone tip resistance (q_T) in clays corresponded to K_o-consolidated undrained triaxial compression (CK_oUC) conditions.

7.2.2. Pore Pressures

The measured excess pore pressures (Δu_m) induced by the advancing probe are due to a combination of changes in (1) octahedral normal stresses due to cavity expansion, (2) normal stresses from elastic total stress path conditions, and (3) shear-induced stresses:

$$\Delta u_m = \Delta u_{oct} + \Delta u_{TSP} + \Delta u_{shear} \qquad [7.2]$$

While it is impossible to decouple the measured pore pressures in reality, the components may be evaluated from an analytical assessment of the soil behavioral aspects. For the excess pore pressures caused by changes in the octahedral normal stress, spherical cavity expansion theory gives (Vesić 1972):

$$\Delta u_{oct} = (4/3)s_u \ln(I_r) \qquad [7.3]$$

The rigidity index (I_r) in Eqs. [7.1] and [7.3] can be eliminated by substituting Eq. [7.1] into Eq. [7.3] to obtain:

$$q_T - p_o = 3.9\ (s_u)_{CK_oUC} + \Delta u_{oct} \qquad [7.4]$$

in which the same cavity expansion form (i.e., spherical) and shearing mode (i.e., CK_oUC) are chosen because q_T and Δu_{oct} are likely to be affected by similar zones of clay that become plastic around the cone tip. They should therefore be consistent for both Type 1 and 2 piezocone penetrometers. Although the possible use of cylindrical cavity expansion for the Type 2 formulation of Δu_{oct} has also been examined, it is believed that spherical cavity expansion is more appropriate for both Type 1 and 2 PCPTs since they focus on the area around the cone tip where an imaginary plastified sphere is formed as the cavity expands. For the selection of the shearing mode, the CK_oUC mode is considered to be dominant for modeling both q_T and Δu_{oct}.

7.2.3. Filter Location

The determination of two other pore pressure components in Eq. [7.2], Δu_{TSP} and Δu_{shear}, relies on the specific filter location on the piezocones. For ease of categorization, piezocone data are divided into three categories as Type 1, 2, and 3 with pore pressure measurements of u_1, u_2, and u_3 (Campanella et al. 1988). In this study, an analytical model is developed to address both Type 1 and 2 piezocones because these are most common in both research and in practice. Few commercial cones focus on a u_3 measurement and therefore a Type 3 model has not been derived herein.

An added complication to the analysis is the fact that piezocone penetrometers from different manufacturers do not have the porous elements at the same exact locations. For instance, the Type 1 piezocone may have the porous element located at the apex, lower mid-face, mid-face, or upper mid-face; while the Type 2 piezocone may have the filter located on the shaft either immediately behind the cone base or alternatively positioned as far as 5

mm from the cone base. A "rainbow" piezocone suggested by Brown (1993) is shown in Figure 7.1 to illustrate this complexity associated with variations in commercial cone designs. The filter thickness and filter material also affect the recorded measurements and magnitudes of pore pressures (Campanella and Robertson 1988). These non-standard features of porous filters complicate and hinder a complete interpretation of piezocone data obtained from a variety of sources.

Although a more systematic approach for distinguishing all possible filter locations of piezocones is desired, in reality, it is difficult to fine tune the model to such a high degree of accuracy. First of all, the large deformations and complicated failure mechanisms around the small cone tip during penetration are more in favor of looking into the "average" soil behavior rather than identifying specific differences in such a small zone. Second, most references usually do not document the exact location of their porous elements to such a degree that the precise difference is known. Third, the magnitude of measured pore pressures is extremely sensitive to testing procedures such as degree of filter saturation, filter material, thickness, and penetrating rate. In the event that the pore pressure is not measured properly, it is less meaningful to distinguish small differences of pore pressure response due to different filter locations.

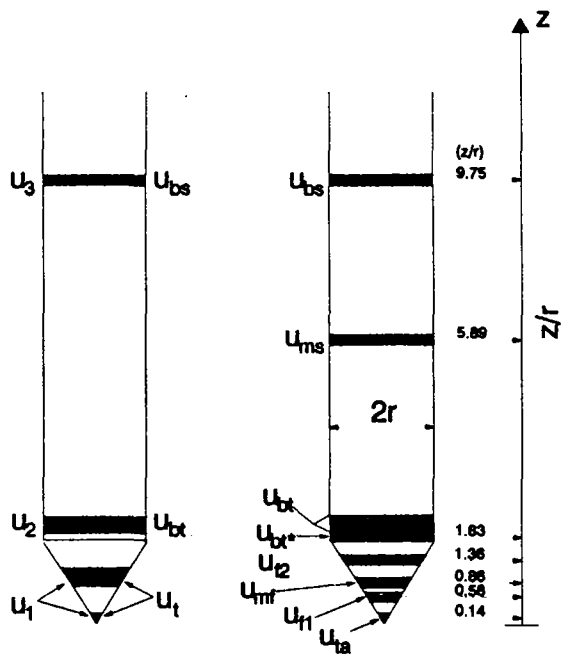

Figure 7.1. The Rainbow Piezocone Illustrating Various Porous Element Locations. (Brown 1993)

7.2.4. Stress Path Analysis

The components Δu_{TSP} and Δu_{shear} can be approximately determined from a stress path analysis. As illustrated in Figure 7.2(a), the soil element is assumed to be initially anisotropically-consolidated under K_o consolidations. The soil is then sheared to failure where the effective stress path intersects the failure envelope. While the magnitude of Δu_{shear} at failure depends solely upon the governing shearing mode, Δu_{TSP} varies with the total stress path as well (Wroth 1984). The slope of the total stress path is determined by the change of loading conditions surrounding the soil element as the penetrometer approaches. As the cone advances into the soil, a wedge is formed in the vicinity of the tip within which the soil exhibits elastic behavior. This phenomenon is illustrated in Figure 7.2(b) which depicts a tri-zonal failure mechanism formed beneath a rigid penetrating probe (Vesić 1975, Vesić 1977). There are three zones produced in the deformed soil: an elastic region (Zone I), radial shear zone (Zone II), and plastic failure or cavity expansion region (Zone III). The induced excess pore pressures in these zones are Δu_{TSP}, Δu_{shear}, and Δu_{oct} for Zones I, II, and III, respectively.

The loading condition of the soil elements located immediately adjacent to the cone tip (Zones I and II) can therefore be evaluated by elasticity theory. As shown in Figure 7.3, a rigid circular loading is assumed at the level of cone base which acts on a semi-infinite elastic medium (Schiffman and Aggarwala, 1961). The ratio of the distributed radial stress to the vertical stress along the cone face increases as the soil element moves from the apex to the cone base. The total stress paths corresponding to different stress ratios vary accordingly and indicate an increase of pore pressure component Δu_{TSP} as the position of the soil element moves from the apex to other points on the cone face. A discontinuity of pore pressure distribution is expected near the base since the pore pressure drops from a theoretical value of infinity to a value which is much smaller than those measured on the face.

Since many Type 1 piezocones have the filter element located between the mid-face and the upper mid-face of the cone, a representative $\Delta\sigma_r/\Delta\sigma_z = ½$ is chosen from that region, indicating a total stress path of 3:4 (V:H) in the Cambridge q-p space [(in which $q = (\sigma_v - \sigma_h)$ and $p' = ⅓(\sigma_v' + 2\sigma_h')$] to represent the typical pore pressure response for

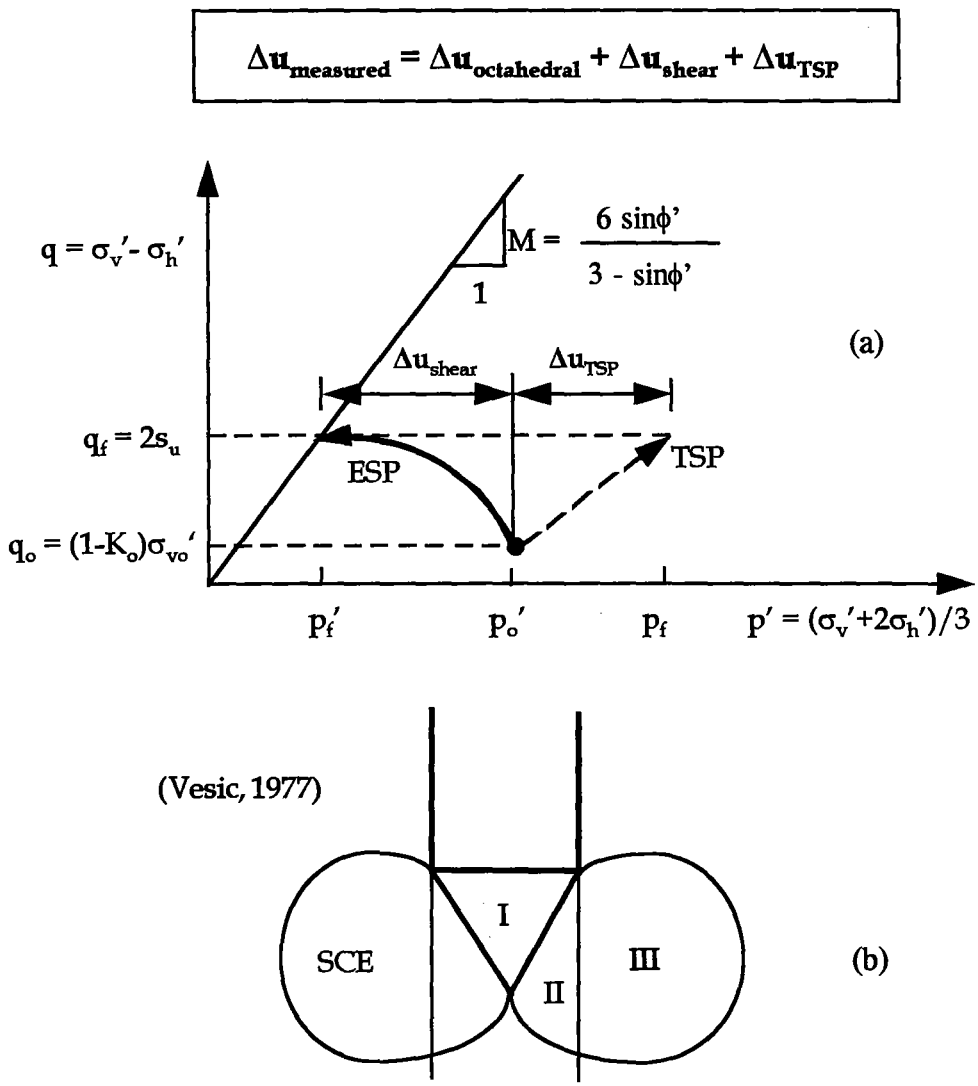

Zone I : Elastic Zone (Δu_{TSP}) from Stress Path Analysis

Zone II : Shear Zone (Δu_{shear}) from Stress Path Analysis

Zone III: Plastic Zone (Δu_{oct}) from Spherical Cavity Expa

Figure 7.2. (a) Stress Path Approach for Obtaining Pore Pressure Components.
(b) Failure Zones Under a Penetrating Point. (Vesic 1977)

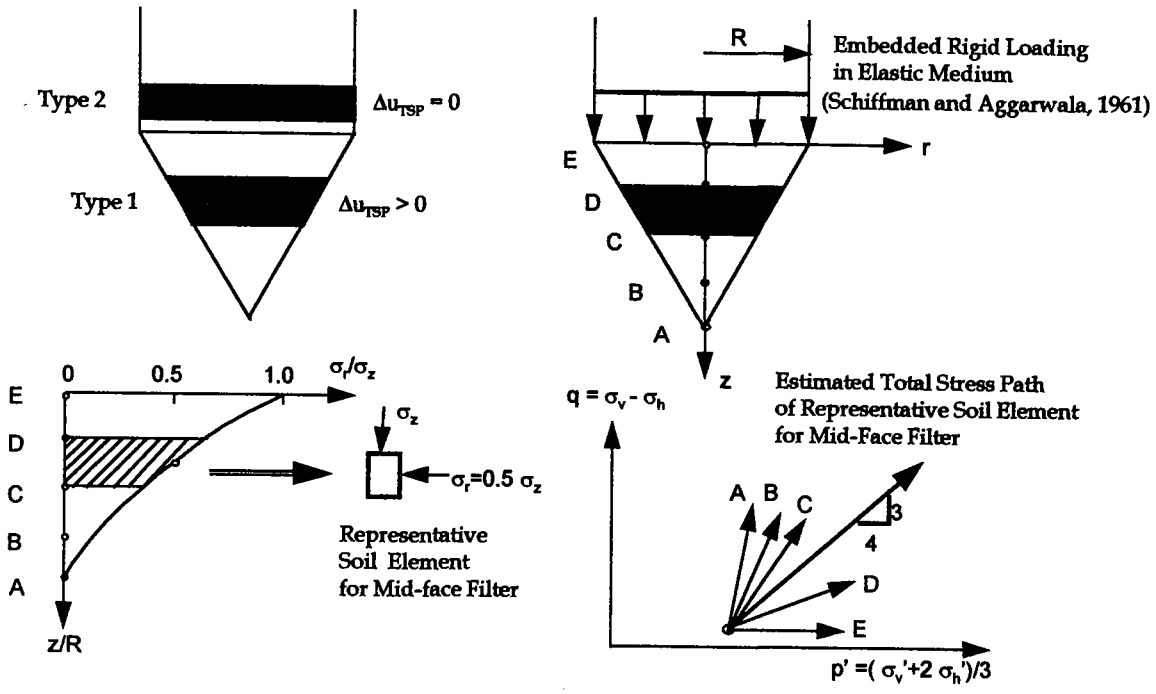

Figure 7.3. An Elasticity Approach for Determining the Magnitude of Excess Pore Pressures Due to the Total Stress Path of Soil Elements Under a Penetrating Cone.

Type 1 piezocones. As a consequence, $\Delta u_{TSP} > 0$ for Type 1 piezocones. For Type 2 piezocones, the porous element is located outside of the elastic compression region. Therefore, the pure shearing action in the governing direct simple shear (DSS) mode implies that all pore pressures generated are shear-induced and $\Delta u_{TSP}=0$.

7.2.5. Strength Anisotropy

The different shearing modes for the components of Δu_{TSP} and Δu_{shear} also distinguish the variation in response for filter locations on the piezocone. Baligh (1984) illustrated the predominant failure modes adjacent to an advancing probe, as shown in Figure 7.4. The dislocation center proposed by Elsworth (1991) has been used to delineate the focal point which describes four regions of loading. In Zone I directly beneath the probe, the major principal strain (or stress) acts in the vertical direction and conditions imposed are

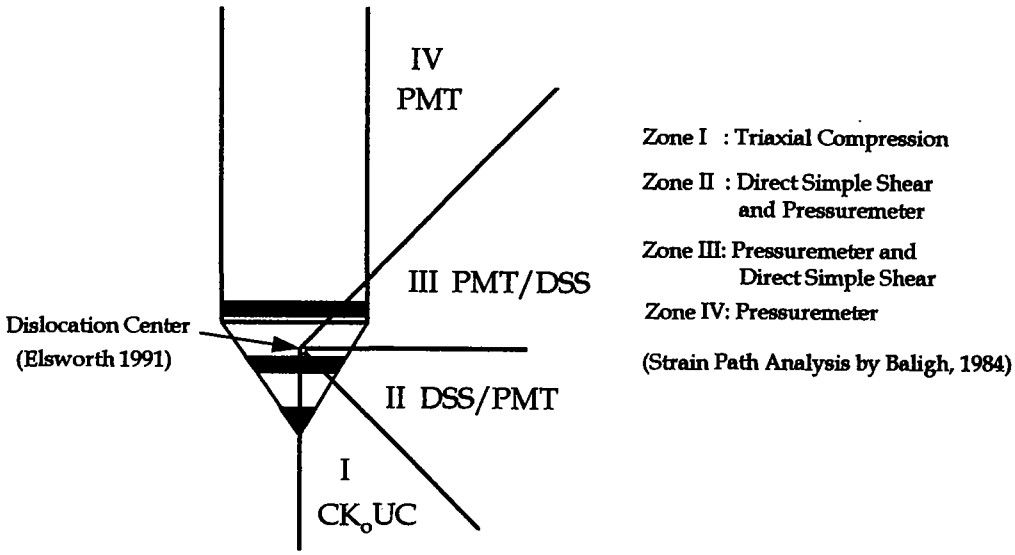

Figure 7.4. Relevance of Strength Anisotropy and Different Shearing Modes Around a Penetrating Cone in Clays. (Baligh 1984)

similar to those of triaxial compression (CK$_o$UC). In Zones II and III, the strains associated with a combined loading in direct simple shear (DSS) and the pressuremeter test (PMT) are more appropriately related. In Zone IV, the major principal strain is that associated with the conditions imposed during a pressuremeter test.

Keaveny and Mitchell (1986) suggested that the CK$_o$UC test corresponds to a strength similar to that mobilized immediately beneath the cone apex. The principal loading direction gradually rotates as the soil element moves along the cone face toward the shaft. Although there exists a transitional zone, the pore pressure measurements with the porous element located behind the tip should be represented by a shearing mode corresponding to DSS and/or PMT. In this regard, Prevost (1979) proposed an elasto-plastic constitutive soil model for interrelating the normalized undrained strength of clays relevant to both DSS and PMT modes and indicated that the difference in s_u/σ_{vo}' between the two tests was fairly small, as shown in Figure 7.5(a). A similar result was obtained from the constitutive model of Ohta et al. (1991), which gives values of s_u/σ_{vo}' of DSS and PMT that are quite

comparable, as illustrated by Figure 7.5(b).

For Type 1 piezocones, both Δu_{TSP} and Δu_{shear} are more properly modeled by the CK_oUC mode because of the high compression zone beneath the cone tip. In fact, positive pore pressures are always observed for Type 1 measurements in clays at all OCR ranges (Mayne et al. 1990). For Type 2 piezocones, the Δu_{shear} term becomes a more predominant component than Δu_{TSP}. Positive Δu are characteristic of Type 2 cones in soft to stiff intact clays but zero to negative pore pressures have been observed for Type 2 piezocones in heavily overconsolidated fissured clays (Lunne et al. 1986b). Negative Δu are often measured in DSS tests on clays at high OCRs. Thus, the pure shearing action in the DSS test gives characteristic pore pressures that are shear-induced with $\Delta u_{TSP} = 0$.

The governing stress paths of soil elements deformed adjacent to a penetrating cone for both Type 1 and Type 2 piezocones are illustrated in Figures 7.6(a) and 7.6(b), respectively. Considering the combined influences of strength anisotropy and total stress path, the components of Δu_{TSP} and Δu_{shear} for Type 1 piezocones can be derived from the stress path analysis and expressed as:

Type 1:

$$\Delta u_{TSP} = \left(\frac{4}{3}\right) [2(s_u)_{CKoUC} - (1-K_o)\sigma'_{vo}] \qquad [7.5a]$$

$$\Delta u_{shear} = p'_o - \frac{2(s_u)_{CKoUC}}{M} + c'\cot\phi' \qquad [7.5b]$$

where the (4/3) term in [7.5a] corresponds to a mid-face element because of the implied stress path. For Type 2 piezocones, a constant p stress path is adopted such that:

Type 2:

$$\Delta u_{TSP} = 0 \qquad [7.6a]$$

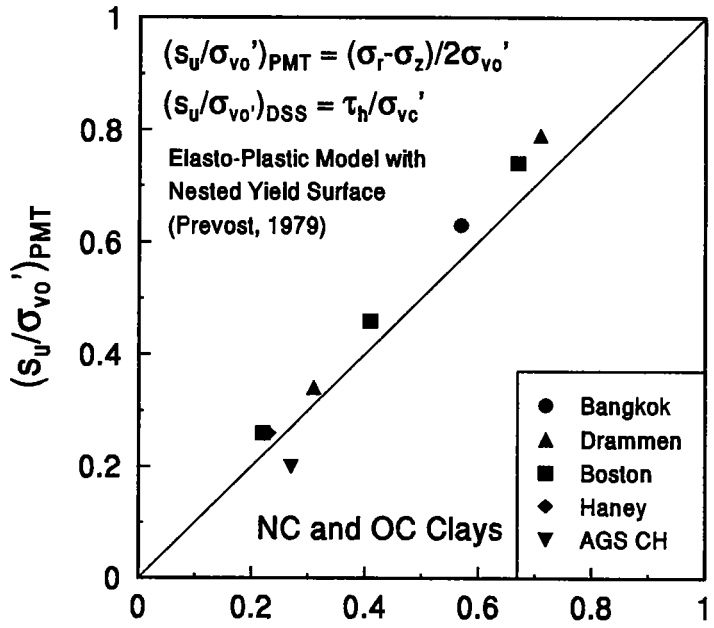

Figure 7.5. (a) Predicted Normalized Undrained Strength for Pressuremeter Test (PMT) vs. Direct Simple Shear (DSS).

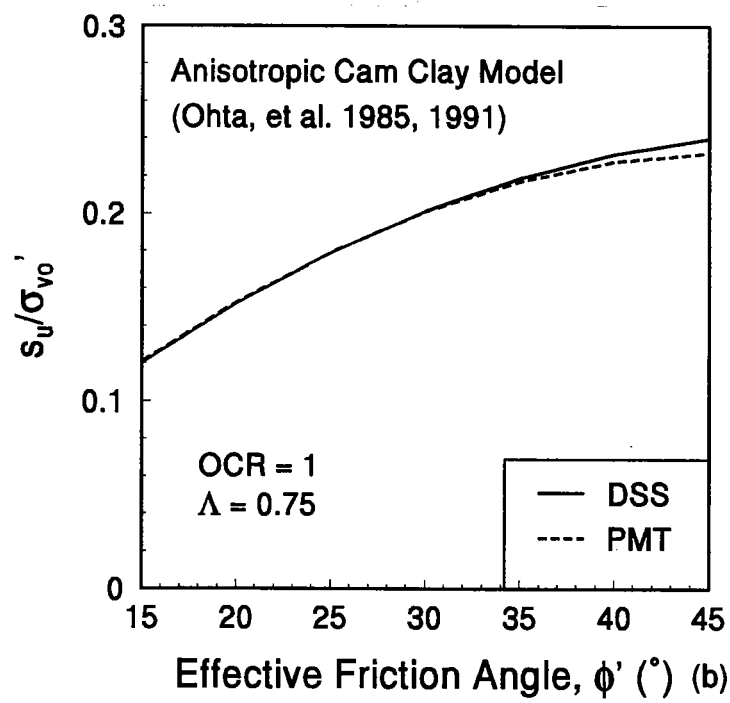

Figure 7.5. (b) Predicted Normalized Undrained Strength for DSS and PMT Modes as Functions of Effective Friction Angle (ϕ').

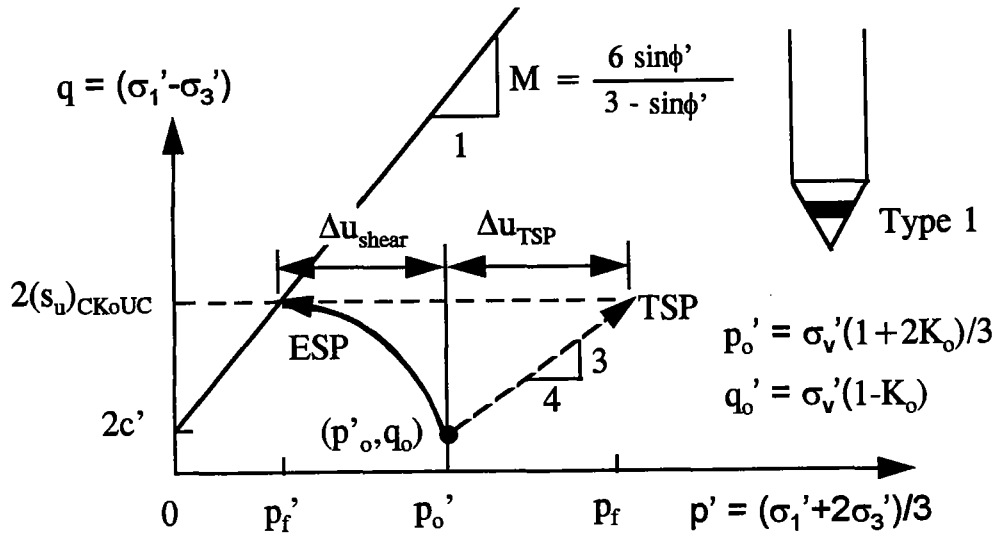

(a)

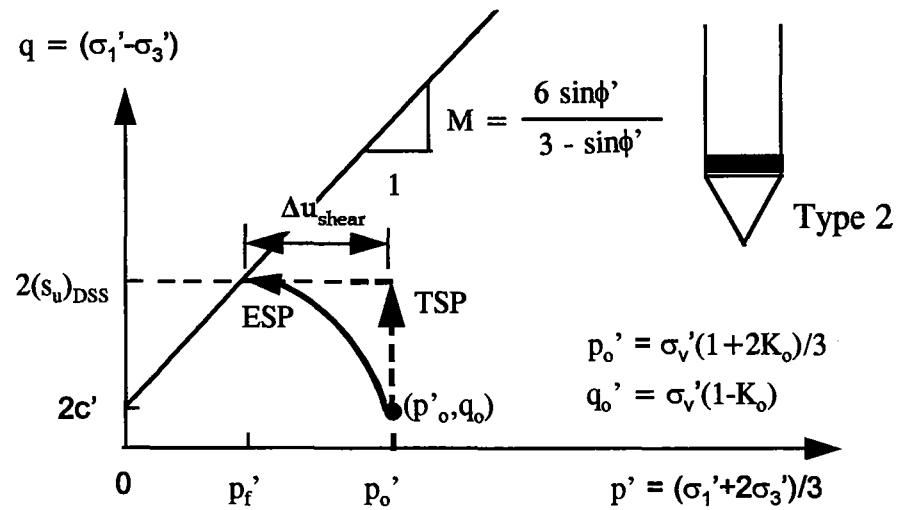

Figure 7.6. Stress Path Analysis of Soil Elements Adjacent to a Penetrating Cone for (a) Type 1 and (b) Type 2 Pore Pressure Measurements.

$$\Delta u_{shear} = p_o' - \frac{2(s_u)_{DSS}}{M} + c'\cot\phi' \qquad [7.6b]$$

For heavily-overconsolidated cohesive materials, an apparent cohesion intercept c' may exist, as illustrated by Figure 7.6. Mayne and Stewart (1988) reported a range of apparent cohesion intercept values of $c'/\sigma_p' = 0.03$ to 0.06 from CK_oUC test data. The value of c' actually reflects that portion of the yield surface above the frictional envelope at states of dry critical. Force fitting of a Mohr-Coulomb envelope to a surface that is, in reality, curved results in values of c' that depend upon confining stress level and other factors (Mesri and Abdel-Ghaffar, 1993).

7.2.6. Constitutive Soil Model

The relevant undrained shear strength (s_u) can be measured using different devices in the laboratory (triaxial, simple shear, plane strain), or else evaluated by various constitutive soil models. The latter approach has been adopted herein. Wroth (1984) derived an expression for the normalized undrained shear strength corresponding to the anisotropically-consolidated triaxial compression (CAUC) test. The initial state of stresses for the NC region was approximated by Jaky's (1944) equation ($K_{oNC} = 1 - \sin\phi'$). For triaxial compression, the normalized undrained shear strength ratio is given by (Wroth and Houlsby 1985):

$$\left(\frac{s_u}{\sigma_{vo}'}\right)_{CAUC} = \frac{\sin\phi'(a^2+1)^{\Lambda}}{2a}\left(\frac{OCR}{2}\right)^{\Lambda} \qquad [7.7]$$

in which $a = (3-\sin\phi')/(6-4\sin\phi')$, Λ = plastic volumetric strain ratio = $1-\kappa/\lambda$, κ = isotropic swelling index, and λ = isotropic compression index. For natural unstructured clays, a value of $\Lambda = 0.75$ is appropriate for compression, $\Lambda = 0.80$ for simple shear, and $\Lambda = 0.85$ for extension (Kulhawy and Mayne, 1990). However, structured, cemented, and/or sensitive materials may be better characterized by $\Lambda = 1.0$ (Brown and Mayne, 1993).

In comparison with actual triaxial test data from 71 natural clays, Figure 7.7(a) shows that the anisotropic Modified Cam Clay model generally predicts the trend of increasing normalized undrained strength $(s_u/\sigma_{vo}')_{CKoUC}$ with ϕ' in the normally-consolidated state. The effect of the parameter Λ has much less influence on the NC strength. Actually, Modified Cam Clay somewhat underpredicts the strengths because it does not consider structural fabric of the soil or natural bonding mechanisms. Modified Cam Clay also provides an evaluation of the undrained strength for overconsolidated clays (Wroth, 1984) and can predict the approximate magnitude of shear-induced pore pressures as well (Kulhawy and Mayne 1990).

The effect of strength anisotropy can be taken into account using the ratio of $(s_u)_{DSS}$ to $(s_u)_{CKoUC}$, or K_{45}. Randolph and Wroth (1981) showed K_{45} to be a function of ϕ' that can be expressed as:

$$K_{45} = \frac{(s_u)_{DSS}}{(s_u)_{CKoUC}} = \frac{(3-\sin\phi') \cos\phi'}{3} \qquad [7.8]$$

Using Eq. [7.8], the ratio $K_{45} = (s_u)_{DSS}/(s_u)_{CKoUC}$ decreases from 0.83 to 0.60 as ϕ' increases from 20° to 40°, with an average value of 0.72 when $\phi' = 30°$. This compares well with lab-measured values of K_{45} for a number of natural clays (Ladd and Edgers 1972; Mayne 1985; Kulhawy and Mayne 1990), as shown in Figure 7.7(b).

The use of Modified Cam Clay or other constitutive soil models for representing the undrained strength should not be taken as complete and encompassing. Many aspects such as sensitivity, fabric, and geologic origin are important, though not considered by these models. Thus, the PCPT-OCR model discussed herein will not account for these facets since these simple constitutive soil models are utilized to represent strength behavior due solely to stress-induced effects.

7.2.7. Strain Rates

The piezocone test is performed at a constant rate of 20 mm/sec, which is much faster than standard laboratory triaxial shear tests. It is well recognized that clay strength

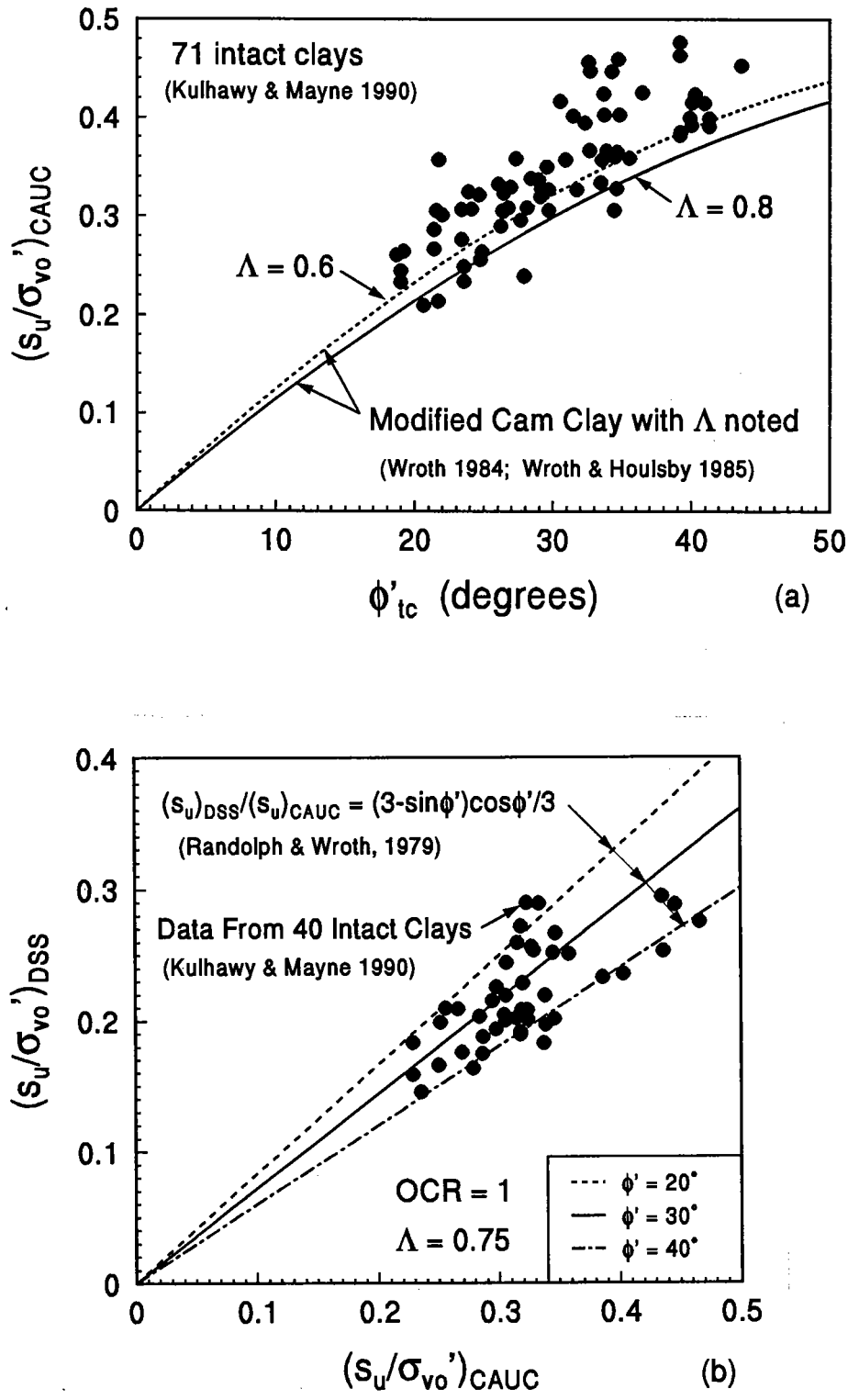

Figure 7.7. Predicted and Measured Strengths for NC Clays in (a) Triaxial Compression and (b) Direct Simple Shear.

increases with strain rate of loading. Ladd and Foott (1974) observed that each log cycle of strain rate is accompanied by a 10% increase in s_u. Kulhawy and Mayne (1990) confirmed this observation by reviewing data from 26 clays tested in triaxial compression, as shown in Figure 7.8. Considering a strain rate ($\dot{\varepsilon} = d\varepsilon/dt$) of 1% per hour as the standard reference rate for laboratory measured s_u, the effect of other strain rates is expressed as a correction factor:

$$a_{Rate} = \frac{(s_u)_{\dot{\varepsilon}}}{(s_u)_{\dot{\varepsilon}=1\%/hr}} = 1.0 + 0.1 \log\dot{\varepsilon} \qquad [7.9]$$

For a 10 cm^2 cone with a diameter of 35.7 mm, the strain rate corresponding to the 20 mm/sec penetration rate is approximately 201,680 % per hour. Thus, according to Eq. [7.9], the s_u obtained from the piezocone test should be 53% higher than that determined by standard laboratory methods conducted at the reference strain rate of 1 % per hour. For a 15 cm^2 cone with a diameter of 43.7 mm, the s_u obtained from the piezocone test is 52% higher. Graham et al. (1983) showed this a_{Rate} is reasonable for other tests, such as direct simple shear and triaxial extension tests as well.

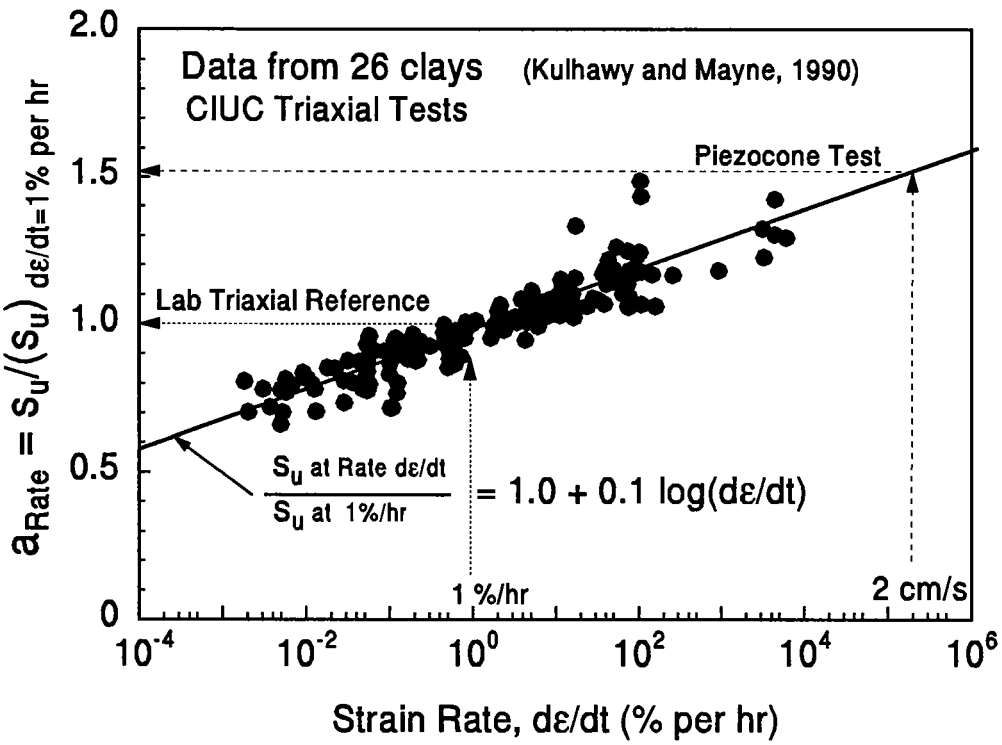

Figure 7.8. Strain Rate Influence on Undrained Strength of Clays. (Kulhawy and Mayne 1990).

7.3. Model Formulation

The three terms of measured excess pore pressures (Δu_m) given by [7.2] can now be expressed for the two types of cones and solved for the octahedral component:

$$\Delta u_{oct} = \Delta u_m - \Delta u_{tsp} - \Delta u_{shear} \qquad [7.10]$$

By introducing the strength term from the anisotropic version of Modified Cam Clay (Eq. [7.7]) and the effect of strength anisotropy (Eq. [7.8]) into the pore pressure equations (Eqs. [7.7] and [7.6]), equations [7.4] and [7.10] can be combined and rearranged to evaluate the OCR in terms of piezocone test parameters. An adjusted undrained shear strength ($a_{Rate} \circ s_u$) is utilized to account for the strain rate effect. The resulting OCR predictions for Type 1 and 2 piezocones can be expressed as follows:

Type 1: [7.11a]

$$OCR = 2\left[\frac{aM}{a_{Rate}\sin\phi'(a^2+1)^{\Lambda}(0.62M+1)}\left(\frac{q_T-u_1}{\sigma'_{vo}}-\frac{1-K_o}{0.75}+\frac{c'\cot\phi'}{\sigma'_{vo}}\right)\right]^{1/\Lambda}$$

Type 2: [7.11b]

$$OCR = 2\left[\frac{aM}{a_{Rate}\sin\phi'(a^2+1)^{\Lambda}[1.95M+(3-\sin\phi')\cos\phi'/3]}\left(\frac{q_T-u_2}{\sigma'_{vo}}+\frac{c'\cot\phi'}{\sigma'_{vo}}\right)\right]^{1/\Lambda}$$

For a piezocone with dual pore pressure measurements, or where both u_1 and u_2 are available from paired soundings, a dual-type model which combines Eqs. [7.11a] and [7.11b] results in:

Dual:

$$OCR = 2\left[\frac{a}{a_{Rate}\sin\phi'(a^2+1)^{\Lambda}\left[\frac{5.85}{(3-\sin\phi')\cos\phi'}-0.62\right]}\left(\frac{\left[\frac{3}{(3-\sin\phi')\cos\phi'}-1\right]q_T}{\sigma'_{vo}}\right.\right.$$

$$\left.\left.+\frac{u_1-\frac{3}{(3-\sin\phi')\cos\phi'}u_2}{\sigma'_{vo}}+\frac{1-K_o}{0.75}+\frac{c'\cot\phi'}{\sigma'_{vo}}\left(\frac{3}{(3-\sin\phi')\cos\phi'}-1\right)\right)\right]^{1/\Lambda} \quad [7.11c]$$

where $M = 6\sin\phi'/(3-\sin\phi')$, $a = (3-\sin\phi')/(6-4\sin\phi')$, and Λ = plastic volumetric strain ratio. The in-situ value of K_o can be measured using the self-boring pressuremeter test or alternatively estimated using a relationship suggested by Mayne and Kulhawy (1982) if a simple load-unload stress history has occurred:

$$K_o = (1 - \sin\phi')\ OCR^{\sin\phi'} \quad [7.12]$$

Iterations are required for solving the value of OCR when Eq. [7.12] is used for the value K_o. It is important to note, however, that the in-situ K_o may be affected by other factors including: reload, cementation, aging, freeze-thaw cycles and geoenvironmental effects (Mayne and Kulhawy, 1990).

7.4. Alternative Constitutive Soil Model

In lieu of the anisotropic Modified Cam Clay model, a more complete constitutive formulation was offered by Ohta et al. (1985), who derived a generalized model for evaluating the undrained response of K_o-consolidated clays under different boundary conditions and stress rotation effects. This model was developed from the original Cam Clay with an induced stress anisotropy caused by rotating the bullet-shape yield envelope along the normally-consolidated K_o line. The generalized equation for expressing s_u as a function of the principal stress direction (θ) is:

$$\frac{s_u}{\sigma'_{vo}} = \frac{OCR^{\Lambda}\,(1+2K_{oNC})\,M\,e^{-\Lambda}}{3\sqrt{3}\,(\sqrt{\cosh\beta - \sinh\beta\,\cos 2\theta})} \qquad [7.13a]$$

where $\beta = \sqrt{3}\eta_o\Lambda/2M$, $\eta_o = 3(1-K_{oNC})/(1+2K_{oNC})$, and θ = the direction of major principal stress. For plane strain conditions, the undrained strength for compression, direct simple shear, and extension tests can be derived by substituting $\theta = 0$, $\pi/4$, and $\pi/2$, respectively. Equations for triaxial compression and extension loading of K_o- consolidated clays (CK_oUC and CK_oUE) can also be expressed in a similar way with an axisymmetric boundary condition. The equations of s_u/σ_{vo}' specific for CK_oUC and DSS are presented as follows:

$$\left(\frac{s_u}{\sigma'_{vo}}\right)_{CKoUC} = \frac{(1+2K_{oNC})}{6}\,M\,\exp\left(\frac{\Lambda\eta_o}{M}\right)\left(\frac{OCR}{e}\right)^{\Lambda} \qquad [7.13b]$$

$$\left(\frac{s_u}{\sigma'_{vo}}\right)_{DSS} = \frac{(1+2K_{oNC})\,M}{3\sqrt{3}\,\cosh\beta}\left(\frac{OCR}{e}\right)^{\Lambda} \qquad [7.13c]$$

where the initial state of stresses for the NC region is again approximated by Jaky's (1944) equation ($K_{oNC} = 1 - \sin\phi'$). The ratio of $(s_u)_{DSS}$ to $(s_u)_{CKoUC}$ using Ohta's criteria is therefore expressed as:

$$K_{45} = \frac{(s_u)_{DSS}}{(s_u)_{CKoUC}} = \frac{2}{\sqrt{3}\,\cos\beta\,e^{a\Lambda}} \qquad [7.13d]$$

By substituting Eqs. [7.13b] and [7.13c] into Eqs. [7.4], [7.5], and [7.6], the Ohta version of PCPT-OCR model is presented as follows:

Type 1:

$$OCR = e\left[\frac{aM}{a_{Rate}\sin\phi' e^{a\Lambda}(0.62M+1)}\left(\frac{q_T-u_1}{\sigma'_{vo}}-\frac{1-K_o}{0.75}+\frac{c'\cot\phi'}{\sigma'_{vo}}\right)\right]^{1/\Lambda} \quad [7.14a]$$

Type 2:

$$OCR = e\left[\frac{aM}{a_{Rate}\sin\phi' e^{a\Lambda}(1.95M+\frac{2}{\sqrt{3}\cosh\beta e^{a\Lambda}})}\left(\frac{q_T-u_2}{\sigma'_{vo}}+\frac{c'\cot\phi'}{\sigma'_{vo}}\right)\right]^{1/\Lambda} \quad [7.14b]$$

Dual:

$$OCR = e\left[\frac{a}{a_{Rate}\sin\phi' e^{a\Lambda}(1.69\cosh\beta e^{a\Lambda}-0.62)}\left(\frac{(0.87\cosh\beta e^{a\Lambda}-1)q_T}{\sigma'_{vo}}+\right.\right.$$

$$\left.\left.\frac{u_1-(0.87\cosh\beta e^{a\Lambda}-1)u_2}{\sigma'_{vo}}+\frac{1-K_o}{0.75}+\frac{c'\cot\phi'}{\sigma'_{vo}}(0.87\cosh\beta e^{a\Lambda}-1)\right)\right]^{1/\Lambda} \quad [7.14c]$$

As indicated earlier, if the approximate representations for K_o and c'/σ_{vo}' are introduced as functions of OCR, the equations [7.14] require iterations for solving OCRs.

7.5. Parametric Study

The predictive PCPT-OCR relationships are presented in their generic formats which require c', ϕ', a_{rate}, Λ, and K_o as input soil parameters. For practical applications, it is desirable to reduce the number of input parameters without imperiling the performance of the model. Parametric studies were performed to evaluate the significance of some input parameters using a compiled piezocone database which contains more than 200 clay sites. Selective data, which have been collected from reliable sources and well-documented with

the required parameters available, are adopted for evaluating the performance of the model. The required parameters include q_T, u_1, u_2, σ_{vo}', ϕ', as well as OCR from oedometer tests. Other parameters such as a_{rate}, Λ, c', and K_o are evaluated either empirically or theoretically since they are seldom reported in routine laboratory tests. For this purpose, there are 34 high-quality clay sites used in the validation for Type 1 piezocones, 47 sites for Type 2 cones, and 26 sites for evaluating dual-type piezocone tests, respectively.

The parameter Λ is essentially constant for natural intact and uncemented clays and averages about 0.75, 0.80, and 0.85 for compression, simple shear, and extension modes, respectively, when evaluated as the slope of log (s_u/σ_{vo}') versus log(OCR) from regression analyses on laboratory test data (Mayne 1988; Kulhawy and Mayne 1990). In certain structured and cemented materials, however, the value of Λ may be as high as 1.0, as indicated by Brown and Mayne (1993). Field vane tests on natural clays also suggest Λ = 1 (Chandler, 1988; Mayne and Mitchell, 1988). A value Λ = 0.75 has been tentatively suggested herein, corresponding to triaxial compression test results on insensitive and unstructured sedimentary clays.

7.5.1. Parametric Effect of K_o

In the proposed model, iterative solutions are required if the coefficient of earth pressure at rest is evaluated by $K_o \sim (1\text{-}\sin\phi')\ OCR^{\sin\phi'}$. For both the Type 1 and dual-type models, the K_o effect in fact has already been partially incorporated during the derivation since $K_{oNC} \sim 1\text{-}\sin\phi'$ was assumed in evaluation of both the Wroth (1984) and Ohta et al. (1985) constitutive soil models. The piezocone prediction will become closed-form and more convenient to use if the $(1\text{-}K_o)/0.75$ term is removed from the equations. For the Type 2 derivation, the $(1\text{-}K_o)/0.75$ term does not occur due to the constant p stress path adopted. Figures 7.9(a) to (c) show that using Eqs. [7.11] without the $(1\text{-}K_o)/0.75$ term still provides a reasonably close approximation for the OCR predictions in normally consolidated (OCR≈1), lightly overconsolidated ($1 \le OCR \le 6$) and medium to heavily OC clays ($4 \le OCR \le 16$). In fact, however, for some NC soft clays, u_1 could be so close to q_T that the term $(q_T\text{-}u_1)/\sigma_{vo}'$ becomes very small and sensitive to measurement errors. Erroneous results are observed once the value of the term $[(1\text{-}K_o)/0.75]$ exceeds the unreasonably small value of

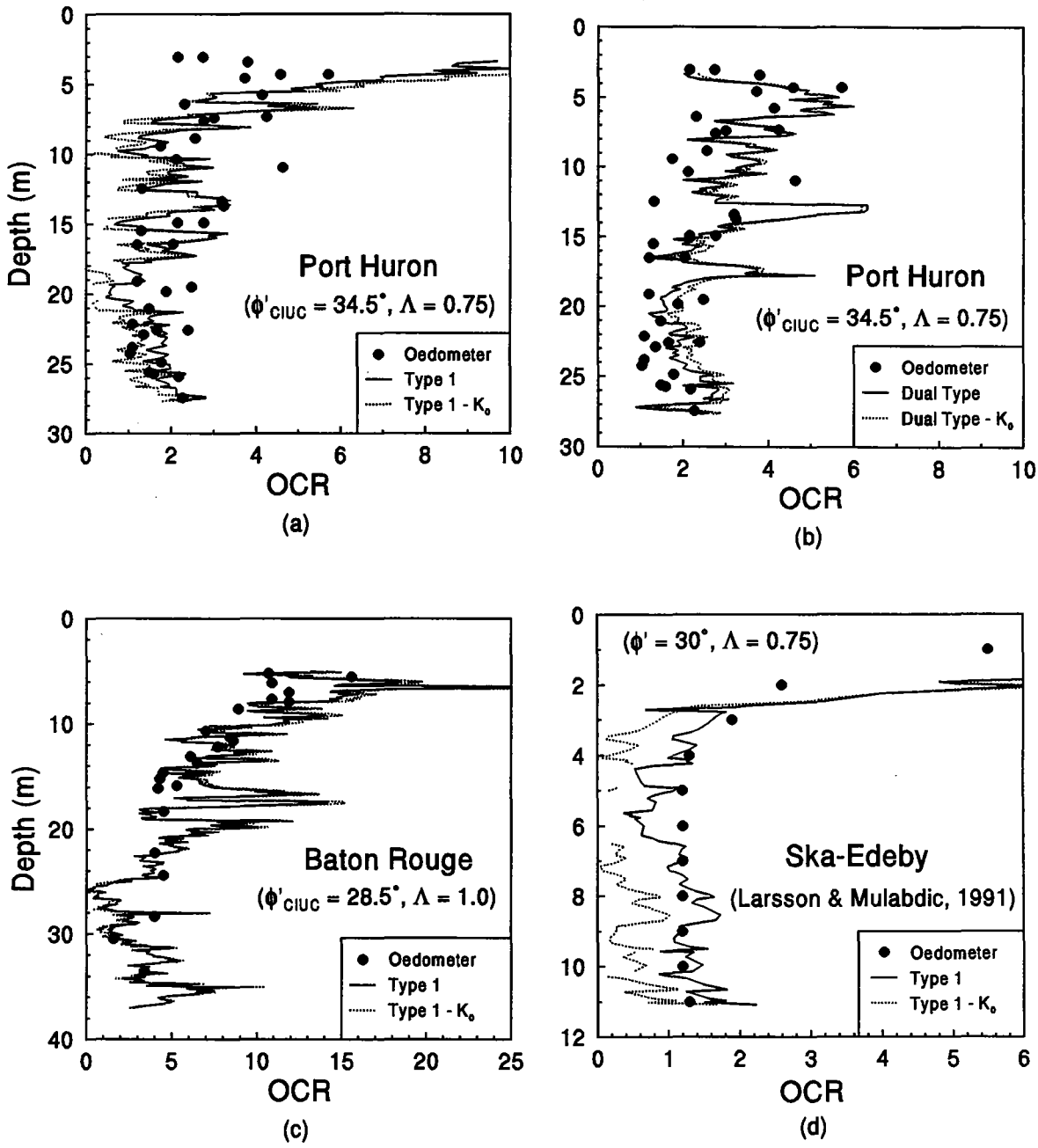

Figure 7.9. Parametric Studies of the K_o-Term Effect on Type 1 and Dual-type Models.
(a) Port Huron - Type 1; (b) Port Huron - Dual Type
(c) Baton Rouge - Type 1; (d) Ska Edeby - Type 1

$(q_T-u_1)/\sigma_{vo}'$, as shown for the plastic organic clay at Ska-Edeby in Figure 7.9(d). It is found that by dropping the term $(1-K_o)/0.75$ from the proposed equations, the erroneous results can be avoided and the prediction becomes more stable even when the $(q_T-u_1)/\sigma_{vo}'$ is very small. For stiffer clays, as that shown in Figure 7.9(c), the term $[(1-K_o/0.75]$ appears to have little influence.

7.5.2 Parametric Effect of c'

The parametric effect of the effective cohesion intercept (c') is evaluated by comparing the actual and predicted OCRs using the selected piezocone database. Here, the value of c' is taken to be about 0.04 σ_p' (Mayne and Stewart 1988; Mesri and Abdel-Ghaffar 1993), or $c'/\sigma_{vo}' = 0.04$ OCR, which requires an iterative solution for evaluating OCR. The ratios of measured to predicted OCR from regression analyses are summarized in Table 7.1 and indicate that the predicted OCRs, in general, agree with those measured (ratio = 1.0 ± 0.1) for both cases investigated: (1) $c'/\sigma_{vo} = 0.04$ and (2) assuming $c'=0$. It is evident that the differences between the two are small. The coefficient of determination (r^2) are similar for both sets with and without c'. Actually, the prediction for Type 1 cones is somewhat improved in the measured to predicted ratio. Therefore, the proposed expressions can be simplified by assuming $c' \approx 0$ while still maintaining reasonable prediction capabilities.

Table 7.1. Parametric Effect of Effective Cohesion Intercept in OCR Predictions.

Type	$c'/\sigma_{vo}' \approx 0.04$ OCR			$c'/\sigma_{vo}' \approx 0$			Difference Calculated in Ratio (%)
	n	r^2	Ratio	n	r^2	Ratio	
1	468	0.839	0.904	468	0.826	0.996	10.2
2	657	0.924	1.081	657	0.916	1.148	6.2
Dual	361	0.864	1.096	361	0.863	1.125	2.6

Notes: n = number of data points
r^2 = coefficient of determination
Ratio = ratio of measured OCR to predicted OCR

Based upon the aforementioned parametric study, modified versions of Eqn. [7.11] using the Wroth-Houlsby-Randolph constitutive soil model are proposed as follows:

Type 1:

$$OCR = 2\left[\frac{aM}{a_{Rate}\sin\phi'(a^2+1)^{\Lambda}(0.62M+1)}\left(\frac{q_T-u_1}{\sigma'_{vo}}\right)\right]^{1/\Lambda} \qquad [7.15a]$$

Type 2:

$$OCR = 2\left[\frac{aM}{a_{Rate}\sin\phi'(a^2+1)^{\Lambda}[1.95M+(3-\sin\phi')\cos\phi'/3]}\left(\frac{q_T-u_2}{\sigma'_{vo}}\right)\right]^{1/\Lambda} \qquad [7.15b]$$

Dual:

$$OCR = 2\left[\frac{a}{a_{Rate}\sin\phi'(a^2+1)^{\Lambda}\left(\frac{5.85}{(3-\sin\phi')\cos\phi'}-0.62\right)}\right.$$

$$\left.\cdot\left(\frac{\left[\frac{3}{(3-\sin\phi')\cos\phi'}-1\right]q_T+u_1-\frac{3}{(3-\sin\phi')\cos\phi'}u_2}{\sigma'_{vo}}\right)\right]^{1/\Lambda} \qquad [7.15c]$$

As discussed previously, the value of strain rate factor $a_{Rate} = 1.53$ can be adopted for cone penetration tests in the above equations for both 10 cm^2 and 15 cm^2 cones.

Similar modifications can be made to obtain simplified expressions with the constitutive soil model by Ohta et al. (1985). The equations are given by Eqs. [7.14] except the $(1-K_o)/0.75$ and $c'\cot\phi'/\sigma_{vo}'$ terms are set equal to zero.

7.5.3. Parametric Effect of Using Different Constitutive Soil Models

The consequences of using different constitutive relationships have been evaluated by comparing measured versus predicted OCRs via regression analyses, as summarized in Table 7.2. It appears that the OCRs predicted using the model by Ohta et al. (1985) are slightly better than those predicted using Wroth (1984) for both Type 2 and dual models, while it is the anisotropic MCC model that is better for the Type 1 piezocones. Nevertheless, the ratio of measured to predicted OCRs between the two constitutive soil models are fairly similar (differences of 1.5 to 8.8%).

Table 7.2. Comparative Studies Using Different Constitutive Soil Models.

Type Cone	Case	Regression Results n	r^2	Ratio	Difference in Ratio (%)
1	Wroth	468	0.826	0.996	1.5
	Ohta	468	0.827	0.981	
2	Wroth	657	0.916	1.148	6.1
	Ohta	657	0.925	1.082	
Dual	Wroth	361	0.863	1.125	8.8
	Ohta	361	0.885	1.034	

Notes: n = number of data points
r^2 = coefficient of determination
Ratio = ratio of measured OCR to predicted OCR

Figures 7.10 to 7.12 show general trends of the measured versus predicted OCRs for Type 1, Type 2, and dual-type piezocones using the PCPT-OCR model (Eq.[7.15]) with the anisotropic Modified Cam Clay model given by Wroth (1984), Wroth and Houlsby (1985), and Randolph and Wroth (1981). Both arithmetic and logarithmic graphs are presented. The full logarithmic plots have been prepared for examining the performance of the model at low OCR ranges. Although not shown here, similar trends are observed for the predicted versus measured OCRs for Type 1, Type 2, and dual-type piezocones anisotropic constitutive soil model proposed by Ohta et al. (1985).

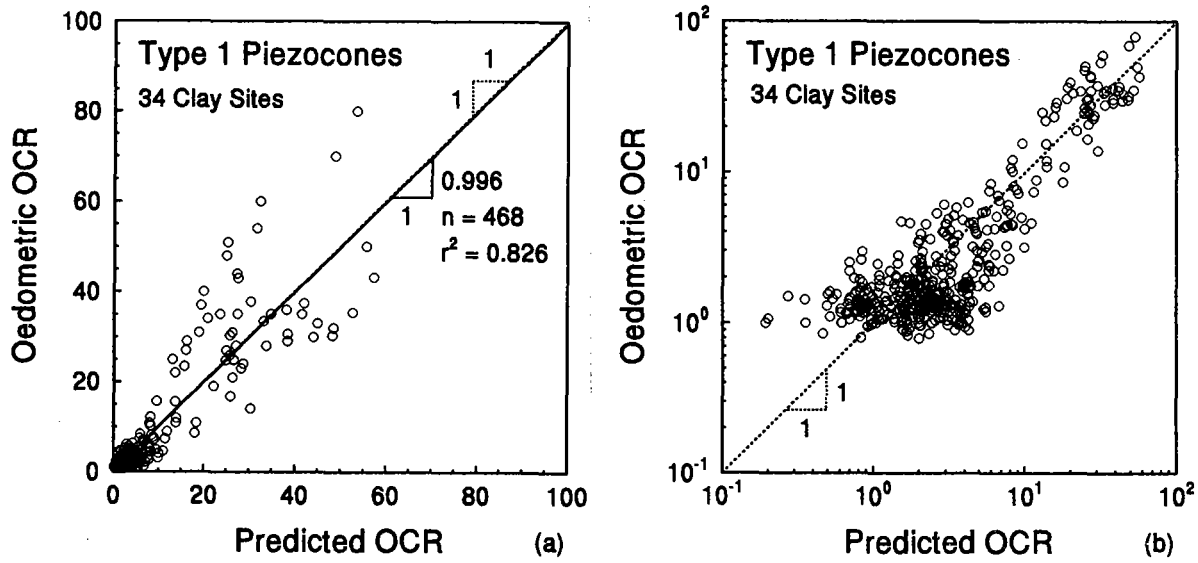

Figure 7.10. Measured versus Predicted OCRs for Type 1 PCPT-OCR Model.

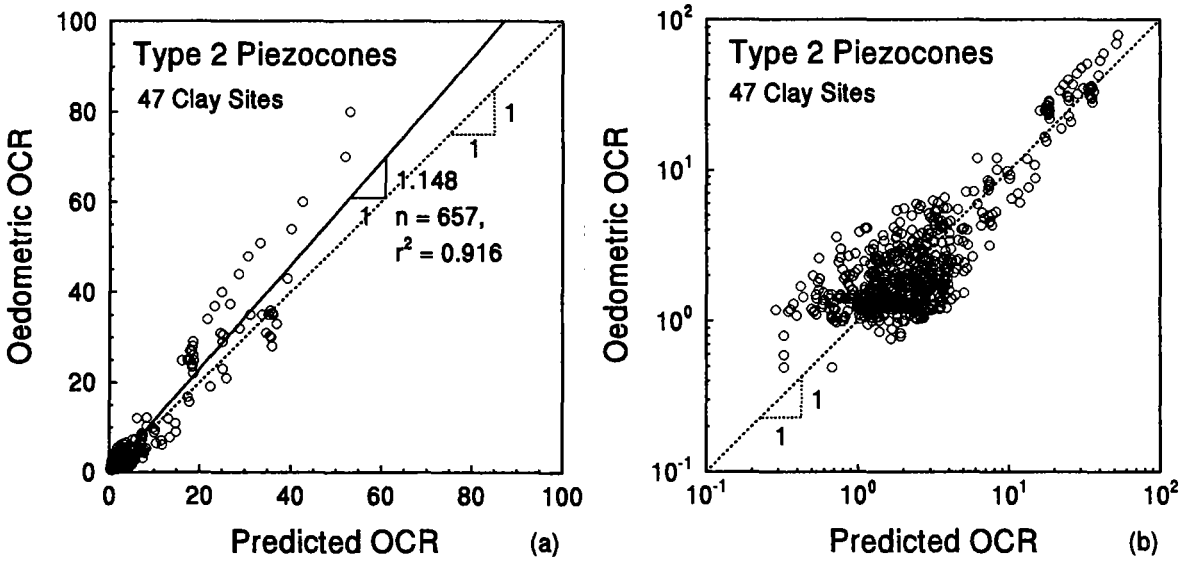

Figure 7.11. Measured versus Predicted OCRs for Type 2 PCPT-OCR Model.

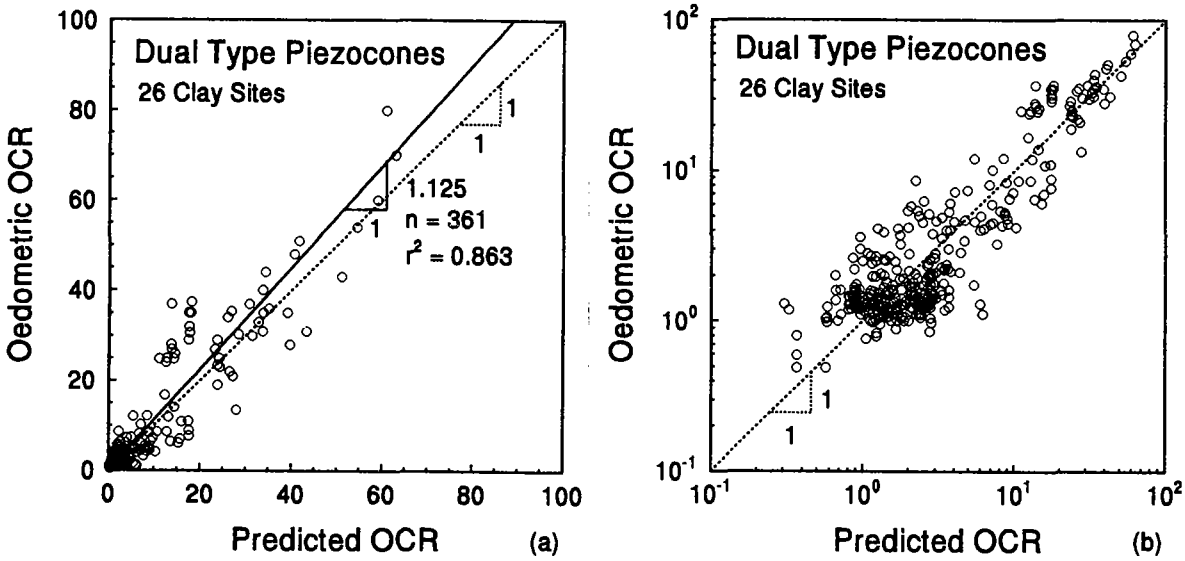

Figure 7.12. Measured versus Predicted OCRs for Dual-Type PCPT-OCR Model.

7.5.4. Recommendations for Practical Applications

The evaluation of in-situ OCR from piezocone data is a valuable supplement to the results of expensive, time-consuming laboratory consolidation tests on undisturbed specimens of clay. The continuous OCR profile interpreted from piezocone test results using the proposed analytical model can be prepared on site immediately as soon as the test is completed. In this regard, the effective friction angle (ϕ') of the clay may not be available on site and will have to be estimated for obtaining an approximate OCR profile. The reliance on the effective friction angle (ϕ') is apparent in the proposed model since many of the terms are the functions of ϕ' ($\sin\phi'$, M, and a). Hence, the parametric effect of ϕ' has been examined for the Type 1, Type 2, and dual-type models. It indicates that the OCR predictions are only slightly affected by varying ϕ', as illustrated by the example given in Figure 7.13(a) for the Lower 232nd Street site in British Columbia (Campanella et al. 1988). The parametric effect of Λ has also been investigated and the results show that $\Lambda = 0.75$ is

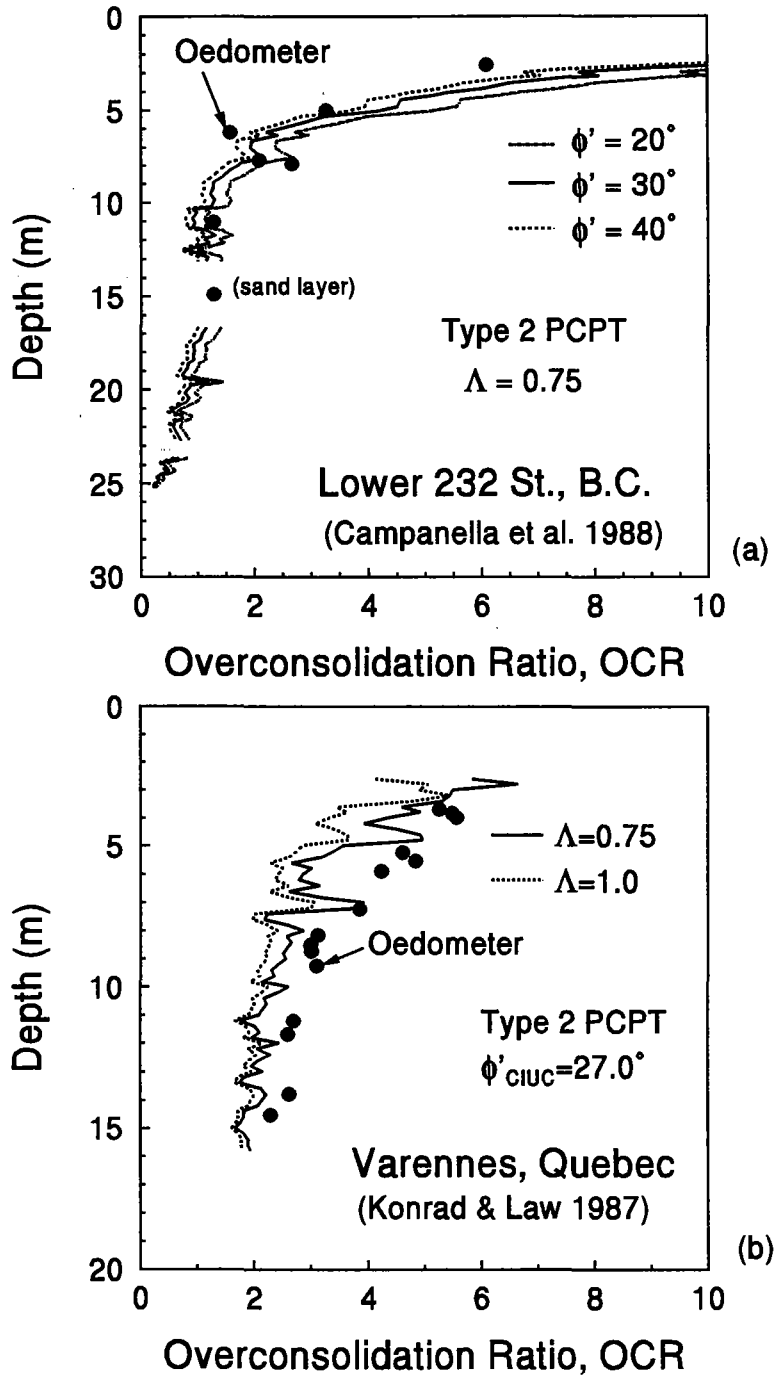

Figure 7.13 Parametric Effects of (a) Effective Friction Angle (ϕ') and (b) Plastic Volumetric Strain Ratio (Λ).

adequate in most cases involving nonstructured clays of low sensitivity. For structured clays, a value of $\Lambda \sim 1.0$ may be more appropriate. Figure 7.13(b) shows the Type 2 OCR predictions for the St. Hilaire clay (LaFleur et al. 1988) using $\Lambda = 0.75$ and 1.0. The effect of Λ at low OCRs is only slight, however. If conservatism is desired, a value of $\Lambda = 1.0$ may be used confidently.

The expressions in Eq. [7.15] can be further simplified to simple functions of ϕ' and Λ by using numerical approximations:

$$\text{Type 1:} \quad OCR \sim 2 \left[(0.51 - 0.14 \sin\phi') \left(\frac{q_T - u_1}{\sigma'_{vo}} \right) \right]^{1/\Lambda} \qquad [7.16a]$$

$$\text{Type 2:} \quad OCR \sim 2 \left[(0.38 - 0.25 \sin\phi') \left(\frac{q_T - u_2}{\sigma'_{vo}} \right) \right]^{1/\Lambda} \qquad [7.16b]$$

Dual: [7.16c]

$$OCR = \left\{ (0.93 - 1.21 \sin\phi')[q_T(1.38 \sin\phi' - 0.275) + u_1 - u_2(1.38 \sin\phi' + 0.725)] / \sigma_{vo}' \right\}^{1/\Lambda}$$

The effect of ϕ' is not particularly significant, however, which is quite different from the previous isotropic model discussed in Chapter V where ϕ' was somewhat important.

In the cases where soil property information is not available beforehand, average values of $\phi' = 30^o$ and $\Lambda = 0.75$ can be adopted in Eqs. [7.15] for obtaining quick and approximate OCR profiles of clay deposits using piezocones. The following expressions are suggested:

$$\text{Type 1:}\quad OCR \approx 0.667 \left(\frac{q_T - u_1}{\sigma'_{vo}} \right)^{1.33} \qquad [7.17a]$$

$$\text{Type 2:}\quad OCR \approx 0.315 \left(\frac{q_T - u_2}{\sigma'_{vo}} \right)^{1.33} \qquad [7.17b]$$

$$\text{Dual:}\quad OCR \approx 0.413 \left(\frac{0.385q_T + u_1 - 1.385u_2}{\sigma'_{vo}} \right)^{1.33} \qquad [7.17c]$$

A more elegant simplification to [7.15] is afforded by the adoption of a conservative value for the plastic volumetric strain ratio, $\Lambda = 1$. Whilst many lab strength tests subjected to load-unload indicate $0.75 \leq \Lambda \leq 0.85$ (Jamiolkowski, et al. 1985), field data from in-situ tests such as the vane suggest that $\Lambda \approx 1$ (Chandler, 1988; Mayne and Mitchell, 1988). In fact, the approach with $\Lambda = 1$ has been applied to many in-situ test methods, including CPT, DMT, FV, PMT, and SPT (Kulhawy and Mayne, 1990). The consequences of adopting values of $\phi' = 30°$ and $\Lambda = 1$ in [7.15] are given in Table 7.3 and these are quite similar to the regression expressions obtained from an empirical assessment of the piezocone database (Tables 3.3 and 3.4).

Of particular note here is that no differentiation has been made regarding whether the clays are intact or fissured. It is well recognized that the undrained strength and cone resistance are affected by degree of fissuring (Marsland and Quarterman, 1982; Powell and Quarterman, 1988). Fissuring also affects the measured distributions of penetration pore water pressures (Campanella, et al. 1986; Powell et al. 1988; Mayne et al. 1990). However, the direct relationship between the overconsolidation ratio and piezocone parameter, $(q_T - u_m)/\sigma_{vo}'$, does not appear to show separate trends for intact and fissured clays. A partial yet incomplete explanation is that the OCR from one-dimensional

consolidation tests is little affected by the presence of fissures during constrained compression, although fissuring can significantly reduce the strengths measured in the triaxial apparatus. A synergistic and interactive effect between the cone readings q_T, u_1, and/or u_2 may also reflect this phenomenon.

Table 7.3. Comparison of Simplified Theoretical Expressions ($\phi' = 30^o$, $\Lambda = 1$) with Results from Regression Analysis of Piezocone Database.

Type of Piezocone	SCE/MCC Theory	Empirical Statistics
Type 1 with pore pressures measured on cone face/tip	$OCR = 0.81(q_T-u_1)/\sigma_{vo}'$	$OCR = 0.78(q_T-u_1)/\sigma_{vo}'$
Type 2 with pore pressures measured at shoulder position	$OCR = 0.46(q_T-u_2)/\sigma_{vo}'$	$OCR = 0.53(q_T-u_2)/\sigma_{vo}'$

It is interesting to note that the Type 2 prediction is also quite similar to the expression derived from an effective stress analysis: $OCR = 0.5(q_T-u_2)/\sigma_{vo}'$ (Konrad and Law 1987; Robertson et al. 1990). Although different theoretical approaches resulted in similar formulations, the major benefit herein is that both Type 1 and 2 piezocones have been addressed in this study.

It is important that the OCR predictions from piezocones be compared with actual oedometer test results. Any discrepancy between the oedometer OCRs and the piezocone OCRs should be carefully examined to determine the possible causes since errors and/or anomalies can occur in both laboratory and field test methods. Disturbances due to sampling, specimen transportation, storage, preparation, and specimen trimming could result in erroneous interpretations of preconsolidation pressures from classical consolidation tests. On the other hand, the inherent geologic variability and errors in field measurements may deviate the piezocone predictions from the true OCR profile. Furthermore, the prediction model is based upon relatively simple constitutive soil models which do not account for aspects such as: soil fabric, sensitivity, mineralogy, aging, geologic origin, and overconsolidation caused by mechanisms other than the simple load-unload scenario. Caution in the use of any predictive method is therefore warranted.

7.6. Applications to Field Data

Individual clay sites from the piezocone database have been selected for the calibration and validation of the developed model. An important selection criterion was that each site contain well-documented data from reliable sources, including: (1) quality piezocone data with continuous profiles of q_T, u_1, and/or u_2; (2) adequate soil information for unit weight, index properties, shear strength (ϕ' and s_u), and oedometer OCR values; and (3) measurements of groundwater level, drawdown, and/or artesian conditions. The selected applications range from NC soft intact clay to heavily OC stiff fissured clay ($1 \leq$ OCRs ≤ 80), that have a wide range of frictional characteristics ($20^o \leq \phi' \leq 40^o$). Subsequently, the PCPT-OCR models given by Equation [7.15] are used to predict profiles of OCR for Type 1 , Type 2, and Dual-type piezocone data.

7.6.1. Data Filtering Technique

In order to demonstrate the methodology taken herein for filtering and validating the developed models, an example is presented using data from an offshore clay site in the Kringalik Plateau of the Beaufort Sea (Jefferies et al. 1987; Hughes et al. 1984), as illustrated in Figure 7.14. A set of raw piezocone data is provided in Figure 7.14(a), indicating significant scatter in cone tip resistance (q_T) due to the inclusion of sand seams within the clay matrix. The raw data were then input to the Type 2 PCPT-OCR model for evaluating the OCR profile. Results shown in Figure 7.14(b) indicate the general trend of OCR variations at the site although additional, but unrelated scatter, due to other factors (sandy zones, soil fabric, etc.) is also observed. As discussed previously in the evaluation of in-situ measurement variability (Chapter 4), the piezocone data were processed using the "moving average" technique over the established vertical autocorrelation distance of 0.30 meters (Kulhawy et al. 1992), as illustrated in Figure 7.14(c). A mathematical function was then used to curve-fit the smoothed data for generating an interpreted trend of OCR with depth. Typically, a power function format was sufficient for many sites with simple stress histories, but multi-linear and segmented layered type interpretations were required for sites with complex stress histories. Figure 7.14(c) shows the results of the smoothed interpretation at Kringalik. In Figure 7.14(d), the trend predicted by piezocone tests is

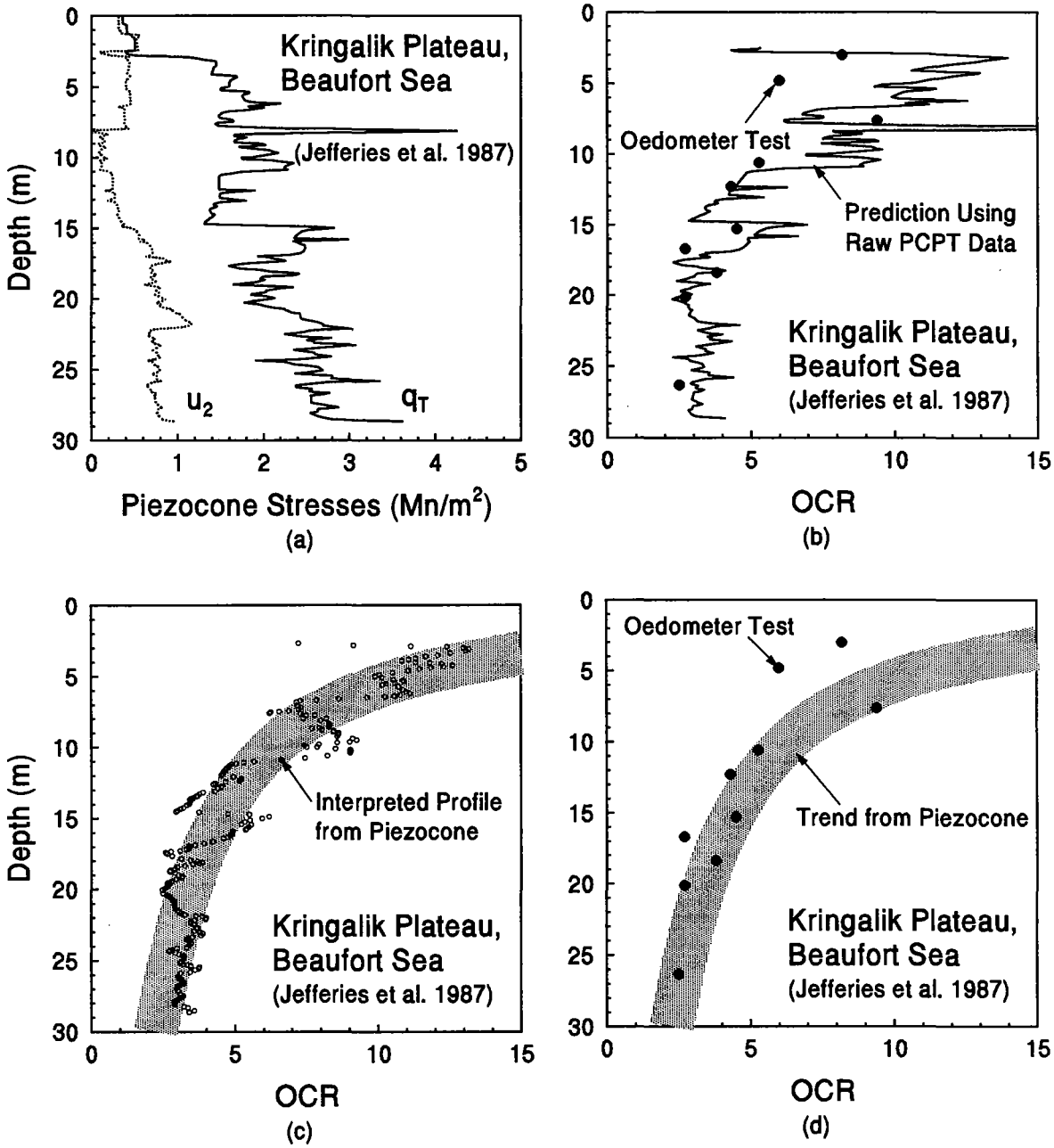

Figure 7.14 An Example showing the Interpreted Trend of OCR Profiles from Raw Piezocone Measurements.

compared with the oedometric OCRs obtained from laboratory consolidation tests. The model apparently works quite well for this site in the Beaufort Sea.

7.6.2. Experimental Test Sites

Piezocone data obtained from the two experimental field test sites at Port Huron and Baton Rouge were used for the calibration of the developed model. For the Port Huron Site, Figure 7.15(a) shows that the Type 1, Type 2, and Dual-type models perform to the same degree of success and are capable of identifying complex OCR profiles, as verified by the laboratory oedometer tests. The Type 1 prediction of OCR at Baton Rouge is illustrated in Figure 7.15(b), indicating very comparable results to the oedometric OCR profile. Both Type 2 and Dual-type models were also evaluated, though not shown here because of desaturation effects measured between the depths of 17 to 28 meters. As discussed in Chapter 4, major difficulties were encountered at Baton Rouge in maintaining continuous u_2 and u_3 measurements. Desaturation may have also affected the Type 1 cone prediction as well, as evidenced by the irregular trends indicated in Figure 7.15(b) below 17-meter depths.

7.6.3. Piezocone Sites with Both Type 1 and Type 2 Data

Six clay sites, where detailed profiles of q_T and both u_1 and u_2 were available, were chosen for demonstrating the consistent prediction performance of the Type 1, Type 2, and Dual-type models. Figure 7.16(a) indicates that the model predicts a reasonable OCR profile for the soft clay at Onsoy, Norway (Lunne et al. 1986). In the depth interval of 7 to 17 meters, the Dual-type model gives the highest prediction, followed by the Type 1 and Type 2. Nevertheless, the variations of OCRs are within 1 to 2 for all cases. The PCPT-OCR model was calibrated for the moderately-overconsolidated clay ($1 < OCR < 14$) at Haga, Norway (Lunne et al. 1986a), as illustrated in Figure 7.16(b). The predicted and measured oedometric OCR profiles are in good agreement. In Figure 7.16(c), the performance of the developed model was evaluated using data from a soft sensitive plastic clay in Ska-Edeby, Sweden (Larsson and Mulabdic 1991). The OCR profile of the normally consolidated glacial and post-glacial clays at Ska-Edeby is well predicted by the Type 1, Type 2, and Dual-type models. Figure 7.16(d) shows the predicted OCR profiles and the oedometer test results

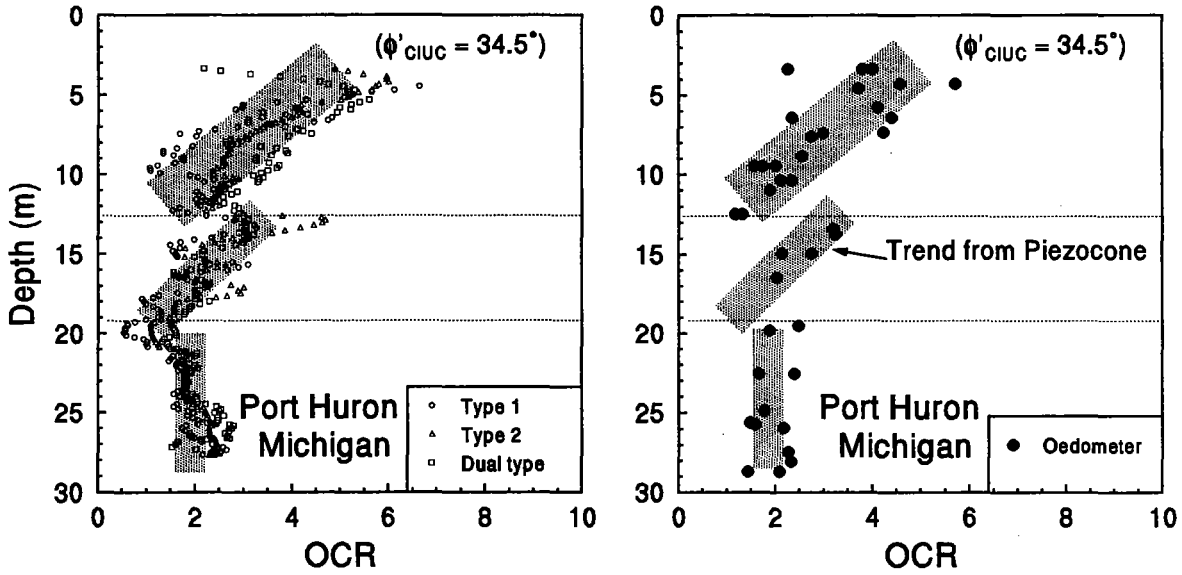

Figure 7.15. (a) Applications of Type 1, 2, and Dual-Type Models to Port Huron Site.

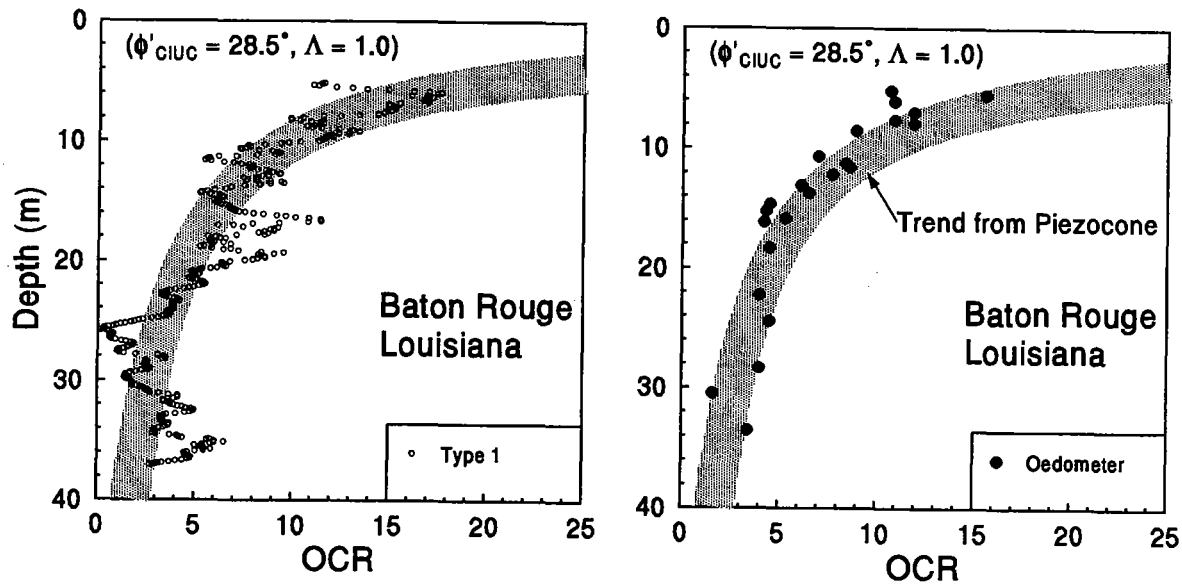

Figure 7.15. (b) Application of Type 1 Piezocone Model to Baton Rouge Site.

within the layered profiles of the soft cohesive materials at Porto Tolle, Italy (Jamiolkowski, et al. 1985; Battaglio, et al. 1986). The OCR predictions are slightly low for the heavily overconsolidated fissured London clays in Brent Cross, UK (Lunne et al. 1986b; Powell et al. 1988), as indicated in Figure 7.16(e). These are some of the highest reported OCRs worldwide and a true measuring of σ_p' in oedometer tests must indeed be difficult. It is also noteworthy that London clay has one of the lowest ϕ' values worldwide for natural clays (Diaz-Rodriguez et al. 1992).

Figure 7.16(f) shows overpredictions for heavily-overconsolidated and fissured Gault clay at Madingley, UK (Lunne et al. 1986b). Again, the reference OCRs from consolidation tests are only approximate in these materials. Nevertheless, the piezocone predictions clearly indicate that the clays at Madingley are very heavily overconsolidated.

7.6.4. Type 1 Piezocone Sites

Figure 7.17 shows four additional OCR predictions using the Type 1 model in soft to stiff to hard clays. Slight underpredictions were observed for slightly organic soft clay at the British national test site in Bothkennar, Scotland (Hight et al. 1992; Powell et al. 1988). Below 9 meter depths, the piezocone model evaluates the materials as normally consolidated to underconsolidation, while the oedometer test results showed $1.5 < OCR < 2.0$. For the offshore site at Troll East in the North Sea (Skomedal and Bayne 1988), the irregular OCR profiles obtained from piezocone assessment possibly reflect factors such as measurement errors and soil geological variations. At the Chek Lap Kok airport site for Hong Kong (Koutsoftas et al. 1987), the boundary between the upper and lower marine clays were identified clearly by the piezocone interpretation of the OCR profile. Both the piezocone and oedometer interpretations indicate that the OCRs for upper marine clay decrease from 5 to 1, while the OCR profile for the lower marine clay lowers from 10 to 1 as the depth increases. Lastly, overpredictions somewhat occurred when the model was applied to the very hard cemented and microfissured clay at Taranto, Italy (Jamiolkowski et al. 1985; Battaglio et al. 1986). Perhaps a more complex stress history interpretation is more appropriate here as well.

7.6.5. Type 2 Piezocone Sites

Since the database contains a large number of Type 2 piezocone data, a total of fifteen clay sites were chosen to provide additional validations for the Type 2 model. In Figure 7.18, good agreement between the predicted and measured OCRs were generally observed for the sensitive Leda clays at the Canadian sites at St. Alban (Roy et al. 1982), St. Hilaire (LaFleur et al. 1988), Gloucester (Konrad and Law 1987), and the National Research Council of Canada test site (Konrad and Law 1987). Overpredictions were observed at shallow depths for the St. Alban and Gloucester sites. The Type 2 piezocone may be the most appropriate for the soft, normally to lightly overconsolidated clays in these areas since significant pore pressures can be measured for the porous filter element located immediately behind the tip.

Four clay sites from the United States are presented in Figure 7.19 for the calibration of the Type 2 model. The OCR predictions for San Francisco Bay Mud at Hamilton Air Force Base, California (Masood and Mitchell 1993), indicates only a fair match between and piezocone and oedometer test results for the normally to lightly overconsolidated clays, as shown in Figure 7.19(a). For the national test site at Amherst, Massachusetts (Lutenegger 1993), the piezocone evaluation of the varved clays also shows comparable results except that slight underpredictions are observed at depths below 17 meters, as indicated by Figure 7.19(b). In Figure 7.19(c), results of the piezocone predictions for the sandy clay of the Yorktown Formation in Newport News, Virginia (Mayne 1989), show a similar trend with that determined by laboratory oedometer tests. For the clay site in Surry, Virginia (Mayne and Gordon 1987), significant variations in predicted OCR profiles were observed and the interpreted trends underpredict the OCRs in three different layers, as shown in Figure 7.19(d).

Results of OCR predictions in two Norwegian clays (Lacasse and Lunne 1982; Sandven 1990)) and two Italian clays (Jamiolkowski et al. 1994; Lancellotta and Pepe 1990; Battaglio et al. 1986) are presented in Figure 7.20. The predicted trend of Drammen appears reasonable (Fig. 7.20a), while that for Glava is only fair (Fig. 7.20b). The Pisa site exhibits significant scatter possibly due to the presence of sand seams in the clay matrix (Fig. 7.20c). In Fig. 7.20d, the Type 2 cone gives a fairly good approximation of the high OCRs

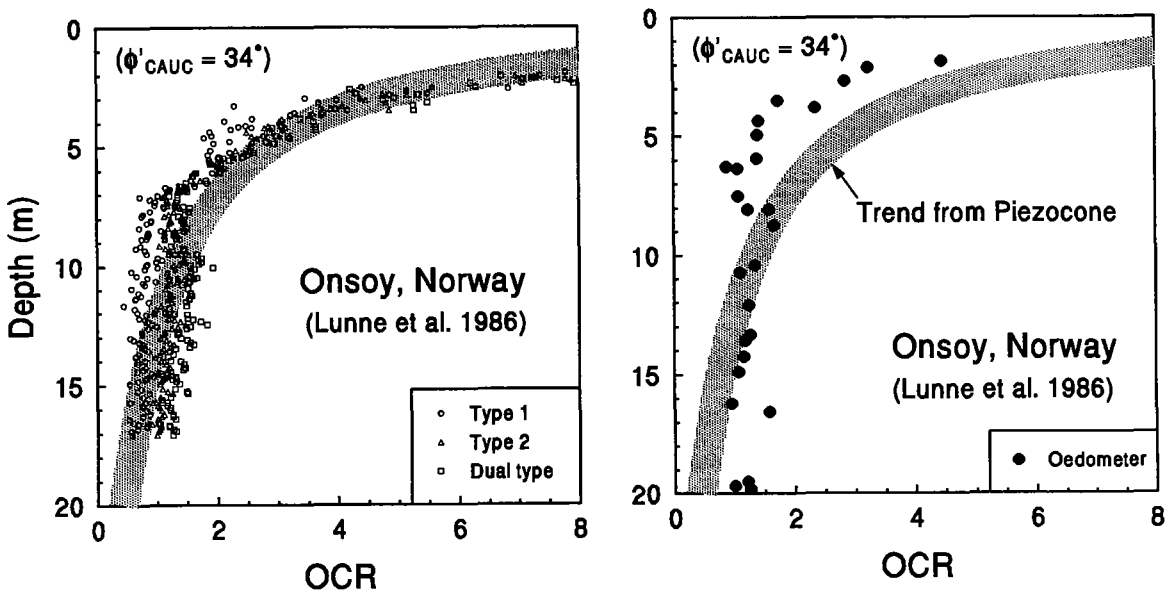

Figure 7.16. (a) Applications of Type 1, 2, and Dual Type Models to Onsoy, Norway.

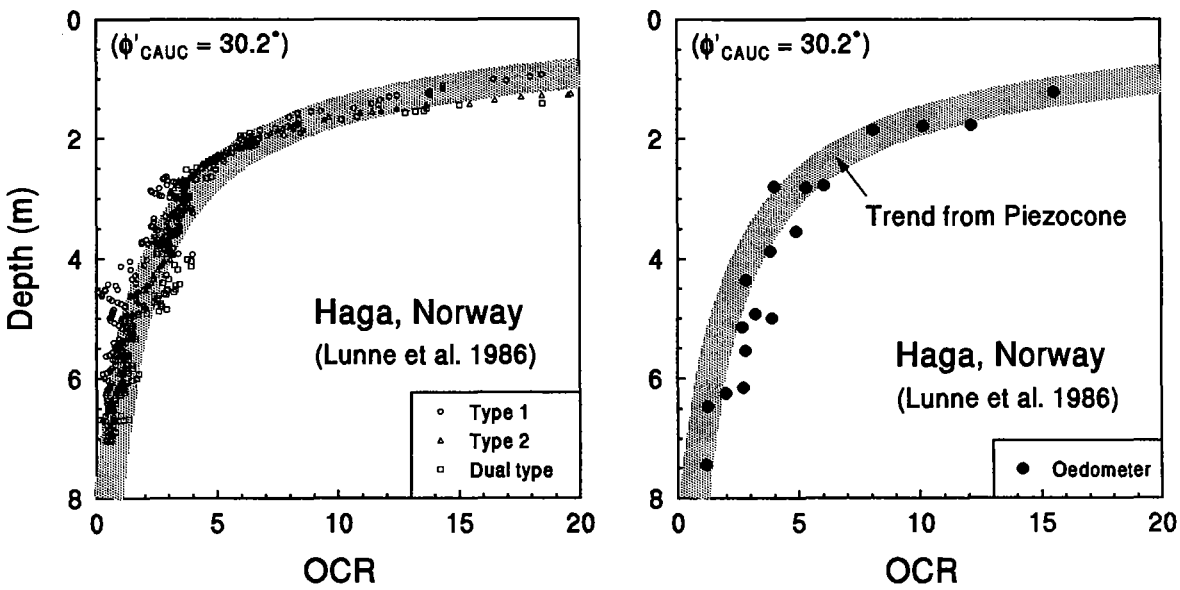

Figure 7.16. (b) Applications of Type 1, 2, and Dual Type Models to Haga, Norway.

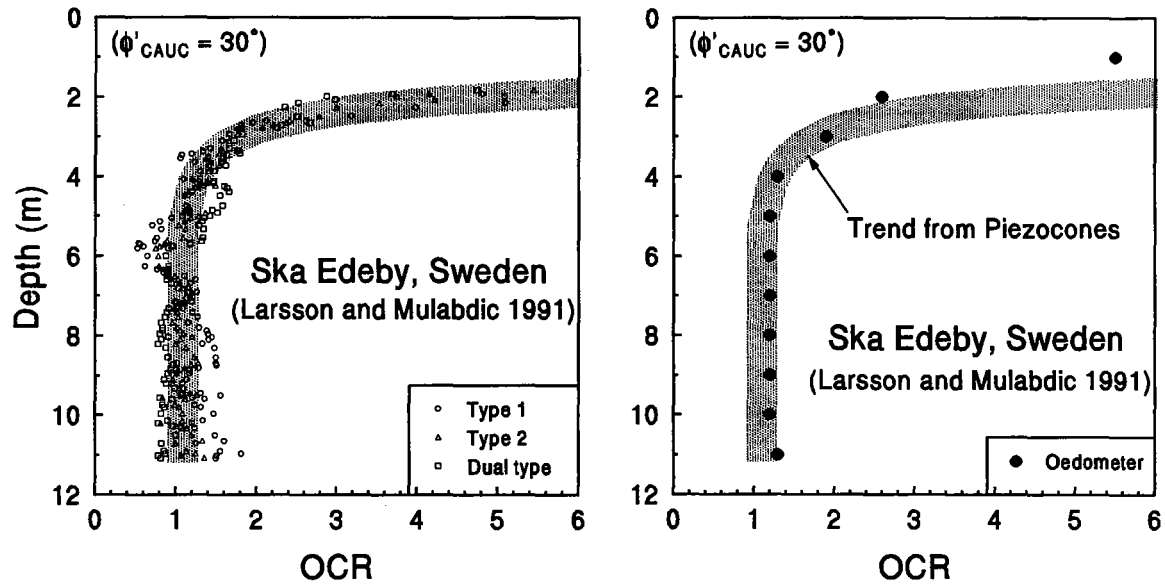

Figure 7.16. (c) Applications of Type 1, 2, and Dual Type Models to Ska-Edeby, Sweden.

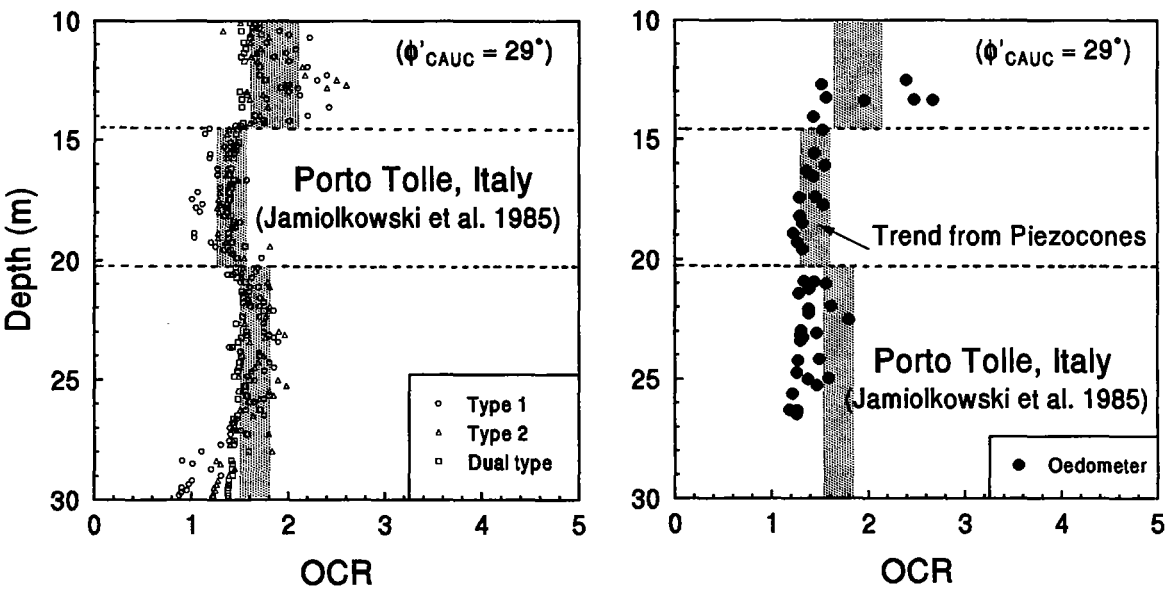

Figure 7.16. (d) Applications of Type 1, 2, and Dual Type Models to Porto Tolle, Italy.

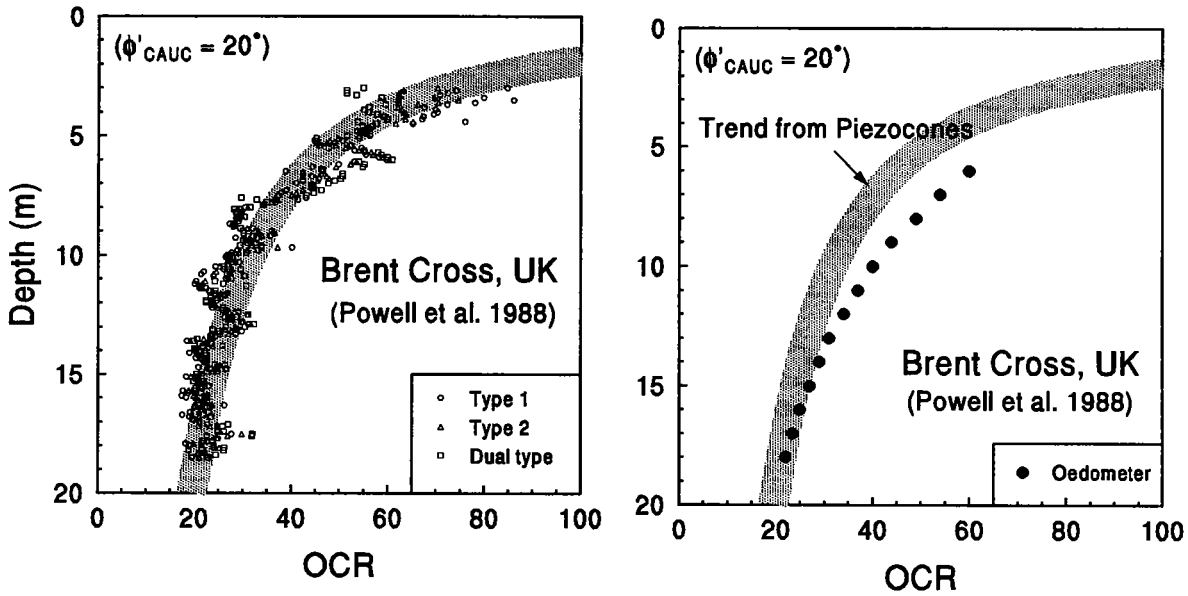

Figure 7.16. (e) Applications of Type 1, 2, and Dual Type Models to Brent Cross, UK.

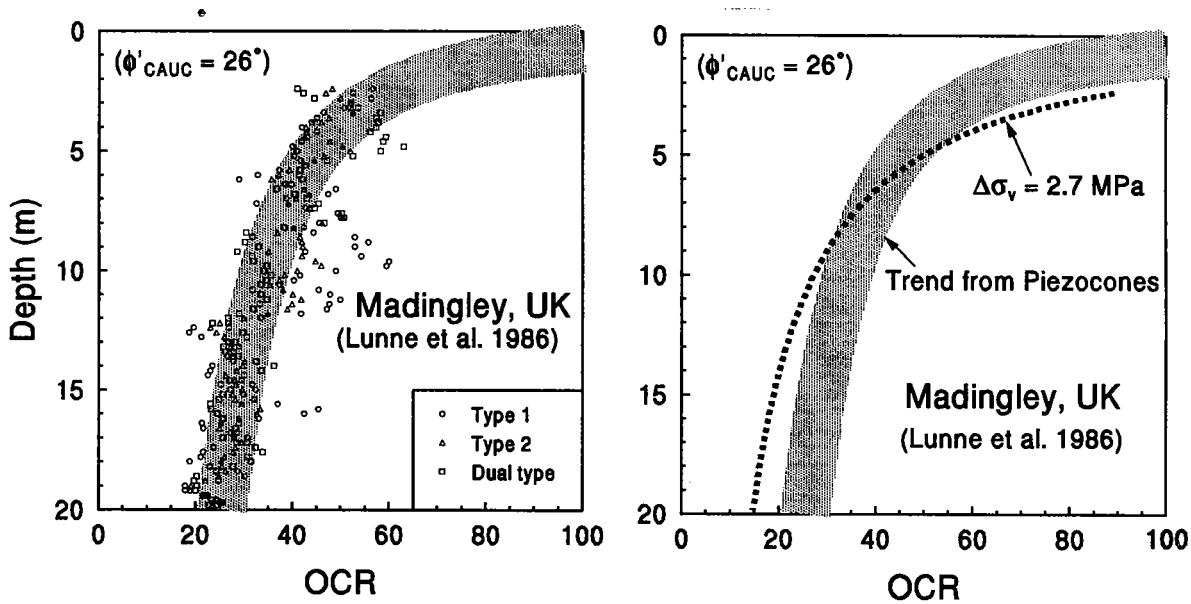

Figure 7.16. (f) Applications of Type 1, 2, and Dual Type Models to Madingley, UK.

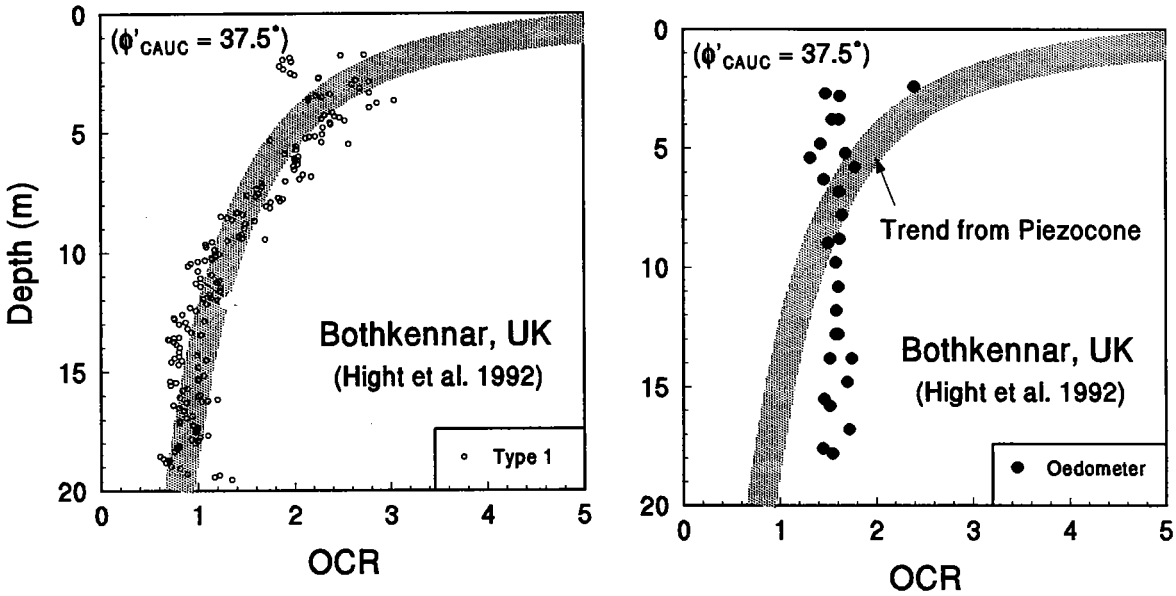

Figure 7.17. (a) Application of Type 1 Model to Bothkennar, UK.

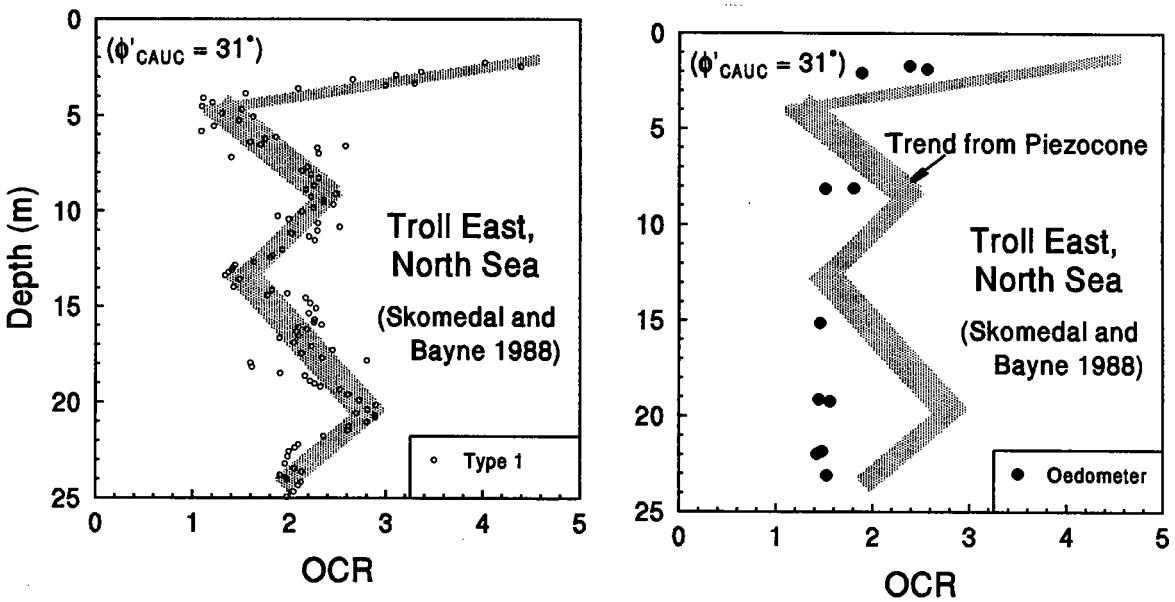

Figure 7.17. (b) Application of Type 1 Model to Troll East, North Sea.

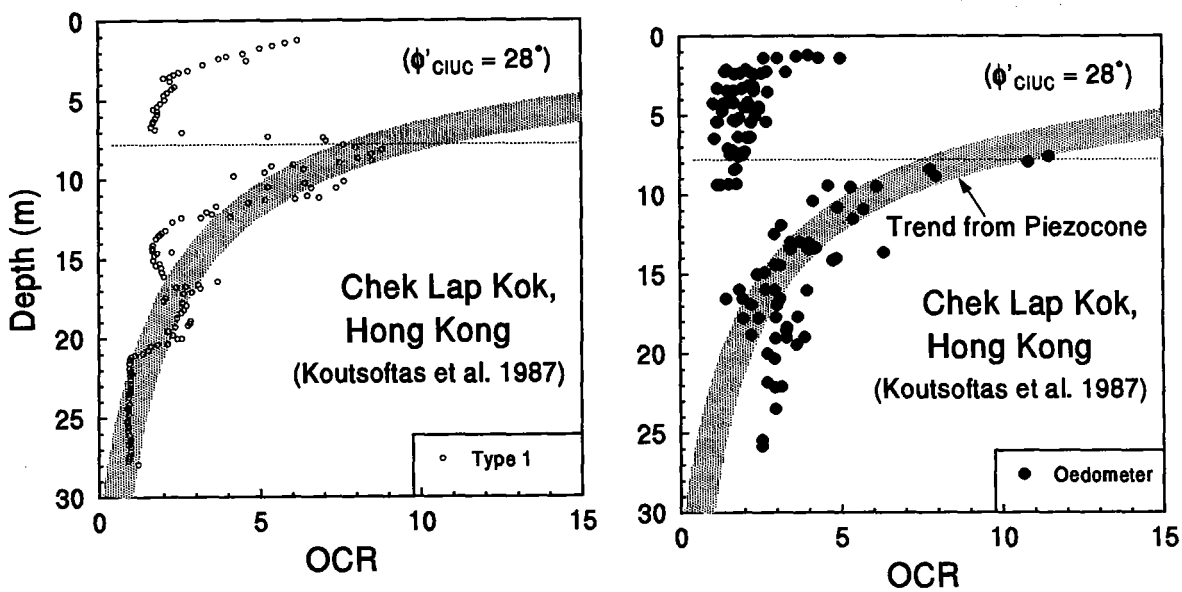

Figure 7.17. (c) Application of Type 1 Model to Chek Lap Kok.

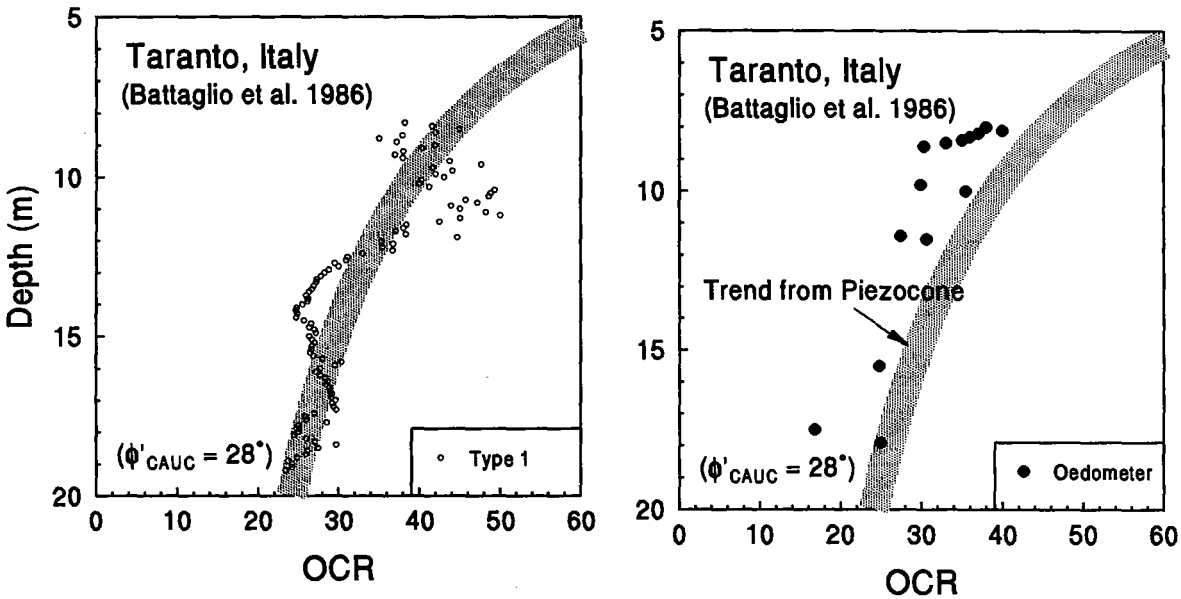

Figure 7.17. (d) Application of Type 1 Model to Taranto, Italy.

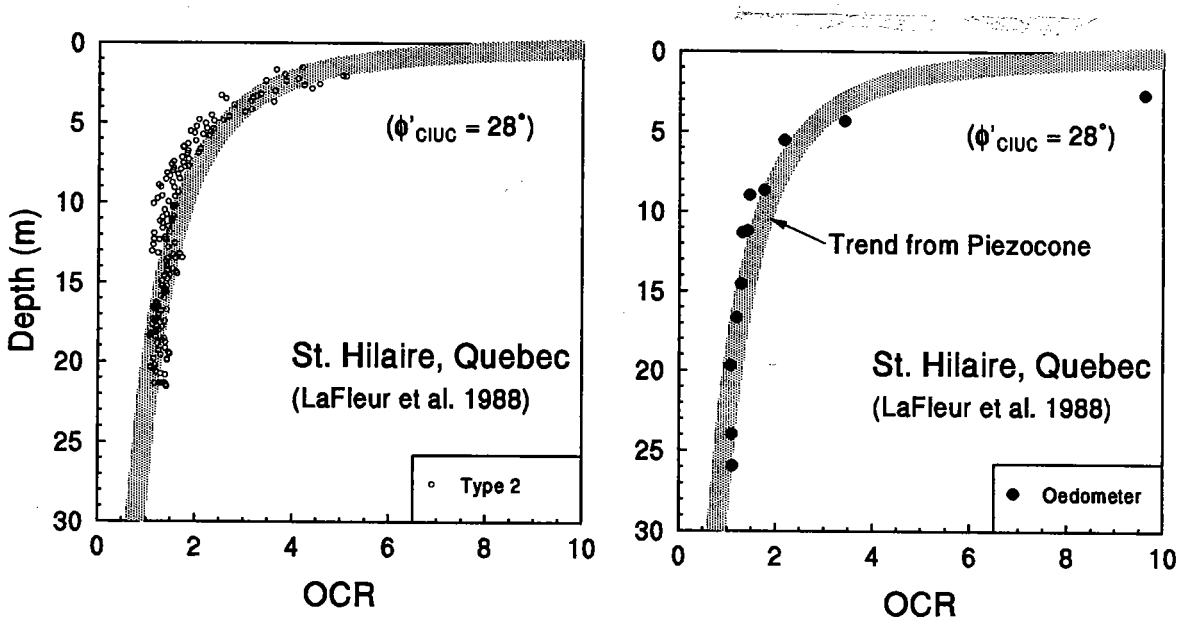

Figure 7.18. (a) Application of Type 2 Model to St. Alban, Quebec.

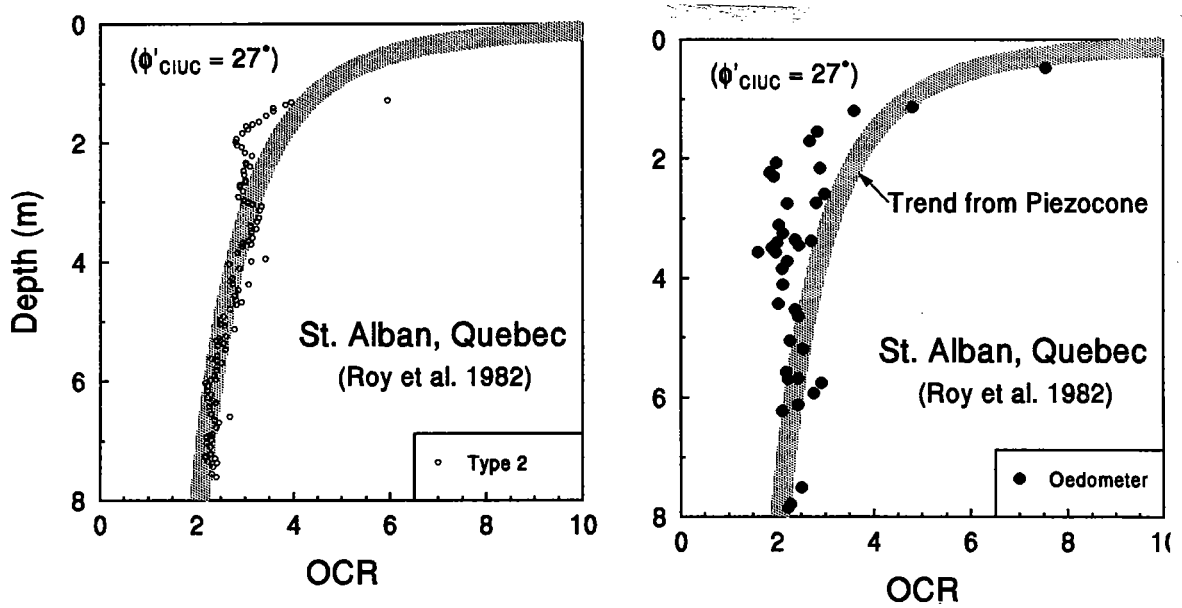

Figure 7.18. (b) Application of Type 2 Model to St. Hilaire, Quebec.

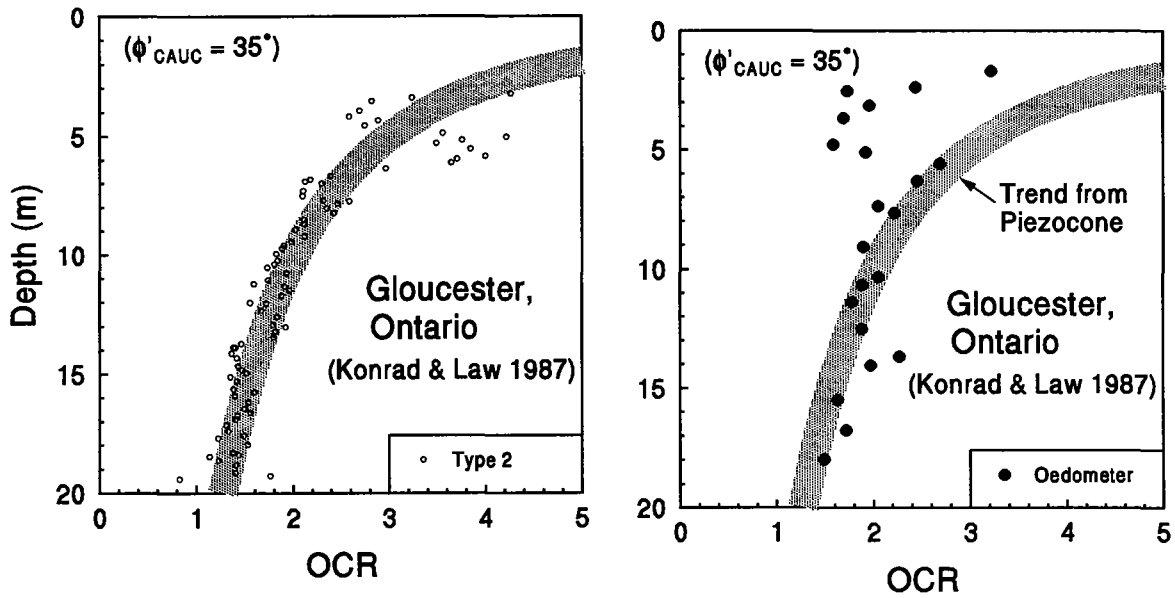

Figure 7.18. (c) Application of Type 2 Model to Gloucester, Ontario.

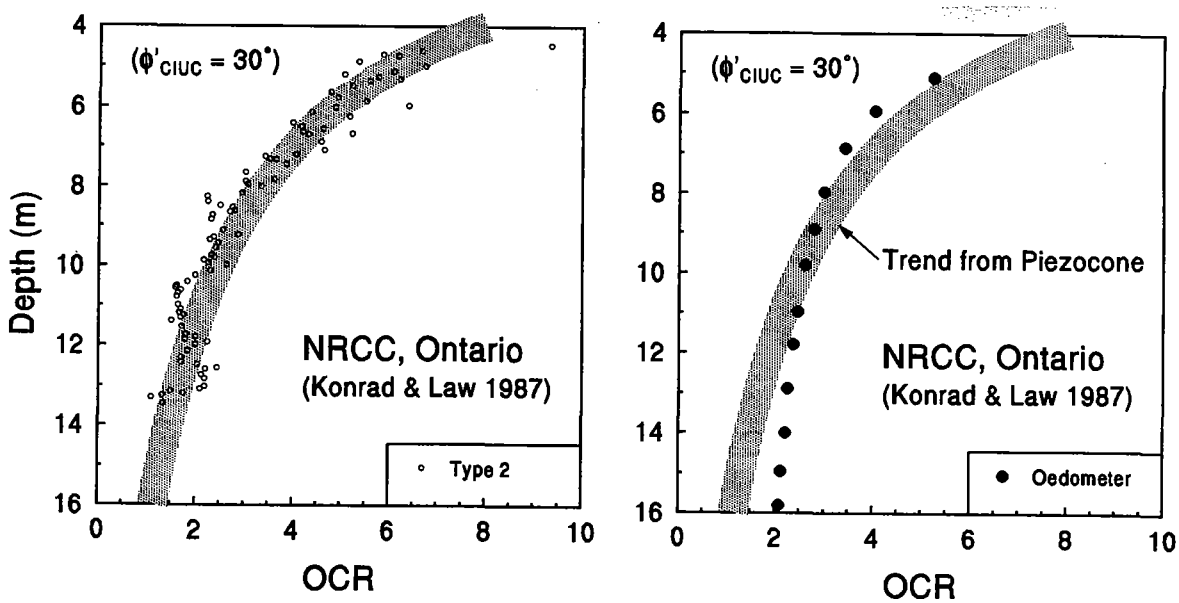

Figure 7.18. (d) Application of Type 2 Model to NRCC, Ontario.

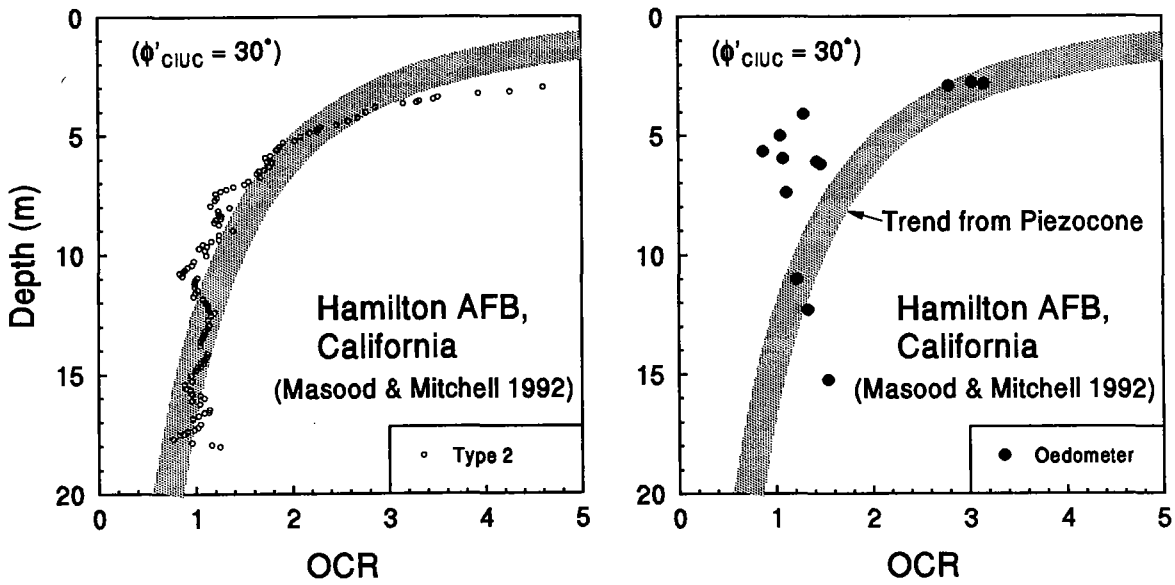

Figure 7.19. (a) Application of Type 2 Model to Hamilton Air Force Base.

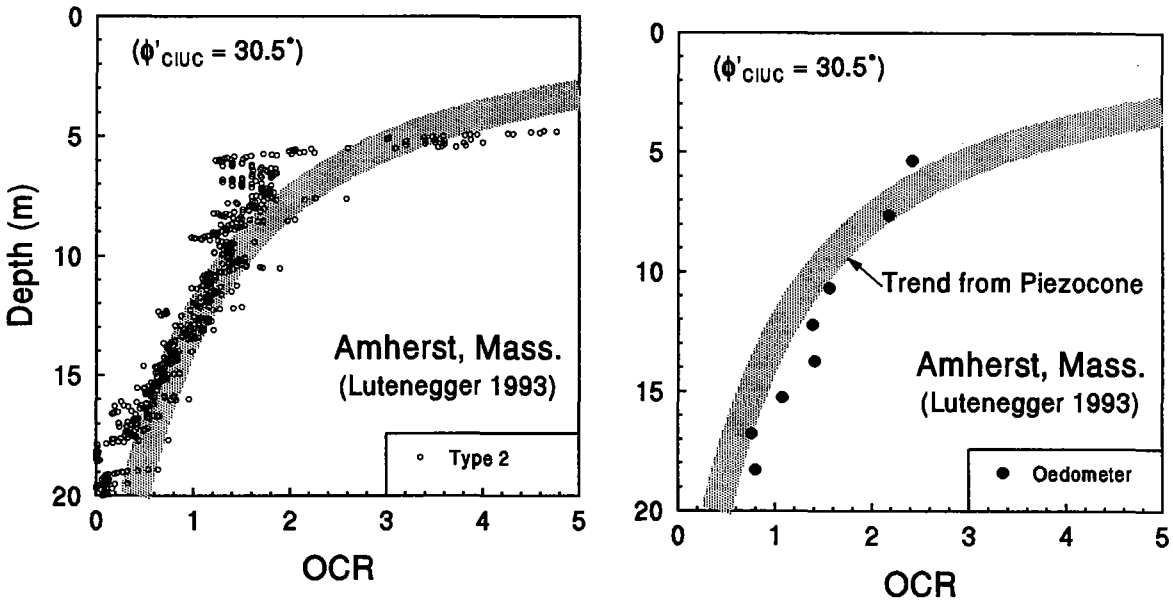

Figure 7.19. (b) Application of Type 2 Model to Amherst, Massachusetts.

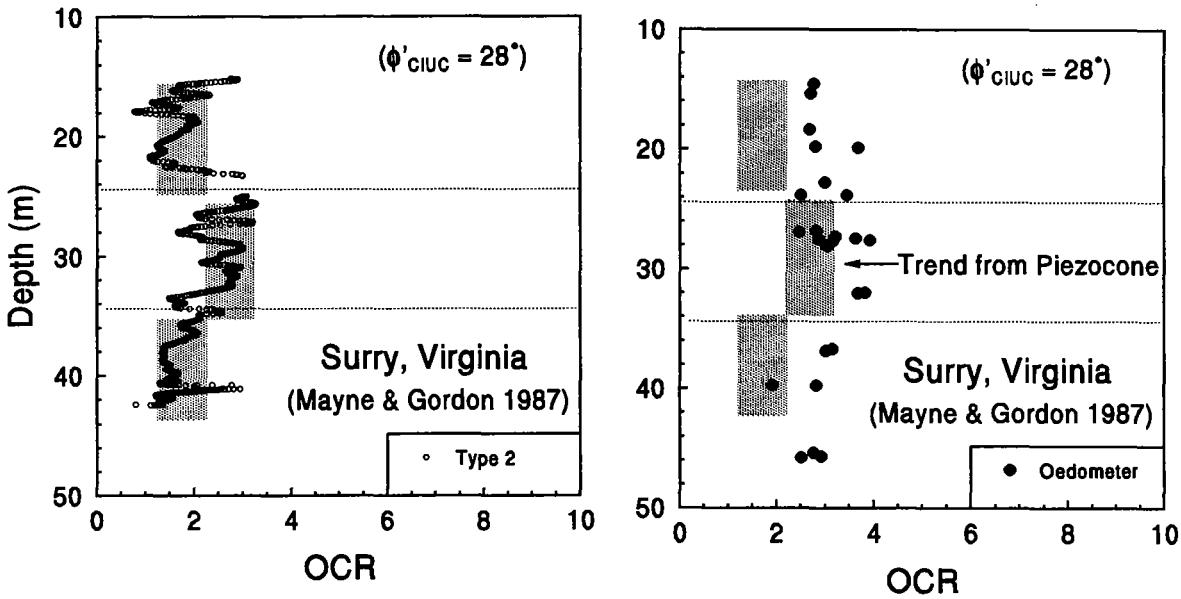

Figure 7.19. (c) Application of Type 2 Model to Yorktown, Virgina.

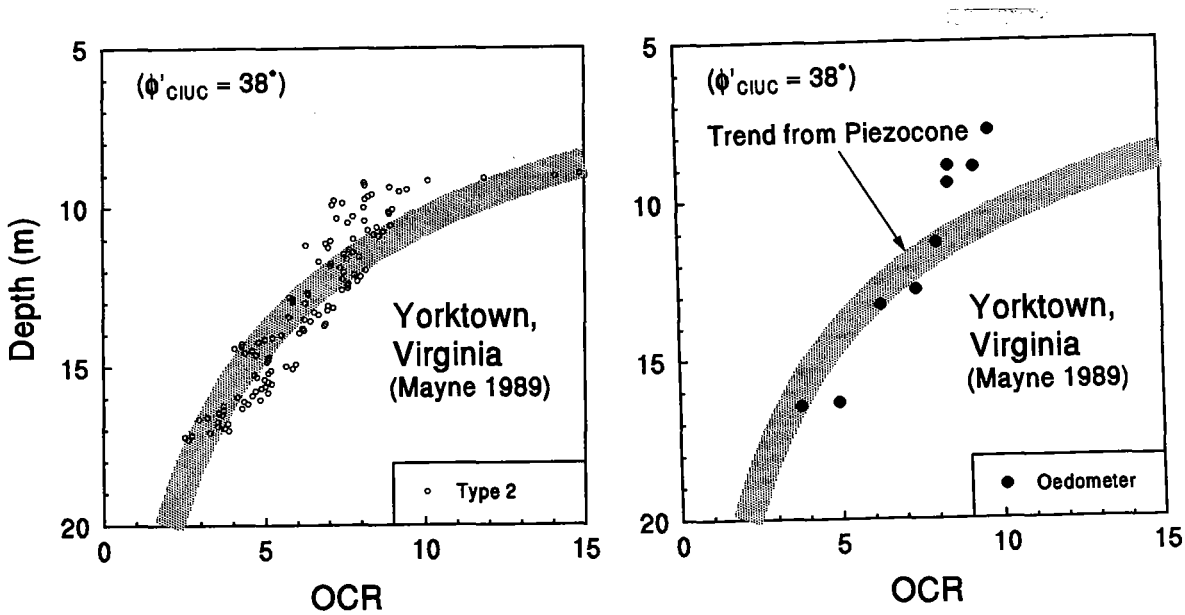

Figure 7.19. (d) Application of Type 2 Model to Surry, Virgina.

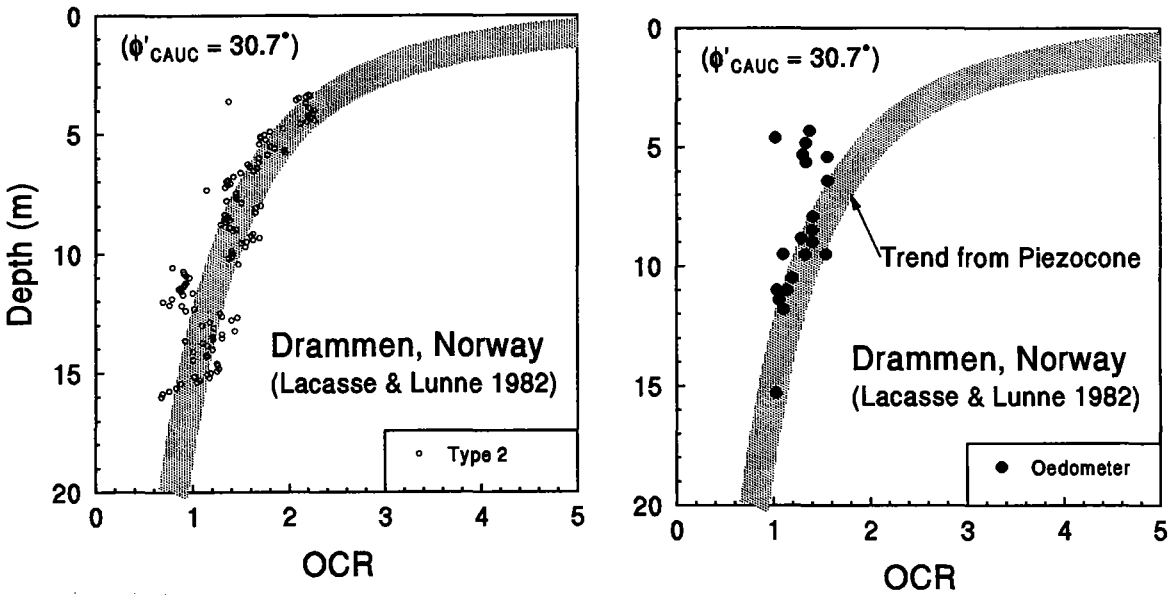

Figure 7.20. (a) Application of Type 2 Model to Drammen, Norway.

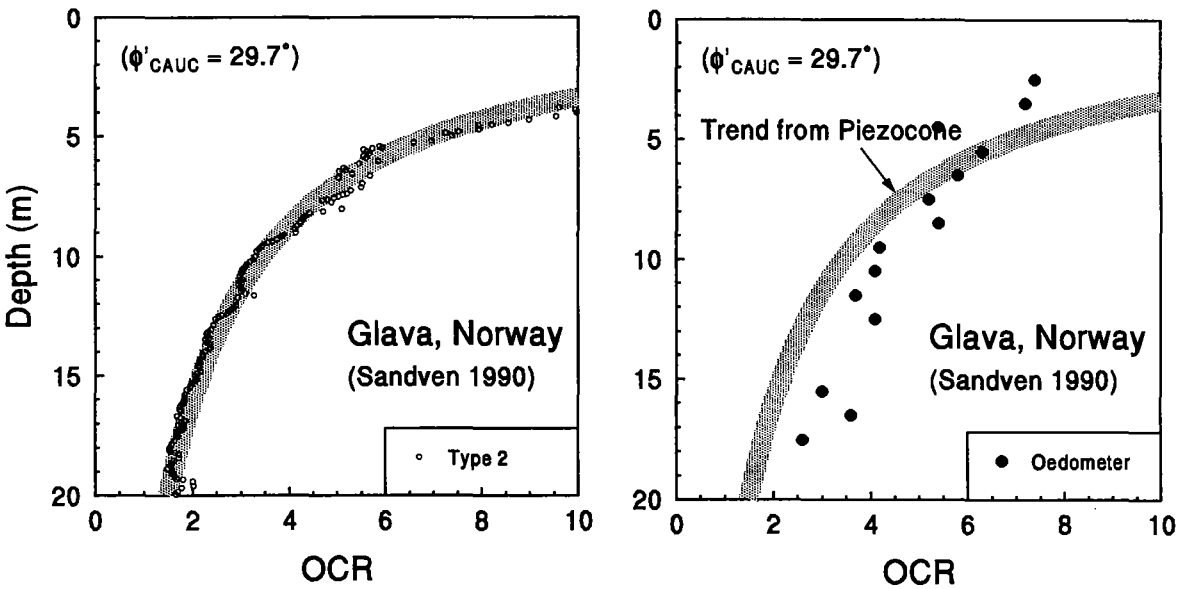

Figure 7.20. (b) Application of Type 2 Model to Glava, Norway.

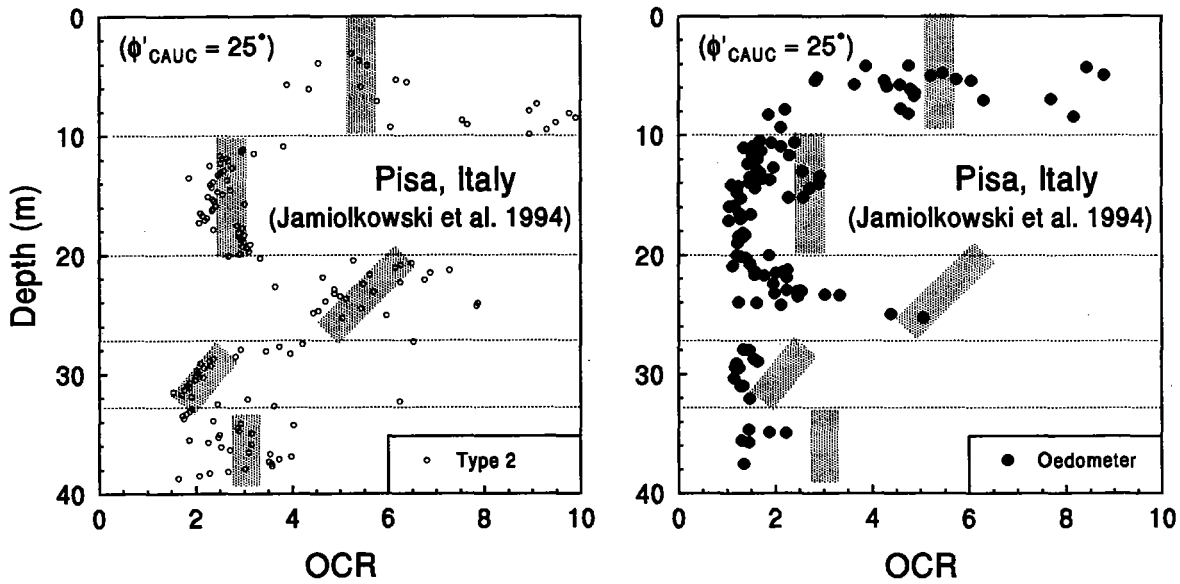

Figure 7.20. (c) Application of Type 2 Model to Pisa, Italy.

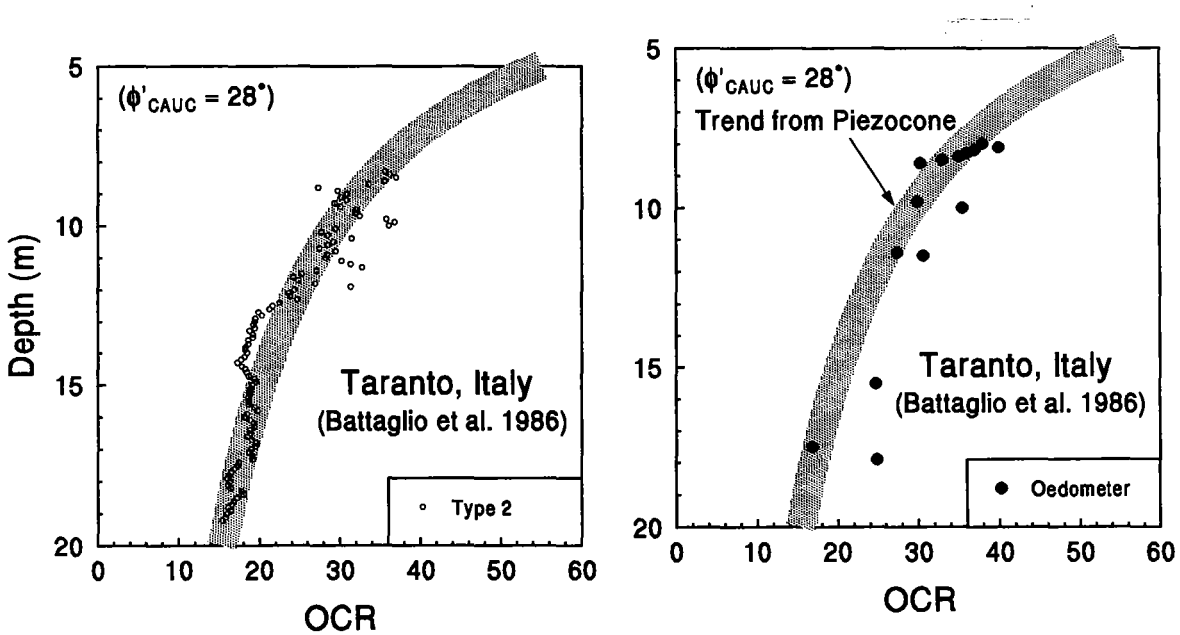

Figure 7.20. (d) Application of Type 2 Model to Taranto, Italy.

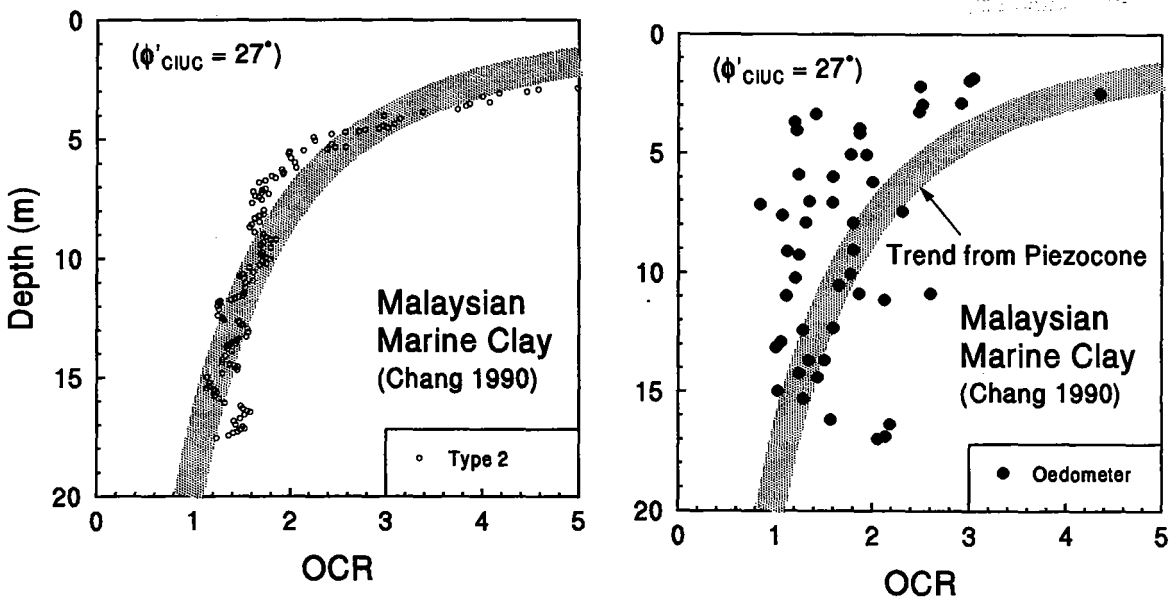

Figure 7.21. (a) Application of Type 2 Model to Malaysian Marine Clay.

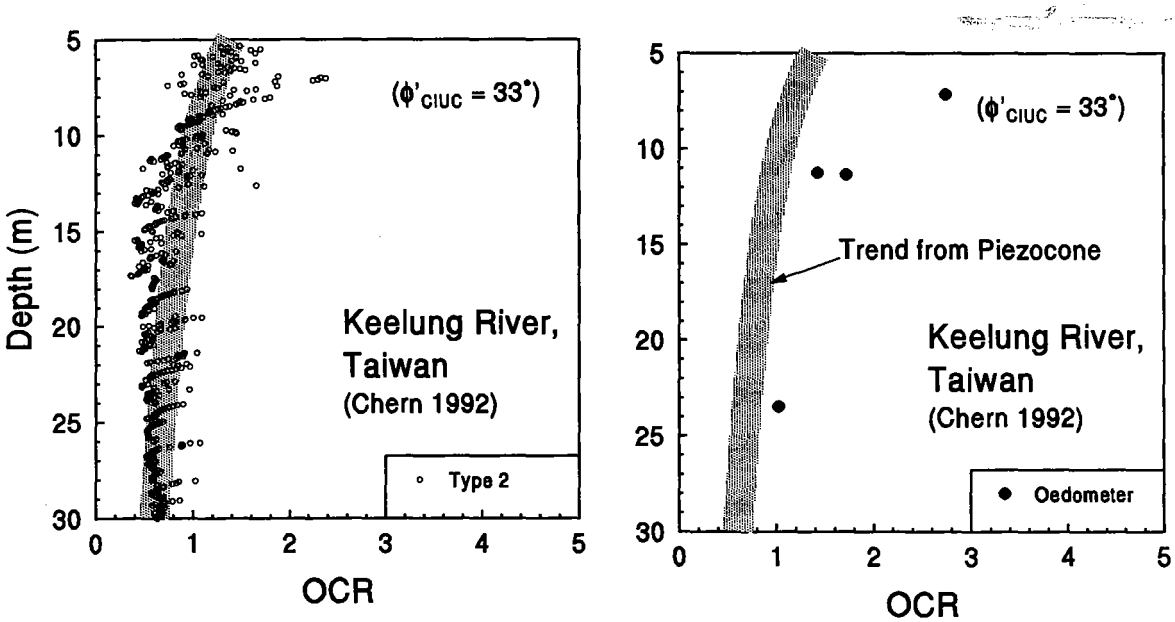

Figure 7.21. (b) Application of Type 2 Model to Keelung River, Taiwan.

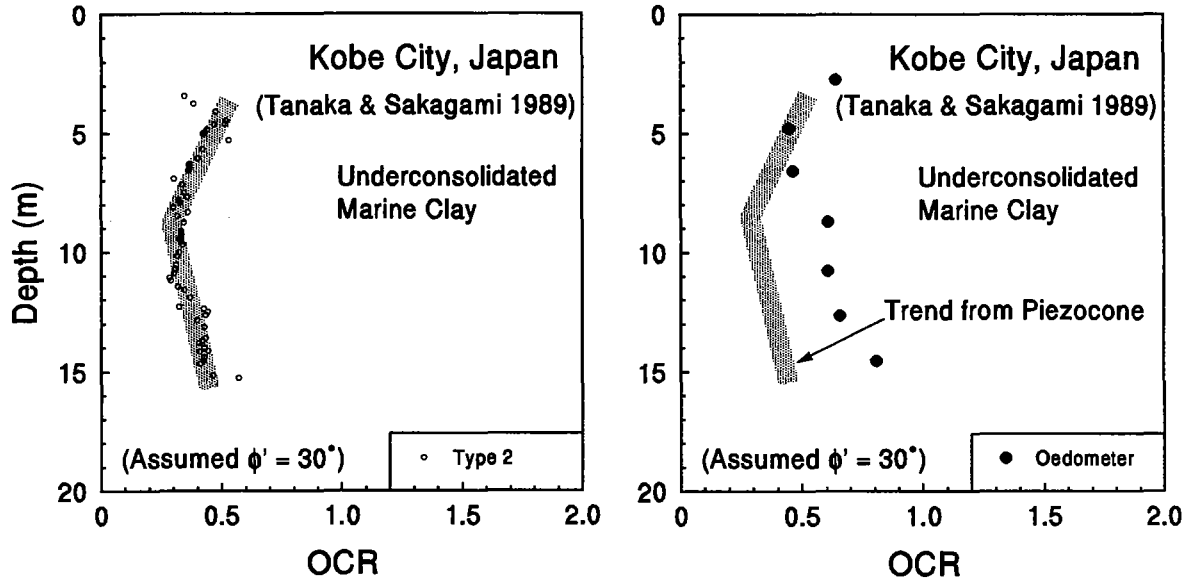

Figure 7.21. (c) Application of Type 2 Model to Kobe City, Japan.

in the hard Taranto clay.

Data from Southeast Asia were also evaluated for their applicability to the developed model. The piezocone predictions of OCRs in Malaysian Marine Clay (Chang 1990) show much less scatter than the oedometric OCR profile (Fig. 7.21a), while underpredictions are apparent for the soft silty clays at Keelung River site in Taiwan (Chern 1992) presented in Fig. 7.21b. Since the influence of ϕ' is particularly not significant for this model, the OCRs of the underconsolidated marine clay in Kobe city, Japan (Tanaka and Sakagami 1989) shown in Fig. 7.21c were evaluated by assuming $\phi' = 30^{o}$. The results confirmed that the clays were indeed underconsolidated, a phenomenon caused by new fill loading placed at the site.

7.7. Conclusions

A soil behavioral model for evaluating the stress history of clays is developed using a framework of spherical cavity expansion theory and constitutive soil models with

considerations of: (1) initial stress state, (2) stress path loading, (3) strength anisotropy, and (4) strain rates. Different positions of the porous filter element for monitoring pore pressure behavior are accommodated for either u_1 (face) and u_2 (shoulder) measurements, or both. The model relates the OCR to the piezocone parameters q_T, u_1, and/or u_2, and effective overburden stress (σ_{vo}'), as well as several common soil parameters: cohesion intercept (c'), effective friction angle (ϕ'), plastic volumetric strain ratio ($\Lambda=1-\kappa/\lambda$), coefficient of earth pressure at rest (K_o), and anisotropic strength ratio $K_{45} = (s_u)_{DSS}/(s_u)_{CKoUC}$. More practical desirable forms of the model are also presented, based on the results of parametric studies, in which only ϕ' and Λ are required for the approximate evaluation. At low OCRs, the model is not particularly sensitive to either ϕ' or Λ. For many insensitive clays, a value of $\Lambda = 0.75$ is sufficient, while $\Lambda = 1.0$ is more indicative of structured clays and affords a conservative estimate of yield stress (σ_p').

Using a compiled database, reasonable success has been observed for predicting OCR profiles from field piezocone test results in natural clay deposits from around the world. In particular, the performance of the dual-type model is proven to be very satisfactory due to its fully utilizing three separate piezocone measurements (q_T, u_1, and u_2).

Since the PCPT-OCR model was developed based upon relatively simple constitutive soil models, it inevitably inherits the shortcomings of neglecting several important factors such as soil fabric, inherent structure, aging, and clay mineralogy. This probably explains why the model sometimes encounters difficulties when used for some highly structured clays, clay matrices with sandy inclusions, or cohesive deposits with complex stress histories caused by sequences of erosion/deposition, cementation, and/or desiccation. Nevertheless, the model has achieved a reasonable degree of accuracy such that an approximate OCR range can be assessed in the field before more expensive and timely laboratory test results become available. The approach provides valuable information in an expedient and cost-effective manner to practicing engineers in quickly assessing the magnitude of preconsolidation stress and yield surface domain of natural clay deposits from piezocone penetration tests.

CHAPTER 8

SUMMARY AND RECOMMENDATIONS

8.1. Synopsis of Research Program

The stress history of clays is normally evaluated by conventional laboratory oedometer tests to determine the magnitude of the effective yield stress or preconsolidation pressure (σ_p') which separates elastic from plastic behavioral responses. This yield point is conveniently expressed as a normalized overconsolidation ratio (OCR = σ_p'/σ_{vo}'), which is dimensionless. The use of in-situ tests for evaluating the profile of σ_p' in clay is attractive since they are conducted rather quickly and inexpensively, thus allowing an immediate assessment of the state of overconsolidation and its variation across the site of study. Also, because of the continuous nature of in-situ tests, it may be possible to discern a rather complicated and varied stress history that includes multiple and compounded effects (e.g., erosion, reloading, aging, plus cementation). Thus, the primary focus of this research program was to evaluate the ability and potential for using piezocone data to delineate OCR profiles as compared with reference values obtained from laboratory oedometer tests.

Current methods of evaluating the stress history of clays using piezocones were reviewed according to empirical, analytical, and numerical approaches. The empirical procedures attempted to relate σ_p' (or OCR) either to direct piezocone measurements (q_T, u_1, u_2, or f_s) or to arbitrarily-chosen parameters (i.e., u_1/q_c, $(u_1-u_2)/u_o$, etc.) without any due rational or reason for a relationship. Some of the parameters acceptable from a engineering mechanics viewpoint have been reviewed by Wroth (1988) and Houlsby (1988) and these include relating OCR to $Q = (q_T-\sigma_{vo})/\sigma_{vo}'$, $\Delta u/\sigma_{vo}'$, and $(q_T-u)/\sigma_{vo}'$. It is interesting to note that a number of independent theoretical methods (Konrad & Law 1987; Houlsby 1988; Senneset et al. 1989; Mayne 1991; Larsson & Mulabdic 1991) concluded that OCR should profile directly with the piezocone parameters $(q_T-u_1)/\sigma_{vo}'$ and $(q_T-u_2)/\sigma_{vo}'$.

A large database containing digitized piezocone soundings from over 205 different

clay deposits was compiled for exploring statistical relationships and use in verification of the developed methodologies. Results from regression analyses on the database determined the following empirical expressions for evaluating σ_p' in natural intact clays:

All Cones:	$\sigma_p' = 0.31(q_T-\sigma_{vo})$,	$n = 1355$,	$r^2 = 0.745$	[8.1a]
Type 1:	$\sigma_p' = 0.40\ \Delta u_1$,	$n = 526$,	$r^2 = 0.667$	[8.1b]
Type 2:	$\sigma_p' = 0.53\ \Delta u_2$,	$n = 811$,	$r^2 = 0.722$	[8.1c]

The effect of soil plasticity was also considered and the results of multiple regression analyses determined the following:

All cones:	$\sigma_p'/p_a = 0.16\left[(q_T-\sigma_{vo})/p_a\right]^{0.72} I_p^{-0.24}$,	$n = 1310$,	$r^2 = 0.717$	[8.2a]
Type 1:	$\sigma_p'/p_a = 0.91\left[(u_1-u_o)/p_a\right]^{0.92} I_p^{-0.21}$,	$n = 484$,	$r^2 = 0.727$	[8.2b]
Type 2:	$\sigma_p'/p_a = 1.03\left[(u_2-u_o)/p_a\right]^{0.93} I_p^{-0.18}$,	$n = 747$,	$r^2 = 0.763$	[8.2c]

The research program included the collection of piezocone data at two experimental test sites: (1) a lightly overconsolidated lean glacial lacustrine clay at Port Huron, Michigan, and (2) a moderately overconsolidated plastic deltaic clay in Baton Rouge, Louisiana. At Port Huron, paired sets of both types of piezocone penetrometers were used to obtain different pore pressure responses. A complex OCR profile indicated a layered deposit, possibly due to a history of loading-unloading-reloading sequences. At Baton Rouge, dual- and triple-element piezocones were used to obtain the penetration pore pressures u_1, u_2, and u_3. Undisturbed soil samples were retrieved from the site for the laboratory tests at Georgia Tech. A nearly constant value of preconsolidation pressure ($\sigma_p' \approx 1.04$ MPa) caused by desiccation was interpreted from the laboratory consolidation test data, resulting a uniformly decreasing profile of OCR in the Baton Rouge clay.

A soil behavioral model for evaluating the stress history of clays was developed for Type 1 (u_1 on cone face), Type 2 (u_2 behind cone tip), and dual-type piezocones (both u_1 and u_2). The method uses spherical cavity expansion theory and constitutive soil models (Wroth and Houlsby 1985; Ohta et al. 1985) and is derived such that (1) initial stress state, (2) stress path loading, (3) strength anisotropy, and (4) strain rates are taken into consideration. The methodology relates OCR to the normalized parameters $(q_T-u_1)/\sigma_{vo}'$ and

$(q_T-u_2)/\sigma_{vo}'$. Generic formats of the model are presented which allow the input of the following soil parameters: cohesion intercept (c'), effective friction angle (ϕ'), plastic volumetric strain ratio ($\Lambda = 1-\kappa/\lambda$), coefficient of earth pressure at rest (K_o), and the anisotropic undrained strength ratio $K_{45} = (s_u)_{DSS}/(s_u)_{CKoUC}$. More practical desirable forms of the model are also presented based on the results of parametric studies, in which only ϕ' and Λ are required as input parameters. Using the compiled database, reasonable predictions of OCR are observed for a variety of natural clay deposits worldwide.

The soil behavioral model presented herein is not particularly sensitive to ϕ'. Also, for insensitive and unstructured natural clays, a value $\Lambda = 0.75$ may be characteristic, while $\Lambda = 1.0$ may be more appropriate for structured and sensitive clays. If conservatism is desired, $\Lambda = 1.0$ can be used confidently since it results in lower OCR predictions. For field vane tests in clay, a value $\Lambda \approx 1$ has been suggested (Chandler 1988; Mayne and Mitchell, 1988). Adopting this value as indicative of natural clays, the predictive form of the PCPT-OCR methodolgy becomes rather simple and quite similar to that derived from regression analyses on the compiled database, as evidenced in the following table.

Table 8.1. Simplified Model Expressions and Regression Equations for OCR.

Type of Piezocone	Soil Behavior Model	Regression Analysis
Type 1 with Face Element	$OCR = 0.81(q_T-u_1)/\sigma_{vo}'$	$OCR = 0.78(q_T-u_1)/\sigma_{vo}'$
Type 2 with Shoulder Element	$OCR = 0.46(q_T-u_2)/\sigma_{vo}'$	$OCR = 0.53(q_T-u_2)/\sigma_{vo}'$

The evaluation of in-situ OCRs from piezocone data can be a valuable supplement to the results of expensive, time-consuming laboratory consolidation tests on undisturbed specimens of clay. The continuous OCR profile interpreted from piezocone test results using the proposed model can be prepared on site immediately as soon as the field testing is completed. However, it is important that the OCR predictions from piezocones be compared with actual oedometer test results. Discrepancies between the oedometer OCR

and interpreted OCR from piezocone tests should be examined to determine possible causes and reasons for the differences.

The empirical regression analyses in Chapter 3 and the analytical approaches discussed in Chapters 5, 6, and 7 fail to incorporate all facets of soil behavior. Aspects such as sensitivity, aging, geology, fabric, and cementation are all neglected. Therefore, on well-documented sites, a calibration procedure for profiling OCR can be adopted by referencing the results of high-quality oedometer tests and using the following formats: $OCR = \mu_a Q$; $OCR = \mu_b \Delta u/\sigma_{vo}'$, $OCR = \mu_c (q_T-u)/\sigma_{vo}'$, and/or $OCR = \mu_d (u_1-u_2)/\sigma_{vo}'$, where the μ terms represent calibration factors. Alternatively, power function formats for the above could be introduced as well.

8.2. RECOMMENDATIONS FOR FUTURE RESEARCH

Based on observations made while performing this study, the authors note several potential directions for future research and improvement for application of piezocone testing and interpretation to geotechnical practice:

8.2.1. Chamber Tests

Series of laboratory calibration chamber tests should be conducted to evaluate the roles of clay mineralogy, sand and silt content, and magnitude of lateral stress, as well as define a better understanding of the complete pore water pressure distribution and effect of filter size, position, material type, and smearing phenomena.

8.2.2. Strength Profiling

In this report, the undrained shear strength of cohesive materials was evaluated for only the isotropic and simplified anisotropic soil models. More comprehensive studies using the soil behavioral model of Chapter 7 could provide a more complete capability that could provide consistent profile of undrained strength that include stress rotation effects (compression, simple shear, extension), boundary constraints (triaxial vs. plane strain), as well as other in-situ test conditions (vane and pressuremeters). For example, the interrelationships of several shearing modes from the Wroth-Houlsby-Randolph constitutive

model are presented in Figure 8.1. Here, the normalized undrained strength ratios for NC clay $(s_u/\sigma_{vo}')_{NC}$ are shown for CIUC triaxial, anisotropic CK_oUC triaxial, plane strain compression (PSC), and direct simple shear (DSS), all as functions of the effective ϕ'. Alternatively, ratios from the more generalized constitutive model of Ohta, et al. (1985, 1991) are summarized in Figure 8.2 for evaluating the normally-consolidated undrained strengths. In this case, the approach also includes extension (CK_oUC and PSE), vane (VST), and pressuremeter (PMT) and therefore is more encompassing. Thus, with a knowledge of the OCR of a given clay, a number of different shearing modes can be evaluated using the approach suggested by Kulhawy and Mayne (1990):

$$(s_u/\sigma_{vo}')_{OC} = a_{RATE}\, a_{OCR}\, (s_u/\sigma_{vo}')_{NC} \qquad [8.3]$$

where $a_{RATE} = 1 + 0.1\log(d\epsilon/dt)$ = correction factor for strain rate effect, $d\epsilon/dt$ = strain rate in percent per hour, $a_{OCR} = OCR^{\Lambda}$ = overconsolidation effect, and Λ = plastic volumetric strain ratio. By this approach, any number of different strength modes can be evaluated for a particular clay deposit.

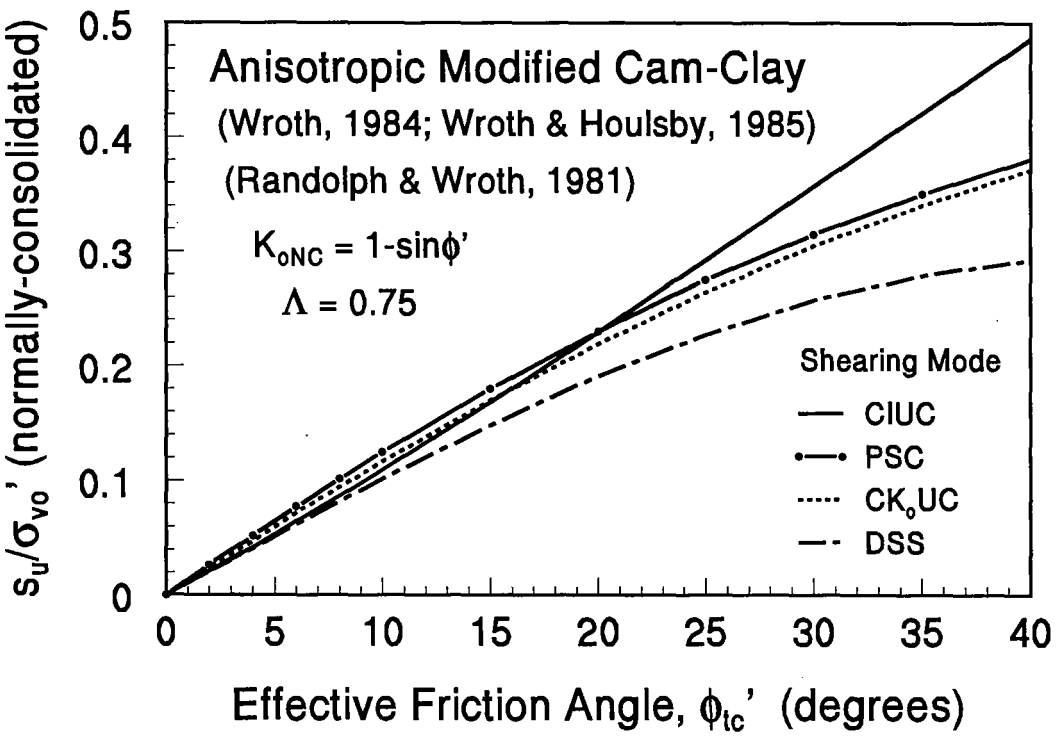

Figure 8.1. Undrained Strengths from Wroth-Houlsby-Randolph Constitutive Model.

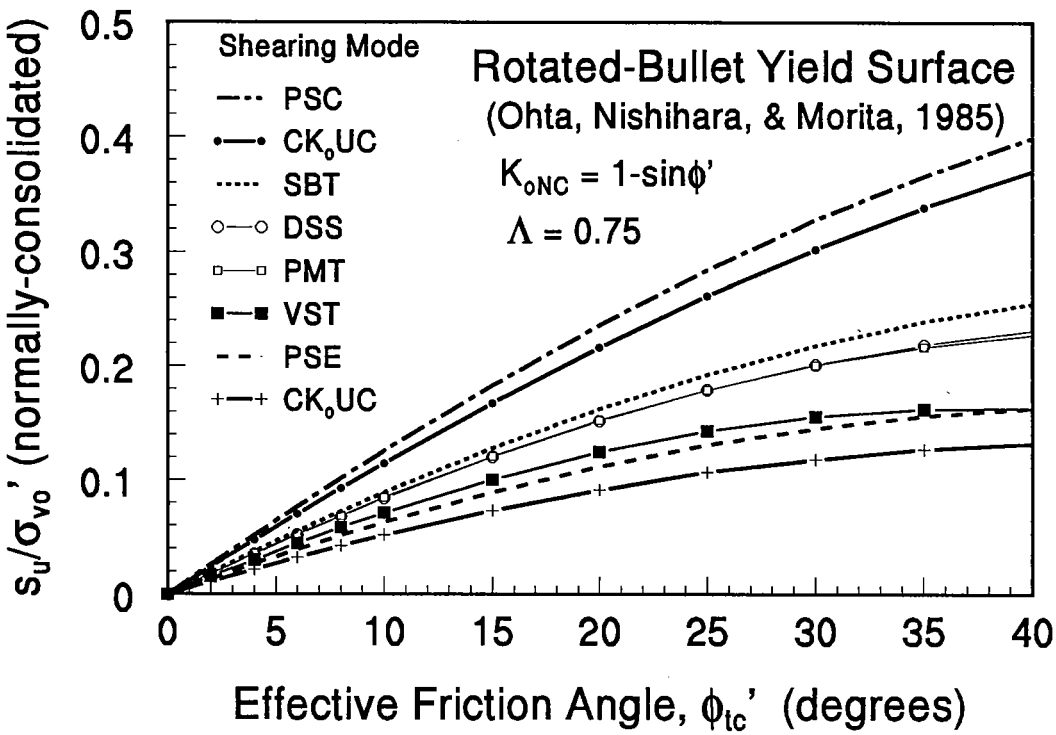

Figure 8.2. Undrained Strength Ratios From Ohta-Nishihara-Morita Constitutive Model.

8.2.3. Rigidity Index

The aforementioned SCE/MCC models can be used to backcalculate the apparent value of rigidity index appropriate to the cone penetration problem. Returning to the bearing factor expression of Vesic (1977), the rigidity index ($I_r = G/s_u$) for the undrained condition is given by:

$$I_r = \exp[(q_T - p_o - 3.90s_u)/(1.33s_u)] \qquad [8.4]$$

The approach can be applied as easily to the pore pressure measurements as well. The backcalculated values can be obtained from either the original isotropic PCPT-OCR model (Chapters 5 and 6), or the newly proposed approach discussed in Chapter 7. Using the original isotropic model, Figure 8.3 illustrates the backcalculated I_r approach applied to data from Onsoy clay in Norway. Results are presented in the form of I_r versus the logarithm of estimated OCR, as is common for this parameter (Wroth and Houlsby, 1985).

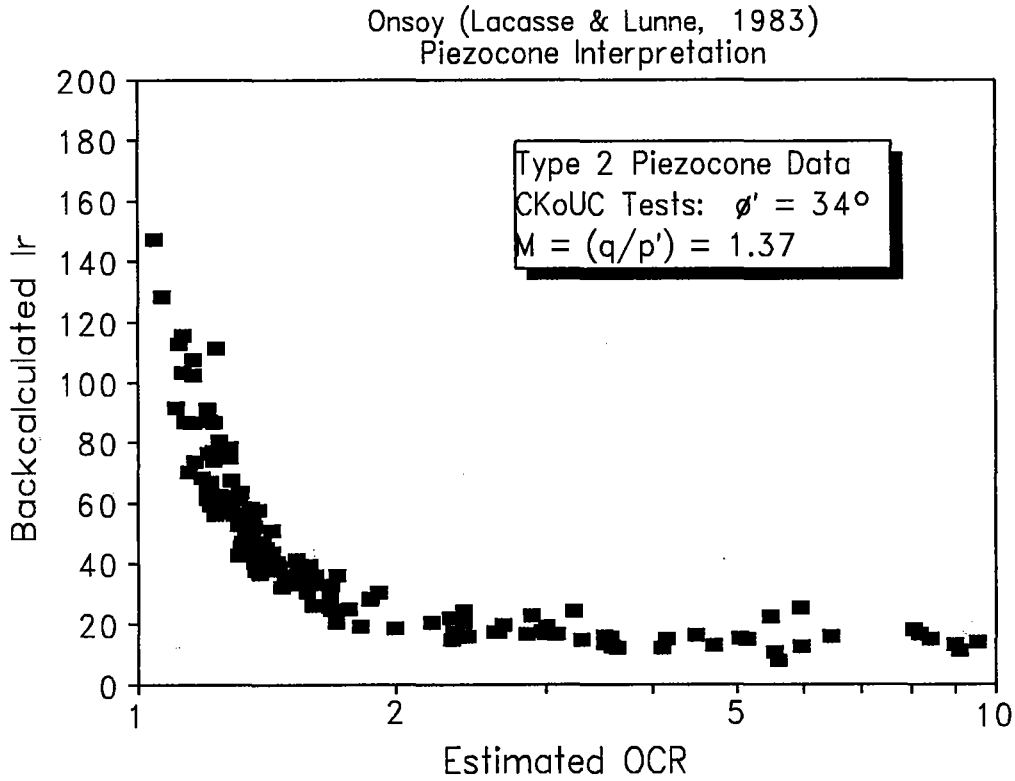

Figure 8.3. Backcalculated Rigidity Index Versus OCR for Onsoy, Norway Using Initial Isotropic SCE/MCC Piezocone Model.

8.2.4. Dissipation Tests

The theory and formulation of the OCR model can be extended to study the time-dependent soil behavior resulting from piezocone dissipation tests. The influence of each pore pressure component discussed in this model to the desired soil engineering properties, such as the coefficient of consolidation (c_h) and hydraulic conductivity (k), should be investigated for better interpretation of the dissipation test results. The soil behavior model presented herein offers the ability to explain the observed trend in dissipation behavior of both Type 1 and Type 2 cones. For example, Type 1 cones always show decreases in Δu_1 dissipations for clays of all consistencies. In contrast, Type 2 cones show decreasing Δu_2 dissipations in soft to stiff intact clays but temporary and transient increases in Δu_2 during dissipation of heavily overconsolidated and fissured clays, followed by decreasing Δu_2 with time (Davidson 1985; Campanella et al. 1980; Sully 1991).

In this regard, the ability to evaluate a value of rigidity index is important since the available approaches for interpreting c_h from piezocone dissipation tests (Jamiolkowski et

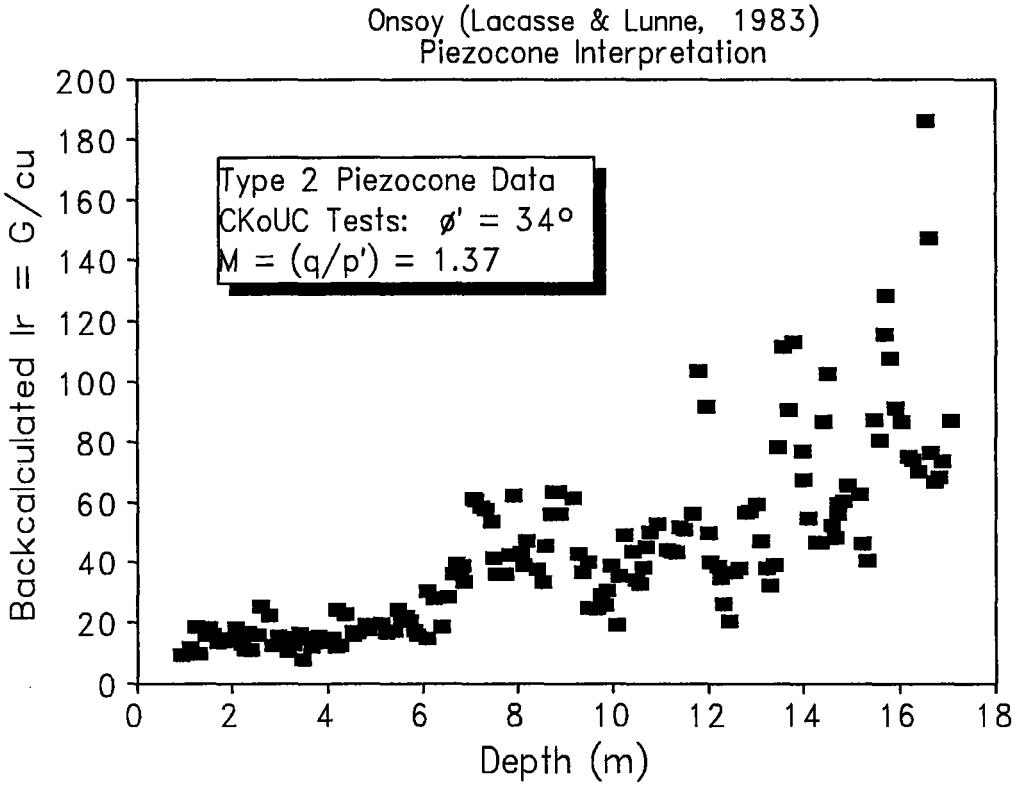

Figure 8.4. Profile of Backcalculated I_r with Depth for Onsoy Clay.

al. 1985; Houlsby and Teh, 1988; Kabir and Lutenegger, 1990; Robertson et al. 1992) require an input value of I_r. The strain path analysis by Houlsby and Teh (1988) and Teh and Houlsby (1988), in fact, present modified time factors (T*) that are normalized by the square root of I_r, for the adopted range of values $50 \leq I_r \leq 500$. Figure 8.4 shows the backcalculated I_r for Onsoy plotted as a function of depth. The backcalculated I_r fall generally within the range of $10 \leq I_r \leq 100$. Similar values have been backfigured by the authors for other sites (Brent Cross, Bothkennar, etc.). While these I_r might be considered low relative to anticipated values, however, it must be reflected that the appropriate I_r depends on strain level which is high during cone penetration. Moreover, the rigidity index is the reciprocal of shear strain level, such that $\epsilon_s = 1/I_r$. In this regard, the above values of $10 \leq I_r \leq 100$ correspond to strains of 1 to 10 percent and represent failure levels of strain indicative of the cone penetration problem.

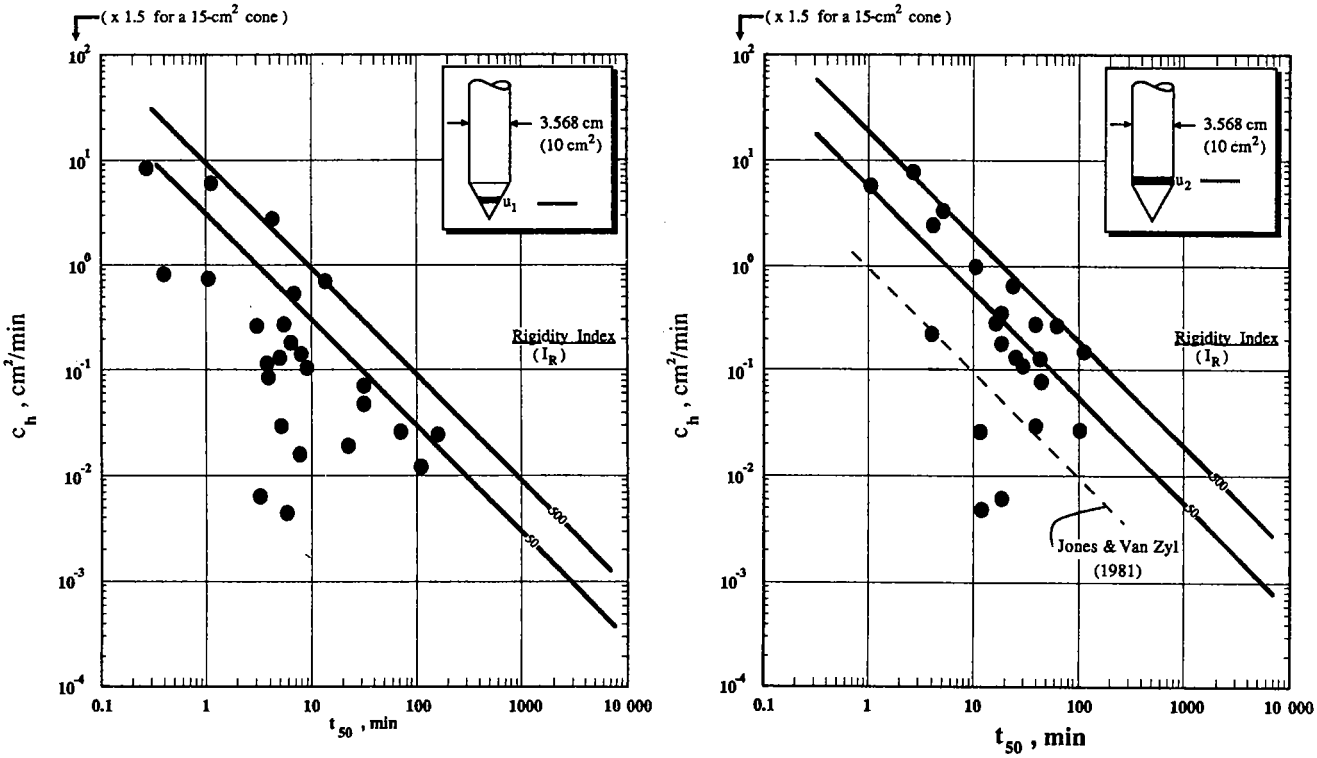

Figure 8.5. Oedometer c_h Values Compared With Piezocone t_{50} Measurements.

Note that other analytical/numerical schemes require I_r as an input yet the cavity expansion/critical-state approaches discussed herein provide I_r as an output parameter. Additional support for the magnitudes of backcalculated I_r is afforded from the study of rates of consolidation in the laboratory, field, and by piezocone dissipation tests by Robertson et al. (1992). Figure 8.5 shows the comparison of the coefficient of consolidation (c_h) versus time for 50% dissipation of excess pore pressures (t_{50}), with the SPM approach of Teh and Houlsby (1988) superimposed. Much of the data imply that a value of $I_r < 50$ would be needed in order to match the c_h values with t_{50} measurements.

8.2.5. Penetration Pore Water Pressures

For a proper assessment of dissipation tests, a finite difference solution that includes all pore pressure components in the time rate of pore pressure decay would be required.

For the analytical piezocone model presented in Chaper 7, the excess penetration pore pressures include:

Type 1: $$\Delta u_1 = \Delta u_{oct} + (\Delta p/\Delta q)[2s_{uTC}-q_o] + p_o' - 2s_{uTC}/M + c'\cot\phi' \quad [8.5a]$$

Type 2: $$\Delta u_2 = \Delta u_{oct} + p_o' - 2s_{uDSS} + c'\cot\phi' \quad [8.5b]$$

where $\Delta u_{oct} = (4/3)s_{uTC}\ln(I_r)$ is the octahedral component due to plastic failure and the stress path for the midface element is given by $\Delta p/\Delta q = 4/3$. Note that a filter element at the apex would require a stress path $\Delta p/\Delta q \approx 1$ or so, and this would provide lower pore pressures than midface.

By combining terms and allowing $c' = 0$, the normalized excess pore pressures from the piezocone become:

Type 1: $$\Delta u_1/\sigma_{vo}' = (4/3)(s_u/\sigma_{vo}')_{TC}\ln I_r + (4/3)[2(s_u/\sigma_{vo}')_{TC}-(1-K_o)] + (1+2K_o)/3 - (2/M)(s_u/\sigma_{vo}')_{TC} \quad [8.6a]$$

Type 2: $$\Delta u_2/\sigma_{vo}' = (4/3)(s_u/\sigma_{vo}')_{TC}\ln I_r + (1+2K_o)/3 - (2/M)(s_u/\sigma_{vo}')_{DSS} \quad [8.6b]$$

Consequently, the penetration pore water pressures can be decoupled for use in developing decay curves that are separate for the shear-induced and total stress path components, which dissipate quickly, from the large octahedral components (Δu_{oct}) that require much longer times for decay since they affect a much larger zone beyond the radius of the cone. The zone of influence is related to the rigidity index. For cylindrical cavity expansion, the radius of the plastic zone to the cone radius equals $(I_r)^{0.5}$, while for spherical cavity expansion, the ratio $r_{plastic}/r_{cone} = (I_r)^{0.333}$.

The shear-induced Δu are affected by a thin zone nearest the cone and therefore will dissipate in shorter time than the octahedral Δu. Figure 8.6 illustrates the conceptual decays of Δu(octahedral) and Δu(shear plus total stress path) using dissipation data from the Baton Rouge site. It is interesting to note that, once the Δu(shear) component has fully equilibrated, both u_1 and u_2 dissipation curves are identical, reflecting the continuing decay of Δu(octahedral). This phenomenon of Δu_2 increasing for a portion of the dissipation and subsequently decreasing at later stages of time is indicative and characteristic of overconsolidated clays (Davidson 1988; Sully and Campanella 1994).

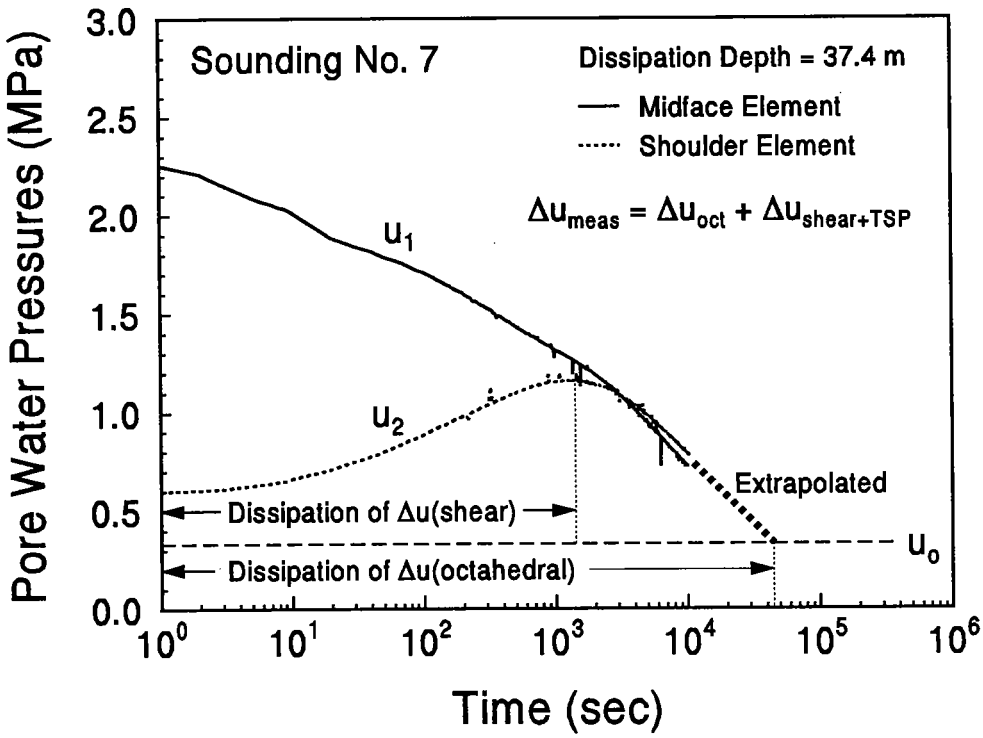

Figure 8.6. Conceptual Separate Decays of Δu Components During Dissipation Tests.

8.2.6. Dual Pore Pressure Model

The combined effect of both Type 1 and 2 pore pressures in Equations [8.6] may be utilized to give the following:

$$\text{Dual:} \quad (\Delta u_1 - \Delta u_2)/\sigma_{vo}' = (4/3)[2(s_u/\sigma_{vo}')_{TC} - 1 - K_o] + (2/M)[(s_u/\sigma_{vo}')_{DSS} - (s_u/\sigma_{vo}')_{TC}] \qquad [8.7]$$

Introducing the Wroth-Houlsby-Randolph expressions for s_u/σ_{vo}' for the TC and DSS modes and the relationship for $K_o = (1-\sin\phi')OCR^{\sin\phi'}$, the above can be adequately approximated and rearranged to give:

$$\text{Dual:} \quad OCR = (2\sin\phi')^{-1}[(u_1 - u_2)/\sigma_{vo}'] + 1 \qquad [8.8]$$

which serves as an expression derived from the soil behavioral model for obtaining overconsolidation ratio from pore pressure measurements only.

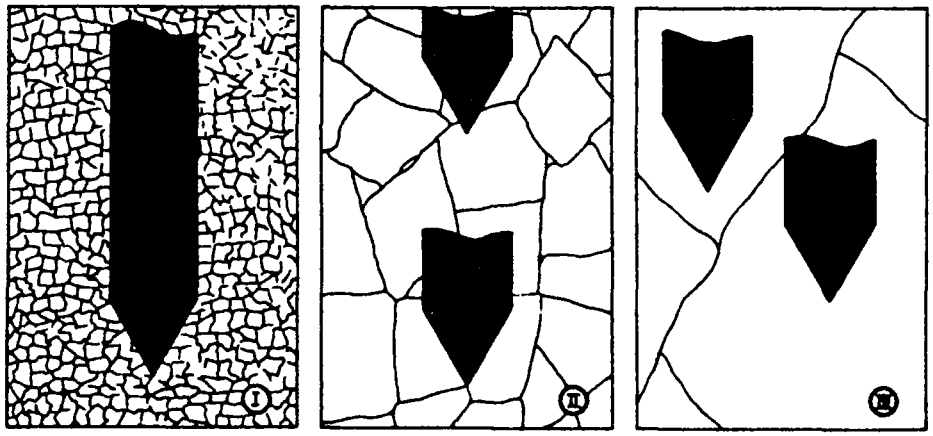

Figure 8.7. Fissuring and Scaling Size Effects (Powell and Quarterman, 1988).

8.2.7. Effect of Fissuring

The effects of fissuring undoubtably affect the results of laboratory and in-situ tests in clays. Degree of fissuring has been noted to affect the response of cone penetration (see Figure 8.7). Perhaps the undrained strength is the most markedly affected parameter (Marsland and Quarterman, 1982). In this regard, normalized undrained strengths vs. OCR give lower relationships than those obtained from intact specimens. Additional studies should be made to quantify the degree and extent of fissuring so that this facet can be quantified for strength evaluations.

8.2.8. Sleeve Friction Measurements

Additional research should be focussed on the improvement and corrections for sleeve friction measurements (f_s and f_T). It is perhaps noteworthy that series of soundings utilizing as many as 14 different commercial/research penetrometers by Lunne et al. (1986a) found little agreement in the magnitudes of recorded f_s **and** corrected f_T. For example, Figure 8.8 shows results from 8 different cone soundings at Onsoy. Quite scattered and inconsistent readings are evident. Results from the Haga site were more varied, with

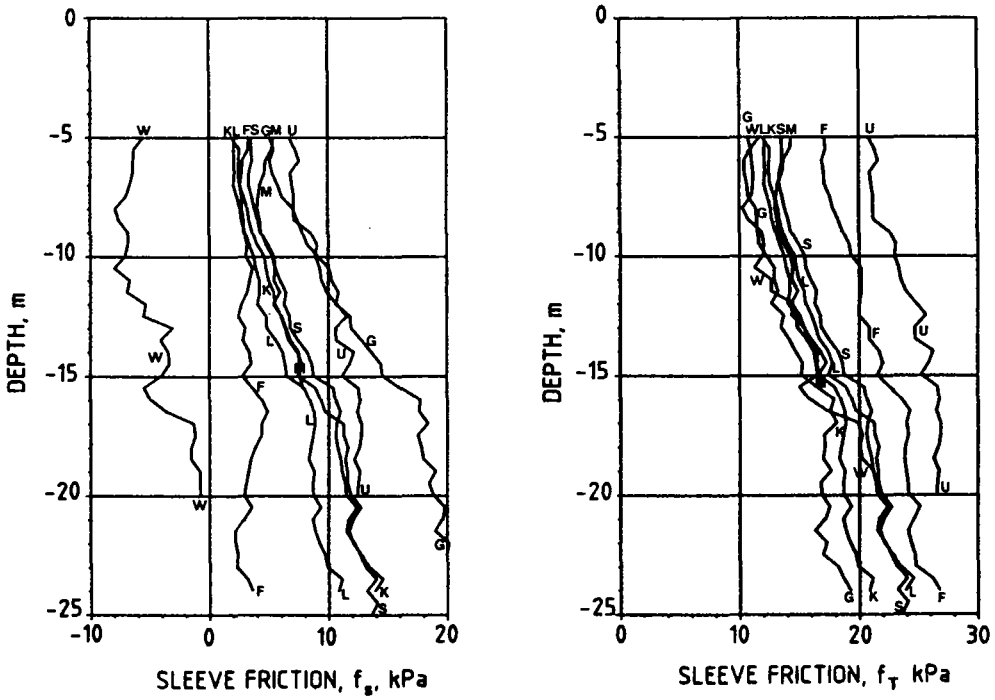

Figure 8.8. Measured and Corrected Friction Sleeve Readings at Onsoy, Norway (Lunne et al. 1986a).

several cones indicating negative f_s! Ongoing work at Laval University is investigating the re-positioning of the f_s measurement further up the shaft in order to provide more consistent measurements (Leroueil, 1994, personal communication).

Perhaps once this measurement difficulty with f_s is overcome, added benefits will accrue in the interpretation of soil parameters. For example, a recent proposal by Masood and Mitchell (1993) suggested that the normalized sleeve friction was related to ϕ':

$$f_s/\sigma_{vo}' = \tan^2(45° + \phi'/2) \tan(\phi'/3) \qquad [8.9]$$

The expression has been used to evaluate ϕ' at the Baton Rouge site, for which the triaxial test series (Chapter 4) indicated a large-strain $\phi' = 27.5°$. Figure 8.9 shows the derived ϕ' profile using the Masood and Mitchell (1993) approach and implies a potential may exist, provided that reliable f_s values can be obtained. If so, the aforementioned [8.9] can be

rearranged and approximated in closed-form to give:

$$\phi' \text{ (deg)} \approx 30.8\,[\log(f_s/\sigma_{vo}') + 1.26] \qquad [8.10]$$

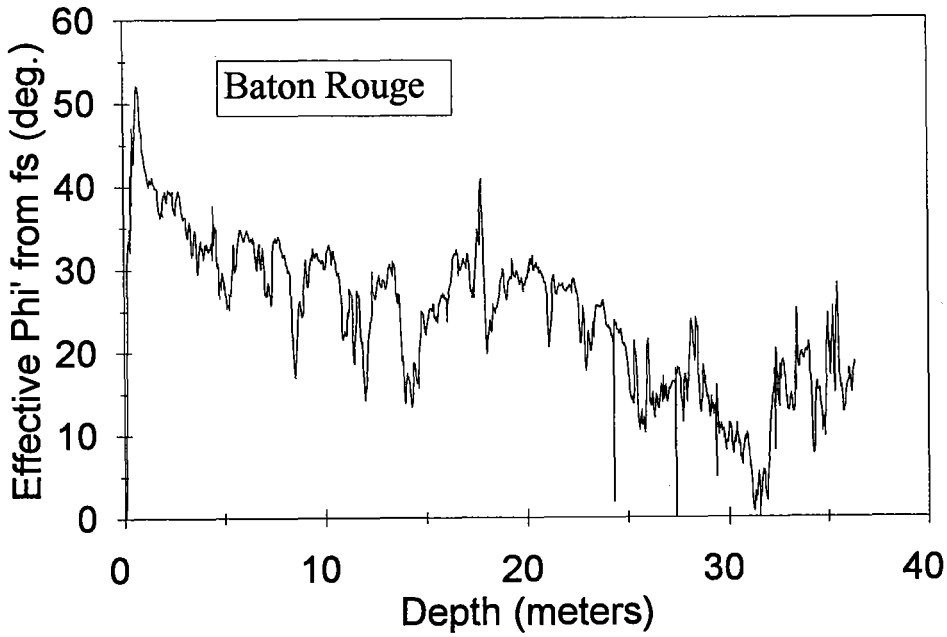

Figure 8.9. Profile of Effective ϕ' Calculated from f_s/σ_{vo}' Measurements.

8.3. Final Comments

The use of piezocone tests for profiling overconsolidation ratio in clays should be tempered with a good understanding of the local geology, history, origins, and past behavior of the deposit. Prudent engineering practices would dictate that high-quality samples be obtained from the site and standard sets of consolidation tests be performed to evaluate σ_p' along portions of the soil profile. The OCRs evaluated by the piezocone results can be used to provide preliminary assessments and complement the results of incremental-load oedometer tests or constant rate-of-strain consolidation tests. Testing with the piezocone should be carried out by experienced personnel to ensure that proper calibrations are assured and that saturation techniques and other details are addressed. In this manner, the use of in-situ tests will provide great economic benefit and fundamental satisfaction to those assigned to work on civil engineering projects.

APPENDIX A

GEORGIA TECH PIEZOCONE SYSTEM

At present, the Georgia Tech piezocone system consists of the following components: one electric cone penetrometer, three electric piezocone penetrometers, 30-meters of EW rods, power supplies, an ultrasonic depth sensor, two analog-to-digital signal convertors, a 286 laptop computer and 486 notebook with data acquisition software. In addition to interfacing with commercial drill rigs, a small hydraulic actuator with 1-m stroke has been mounted on a trailer and used mainly for teaching demonstrations.

During penetration, strain gages and pressure transducers within the piezocone continuously monitor q_c, f_s, and u_m and send electronic analog signals via cable to the signal convertor. This convertor receives and conditions the signals and then transmits them in digital form to the laptop computer, where they are processed by the data acquisition software and stored in tabular form on the computer's hard disk drive. Figure A.1 shows a schematic chart describing the electronic link between the piezocone and the supporting components.

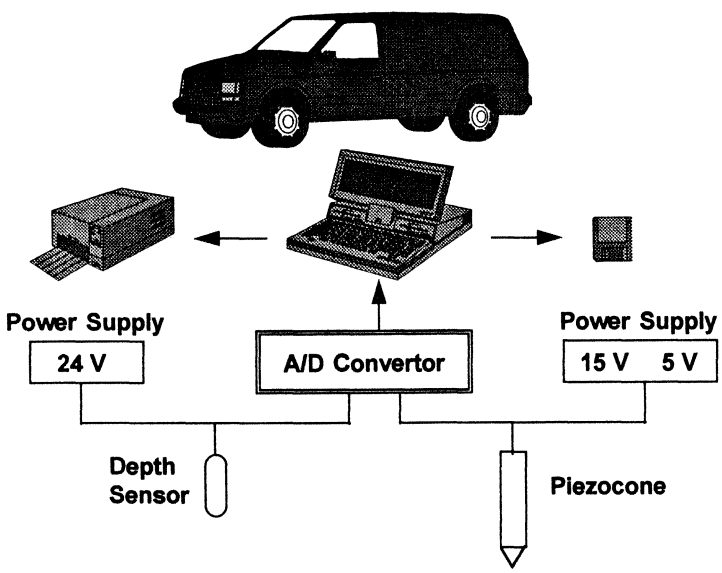

Figure A.1. Flow Diagram Showing Electronic Path Signals From Piezocone.

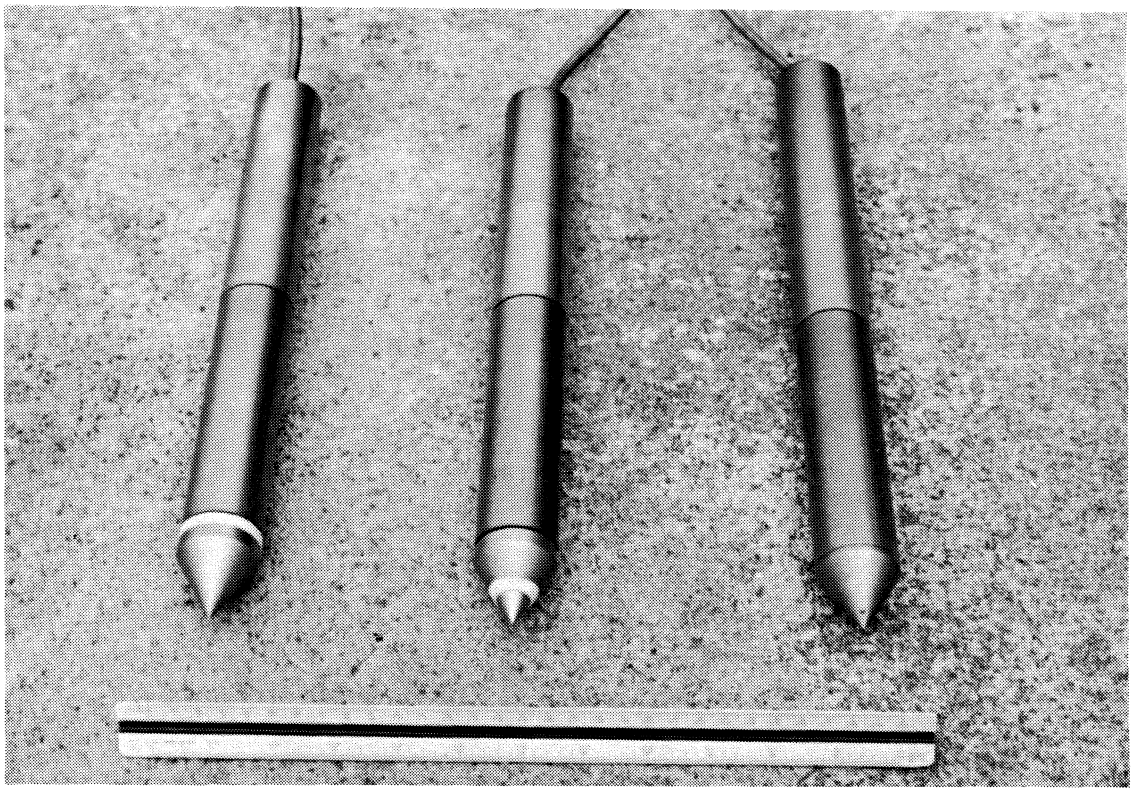

Figure A.2. L-D Type Penetrometers (from left to right) including: (a) Type 2 Piezocone, (b) Type 1 Piezocone, and (c) Standard Electric Cone.

A.1. Piezocone Penetrometers

The GT system utilizes one electric cone and two electric piezocones built by Dr. Alan J. Lutenegger of University of Massachusetts-Amherst and Mr. Carl Davey of Clarkson University (designated L-D type). A recent addition includes a Hogentogler-type seismic piezocone with inclinometer and interchangeable filters and tips. The cone and piezocones are 35.7 mm in diameter and have 10-cm^2 tips with a 60° apex angle and friction sleeves with 150 cm^2 of surface area. The penetrometers shown in Figure A.2 are made of tool steel, including the tip, the friction sleeve, and the internal rod to which the strain gages are affixed. The newer piezocone (not shown) is constructed of stainless steel. Spare tips and sleeves are replaceable in case of damage. The filter element is machined to fit each piezocone and provides access for the water to reach the pressure transducer.

A.1.1. Load Cells and Pressure Transducer

The load cells of the L-D type piezocone consist of strain gages which measure q_c and f_s independently. Such penetrometers are often referred to as tension-type penetrometers, in contrast to the subtraction-type penetrometer (Larsson and Mulabdić, 1991). The gages used are bonded-foil strain gages and are configured in four separate two element-rosettes, an arrangement commonly used when the direction of principal stresses or strains is known. The gages function by responding to externally applied strains with changes in resistance. These changes in resistance are monitored by a Wheatstone bridge, a circuit designed to convert the changes in resistance to a more recognizable voltage signal. A pressure transducer is required in each of the piezocones to measure u_m. This pressure transducer, which also operates using the strain gage/Wheatstone bridge formation, is an AB type model manufactured by Data Instruments Inc. and has a capacity of 1400 kN/m^2.

The wiring diagram for the L-D type piezocones is shown in Figure A.3. As indicated in the diagram, the load cells used to measure q_c and f_s require a 15 volt DC (maximum) excitation, while the pressure transducer which measures u_m uses a 5 volt DC

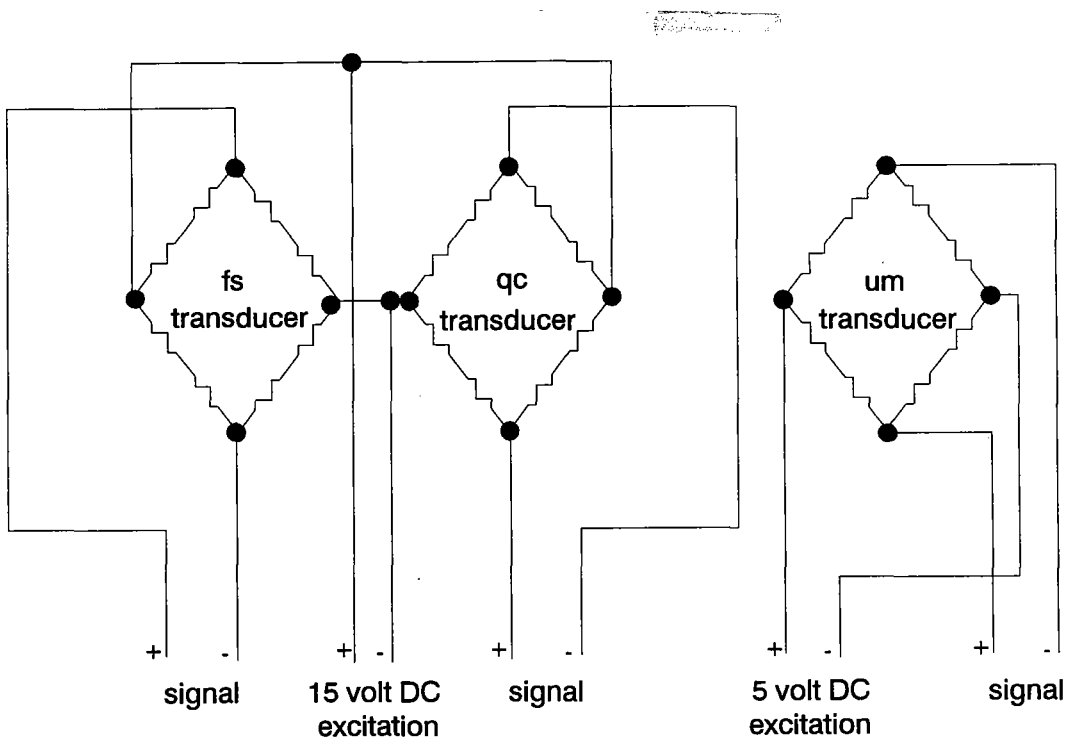

Figure A.3. Wiring Diagram for L-D Type Piezocone Penetrometers.

(6 volt maximum) excitation. The power supply used for this system is the Omega Engineering Inc. Triple Power Supply (PSS-T15). This power supply uses an input 115 volts AC house current and is capable of delivering 15 volts (@ 100 mA) and 5 volts (@ 50 mA) simultaneously, or an option of 30 volts output. The power supply generates a frequency of 50/60 Hz and provides a stable power source with a voltage accuracy of $\pm 1\%$.

The newer Hogentogler-type piezocone has internal signal conditioners and completely different arrangement.

A.2. Laboratory Calibration of Load Cells and Transducers

Careful calibration of the strain gage load cells and transducers is essential to the operation of the piezocone system. The purpose of this calibration is to determine the scale factor for the load cell and transducer and also to define the linearity, hysteresis, non-return to zero, and zero shift of the strain gage system. The scale factor is determined by relating the electrical output of the load cell and transducer to the desired engineering quantity, in this case q_c, f_s, and u_m, and is usually defined as the slope of the calibration curve.

A.2.1. Calibration of Load Cells

The setup to generate the calibration curve for the q_c load cell in the piezocones is shown in Figure A.4(a). Data for the calibration curve are generated using a Tinius Olsen compression machine to apply a series of known loads to the piezocone. The electrical response of the load cell is recorded as each load is applied. To convert the load into the desired engineering quantity of stress, the applied load must be divided by the area over which it acts (A_t = 10 cm^2). This allows a plot of gage output versus applied stress, which defines the calibration curve. Linear regression analyses are used to determine the best fit line through the data. In these analyses, n is the number of data and r^2 is the coefficient of determination.

An example calibration curve for the q_c load cell in Type 1 piezocone is shown in Figure A.5(a). This calibration curve shows excellent linearity and almost no hysteresis, and is representative of the repeatability and relationships determined for the other strain gages and pressure transducers.

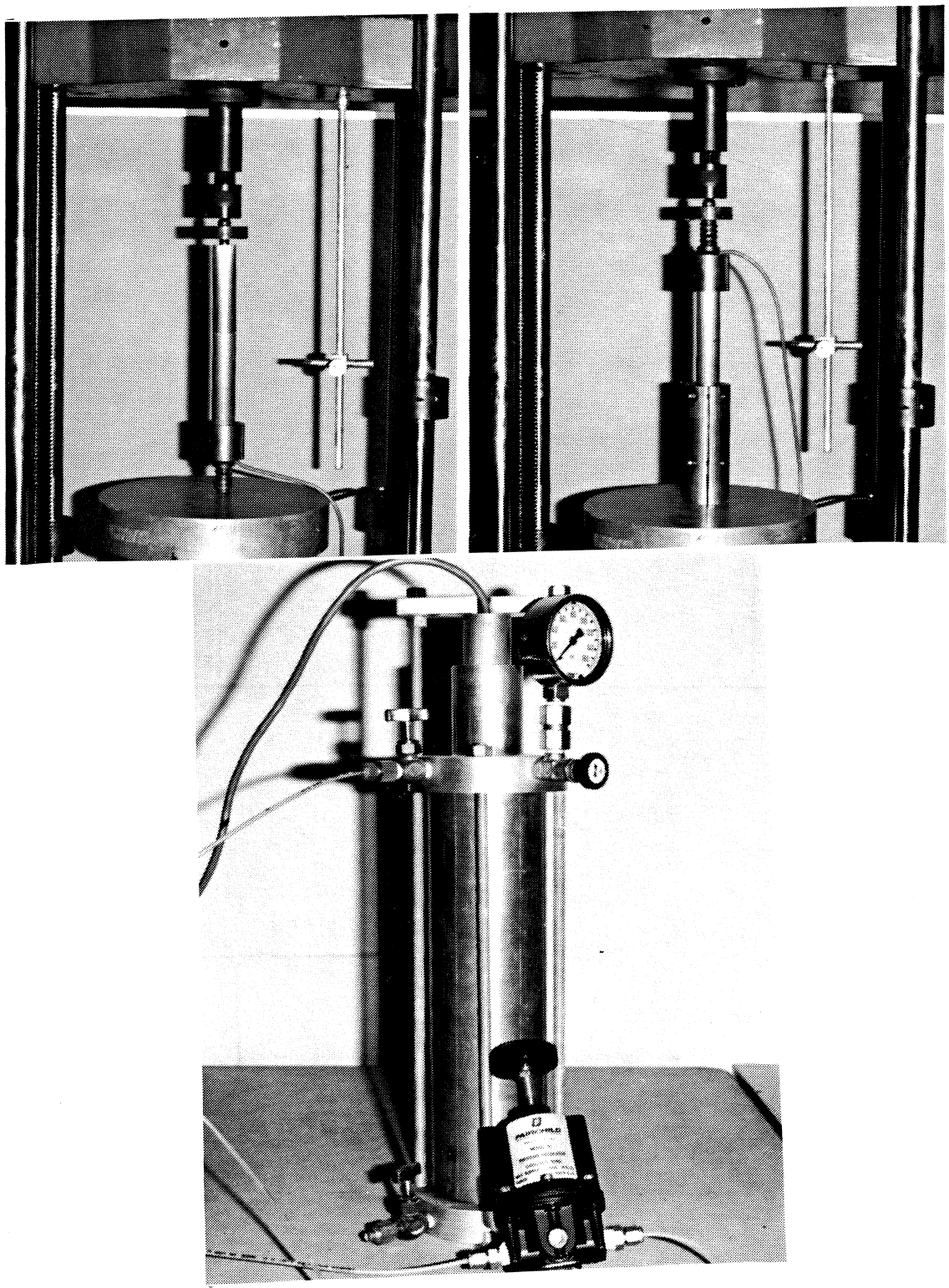

Figure A.4. Calibration Setup of (a) Axial Force for Cone Tip Resistance, (b) Force for Sleeve Friction, and (c) Pore Water Pressure Transducer.

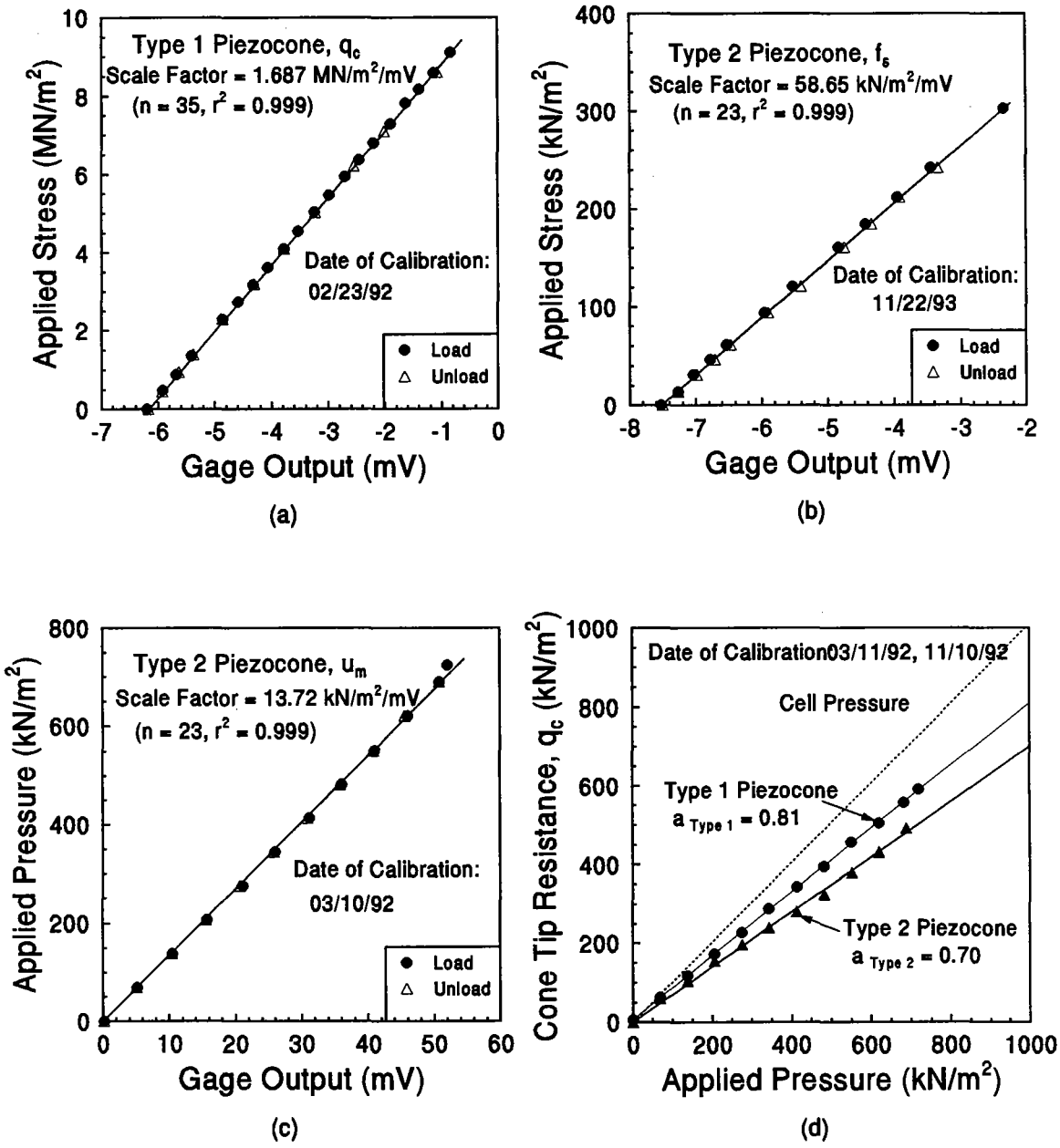

Figure A.5. Typical Calibration Results for (a) Cone Tip Resistance, (b) Sleeve Friction, (c) Pore Water Pressure Measurements, and (d) Net Area Ratio.

The setup used for determining the calibration factor for the f_s load cell is shown in Figure A.4(b). A metal sleeve capable of clamping the friction sleeve is used to allow a direct transfer of load from the loading frame to the friction sleeve. The metal sleeve is lined with a rubber membrane and can be tightened to ensure that no slippage occurs between the clamp and the friction sleeve during load application. To convert the load to the desired engineering quantity of stress, the applied load must be divided by the area over which it acts (A_s = 150 cm^2). An example calibration curve for the f_s load cell in Type 2 piezocone is shown in Figure A.5(b).

A.2.2. Calibration of Pressure Transducer

The pressure transducer measuring u_m must also be calibrated. This calibration is performed by submerging the tip of the piezocone in a water filled pressure chamber, as shown in Figure A.4(c). The pressure chamber is made of aluminum and measures 305 mm in height and 76 mm in inside diameter. The chamber is capable of holding the maximum house pressure of 700 kN/m^2. The top cap of the chamber has an inside diameter slightly larger than the cone diameter (37.5 mm) and has two layers of O-ring along the inside wall which provides a seal once the piezocone is inserted. A secure plate is tightened on the top of the inserted cone to prevent the cone from being pushed out under high pressure. By applying known increments of pressure, through a pressure regulator, to the inside of the chamber and recording the transducer response, the scale factor can be determined as previously described. An example calibration curve for the u_m load cell in both types of piezocone is shown in Figure A.5(c).

A.2.3. Calibration to Determine Net Area Ratio

The importance of calculating the corrected cone tip resistance, q_T, requires experimental determination of the net area ratio ($a = A_N/A_T$). The evaluation of the net area ratio is performed during the calibration of the pressure transducer and requires that the response of the q_c load cell also be recorded as the cell is pressurized. A prior knowledge of the scale factor of q_c load cell is required. A plot of the q_c load cell response (in engineering units) versus the applied cell pressure is then generated and used to

determine the net area ratio, which is simply the ratio of the load cell response to the applied cell pressure. Figure A.5(d), which illustrates this behavior for the L-D Type piezocones, shows the net area ratio to be 0.81 and 0.70 for the L-D Type 1 and Type 2 piezocones, respectively.

A.2.4. Calibration Factors

Slight variations of the calibration factor of strain gages and pressure transducer may be observed over a period of time, possibly due to variations in environmental conditions (such as temperature, humidity, dust, and magnetic field). Routine maintenance and calibration are required if high-quality test results are expected. The Georgia Tech cone and piezocone penetrometers are normally calibrated before and after each use, on an average time interval of every two to three months. The most recent results of the calibrations of the L-D type cone and piezocones, including the scale factor for each of the load cells and pressure transducers and the net area ratio for each piezocone, are presented in Table A.1.

Table A.1. Calibration Factors for L-D Type Penetrometers (kPa/mV).

Cone Type	q_c	f_s	u_m	a
Standard	1963	54.8	NA	NA
Type 1	1713	47.7	13.7	0.81
Type 2	1744	58.7	13.7	0.70

Notes: NA - not available

The net area ratio for the new Hogentogler cone was determined to be 0.80. Signal conditioners within the cone electronics allow it to operate without amplification.

A.2.5. Problems Encountered in Calibration

Two major problems encountered during the calibration of cone and piezocone penetrometers include zero drift and cross talk. The zero drift is defined as the change in

zero-load output with time, possibly caused by (1) variation of temperature, (2) change in humidity, and (3) electronic noise. The effect of thermal zero drift on test results can be minimized by allowing the piezocone strain gages to come to equilibrium at the in-situ temperature before testing. Once the penetrometer enters the ground, the influence of temperature variation becomes less significant. This is done in the field by suspending the cone in a prebored hole to a depth just below the water table elevation and allowing the zero readings to stabilize, then re-zero all output readings to minimize the temperature effect. If the temperature variation is expected to be more significant in extreme climate conditions, evaluation of the thermal zero shift is necessary. This can be done by submerging the penetrometers into a water bath with constant temperature control and monitoring the output signals with varying temperature. Although the GT cone penetrometers are not equipped with temperature sensors, some commercial cone designs do provide temperature records during penetration that can be used for correcting the thermal zero shift.

In addition to thermal zero drift, humidity by itself and the excessive residues accumulated in the vicinity of strain gages due to humidity intrusion can also cause changes in zero load output. During the two year periods, both Type 1 and Type 2 L-D piezocones experienced some humidity problems and had to be repaired by replacing the strain gages. Nevertheless, the humidity problem has been alleviated by an improvement on the original seal design, more effective cleaning of the cone after each use, and a sealed storage environment with a desiccant inside.

Electronic noise is related to the performance of strain gages and the transducer, as well as the quality of connections to other peripheral electronic devices. An electronic filter device is often used to eliminate some of these noises. Larsson and Mulabdic (1991) recommended that the allowable limits for the maximum error be 20 kN/m^2, 2 kN/m^2, and 1 kN/m^2 for q_c, f_s, and u_m, respectively. By careful maintenance and occasional repair, the L-D type piezocones were found to meet these requirements at all times.

One additional item that must be considered during calibration is the electrical and mechanical cross-talk that can occur between the load cells and the pressure transducer for each piezocone. For the L-D type piezocones, electrical cross talk is eliminated by using a sufficiently slow sampling rate (1 sample per 0.75 second). Mechanical cross-talk is

more difficult to eliminate since its occurrence is related to the cone design and manufacture. The only mechanical cross-talk observed for the GT penetrometers is a slight increase of u_m when the load is applied to q_c for Type 1 piezocone during mechanical calibration, although it is found that pressurizing the pore pressure transducer does not affect the q_c reading. While it is very likely that this one-way cross-talk is related to the test setup during q_c calibration, the problem can be corrected by subtracting 5 kN/m^2 from u_m readings per 1000 kN/m^2 of q_c, if necessary.

A.3. Filter Elements

Several aspects concerning the porous filter elements used for pore water pressures are important, including the specific location, material type, and saturation procedures.

A.3.1. Filter Location

The two L-D type piezocones are distinguished only by the location of their filter element. On the Type 1 piezocone, the filter is 5 mm in thickness and is located at the mid-height of the cone face, approximately 15 mm from the cone tip apex (as measured to the center of the filter). On the Type 2 piezocone, the filter is 6 mm in thickness and is located on the cone shaft 5 mm behind the cone tip shoulder. The new Hogentogler piezocone has an interchangeable element.

A.3.2. Filter Type

Sintered metal (steel and bronze), ceramic, and plastic can be used as the filter material for piezocones. The filter material currently being used for the L-D penetrometers is a coarse high-density polyethylene (HDPE) plastic termed Product No. X-4907 that is manufactured by Porex Technologies of Fairburn, Georgia. Table A.2 lists some of the technical data for this material. While the plastic filter may be compressible and involving a risk of clogging during the test, there is yet little agreement regarding what is the most suitable filter material for measuring pore pressure with piezocones (Jamiolkowski et al. 1985; Larsson and Mulabdic, 1991). To avoid the risk of excessive clogging, the current practice at Georgia Tech is to use a new filter before each test since they are inexpensive.

Table A.2. Technical Data for High-Density Polyethylene Filter Material

Softening Point	130°C
Melting Point	160°C
Average Pore Size	150 micron
Void Volume	35-50 %

A.3.3. Saturation of Filter

The importance of saturating the porous filter and the cavity between the filter and transducer has been recognized (Lacasse and Lunne, 1982). Detailed methods for achieving this saturation have been described elsewhere (Senneset et al., 1989; Juran and Tumay, 1989). At Georgia Tech, different laboratory and field techniques are used to achieve saturation of the piezocone. These techniques are as follows:

1. Laboratory saturation of the filter elements overnight is achieved by submersing them in deaired water in a sealed chamber under vacuum (typically 500 mm Hg or -80 kN/m^2).
2. Field saturation of the filter elements (to negate the effects of transportation-induced aeration) is performed using a small vacuum chamber and a portable vacuum pump.
3. Field saturation of the cavity between the filter and the pressure transducer is accomplished using a water-filled hypodermic needle.
4. The cone tip and filters are assembled while being held underwater.

Larsson and Mulabdic (1991) reported identical results when using either water or glycerin as the saturating fluid. For the results reported herein, water was used for all saturation procedures. However, in the most recent soundings with the new Hogentogler cone, a 50-50 glycerin/water solution proved more effective.

One additional step often taken involves preboring a hole to the depth of the water table and filling the hole with water. The purpose of preboring (or prepunching with a

dummy cone) is to prevent the loss of cone saturation during the penetration of dry desiccated layers of soil. Also, in the absence of a vacuum source, an alternative means of achieving filter saturation is by boiling the filters in a water bath. With the newer glycerin/water approach, no preboring efforts were required.

A.4. Piezocone Cable

The signals generated at the piezocone during its penetration are transmitted to the ground surface using a cable. The type used in the L-D system is Belden Cable No. 9540 and is rated for underground use. This 24-gage cable provides 10 leads plus ground and is 6.35 mm in nominal diameter. In the cases of pinched cable or extension, each lead is soldered together and insulated with plastic heat shrink, followed by finishing with silicone sealant and electrical tape. The cable has to be threaded through all the rods before each test, with one free end connected to the data acquisition system. Handling the cable is apparently a major burden in the field operation of piezocone penetration test, therefore, an improvement of using a cableless testing system will definitely make the test more attractive in the future.

A.5. Analog-to-Digital Signal Convertor

The analog-to-digital (AD) signal convertor is required to convert the electronic signals received from the strain gages on the piezocone and from the depth sensor into a format that is recognizable by the laptop computer. When signals arrive via the piezocone cable at the convertor box, they are in analog form and represent the voltage changes sensed at the strain gages. The function of the convertor is to monitor this analog input and produce a representative binary (digital) number, which sends this number to the data acquisition software on the laptop computer.

The AD convertor used at Georgia Tech is the ADC-1 model manufactured by Remote Measurement Systems of Seattle. This convertor, pictured in Figure A.6, is capable of receiving 16 channels of analog input, although only four of these are required for the L-D cones (channels 1 to 3 to monitor the gages on the piezocones and channel 4 to monitor signals from the depth sensor). Since the strain gages used on the L-D cones produce

Figure A.6. View of the ADC-1 Analog-Digital System.

output voltages of only a few millivolts, the input voltages are amplified in channels 1 to 8 by a 50-gain amplifier before arriving at the convertor. Signals through channels 1 to 8 have an option of either being amplified or unamplified while channels 9 to 16 remain unamplified. This amplification improves the resolution of the ADC-1 to 0.002 mV over a range of $\pm$ 8.19 mV, which is especially important for the q_c load cell. A second ADC-1 convertor, which uses a 20-gain amplifier, is also available to provide a wider range ($\pm$ 20.48 mV) but a lower resolution (0.005 mV) of signal outputs. Signals on all four channels are monitored for a period of approximately 15 milliseconds and then averaged before being converted to digital output. In addition to convert the analog signal to digital, the ADC-1 can also receive digital input, provide controlled output, and serve as a +5 V

DC (@ 5 mA) power source. As noted earlier, the Hogentogler cone requires no amplification.

The ADC-1 is a lightweight, accurate, and rugged AD converter, nevertheless, has its limitation of not providing sufficient readable voltage range. Unlike full-scale AD converters with signal conditioners, which can change the initial zero reading and the scale factor by adjustments, the ADC-1 can only make limited adjustments through programming. Therefore, it may be more desirable to obtain a more sophisticated but lightweight AD converter in future improvements.

A.6. Laptop Computer and Data Acquisition Software

The digital signals produced by the AD convertor are sent to a laptop computer for processing. The laptop computer used herein was a Zenith SuperSport 286 Portable Computer which has a 80286 processor and a math coprocessor. More recently, a 486 Toshiba notebook was added to the system.

The data acquisition program is written and edited in QUICK BASIC computer language, which has several different versions, with the one currently used in the field called GTFLD. The user must interact with the software to define which channels are to be read, which input source is being read by which channel, and the zero-reading and scale factor for each channel. The program is written to have the capability of performing regular electric cone penetration test, piezocone penetration test, and dissipation test. The software samples incoming data at a rate of 1 sample every 0.75 seconds, or 1 sample every 20 mm if the test is performed at the standard penetration rate of 20 mm/sec. The software sends a copy of the data to the screen during the test and a copy to the computer's hard disk or to a floppy disk. The data are then imported to a pre-formatted spreadsheet for data reduction and final presentation. A dot matrix printer is used to provide a hard copy of the data. The data acquisition devices, including ADC-1 AD convertor, power supply, and laptop computer, are normally set up inside a cargo van for mobility and protection. For test locations where the access is difficult, they may be set up remotely from the vehicle to perform the test.

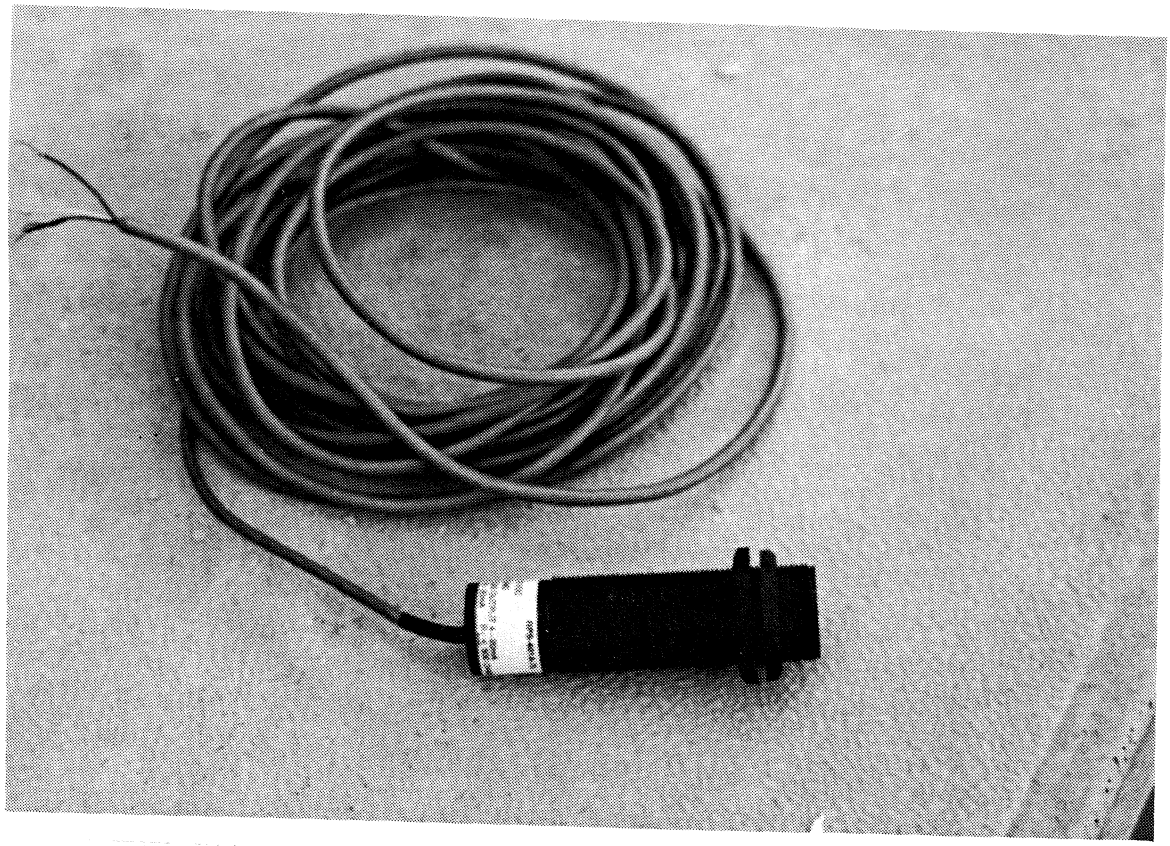

Figure A.7. Migatron-Type Ultrasonic Depth Sensor.

A.7. The Ultrasonic Depth Sensor

To take full advantage of the continuously monitored q_c, f_s, and u_m, the depth at which the readings are taken must also be profiled continuously. This is often done either using an electric potentiometer or mechanical encoder. For the Georgia Tech system, an ultrasonic depth sensor is used to continuously monitor the depth during the test. The depth sensor used by Georgia Tech is the RPS-401A model manufactured by Migatron Corporation of Woodstock, Illinois (see Figure A.7). This cylindrical-shaped device monitors distance changes over a range of 200 mm to 1,830 mm by recording the time interval between the transmission and reflection of an ultrasonic sound wave. The depth sensor requires 24 volts DC as input (provided by a separate power source) and delivers an analog signal as output. A product specification is listed as shown in Table A.3.

Table A.3. Detail Specifications of Migatron Ultrasonic Depth Sensor

Operational Range	200 to 1,830 mm
Power Input	20 to 30 Volts
Current Input	50 Amps
Output	4 to 20 mA
Accuracy	2.5 mm
Frequency	150 kHz
Response Time	50 msec
Ambient Temperature	0 to 60 °C

A target plate such as wood or plastic or a level ground surface way be used to reflect the signal back to the receiver. Due to the phenomenon of beam spread, the target must be level and have a minimum diameter of 600 mm for the maximum 1,830 mm distance, in order to reflect the signal properly. During a piezocone test, the setup for the depth sensor and target requires that the depth sensor be mounted to the top of the drill rod string using a clamp with an extension arm. Like the strain gages on the piezocone, the depth sensor must also be calibrated to determine its scale factor. The scale factor for the depth sensor was determined to be 4.9 mm/mV.

A.8. Hydraulic Drill Rig

A final component of the piezocone system at Georgia Tech is the equipment used to push the piezocone and other in-situ devices (such as the flat dilatometer) into the ground. The main equipment is a hydraulic actuator mounted on a surplus Army ammunition trailer to provide mobility. The portable rig can be operated on the top of the trailer (Figure A.8), or be removed from the trailer to operate in a limited access area if necessary.

The rig is hydraulically operated and has a thrust capacity of approximately 40 kN. This capacity is limited, however, by the amount of reaction force available. Currently, screw anchors with several different sizes, such as 1,000 mm long (single 100 mm helix) and 750 mm long (twin 100 mm helixes), are used to provide this reaction force and have produced soundings of up to 8 meters deep. An electric anchor drive machine was

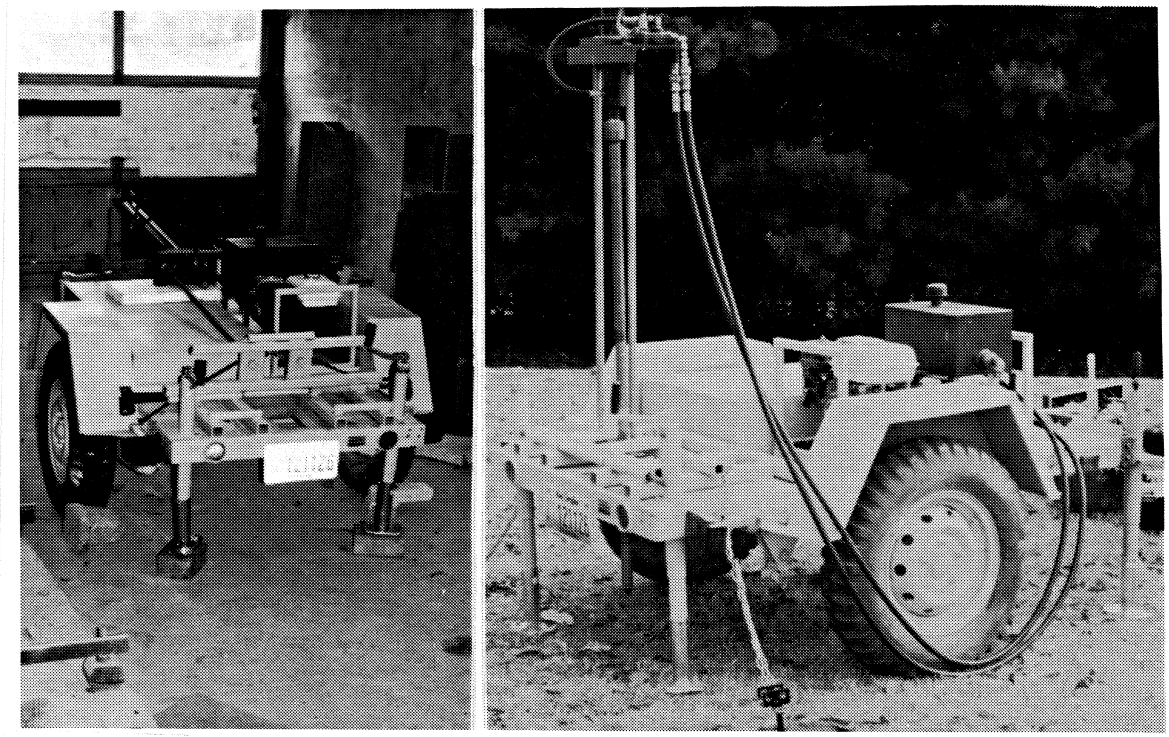

Figure A.8. Portable Trailer System with Hydraulic Actuator and Pump Station.

purchased to install the anchor into the ground more efficiently.

The hydraulic actuator on the rig has a maximum stroke of one meter, permitting the use of 0.9 m long, EW-size (35 mm outer diameter) drill rods. The piezocone is attached to the drill rods using a threaded adaptor. A friction reducer consists of a portion of the adapter 14 mm in length and is approximately 9 mm larger in outside diameter than the EW rods. The friction reducer is designed to minimize frictional resistance along the drill rods behind the cone penetrometer during penetration. Another special adapter, positioned at the interface between the topmost drill rod and the drill rig piston, was designed with a thin open slit on one side to allow exit of the piezocone cable.

The trailer, with an empty weight of approximately 2.5 kN, has been modified and equipped with four 13.5-kN jack at the corners and can carry the actuator, hydraulic pump,

drill rods, and tools. The actuator is hinged near the rear end of the trailer, which permits a horizontal position during transportation. When operated with the trailer, the hydraulic actuator extends and pushes the rods into the ground through a square hole near the end of the trailer. Upgrades are still being pursued to improve its performance.

The portable drill rig is primarily used for for classroom demonstrations. When deep soundings are required, larger drill rigs are employed that provide the necessary thrust capacity and reaction force. The GT equipment has been used in conjunction with commercial drill rigs to successfully obtain soundings of up to 30 meters in depth.

A.9. Applications of GT Piezocone System

The GT cone system has been used successfully on campus and several test sites in the United States. Table A.4 summarizes the applications of the GT piezocone testing system in chronological order.

Table A.4. Summary of Applications of GT Piezocone Testing System.

Test Site	Location	Drill Rig	Type	Qty	Depth	Date	Temperature
GT Campus	Georgia	CME-55	CPT	2	20 m	06/92	80-85°F
Plymouth	N. Carolina	Mudbug	CPT	1	8 m	08/92	80-90°F
Jonesboro	Georgia	GT Rig	PCPT	4	8 m	09/92	80-90°F
Port Huron	Michigan	CME-75	PCPT	7	29 m	11/92	35-45°F
Savannah	Georgia	CME-55	PCPT	7	10 m	07/93	95-100°F
Bagdad	Arizona	CME-75	PCPT	5	28 m	11/93	55-75°F
Mayaguez	Puerto Rico	CME-55	PCPT	12	25 m	03/94	80-85°F
San Manuel	Arizona	CME-75	PCPT*	3	26 m	08/94	±110°F

* Note: Seismic piezocone test

The results for the tests in lacustrine clays at Port Huron were discussed in Chapter 4. Tests at the GT Campus and Jonesboro sites involved residual silty sands of the Piedmont Province. Tests at Savannah and Plymouth involved interbedded sands and clays of the Atlantic Coastal Plain and mixed profiles of sediment and residuum encountered at Mayaguez. Finally, piezocone tests at Bagdad and San Manuel involved copper mine tailings.

APPENDIX B

REFERENCE LISTING OF PIEZOCONE SITES

A summary table is presented in this appendix which lists the clay sites tested by piezocones used in compiling the database and the references sources of data for each site. A more complete listing of the relevant information is given in Chen (1994). The full listing includes: (1) site name, (2) data completeness rating, (3) site location, (4) country, (5) soil type and description, (6) natural water content, (7) liquid limit, (8) plasticity index, (9) sensitivity, (10) reference values of overconsolidation ratio from oedometer tests, (11) undrained shear strengths, (12) effective friction angle, (13) cone tip area, (14) porous filter location, and (15) reference source. In this abbreviated appendix, only the specific listing of the clay site, type of piezocone porous element, and reference source of data are listed. Sites are listed alphabetically by name. References cited in the table are given in Appendix D of this technical report.

Most sites were tested by piezocones which had standard 10-cm^2 cone tip areas. A few sites were tested with both 10- and 15-cm^2 tips (Onsoy, Haga, and Surry/Virginia). Negligible differences in the recorded q_c are observed in clays between these tip areas. In the following table, an asterisk (*) appearing after the site name indicates that cone tip area of the cone was 15 cm^2. Likewise, a double asterisk (**) indicates a miniature cone with 4- to 5-cm^2 tip. Under the category of "u type", the pore pressures were measured at the tip apex (u_{1t}), the tip face (u_{1f}), behind the tip (u_2), and behind the friction sleeve (u_3). For additional details, see the full listing given by Chen (1994).

PIEZOCONE DATABASE

SITE	U TYPE	REFERENCE
200th Street	1f, 2, 3	Sully (1991)
Adriatic Sea	?	Pelli & Ottaviani (1993) in Italian
Alex Fraser Bridge	2	Robertson et al. (1990); Woeller et al. (1991)
Amherst	2	Saxena et al. (1978); Private communication with Luttenegger
Anacostia (*)	2	Mayne & Frost (1986); Mayne & Holtz (1988); Mayne (1987)
Antibes	2	Smits & Bruzzi (1988)
Arnprior	2, 3	Konrad (1986)
Arthur Laing Bridge	2	Campanella & Kokan (1993)
Askersund	1t	Bergenstahl (1991)
Atchafalaya	1t	Baligh et al. (1980)
Backebol	1f, 2, 3	Larsson & Mulabdic (1991)
Bagdad Cyprus	1f, 2	GT Internal Report
Bakklandet	1f, 2, 3	Sandven (1990)
Baltimore	2	Myers (1993)
Bastican	2	Tavenas (1981); Tavenas et al (1982)
Baton Rouge (*)	1f, 2, 3	GT Internal File
Bay Farm Island	2	Masood et al (1988); Masood & Mitchell (1992)
Bayonne	1f	Bensaid (1985) French Report
Berthierville	1f, 2	LaRochelle et al. (1988)
Bologna	2	Robertson (1989); Belfiore et al (1989)
Borgne Canal	1f	Tumay et al (1981); Canou & Tumay (1986)
Borlagne	2	Torstensson (1982)
Boston (East)	2	Whittle et al. (1990); Sweeney & Kraemer (1993)
Boston (South)	2	Whittle et al. (1990); Sweeney & Kraemer (1993)
Boston Blue Clay	1t, 2	Baligh et al (1980); Baligh et al (1981); Levadoux & Baligh (1986)
Bothkennar	1f, 2	Hight etal (1992); Hawkins et al (1989); Jacob & Coutts (1992)
Bowie	1f, 2	Franz & Hull (1993)
Brage	1f	Senneset et al. (1988)
Brage 2	1f	Rad & Lunne (1988)
Brazil	2	Tanaka & Diniz (1993)
Brent Cross (Hendon)	1t, 1f, 2	Powell et al. (1988); Lunne et al (1986); Rad & Lunne (1988)
Broadway	1f, 2	Chameau et al. (1991)
Burnaby	2	Gillespie & Campanella (1981)
Canons Park	1f	Powell et al. (1988)
Charles City County	1f, 2	Houlihan & Blodgett (1989)
Chek Lap Kok (Lower) (*)	1f	Koutsoftas & Foott (1982)
Chep Lap Kok (Upper) (*)	1f	Koutsoftas & Foott (1982)
Cloverdale	2	Greig et al. (1988)
Colebrook Road (*)	2	Crawford & Campanella (1991); Campanella & Weemees (1990)
Cornell Clay (**)	1t, 2	Mayne et al. (1992)
Cowden	1t, 1f, 2	Lunne et al (1986); Powell & Uglow (1985); Rad & Lunne (1988)

PIEZOCONE DATABASE

SITE	U TYPE	REFERENCE
Cran	1f	Juran (1983); Bensaid (1985)
Cretaceous (*)	2	Mayne & Frost (1986); Frost & Mayne (1986)
Deerhaven Power House	?	Gupta (1983)
Drammen	1t, 2	Lacasse & Lunne (1982)
Dunkerque	1f, 2	Juran & Tumay (1989); Bensaid (1985)
El Camino Real	1f	Stark & Juhrend (1989); Private Communication with Spang
Eberg	2	Sandven (1990)
Emmerstad	1t, 2	Rad & Lunne (1988); Aas et al (1986)
Empire	1t	Azzouz & Lutz (1986)
Evanston	1f	Finno (1988)
Evanston 2 (*)	1f	Saines et al. (1989)
Fort Road	2	Chang (1990)
Fredericton	2	Konrad & Law (1987)
Gault (Remolded) (**)	2	Almeida & Parry (1985)
Glava	1f, 2, 3	Sandven (1990)
Gloucester	2	Konrad & Law (1987)
Grand Isle (*)	1f, 3	Juran & Tumay (1989)
Grangemouth	1f, 2	Hawkins et al. (1989); Jacob & Coutts (1992); Powell et al. (1988)
Gulf of Mexico	?	Private Communication with Macari
Hachirogata	2	Shibata et al. (1993)
Haga	1t, 2	Lunne et al (1986); Rad & Lunne (1988); Gillespie et al (1984); Christopher & Lacasse (1984)
Halsen	1t, 2	Sandven (1990)
Haltenbanken	1f, 2	Rad & Lunne (1988); Private Communication with Lunne
Hamilton AFB	2	Masood et al (1988); Masood & Mitchell (1992)
Haney	1f, 2	Wickremesinghe & Campanella (1991); Sully et al. (1988); Robertson et al. (1986)
Helsinki	?	Rathmayer (1979)
Hibernia	2	Taylor (1993)
Himeji	2	Shibata et al. (1993)
Holland A	2	Smits (1982)
Holland B	2, 3	Smits (1982)
Homestake Mine	1f	East & Ulrich (1989); East et al (1988)
Houston	1f, 2	Mahar & O'Neill (1983); Private Communication with O'Neill
I-90 Bridge	2	Kramer et al. (1990)
ICI (*)	1f	Reid & Turnbull (1988)
Imperial Valley	1f, 2	Campanella et al. (1986); Sully et al. (1988); Campanella & Robertson (1988)
Inchinnan	1f, 2, 3	Sills et al. (1988)
Japan	2	Sugawara & Chikaraishi (1988)
Japan NM	2	Shrivastava & Mimura (1991)
Jonesboro	1f, 2	GT Internal File
Kallang Basin	2	Chang (1990)
Kaolin K-50	1f, 2	Kurup et al. (1992); Kurup (1993)

PIEZOCONE DATABASE

SITE	U TYPE	REFERENCE
Kaolin K-55	1f, 2	Smits (1982)
Keelung River	2	Chern (1992)
Kettner	1f	Private Communication with Spang
Kinkai	2	Shibata et al. (1993)
Kobe City 1 (*)	2	Tanaka & Sakagami (1989)
Kobe City 2 (*)	2	Tanaka & Sakagami (1989)
Koshien	2	Shibata et al. (1992)
Kringalik Plateau	2	Jefferies et al. (1987); Hugh et al. (1984)
Kyobashi	2	Shibata et al. (1992)
Labenne	1f	Bensaid (1985) French Report
Lagunillas	?	Sully et al. (1988) ; Sully & Murria (1987) ; Ladd & Lamb (1963)
Lake Alice	1t	Gupta (1983)
Lake Mjosa	2	Senneset et al (1982); Senneset et al (1985)
Lake Wauberg	1t	Gupta (1983)
Langley	2	Greig et al. (1988); Robertson et al. (1988)
Lierstranda	2	Masood & Mitchell (1992)
Lilla Mellosa	1f, 2, 3	Larsson & Mulabdic (1991)
Lopez Ridge	1f	Stark & Juhrend (1989); Private Communication with Spang
Louiseville	2	LaRochelle et al (1988); Tavenas (1981); Tavenas et al (1982); Silvestri & Aubertin (1988)
Lower 232nd Street	1f, 2, 3	Greig et al. (1988); Campanella et al. (1988); Sully & Campanella (1990); Sully (1991)
Lulu Island	2	Robertson et al. (1988)
Madingley	1f, 2	Lunne et al. (1986); Marsland & Powell (1988)
Makuhari 4-3	2	Tsuchiya et al. (1988)
Maskinonge	1f, 2	Roy & Mercier (1989)
Massena IDA	2	Lutenegger & Kabir (1987); Lutenegger & Kabir (1988)
Massena MHS	2	Lutenegger & Kabir (1987); Lutenegger & Kabir (1988)
Massena RRC	2	Lutenegger & Kabir (1988)
Massena SLS	2	Lutenegger & Kabir (1988)
Matagami	2	Tavena et al. (1982)
Merville	2	Amar et al. (1989)
Muar	2	Chang (1990)
Muni Metro (*)	1f	Koutsoftas (1989)
Munkedal	1f, 2, 3	Larsson & Mulabdic (1991)
Museum Park	2	Masood & Mitchell (1992)
NRCC	1f, 2, 3	Konrad & Law (1987); Konrad (1986)
National Stadium	2	Chang (1990)
Netherlands C	2	Cheng-hou et al. (1990)
Netherlands D (JDR)	1f	De Ruiter (1982)
Netherlands Z	1f	Zuidberg et al. (1982)
New Westminster	1f, 2	Bensaid (1985) French Report
Nice (*)	1f	Juran & Tumay (1989)

PIEZOCONE DATABASE

SITE	U TYPE	REFERENCE
Norco (Laplace)	1f	Tumay & Acar (1985); Bensaid (1985); Tumay & deSeze (1983)
Norfolk Road	2	Chang (1990)
Norrkoping	1f, 2, 3	Larsson & Mulabdic (1991)
North Anna (*)	2	Gordon & Mayne (1987)
North Sea (*)	1f	Richards & Zuidberg (1985)
North Sea GA (*)	1t	Lunne et al. (1985)
North Sea GC (*)	1f, 2, 3	Lunne et al. (1985); Bayne & Tjelta (1987); Skomedal & Bayne (1988)
North Sea S (*)	1f, 2, 3	Private Communication with NGI
North Sea T (*)	1f, 2, 3	Skomedal & Bayne (1988); Private Communication with NGI
Northern Nevada	?	Ulrich (1993)
Noto Peninsula	?	Matsumoto et al. (1993)
Odiel River	2	Cuellar et al. (1985)
Onsoy	1t, 1f, 2	Lunne et al (1986); Lacasse & Lunne (1983); Rad & Lunne (1988)
Orinoco E1	1t	Azzouz et al. (1982)
Orinoco F1	1t	Azzouz et al. (1982)
Ottawa STP	2	Konrad & Law (1987)
Peak Down Mine	2	Simons (1993)
Pisa	1t, 2	Jamiolkowski et al. (1994); Lancellota & Pepe (1990); Battaglio et al. (1986)
Plancoet	1f	Bensaid (1985) French Report
Pontida	1t, 2, 3	Jamiolkowski et al. (1985)
Port Huron	1f, 2	GT Internal Report
Porto Tolle	1t, 2	Jamiolkowski et al (1985)
Prince George County	2	Private Communication with Clemente
Pyramid Carousel	2	Mayne (1989)
Ravenna	1t	Battaglio et al. (1986)
Richards Island	2	Woeller et al. (1991); Campanella et al. (1986); Kurfurst & Wowller (1988)
Richmond	2	Gillespie & Campanella (1981)
Rio de Janeiro	1f, 2, 3	Sills et al. (1988); Rocha Filho & Alencar (1985); Rad & Lunne (1988)
Santa Maria	1f	Villet & Darragh (1985); Keaveny & Mitchell (1986)
Saro Rd 6/900	1f, 2, 3	Larsson & Mulabdic (1991)
Saro Rd 7/600	1f, 2, 3	Larsson & Mulabdic (1991)
Savannah	1f, 2	GT Internal Report
Savannah River Site	2	Private Communication with Bechtel
Sea Island	1f, 2, 3	Konrad (1985); Robertson et al. (1988); Greig et al. (1988); Masood & Mitchell (1992)
Shanghai G	2	Tang & Zhu (1988)
Sicily	2	Ventura (1983)
Singapore	?	Karunaratne (1991)
Ska-Edeby	1f, 2, 3	Larsson & Mulabdic (1991)
Sleipner 2	1f	Lunne et al. (1985)
Sleipner 4	1f	Lunne et al. (1985)
South Africa	1f, 2	Jones & Van Zyl (1981); Jones & Rust (1982)

PIEZOCONE DATABASE

SITE	U TYPE	REFERENCE
South Killingholme	2	Baker & Gardener (1988)
St. Alban	1t, 1f, 2	Roy et al. (1982)
St. Hilaire	2	LaFleur et al. (1988)
St. Jean Vianney	1f, 2	LaRochelle et al. (1988)
St. Marcel	2	Konrad & Law (1986)
Stjordal	1t, 2	Senneset et al. (1988)
Strong Pit (*)	1f, 2, 3	Campanella et al. (1988); Campanella & Weemees (1990); Sully & Campanella (1990)
Surrey	1f	Long & O'Riordan (1988)
Surry Miocene	2	Mayne & Gordon (1987)
Surry Pleistocene	2	Mayne & Gordon (1987)
Swale	2	Hawkins et al. (1989)
Tablazo Bay	1f, 2	Sully et al. (1988); Sully & Murria (1987)
Taipei	2	Moh & Hwang (1993); Chin et al. (1993)
Taranto	1t, 2, 3	Battaglio et al. (1986); Jamiolkowski et al (1988)
Tarsuit	2	Crooks et al. (1988); Jefferies et al. (1987)
Telegraph Hill	1f, 2	Chameau et al. (1991)
Texas A&M	1f	Private Communication with Gibbens & Briaud
Tiller	2	Sandven (1990)
Tinker AFB	2	Private Communication with ARA
Tokyo	2	Sugawara (1988)
Tokyo Bay	?	Tanaka et al. (1991)
Tongji	2	Du et al. (1992)
Troll 2	1f	Rad & Lunne (1988)
Troll East	1f, 2, 3	Skomedal & Bayne (1988)
Troll East Area 2	1t, 1f, 2	Sandven (1990)
Trondheim	2	Senneset & Janbu (1985)
Tuve	1f, 2, 3	Larsson & Mulabdic (1991)
Umeda	2	Shibata et al. (1992)
Upper 232nd Street	2	Greig et al. (1988)
Urayasu 2	2	Tsuchiya et al. (1988)
Vagnharad	2	Torstensson (1982)
Valen	1f, 2, 3	Larsson & Mulabdic (1991)
Valoya	1f, 2	Sandven (1990)
Vancouver	1f, 2	Rad & Lunne (1988)
Varennes	2	Konrad & Law (1987)
Veslefrikk (*)	1f, 2, 3	Skomedal & Bayne (1988)
Wayne County	?	Private Communication with Niehoff
Winthrop Harbor (*)	1f	Saines et al. (1989)
Yerba Buena Cove	1f, 2	Chameau et al. (1991)
Yorktown	2	Mayne (1989)

APPENDIX C

COMPILED PIEZOCONE DATABASE FROM CLAY SITES

This appendix provides a listing of a spreadsheet containing the discrete data points of overconsolidation ratio (OCR = σ_p'/σ_{vo}') from laboratory oedometer tests and corresponding piezocone measurements (q_T, u_1, u_2, and u_3) at the same depths. Corrected cone tip resistances (q_T) are listed, as appropriate. The pore pressures were measured at various locations such as the tip apex (u_{1t}), the tip face (u_{1f}), behind the tip (u_2), and behind the friction sleeve (u_3). Other pertinent information given in the spreadsheet includes: soil type, total (σ_{vo}) and effective overburden stress (σ_{vo}'), hydrostatic pore pressure (u_o), and approximate plasticity index (PI or I_p).

It was necessary in certain instances that data points be filtered from the spreadsheet when measured anomalies occurred either within a desiccated crustal layer or where silty or sandy lenses and seams were encountered. Other data points excluded from the analysis included irregular pore pressure measurements (e.g. $u_m > q_T$) or uncertain u_T corrections for corrected cone tip resistance. In the latter, either the value of net area ratio "a" or penetration pore pressures behind the tip (u_2) were not known. In other cases, a random stone or gravel was encountered in the profile, or else the pore pressure filter became de-saturated. The full spreadsheet contains approximately 1,450 data points. Herein, only a selected sampling of compiled values are presented and reference is made to Chen (1994) for a more complete listing.

Piezocone Site -	SOIL TYPE	DEPTH (m)	PI (%)	OED. OCR	Svo (kN/m2)	Svo' (kN/m2)	uo (kN/m2)	qT (kN/m2)	u1t (kN/m2)	u1f (kN/m2)	u2 (kN/m2)	u3 (kN/m2)
ALEX FRASER BRIDGE	silt	40.00	10	1.38	740.0	362.0	378.0	1855			810	
ALEX FRASER BRIDGE	silt	49.00	10	1.41	907.0	425.0	482.0	2891			1407	
AMHERST	intact	5.33	25	2.42	95.9	43.6	52.3	609			310	
AMHERST	intact	7.62	25	2.18	137.2	62.4	74.8	712			414	
AMHERST	intact	10.67	25	1.56	192.1	87.4	104.7	765			518	
AMHERST	intact	12.19	25	1.39	219.4	99.8	119.6	795			490	
AMHERST	intact	18.29	25	0.80	329.2	149.8	179.4	674			656	
ANACOSTIA	intact	1.92	22	2.73	27.9	18.8	9.0	1033			15	
ANACOSTIA	intact	4.01	17	2.48	58.1	28.6	29.5	570			150	
ANACOSTIA	intact	4.84	38	2.32	70.2	32.5	37.7	567			171	
ANACOSTIA	intact	7.97	25	2.00	115.6	47.2	68.4	606			224	
ANACOSTIA	intact	9.10	25	2.30	132.0	52.0	80.0	547			255	
ANACOSTIA	intact	10.77	36	1.78	156.2	60.3	95.8	708			318	
ANACOSTIA	intact	11.44	50	1.56	165.8	63.4	102.4	727			318	
ANACOSTIA	intact	14.29	27	1.72	207.2	76.8	130.4	896			415	
ANACOSTIA	intact	20.85	26	1.41	302.4	107.6	194.8	1417			592	
ARNPRIOR	intact	6.00	35	1.60	108.0	48.0	60.0	500			345	176
ARNPRIOR	intact	10.00	35	1.60	180.0	80.0	100.0	594			459	248
ARNPRIOR	intact	14.00	35	1.60	252.0	112.0	140.0	824			608	358
ARNPRIOR	intact	18.00	35	1.60	324.0	144.0	180.0	946			702	436
ASKERSUND	intact	5.00		1.68	68.0	28.0	40.0	266		175		
ASKERSUND	intact	7.00		1.88	102.0	42.0	60.0	370		247		
ASKERSUND	intact	9.00		1.25	137.0	57.0	80.0	418		287		
ATCHAFALAYA	intact	12.30	40	1.24	165.2	64.2	101.0	362	182			
ATCHAFALAYA	intact	15.71	41	1.10	224.0	89.5	134.5	525	335			
ATCHAFALAYA	intact	19.25	43	1.11	285.2	116.0	169.2	740	340			
ATCHAFALAYA	intact	20.03	45	1.16	299.9	123.0	176.9	800	350			
ATCHAFALAYA	intact	24.89	50	1.73	382.6	158.0	224.6	979	440			
ATCHAFALAYA	intact	30.82	60	1.19	480.7	198.0	282.7	1282	602			
ATCHAFALAYA	intact	34.24	80	1.04	543.3	227.0	316.3	1385	637			
BACKEBOL	intact	2.50	40	2.20	42.6	22.0	20.6	308		177	170	100
BACKEBOL	intact	3.50	40	1.57	57.9	27.5	30.4	340		232	199	135
BACKEBOL	intact	5.00	45	1.27	80.1	35.0	45.1	330		232	204	145
BACKEBOL	intact	7.00	35	1.23	110.7	46.0	64.7	357		262	232	160
BACKEBOL	intact	10.00	50	1.06	188.2	94.0	94.2	515		393	343	225
BAKKLANDET	intact	4.50	8	3.30	91.8	82.0	9.8	616		527	470	270
BAKKLANDET	intact	10.50	5	2.80	208.7	140.0	68.7	711		645	576	245
BAKKLANDET	intact	16.50	5	1.90	326.5	199.0	127.5	920		816	728	318
BAKKLANDET	intact	20.50	8	1.80	406.0	238.0	168.0	1096		1010	905	466
BASTICAN	leda	7.00	21	1.47	112.0	58.0	54.0	540			275	
BASTICAN	leda	15.00	21	1.30	239.0	107.0	132.0	940			500	
BASTICAN	leda	27.00	21	1.10	432.0	182.0	250.0	1341			785	
BATON ROUGE	fissured	5.50	26	15.60	101.8	92.0	9.8	2127		1468	327	-60
BATON ROUGE	fissured	7.92	35	11.90	142.0	108.4	33.6	2115		1088	414	-56
BATON ROUGE	fissured	11.28	36	8.40	202.0	135.5	66.5	1723		1042	332	-33
BATON ROUGE	fissured	15.90	35	5.30	293.8	182.0	111.8	3036		1892	1027	131
BATON ROUGE	fissured	28.40	17	4.00	524.5	290.0	234.5	3123		2281	31	87
BATON ROUGE	fissured	33.50	40	3.40	620.5	336.0	284.5	3453		2352	1281	644
BERTHIERVILLE	leda	2.50	28	1.57	46.5	33.8	12.7	321		134	116	
BERTHIERVILLE	leda	4.42	18	1.13	82.3	50.7	31.6	370		200	168	
BOSTON BLUE CLAY	intact	7.85	15	5.58	135.8	68.6	67.2	824	400		360	
BOSTON BLUE CLAY	intact	12.41	25	2.96	214.7	102.8	111.9	680	438		394	
BOSTON BLUE CLAY	intact	17.61	18	1.98	304.7	141.7	162.9	1013	764		688	
BOSTON BLUE CLAY	intact	20.38	18	1.48	352.6	162.5	190.1	1080	887		798	
BOSTON BLUE CLAY	intact	30.13	20	1.37	521.2	235.5	285.8	1401	1126		1013	
BOSTON BLUE CLAY	intact	30.17	20	1.29	521.9	235.8	286.2	1401	1126		1013	
BOSTON BLUE CLAY 2	intact	14.20	25	3.40	233.0	104.0	129.0	895	600	662	554	440
BOSTON BLUE CLAY 2	intact	18.30	18	2.20	320.0	150.0	170.0	1078	760	834	714	574
BOSTON BLUE CLAY 2	intact	21.30	18	1.60	372.0	173.0	199.0	1036	821	894	767	640
BOSTON BLUE CLAY 2	intact	24.40	20	1.40	425.0	196.0	229.0	1074	827	874	774	680
BOSTON BLUE CLAY 2	intact	27.40	20	1.20	476.0	217.0	259.0	1226	927	981	844	734
BOTHKENNAR	intact	2.06	41	3.54	41.4	30.0	11.4	295		226	127	
BOTHKENNAR	intact	2.16	41	2.06	43.4	31.0	12.4	280		235	140	
BOTHKENNAR	intact	3.62	41	1.42	66.7	40.0	26.7	408		281	178	
BOTHKENNAR	intact	9.02	41	1.61	153.7	74.0	79.7	658		522	243	
BOTHKENNAR	intact	13.93	41	1.37	231.8	104.0	127.8	898		780	499	
BOTHKENNAR	intact	17.89	41	1.72	296.7	130.0	166.7	1130		957	593	
BRAGE 2	intact	4.00	24	3.60	71.0	31.0	40.0	350		300		
BRAGE 2	intact	35.00	25	1.70	682.0	328.0	354.0	2890		2380		

Piezocone Site -	SOIL TYPE	DEPTH (m)	PI (%)	OED. OCR	Svo (kN/m2)	Svo' (kN/m2)	uo (kN/m2)	qT (kN/m2)	u1t (kN/m2)	u1f (kN/m2)	u2 (kN/m2)	u3 (kN/m2)
BRAGE 2	intact	42.00	21	2.00	820.0	396.0	424.0	4320		3150		
BRENT CROSS	fissured	4.00	50	80.00	77.6	48.6	29.0	1900	705	688	-6	
BRENT CROSS	fissured	6.00	50	60.00	116.4	66.4	50.0	2200	940	1062	-9	
BRENT CROSS	fissured	8.00	50	48.00	155.2	85.2	70.0	2200	823	1000	-9	
BRENT CROSS	fissured	13.00	50	31.00	252.2	132.2	120.0	2885	900	1371	-22	
BRENT CROSS	fissured	18.00	50	22.00	349.2	179.2	170.0	3192		1594	-11	
BROADWAY	intact	14.26	45	1.00	224.0	109.0	115.0	873			661	
CANONS PARK	fissured	6.00	42	50.00	120.0	67.0	53.0	2913		1100		
CANONS PARK	fissured	7.00	42	43.20	140.0	77.0	63.0	3700		1572		
CANONS PARK	fissured	8.00	42	37.80	160.0	87.0	73.0	2835		1341		
CANONS PARK	fissured	9.00	42	33.50	180.0	97.0	83.0	3386		1603		
CANONS PARK	fissured	10.00	42	30.30	200.0	107.0	93.0	3228		1607		
CHARLES CITY COUNTY	intact	23.20	47	2.95	383.2	203.2	180.0	2873		1943	1394	
CHEK LAP KOK (LOWER	intact	7.61	60	11.46	204.7	31.9	172.8	1090		907		
CHEK LAP KOK (LOWER	intact	9.51	60	6.12	231.2	39.8	191.4	1248		1042		
CHEK LAP KOK (LOWER	intact	12.97	60	3.75	279.7	54.4	225.4	886		726		
CHEK LAP KOK (LOWER	intact	14.45	60	3.12	300.4	60.5	239.9	800		651		
CHEK LAP KOK (LOWER	intact	18.53	60	3.31	357.5	77.6	279.9	1784		1487		
CHEK LAP KOK (LOWER	intact	25.82	60	2.55	459.5	108.2	351.4	1117		906		
CHEK LAP KOK (UPPER)	intact	2.27	40	2.73	129.8	9.5	120.3	126		90		
CHEK LAP KOK (UPPER)	intact	3.47	40	1.49	146.6	14.5	132.1	120		83		
CHEK LAP KOK (UPPER)	intact	4.49	40	2.18	160.9	18.8	142.1	165		121		
CHEK LAP KOK (UPPER)	intact	6.39	40	2.20	187.6	26.8	160.8	203		150		
CHEK LAP KOK (UPPER)	intact	7.53	40	1.96	203.5	31.5	171.9	1090		907		
COLEBROOK ROAD	intact	5.24	11	1.59	94.0	52.0	42.0	353			64	
COLEBROOK ROAD	intact	7.45	11	1.33	132.1	59.6	72.5	510			167	
COLEBROOK ROAD	intact	12.01	11	1.19	212.0	117.0	95.0	592			299	
COLEBROOK ROAD	intact	15.00	11	1.10	268.0	120.0	148.0	640			340	
COLEBROOK ROAD	intact	18.10	11	1.00	326.0	145.0	181.0	698			461	
CORNELL CLAY UU	lab	0.13	11	43.40	2.3	1.0	1.3	67	32		-5	
CORNELL CLAY UU	lab	0.22	11	26.34	4.0	1.8	2.2	67	51		-2	
CORNELL CLAY UU	lab	0.27	11	21.40	4.9	2.2	2.7	65	54		1	
CORNELL CLAY UU	lab	0.55	11	11.04	9.9	4.4	5.5	74	64		10	
CORNELL CLAY UU	lab	1.12	11	5.97	20.2	9.0	11.2	95	85		29	
CORNELL CLAY XX	lab	0.05	11	53.95	0.9	0.4	0.5	34	33		-1	
CORNELL CLAY XX	lab	0.09	11	32.45	1.6	0.7	0.9	38	35		-7	
CORNELL CLAY XX	lab	0.22	11	13.46	4.0	1.8	2.2	42	35		5	
CORNELL CLAY XX	lab	0.62	11	5.43	11.2	5.0	6.2	53	52		17	
COWDEN	fiss. till	3.00	21	15.00	47.0	27.0	20.0	2550	850		-100	
COWDEN	fiss. till	6.00	19	4.50	93.0	43.0	50.0	2350	750		-100	
COWDEN	fiss. till	17.00	16	2.80	387.0	227.0	160.0	2366	1102	1278	472	
CRAN	intact	1.50	55	2.46	26.0	11.0	15.0	423		209		
CRAN	intact	4.50	55	2.01	76.0	32.0	44.0	354		145		
CRAN	silt	10.00	55	1.50	170.0	80.0	90.0	650		500		
CRAN	silt	16.00	55	1.20	272.0	122.0	150.0	824		560		
CRETACEOUS	fissured	15.20	25	20.60	304.0	165.0	139.0	3151			38	
CRETACEOUS	fissured	16.80	25	18.80	336.0	181.0	155.0	3337			19	
DRAMMEN	intact	7.00	22	1.50	122.0	65.0	57.0	405	390		280	
DRAMMEN	intact	9.00	25	1.50	157.0	80.0	77.0	462	452		345	
DRAMMEN	intact	13.00	17	1.20	229.0	113.0	116.0	563	480		405	
DRAMMEN	intact	15.00	10	1.20	266.0	131.0	135.0	656	570		420	
DRAMMEN 2	intact	6.00	22	1.48	105.0	58.0	47.0	384			197	
DRAMMEN 2	intact	8.00	22	1.53	140.0	73.0	67.0	473			263	
DRAMMEN 2	intact	10.00	15	1.20	178.0	91.0	87.0	521			303	
DRAMMEN 2	intact	12.00	10	1.33	208.0	102.0	106.0	494			310	
DRAMMEN 2	intact	16.00	10	1.08	288.0	143.0	145.0	631			463	
DRAMMEN 2	intact	18.00	10	1.17	320.0	155.0	165.0	755			531	
DUNKERQUE	intact	20.00		1.00	360.0	210.0	150.0	947		768		
DUNKERQUE	intact	22.00		1.00	396.0	216.0	180.0	926		742		
DUNKERQUE	intact	24.00		1.00	432.0	222.0	210.0	1474		742		
EBERG	intact	3.50	12	2.78	55.0	40.0	15.0	230			183	
EBERG	intact	5.50	12	2.19	87.0	52.0	35.0	319			200	
EBERG	intact	8.50	10	1.70	135.0	72.0	63.0	1008			203	
EMMERSTAD	intact	4.00	10	3.90	107.0	73.0	34.0	370	350		200	
EMMERSTAD	intact	6.00	4	2.40	163.0	108.0	55.0	450	440		325	
EMMERSTAD	intact	8.00	4	1.90	221.0	144.0	77.0	460	415		350	
EMMERSTAD	intact	10.00	8	1.50	278.0	179.0	99.0	475	460		390	
EMMERSTAD 2	intact	3.65	10	5.35	54.0	28.0	26.0	272			98	

Piezocone Site -	SOIL TYPE	DEPTH (m)	PI (%)	OED. OCR	Svo (kN/m2)	Svo' (kN/m2)	uo (kN/m2)	qT (kN/m2)	u1t (kN/m2)	u1f (kN/m2)	u2 (kN/m2)	u3 (kN/m2)
EMMERSTAD 2	intact	4.50	10	3.29	69.3	35.0	34.3	350			115	
EMMERSTAD 2	intact	5.95	4	2.84	93.6	45.0	48.6	430			186	
EMMERSTAD 2	intact	8.00	4	2.50	120.7	52.0	68.7	500			255	
EMPIRE	intact	35.29	55	1.77	550.5	158.6	391.9	1801	1466			
EMPIRE	intact	42.50	55	1.60	663.0	203.4	459.5	2074	1630			
EMPIRE	intact	49.98	55	1.50	779.7	250.0	529.7	2344	1890			
EVANSTON	intact	9.00	18	1.30	166.5	122.4	44.1	510		464		
EVANSTON	intact	13.56	18	1.35	250.9	162.0	88.9	710		600		
EVANSTON	intact	18.10	18	1.40	334.9	201.4	133.4	1280		970		
EVANSTON	intact	19.51	18	1.50	360.9	213.7	147.2	1310		990		
FORT ROAD	intact	7.58	40	1.32	154.0	84.5	69.5	718			324	
FORT ROAD	intact	14.10	45	1.60	260.0	126.6	133.4	814			448	
FORT ROAD	intact	24.40	45	1.28	420.0	185.5	234.5	1050			700	
GAULT	lab		35	1.00	126.0	126.0	0.0	493	380			
GAULT	lab		35	1.90	66.0	66.0	0.0	395	285			
GAULT	lab		35	7.00	18.0	18.0	0.0	318	210			
GLAVA	intact	2.50	15	7.40	47.0	32.0	15.0	563		299	233	85
GLAVA	intact	6.50	14	5.80	124.0	69.0	55.0	805		569	476	302
GLAVA	intact	10.50	15	4.10	200.0	105.0	95.0	852		772	581	420
GLAVA	intact	17.50	12	2.60	333.0	168.0	165.0	1050		985	799	585
GLOUCESTER	leda	1.69	35	3.22	21.0	21.0	0.0	475			8	
GLOUCESTER	leda	5.57	20	2.68	74.0	39.0	35.0	517			254	
GLOUCESTER	leda	12.51	35	1.88	173.1	70.0	103.1	750			486	
GLOUCESTER	leda	17.97	25	1.50	264.7	108.0	156.7	1014			645	
GRANGEMOUTH	intact	2.00	45	3.00	32.0	32.0	0.0	365		225	136	
GRANGEMOUTH	intact	7.00	45	1.43	112.0	63.0	49.0	417		378	249	
GRANGEMOUTH	intact	14.00	45	1.35	225.0	107.0	118.0	857		708	473	
HAGA	intact	1.20	13	15.53	23.0	23.0	0.0	636	418		108	
HAGA	intact	3.55	16	4.90	66.0	66.0	0.0	871	665		500	
HAGA	intact	6.25	17	1.98	117.0	117.0	0.0	912	833		674	
HAGA 2	intact	1.50	13	12.00	30.0	30.0	0.0	713	533		438	
HAGA 2	intact	3.50	16	4.50	70.0	70.0	0.0	807	703		541	
HAGA 2	intact	4.50	35	4.00	88.0	88.0	0.0	1045	953		662	
HAGA 2	intact	6.00	17	2.20	118.0	118.0	0.0	885	768		654	
HAGA 2	intact	7.00	12	2.00	135.0	135.0	0.0	924	850		735	
HALSEN	silt	10.00		2.00	190.0	100.0	90.0	673	384		225	
HALSEN	silt	15.50		1.25	295.0	150.0	145.0	1291	531		282	
HALTENBANKEN	intact	2.00	18	8.60	44.0	24.0	20.0	780		500	350	
HALTENBANKEN	intact	6.00	18	5.00	125.0	65.0	60.0	1220		750	530	
HALTENBANKEN	intact	8.80	18	5.00	188.0	100.0	88.0	729		489	287	
HALTENBANKEN	intact	11.00	18	4.60	238.0	128.0	110.0	1396		886	515	
HAMILTON AFB	intact	2.75	70	3.03	39.9	36.8	3.1	350			-30	
HAMILTON AFB	intact	6.10	80	1.43	88.5	52.5	35.9	310			43	
HAMILTON AFB	intact	11.00	75	1.22	159.5	75.5	84.0	367			233	
HAMILTON AFB	intact	15.25	75	1.54	221.1	95.4	125.7	510			360	
HOMESTAKE MINE	tailings	9.80		1.00	176.0	88.0	88.0	309		205		
HOMESTAKE MINE	tailings	12.80		1.00	230.0	111.0	119.0	486		349		
HOMESTAKE MINE	tailings	14.60		1.00	263.0	126.0	137.0	684		416		
HOMESTAKE MINE	tailings	16.80		1.00	302.0	143.0	159.0	823		519		
HOUSTON	fissured	7.50	52	6.20	139.0	74.0	65.0	2645		1705	-62	
HOUSTON	fissured	8.00	52	4.30	148.0	78.0	70.0	2220		1450	-52	
HOUSTON	fissured	11.30	15	5.10	209.0	106.0	103.0	3750		2000	60	
HOUSTON	fissured	18.00	3	5.00	333.0	163.0	170.0	4440		1250	42	
IMPERIAL VALLEY	fissured			16.00	144.0	68.0	76.0	2328		960	40	
IMPERIAL VALLEY	fissured			16.00	205.0	97.0	108.0	2512		878	80	
INCHINNAN	intact	3.00	12	1.41	57.0	47.0	10.0	304		282	155	116
INCHINNAN	intact	7.00	15	1.52	133.0	84.0	49.0	355		339	219	181
INCHINNAN	intact	9.00	15	1.27	171.0	102.0	69.0	445		430	283	240
JAPAN	tailings	4.00		1.00	73.0	33.0	40.0	285			152	
JAPAN	tailings	8.00		1.00	147.0	67.0	80.0	590			369	
JAPAN	tailings	12.00		1.00	220.0	100.0	120.0	755			443	
JAPAN	tailings	16.00		1.00	293.0	133.0	160.0	1513			581	
KAOLIN K55	lab			1.00	402.0	2.0	400.0	2143		1645	846	
KAOLIN K55	lab			1.00	402.0	2.0	400.0	1082		754	564	
KAOLIN K55	lab			1.00	402.0	2.0	400.0	7902		5633	2422	
KEELUNG RIVER	intact	7.15	15	2.74	135.0	63.0	72.0	314			86	
KEELUNG RIVER	intact	11.25	15	1.43	211.0	98.0	113.0	607			288	
KEELUNG RIVER	intact	11.35	15	1.72	213.0	99.0	114.0	540			247	

Piezocone Site -	SOIL TYPE	DEPTH (m)	PI (%)	OED. OCR	Svo (kN/m2)	Svo' (kN/m2)	uo (kN/m2)	qT (kN/m2)	u1t (kN/m2)	u1f (kN/m2)	u2 (kN/m2)	u3 (kN/m2)
KOBE CITY 1	intact	5.20	80	1.00	94.0	42.0	52.0	113			66	
KOBE CITY 1	intact	8.90	80	1.00	161.0	72.0	89.0	299			141	
KOBE CITY 2	intact	5.00	70	0.47	487.0	287.0	200.0	1109			736	
KOBE CITY 2	intact	15.00	70	0.80	665.0	365.0	300.0	1523			1081	
KRINGALIK PLATEAU	fissured	3.00	23	8.20	341.0	31.0	310.0	1234			413	
KRINGALIK PLATEAU	fissured	7.60	23	9.40	437.0	78.0	359.0	1445			384	
KRINGALIK PLATEAU	fissured	12.30	23	4.30	531.0	126.0	405.0	1485			248	
KRINGALIK PLATEAU	fissured	20.10	23	2.70	686.0	206.0	480.0	2054			857	
KRINGALIK PLATEAU	fissured	26.30	23	2.50	813.0	271.0	542.0	2483			679	
LIERSTRANDA	intact	5.00	20	2.50	90.0	60.0	30.0	294			227	
LIERSTRANDA	intact	9.00	20	2.50	163.0	93.0	70.0	724			367	
LIERSTRANDA	intact	13.00	20	1.75	236.0	126.0	110.0	851			524	
LIERSTRANDA	intact	17.00	20	1.10	318.0	158.0	160.0	872			605	
LIERSTRANDA	intact	21.00	20	1.00	391.0	191.0	200.0	982			699	
LILLA MELLOSA	intact	2.00	90	1.11	29.0	18.0	11.0	200		160	74	52
LILLA MELLOSA	intact	6.00	75	1.00	86.0	36.0	51.0	310		230	170	130
LILLA MELLOSA	intact	10.00	55	1.25	147.0	57.0	91.0	431		364	285	225
LOUISEVILLE	leda	1.66	40	3.32	32.3	26.0	6.3	204			60	
LOUISEVILLE	leda	5.02	40	2.01	95.3	55.3	40.0	489			316	
LOUISEVILLE	leda	10.00	40	1.90	180.0	90.0	90.0	671			492	
LOUISEVILLE	leda	18.00	40	1.60	324.0	154.0	170.0	1047			712	
LOWER 232nd ST.	intact	2.57	19	6.10	46.0	20.0	26.0	409		178	165	78
LOWER 232nd ST.	intact	5.00	19	3.27	86.5	36.5	50.0	502		275	254	136
LOWER 232nd ST.	intact	9.10	19	1.20	157.0	66.0	91.0	520		408	339	239
LOWER 232nd ST.	intact	15.50	19	1.28	267.0	112.0	155.0	885		450	276	327
LOWER 232nd ST.	intact	20.50	19	1.00	352.0	147.0	205.0	824		746	643	527
LOWER 232nd ST.	intact	33.00	19	1.00	561.0	231.0	330.0	846			727	596
MADINGLEY	fissured	4.00	45	51.00	76.0	56.0	20.0	1700		880	-14	
MADINGLEY	fissured	6.00	45	35.00	114.0	74.0	40.0	2150		1120	-7	
MADINGLEY	fissured	8.00	45	28.00	153.0	93.0	60.0	3000		1300	-14	
MADINGLEY	fissured	12.00	45	21.00	229.0	129.0	100.0	3200		1250	-67	
MADINGLEY	fissured	14.00	45	19.00	267.0	147.0	120.0	3300		1350	-30	
MASSENA IDA	leda	4.00	14	1.00	64.0	24.0	40.0	303			213	
MASSENA IDA	leda	8.00	14	1.00	129.0	49.0	80.0	487			319	
MASSENA IDA	leda	12.00	14	1.00	193.0	73.0	120.0	651			433	
MASSENA MHS	leda	3.00	25	5.27	51.0	31.0	20.0	801			352	
MASSENA MHS	leda	6.00	25	2.09	102.0	53.0	49.0	781			431	
MASSENA RRC	leda	2.40	22	8.82	41.0	37.0	4.0	1416			373	
MASSENA RRC	leda	3.70	40	6.64	63.0	46.0	17.0	1440			452	
MASSENA RRC	leda	6.00	25	1.36	102.0	63.0	39.0	870			436	
MASSENA RRC	leda	9.70	25	1.00	165.0	89.0	76.0	886			490	
MASSENA SLS	leda	3.05	25	5.27	52.0	36.8	15.2	690			140	
MASSENA SLS	leda	7.01	30	2.23	120.0	65.5	53.9	1135			412	
MASSENA SLS	leda	7.62	30	2.12	130.0	69.9	60.0	1092			401	
MASSENA SLS	leda	9.15	40	1.87	156.0	80.9	75.0	1330			519	
MATAGAMI	leda	3.00		1.80	45.0	16.0	29.0	175			106	
MATAGAMI	leda	8.00		1.80	120.0	42.0	78.0	452			303	
MUAR	intact	2.94	50	2.52	42.6	18.7	23.9	190			76	
MUAR	intact	4.14	45	1.88	60.0	24.3	35.7	225			114	
MUAR	intact	7.91	50	1.32	114.7	42.0	72.7	325			194	
MUAR	intact	12.39	50	1.29	179.7	63.0	116.6	482			324	
MUAR	intact	16.99	35	2.06	246.4	84.6	161.8	701			460	
MUNI METRO	intact	15.24	30	1.02	275.0	204.0	71.0	745		370		
MUNI METRO	intact	24.69	30	1.16	444.0	281.0	163.0	1075		954		
MUNI METRO	intact	29.41	30	1.23	530.0	320.0	210.0	1150		1006		
MUNI METRO	intact	32.31	30	1.25	583.0	344.0	239.0	1281		1097		
MUNKEDAL	intact	4.25	33	2.27	78.0	46.0	32.0	570		382	331	247
MUNKEDAL	intact	8.00	31	1.64	153.0	83.0	70.0	691		500	433	314
MUNKEDAL	intact	12.00	29	1.26	232.0	122.0	110.0	801		686	524	392
MUNKEDAL	intact	16.00	27	1.15	311.0	161.0	150.0	826		803	598	480
MUNKEDAL	intact	21.00	23	1.12	384.0	259.0	125.0	958		803	716	533
MUSEUM PARK	intact	12.00		1.30	217.0	97.0	120.0	747			426	
MUSEUM PARK	intact	18.00		1.30	327.0	147.0	180.0	875			509	
MUSEUM PARK	intact	21.00		1.00	381.0	171.0	210.0	862			618	
MUSEUM PARK	intact	24.00		1.00	436.0	196.0	240.0	1073			796	
NETHERLANDS Z	intact	8.00		1.30	142.0	64.0	78.0	321		300		
NETHERLANDS Z	intact	18.00		1.30	321.0	144.0	177.0	829		600		
NORCO	intact	6.50	80	1.44	117.0	63.0	54.0	445		58	52	

Piezocone Site -	SOIL TYPE	DEPTH (m)	PI (%)	OED. OCR	Svo (kN/m2)	Svo' (kN/m2)	uo (kN/m2)	qT (kN/m2)	u1t (kN/m2)	u1f (kN/m2)	u2 (kN/m2)	u3 (kN/m2)
NORCO	intact	9.00	85	1.18	162.5	84.0	78.5	255		212	190	
NORCO	intact	13.20	55	1.03	238.7	119.0	119.7	470		329	296	
NORCO	intact	29.00	60	1.60	530.7	256.0	274.7	1153		750	680	
NORCO	intact	34.50	60	1.58	623.6	295.0	328.6	1445		871	784	
NORFOLK ROAD	intact	4.80	80	1.66	97.0	69.0	28.0	253			132	
NORFOLK ROAD	intact	8.00	60	1.60	162.0	102.0	60.0	413			182	
NORFOLK ROAD	intact	22.00	45	1.40	444.0	244.0	200.0	933			647	
NORRKOPING	intact	2.00	44	1.54	32.0	27.0	5.0	238		151	133	75
NORRKOPING	intact	6.00	39	1.27	90.0	45.0	45.0	336		249	207	152
NORRKOPING	intact	12.00	20	1.51	185.0	80.0	105.0	470		387	318	276
NORTH SEA	intact	4.00	25	1.00	72.0	33.0	39.0	200		180		
NORTH SEA	intact	20.00	25	1.00	360.0	164.0	196.0	930		780		
NORTH SEA GA	intact	11.00	27	5.20	217.0	110.0	107.0	3727	2000			
NORTH SEA GA	intact	26.50	27	3.10	520.0	265.0	255.0	2545	1909			
NORTH SEA GA	intact	31.00	27	3.10	614.0	310.0	304.0	3818	2272			
NORTH SEA GC	intact	3.40	22	2.50	68.0	34.0	34.0	295		223	175	150
NORTH SEA GC	intact	5.70	22	2.18	114.0	57.0	57.0	444		377	265	203
NORTH SEA GC	intact	7.40	22	2.55	148.0	74.0	74.0	544		433	318	266
NORTH SEA S	intact	44.14		1.00	794.0	353.0	441.0	2476		1566	1335	817
NORTH SEA S	intact	51.20		1.40	922.0	410.0	512.0	2502		1877	1427	202
NORTH SEA T	fissured	10.40	35	4.80	209.0	107.0	102.0	1369		973	281	252
NORTH SEA T	fissured	15.80	35	5.10	316.0	161.0	155.0	2497		1616	696	99
NRCC	leda	5.00	35	5.23	80.0	41.0	39.0	873			476	290
NRCC	leda	10.00	35	2.84	160.0	72.0	88.0	827			526	386
NRCC	leda	13.00	35	2.26	208.0	90.0	118.0	993			614	425
ONSOY	intact	7.50	30	1.07	121.0	47.0	74.0	330	283	311	205	
ONSOY	intact	14.90	40	1.06	238.0	92.0	146.0	734	530	602	470	
ONSOY 2	intact	1.00	30	14.00	16.0	6.2	9.8	200		92	55	
ONSOY 2	intact	2.00	30	4.40	32.0	12.4	19.6	226		150	92	
ONSOY 2	intact	4.94	30	1.39	78.0	29.5	48.5	292		224	145	
ONSOY 2	intact	10.42	30	1.33	164.4	62.2	102.2	463		400	284	
ONSOY 2	intact	25.00	40	1.20	404.0	164.0	240.0	1020		950	730	
ORINOCO E1	intact	8.56	50	1.23	402.0	57.0	345.0	602	498			
ORINOCO E1	intact	22.86	50	1.02	654.0	166.0	488.0	1223	925			
ORINOCO E1	intact	34.17	50	1.07	843.0	229.0	614.0	1626	1301			
ORINOCO E1	intact	44.19	50	1.15	995.0	288.0	707.0	1983	1536			
ORINOCO F1	intact	11.00	50	1.80	198.0	88.0	110.0	373	303			
ORINOCO F1	intact	17.44	50	1.18	535.0	105.0	430.0	1100	805			
ORINOCO F1	intact	29.39	50	1.37	731.0	178.0	553.0	1461	1058			
ORINOCO F1	intact	38.96	50	1.17	889.0	236.0	653.0	1752	1306			
OTTAWA STP	leda	6.77	38	4.07	114.0	77.0	37.0	1276			821	
OTTAWA STP	leda	12.02	30	3.29	212.5	124.0	88.5	1660			1083	
OTTAWA STP	leda	16.63	10	3.17	297.7	164.0	133.7	1843			1205	
PISA	intact	4.14	14	4.77	73.7	52.7	21.0	744			170	
PISA	intact	9.36	42	2.12	166.6	94.4	72.2	1381			260	
PISA	intact	20.04	26	1.87	356.8	179.8	177.0	1641			615	
PISA	intact	23.22	33	1.99	413.3	205.1	208.1	2480			500	
PISA	intact	29.52	33	1.21	525.4	255.5	270.0	2115			1023	
PISA	intact	34.89	33	1.89	621.0	298.4	322.6	2819			958	
PLANCOET	intact	2.60		4.41	43.3	22.7	20.6	600		50		
PLANCOET	intact	7.50		1.42	125.0	56.3	68.9	2200		55		
PONTIDA	intact	6.00		4.50	114.0	66.9	47.1	962	800		400	325
PONTIDA	intact	7.50		3.60	142.5	80.7	61.8	705	500		420	330
PONTIDA	intact	13.50		2.95	256.5	135.8	120.7	859	700		550	470
PONTIDA	intact	20.50		2.95	389.5	200.2	189.3	2018	1900		1600	1200
PORT HURON	intact	3.40	12	3.80	33.0	28.0	5.0	890		24	-3	
PORT HURON	intact	8.84	12	2.56	170.0	112.7	57.3	1077		838	278	
PORT HURON	intact	14.94	12	2.15	287.2	170.1	117.1	1188		650	444	
PORT HURON	intact	22.56	20	2.40	433.8	241.9	191.8	1779		1243	754	
PORT HURON	intact	27.43	20	2.27	527.5	287.9	239.7	2365		1474	846	
PORTO TOLLE	intact	12.50	31	2.39	231.2	118.4	112.8	672	290		227	
PORTO TOLLE	intact	18.91	31	1.23	349.9	174.2	175.7	1218	559		412	
PORTO TOLLE	intact	23.07	31	1.47	426.7	210.3	216.5	1163	613		515	
PORTO TOLLE	intact	26.48	31	1.26	490.0	240.0	250.0	1387	764		560	
PRINCE GEORGE COUN	silt	3.40	58	1.95	63.0	59.0	4.0	700			-4	
PRINCE GEORGE COUN	silt	4.95	53	2.50	91.5	72.0	19.5	700			19	
PRINCE GEORGE COUN	silt	9.50	12	1.58	176.0	111.0	65.0	700			107	
RIO DE JANEIRO	intact	1.00	85	5.76	13.2	3.4	9.8	134		60	41	15
RIO DE JANEIRO	intact	5.00	60	1.74	65.8	16.8	49.0	176		139	116	80

Piezocone Site -	SOIL TYPE	DEPTH (m)	PI (%)	OED. OCR	Svo (kN/m2)	Svo' (kN/m2)	uo (kN/m2)	qT (kN/m2)	u1t (kN/m2)	u1f (kN/m2)	u2 (kN/m2)	u3 (kN/m2)
RIO DE JANEIRO	intact	8.00	60	1.60	106.0	26.0	80.0	283		202	178	150
RIO DE JANEIRO 2	intact	0.43	85	12.67	5.7	1.4	4.2	140		48	9	
RIO DE JANEIRO 2	intact	2.50	85	2.43	32.9	8.4	24.6	129		89	68	
RIO DE JANEIRO 2	intact	5.14	60	1.84	67.6	17.2	50.4	199		136	124	
RIO DE JANEIRO 2	intact	8.13	60	1.85	106.9	27.2	79.8	273		205	169	
SANTA MARIA	intact	24.38	19	5.50	465.0	222.0	243.0	3113		2040		
SANTA MARIA	intact	30.48	19	4.60	582.0	278.0	304.0	2864		2300		
SANTA MARIA	intact	58.82	19	2.90	1118.0	530.0	588.0	5604		3880		
SANTA MARIA	intact	101.49	19	2.10	1930.0	920.0	1010.0	8219		6710		
SARO RD 6/900	intact	2.00	100	1.49	30.0	20.0	10.0	247		108	55	45
SARO RD 6/900	intact	3.00	90	1.20	40.0	20.0	20.0	253		121	81	55
SARO RD 6/900	intact	6.00	102	1.18	77.0	27.0	50.0	390		200	138	105
SARO RD 6/900	intact	7.00	105	1.16	90.0	30.0	60.0	410		233	180	120
SARO RD 7/600	intact	2.00	100	1.63	31.0	21.0	10.0	237		138	82	49
SARO RD 7/600	intact	4.00	80	1.25	54.0	24.0	30.0	300		177	120	80
SARO RD 7/600	intact	5.00	75	1.22	66.0	26.0	40.0	335		205	145	85
SARO RD 7/600	intact	6.00	90	1.16	78.0	28.0	50.0	355		224	164	113
SEA ISLAND	intact	16.00	15	1.00	300.0	160.0	140.0	973		801	501	352
SEA ISLAND	intact	19.00	15	1.00	357.0	187.0	170.0	956		762	596	450
SINGAPORE	intact	20.00	40	2.05	306.0	131.0	175.0	969			562	
SINGAPORE	intact	30.00	40	1.75	506.0	231.0	275.0	1276			812	
SKA-EDEBY	intact	2.00	55	2.60	25.0	15.0	10.0	201		135	108	65
SKA-EDEBY	intact	8.00	30	1.19	119.0	49.0	70.0	363		271	241	174
SKA-EDEBY	intact	11.00	30	1.30	168.0	68.0	100.0	520		396	352	265
SLEIPNER 2	intact	20.00	28	3.00	400.0	200.0	200.0	2105		1114		
SLEIPNER 2	intact	35.00	28	1.50	700.0	350.0	350.0	1486		1238		
SLEIPNER 4	intact	35.00	32	2.00	700.0	350.0	350.0	2057		1542		
SLEIPNER 4	intact	40.00	32	2.00	800.0	400.0	400.0	2514		1828		
SOUTH AFRICA	intact	6.00	25	1.24	87.0	37.0	50.0	309		204	128	
SOUTH AFRICA	intact	8.00	25	1.24	120.0	50.0	70.0	405		261	214	
ST. ALBAN	leda	1.54	28	2.85	22.9	14.6	8.3	190	105	105	88	
ST. ALBAN	leda	1.71	28	2.69	25.3	15.4	9.9	182	105	105	87	
ST. ALBAN	leda	3.25	20	2.12	48.0	23.1	25.0	276	131	131	121	
ST. ALBAN	leda	4.11	18	2.13	60.8	27.4	33.4	321	165	165	155	
ST. ALBAN	leda	6.22	20	2.12	92.1	37.9	54.2	406	270	250	229	
ST. ALBAN	leda	7.51	20	2.51	111.1	44.3	66.8	512	335	315	302	
ST. HILAIRE	leda	2.50	42	5.52	43.0	19.0	24.0	232			145	
ST. HILAIRE	leda	8.98	42	1.46	151.1	63.0	88.1	452			336	
ST. HILAIRE	leda	16.64	35	1.19	279.2	116.0	163.2	791			586	
ST. HILAIRE	leda	19.64	35	1.07	329.7	137.0	192.7	982			712	
ST. JEAN VIANNEY	leda	2.00	8	37.00	36.0	16.0	20.0	2490			1439	
ST. JEAN VIANNEY	leda	3.00	8	34.00	54.0	24.0	30.0	2470			1660	
ST. JEAN VIANNEY	leda	4.00	8	27.00	72.0	32.0	40.0	3120			1590	
ST. JEAN VIANNEY	leda	4.50	8	26.60	81.0	36.0	45.0	3226			1954	
ST. MARCEL	leda	4.00	35	1.86	66.0	31.0	35.0	306			161	
ST. MARCEL	leda	8.00	35	1.44	131.0	58.0	73.0	425			269	
ST. MARCEL	leda	12.00	35	1.20	197.0	84.0	113.0	645			430	
STJORDAL	silt	10.00		1.43	190.0	105.0	85.0	888	394		222	
STJORDAL	silt	20.00		1.19	380.0	210.0	170.0	1259	548		342	
STRONG PIT	intact	1.50	15	14.00	26.0	26.0	0.0	2130		1500	750	320
STRONG PIT	intact	2.00	15	10.20	36.0	36.0	0.0	1410		1450	800	450
STRONG PIT	intact	3.55	15	7.50	67.0	67.0	0.0	2173		2180	1120	500
STRONG PIT	intact	6.30	15	3.90	122.0	122.0	0.0	2170		1700	1200	500
SURREY	fissured	8.00	45	12.80	160.0	111.0	49.0	2880		1370		
SURREY	fissured	10.00	45	11.00	199.0	131.0	68.0	3030		1570		
SURREY	fissured	14.00	45	8.60	280.0	172.0	108.0	2917		1230		
SURREY	fissured	18.00	45	7.15	360.0	213.0	147.0	3920		2120		
SURRY (MIOCENE)	intact	26.80	37	2.82	473.3	284.0	189.3	2628			1503	
SURRY (MIOCENE)	intact	32.06	37	3.69	570.9	330.0	240.9	3393			1897	
SURRY (MIOCENE)	intact	39.75	37	2.83	713.4	397.0	316.4	3198			1825	
SURRY (PLEISTOCENE)	intact	15.32	25	2.71	287.0	209.0	78.0	1352			750	
SURRY (PLEISTOCENE)	intact	22.75	25	3.00	395.0	258.0	137.0	1778			1080	
TARANTO	fissured	8.00	27	38.00	160.0	91.3	68.7	157	200		72	20
TARANTO	fissured	10.00	27	35.00	239.0	150.7	88.3	4560	1720		880	846
TARANTO	fissured	15.00	27	26.00	301.0	163.0	138.0	5090	2640		1780	1107
TARANTO	fissured	17.90	27	24.90	358.0	192.2	165.8	5575	2765		2074	1320
TARSIUT	fissured	3.00	25	8.08	60.0	30.0	30.0	930			170	
TARSIUT	fissured	12.00	25	5.25	240.0	120.0	120.0	2558			390	
TARSIUT	fissured	27.00	25	2.02	540.0	270.0	270.0	2441			878	

Piezocone Site -	SOIL TYPE	DEPTH (m)	PI (%)	OED. OCR	Svo (kN/m2)	Svo' (kN/m2)	uo (kN/m2)	qT (kN/m2)	u1t (kN/m2)	u1f (kN/m2)	u2 (kN/m2)	u3 (kN/m2)
TILLER	intact	2.50	5	7.60	50.0	45.0	5.0	628			90	
TILLER	intact	6.50	5	3.30	126.0	81.0	45.0	524			158	
TILLER	intact	16.50	5	2.62	316.0	171.0	145.0	1246			928	
TOKYO	intact	3.00		3.08	51.0	51.0	0.0	401			189	
TOKYO	intact	7.00		1.88	119.0	99.0	20.0	563			218	
TOKYO	intact	15.00		1.50	255.0	155.0	100.0	921			434	
TONGJI	intact	17.00		1.50	298.0	140.0	158.0	873			461	
TONGJI	intact	18.00		1.50	320.0	152.0	168.0	861			466	
TONGJI	intact	19.00		1.50	333.0	155.0	178.0	1002			544	
TROLL 2	intact	5.00	37	1.60	109.0	29.0	80.0	217		145		
TROLL 2	intact	20.00	20	1.60	474.0	136.0	338.0	1506		1100		
TROLL 2	intact	30.00	19	1.63	516.0	216.0	300.0	1698		1183		
TROLL EAST, AREA 2	intact	8.00	15	1.50	127.3	48.8	78.5	347	309	329	239	
TROLL EAST, AREA 2	intact	13.00	15	1.40	206.7	79.1	127.5	552	456	493	417	
TROLL EAST, AREA 2	intact	20.00	14	1.30	323.0	126.8	196.2	884	781	875	587	
TUVE	intact	5.00	50	1.68	62.0	14.0	48.0	229		198	136	97
TUVE	intact	10.00	58	1.83	128.0	30.0	98.0	474		396	312	229
TUVE	intact	15.00	50	1.63	197.0	49.0	148.0	599		546	432	339
TUVE	intact	20.00	40	1.50	272.0	74.0	198.0	784		681	577	452
UPPER 232nd ST.	intact	8.00	19	1.00	144.0	94.0	50.0	254			194	
VALEN	intact	3.05	70	1.24	37.5	15.0	22.5	268		131	114	99
VALEN	intact	5.24	65	1.24	68.4	24.0	44.4	319		189	154	142
VALEN	intact	7.00	60	1.30	96.0	34.0	62.0	304		245	189	171
VALOYA	intact	5.50	15	5.70	114.0	89.0	25.0	1300		770	400	
VALOYA	intact	10.50	20	8.00	207.0	132.0	75.0	1558		1075	689	
VALOYA	intact	17.50	14	5.67	341.0	196.0	145.0	1643		1350	943	
VALOYA	intact	19.50	10	2.64	380.0	215.0	165.0	1679		1371	1007	
VANCOUVER	intact	18.00	9	1.60	348.0	178.0	170.0	960		693	522	
VANCOUVER	intact	23.00	16	1.50	441.0	221.0	220.0	1150		900	675	
VARENNES	leda	3.50	40	6.00	48.0	28.0	25.0	692			444	
VARENNES	leda	5.50	40	4.84	89.0	44.0	45.0	760			534	
VARENNES	leda	11.60	40	2.59	188.0	82.0	106.0	1011			693	
VARENNES	leda	14.50	40	2.29	235.0	100.0	135.0	1110			788	
YERBA BUENA COVE	intact	11.03	37	1.30	176.0	94.0	82.0	756			429	
YORKTOWN	intact	7.60	4	9.90	140.0	86.0	54.0	2383			1182	
YORKTOWN	intact	13.70	4	6.60	247.0	133.0	114.0	2431			1518	
YORKTOWN	intact	16.80	4	5.60	302.0	158.0	144.0	2581			1897	

APPENDIX D - REFERENCES

Aas, G., Lacasse, S., Lunne, T., and Hoeg, K. 1986. Use of In-Situ Tests for Foundation Design on Clay. Use of In-Situ Tests in Geotechnical Engineering (GSP 6), American Society of Civil Engineers, New York, 1-30.

Acar, Y.B. and Tumay, M.T. 1986. Strain Field Around Cones in Steady Penetration. Journal of Geotechnical Engineering, ASCE, Vol. 112, No. 2, 207-213.

Almeida, M. and Parry, R.H.G. 1985. Small Cone Penetrometer/and Piezocone Tests in Laboratory Consolidated Clay. Geotechnical Testing Journal, Vol. 8, No. 1, 14-24.

Amar, S., Corte, J.F., and Waschkowski, E. 1989. Some Applications of Piezocone Testing. Proceedings, 12th International Conference on Soil Mechanics and Foundation Engineering, Rio de Janeiro, Brazil, Vol. 2, 151-152.

Arman, A. and McManis, K.L. 1977. The Effect of Conventional Soil Sampling Methods on the Engineering Properties of Cohesive Soils in Louisiana. Engineering Research Bulletin No. 117, Louisiana State University, Baton Rouge, Louisiana, 294 p.

Azzouz, A., Baligh, M.M. and Ladd, C.C. 1983. Cone Penetration and Engineering Properties of Soft Orinoco Clay. Proceedings, 3rd International Conference on Behavior of Offshore Structures, Cambridge, Massachusetts, Vol. 1, 161-180.

Azzouz, A. and Lutz, D. 1986. Shaft Behavior of Pile in Plastic Empire Clay. Journal of Geotechnical Engineering, ASCE, Vol. 112, No. 4, 389-406.

Baker, P.J. and Gardener, R. 1988. Penetration Testing in Glacial Till. Penetration Testing in the U.K., Thomas Telford, London, 223-226.

Baligh, M.M. 1975. Theory of Deep Site Static Cone Penetration Resistance. Research Report No. R75-56, Department of Civil Engineering, Massachusetts Institute of Technology, Cambridge, Massachusetts, 133 p.

Baligh, M.M. 1984. The Simple-Pile Approach to Pile Installation in Clay. Analysis and Design of Pile Foundations, ASCE, New York, 310-330.

Baligh, M.M. 1985. Strain Path Method. Journal of Geotechnical Engineering, ASCE, Vol. 111, No. 9, 1108-1136.

Baligh, M.M. 1986b. Undrained Deep Penetration, II: Pore Pressures. Geotechnique, Vol. 36, No. 4, 486-501.

Baligh, M.M. 1986a. Undrained Deep Penetration, I: Shear Stresses. Geotechnique, Vol. 36, No. 4, 471-485.

Baligh, M.M., Azzouz, A., Wissa, A., Martin, R., and Morrison, M. 1981. The Piezocone Penetrometer. Cone Penetration Testing and Experience, American Society of Civil Engineers, New York, 247-263.

Baligh, M.M. and Levadoux, J.N. 1986. Consolidation After Undrained Piezocone Penetration, II: Interpretation. Journal of Geotechnical Engineering, Vol. 112 (7), 727-745.

Baligh, M.M., Vivatrat, V., and Ladd, C.C. 1980. Cone Penetration in Soil Profiling. Journal of the Geotechnical Engineering, ASCE, Vol. 106, No. 4, 447-461.

Battaglio, M., Bruzzi, D., Jamiolkowski, M., and Lancellotta, R. 1986. Interpretation of CPT's and CPTU's. Proceedings, Fourth International Geotechnical Seminar: Field Instrumentation and In-Situ Measurements, Singapore, 129-143.

Battaglio, M., Jamiolkowski, M., Lancellotta, R., and Maniscalso, R. 1981. Piezometer Probe Test in Cohesive Deposits. Cone Penetration Testing and Experience, American Society of Civil Engineers, New York, 264-302.

Bayne, J.M. and Tjelta, T.I. 1987. Advanced Cone Penetrometer Development for In-Situ Testing at Gullfaks C. Proceedings, 19th Offshore Tech. Conf., Houston, Vol. 4, 531-540.

Becker, D.E., Crooks, J.H.A., Been, K., and Jefferies, M.G. 1987. Work as a Criterion for Determining In-Situ and Yield Stresses in Clays. Canadian Geotechnical Journal, Vol. 24 (4), 549-564.

Belfiore, F., Colombo, P.F., Pezzetti, G., and Villani, B. 1989. A Contribution to the Study of Subsidence of Bologna. Proceedings, 12th International Conference on Soil Mechanics and Foundation Engineering, Rio de Janeiro, Brazil, Vol. 3, 1791-1795.

Bensaid, M.A. 1985. Mesures In-Situ Des Pressions Interstitielles - Application à la Reconnaissance Des Sols. Ph.D. Thesis, Ecole Nationale Des Ponts et Chaussées, Paris, 371 p. (in French)

Bergenstahl, L. 1991. Preloading of an Embankment on Deep Soft Clay. Proceedings, 10th European Conf. on Soil Mechanics and Foundation Engrg., Firenze, Vol. 2, 307-310.

Bishop, A.W. and Henkel, D.J. 1957. The Measurement of Soil Properties in the Triaxial Test, Edward Arnold, Ltd., London, 225 p.

Bjerrum, L. 1972. Embankments on Soft Ground. Performance of Earth and Earth-Supported Structures. ASCE Conference, Purdue University, Vol. 2, 1-54.

Boudali, M., Leroueil, S., and Srinivasa, B.R. 1994. Viscous Behavior of Natural Clays. 13th Intl. Conf. on Soil Mechanics and Foundation Engrg., New Delhi, Vol. 1, 411-416.

Briaud, J-L and Miran, J. 1992. The Cone Penetration Test. Report FHWA-SA-91-043, Federal Highway Admintration, Washington, D. C., 161 p.

Broms, B.B. and Flodin, N. 1988. History of Soil Penetration Testing. Penetration Testing 1988 (Proc. ISOPT-1), Balkema, Rotterdam, Vol. 1, 157- 220.

Brown, D.N. 1993. Determination of Stress State of Clays by Piezocone. MS Thesis, School of Civil Engineering, Georgia Institute of Technology, Atlanta, GA, 168 p.

Brown, D.N. and Mayne, P.W. 1993. Stress History Profiling of Marine Clays by Piezocone. Proceedings, 4th Canadian Conference on Marine Geotechnical Engineering, St. John's, Newfoundland, Vol. 1, 176-191.

Burland, J.B. 1965. The Yielding and Dilation of Clay. Geotechnique, Vol. 15, No. 1, 211-214.

Burland, J.B. 1969. Deformation of Soft Clay Beneath Loaded Area. Proceedings, 7th Intl. Conference on Soil Mechanics and Foundation Engineering (1), Mexico City, 55-63.

Butterfield, R. 1979. A Natural Compression Law for Soils (An advance on e-log p'). Geotechnique. Vol. 29, No. 4, 468-480.

Campanella, R.G., Gillespie, D., and Robertson. P.K. 1982. Pore Pressures During Cone Penetration. Proceedings, 2nd European Symposium on Penetration Testing, Amsterdam, Vol. 2, 507-512.

Campanella, R.G. and Kokan, M.J. 1993. A New Approach to Measuring Dilatancy in Saturated Sands. Geotechnical Testing Journal, ASTM, Vol. 16, No. 4, 485-495.

Campanella, R.G. and Robertson, P.K. 1981. Applied Cone Research. Cone Penetration Testing and Experience. American Society of Civil Engineers, New York, 343-362.

Campanella, R.G., Robertson, P.K., and Gillespie, D. 1986a. Factors Affecting the Pore Water Pressure and Its Measurement Around a Penetrating Cone. Proceedings, 39th Canadian Geotechnical Conference, Ottawa, 291-299.

Campanella, R.G., Robertson, P.K., Gillespie, D., Liang, N., and Kurfurst, P.J. 1986b. Seismic Cone Penetration Testing in the Beaufort Sea. Proceedings, 3rd Canadian Conference on Marine Geotechnical Engineering, St. John's, Newfoundland, 253-271.

Campanella, R.G. and Robertson, P.K. 1988. Current Status of the Piezocone Test. Penetration Testing 1988 (ISOPT-1), Balkema, Rotterdam, Vol. 1, 93-116.

Campanella, R.G. and Robertson, P.K. 1991. Use and Interpretation of a Research Dilatometer. Canadian Geotechnical Journal, Vol. 28, No. 1, 113-126.

Campanella, R.G., Sully, J.P., and Robertson, P.K. 1988. Interpretation of Piezocone Soundings in Clay. Penetration Testing in the UK, Thomas Telford, London, 203-208.

Campanella, R.G. and Weemes, I. 1990. Development and Use of an Electrical Resistivity Cone for Groundwater Contamination Studies. Canadian Geotechnical Journal, Vol. 27, No. 4, 557-567.

Canou J. and Tumay, M.T. 1986. Field Evaluation of French Self-Boring Pressuremeter PAF 76 in A Soft Deltaic Louisiana Clay. Pressuremeter and Its Marine Applications (STP 950), American Society for Testing Materials, Philadelphia, 97-118.

Casagrande, A. 1936. The Determination of the Preconsolidation Load and Its Practical Significance. Proceedings, 1st International Conference on Soil Mechanics and Foundation Engineering, Cambridge, U.K., Vol. 3, 60-64.

Chameau, J.L., Reyna, F., and Frost, J.D. 1991. Ground Motion Analyses at Several Sites in San Francisco After the Loma Prieta Earthquake. Geotechnical Report 91/9, Purdue University, West Lafayette, 285 p.

Chandler, R.J. 1988. The In-Situ Measurement of the Undrained Shear Strength of Clays Using the Field Vane. Vane Shear Strength Testing in Soils (STP 1014), American Society for Testing Materials, Philadelphia, 13-44.

Chang, M.F. 1991. Interpretation of OCR from In-Situ Tests in Recent Clay Deposits in Singapore and Malaysia. Canadian Geotechnical Journal, Vol. 28 (2), 210-225.

Chen, B.S.Y. 1994. Profiling Stress History of Clays Using Piezocones With Dual Pore Pressure Measurements. PhD Thesis, School of Civil & Environmental Engineering, Georgia Institute of Technology, Atlanta, Georgia, 350 p.

Chen, B.S.Y. and Mayne, P.W. 1993. Piezocone Evaluation of Undrained Shear Strength in Clays. Proceedings, 11th Southeast Asian Geotechnical Conference, Singapore, 91-98.

Chen-Hou, Z., Greeuw, G., Jekel, J., and Rosenbrand, W. 1990. A New Classification Chart for Soft Soils Using the Piezocone Test. Engineering Geology, Vol. 29 (1), 31-47.

Chern, J.C. 1992. Geotechnical Investigation of the Keelung River Site. Draft Internal Report, Sinotech Engineering Consultants, Inc., Taiwan.

Chin, C.T., Crooks, J.H.A., Enriquez, A.S., and Hu, I.C. 1993. Interpretation of Piezocone Data After partially Drained Penetration. Proceedings, 11th Southeast Asian Geotechnical Conference, Singapore, 99-103.

Christopher, H.P. and Lacasse, S. 1984. Laboratory Tests on Haga Clay. Internal Report No. 40019-8, Norwegian Geotechnical Institute, Oslo, Norway, 51 p.

Crawford, C.B. and Campanella, R.G. 1991. Comparison of Field Consolidation with Laboratory and In-Situ Tests. Canadian Geotechnical Journal, Vol. 28 (1), 103-112.

Crooks, J.H.A., Been, K., Becker, D.E., and Jefferies, M.G. 1988. CPT Interpretation in Clays. Penetration Testing 1988 (ISOPT-1), Balkema, Rotterdam, Vol. 2, 715-722.

Davidson, J.L. 1988. Pore Pressures Generated During Cone Penetration Testing in Heavily Overconsolidated Clays. Proceedings, 11th International Conference on Soil Mechanics and Foundation Engineering (4), San Francisco, 2699.

DeBeer, E.E., Goelen, E., Heynen, W.J., and Joustra, K. 1988. Cone Penetration Testing: International Reference Test Procedures. Penetration Testing 1988 (ISOPT-1), Balkema, Rotterdam, Vol. 1, 27-51.

DeGroot, D.J., Ladd, C.C., and Germaine, J.T. 1992. Direct Simple Shear Testing of Cohesive Soils. Report No. R92-18, Mass. Inst. of Tech., Cambridge, 153 p.

DeRuiter, J. 1982. The Static Cone Penetration Test - State of the Art Report. Proc. 2nd European Symposium on Penetration Testing, Amsterdam, Vol. 1, 389-405.

Díaz-Rodríguez, J.A., Leroueil, S., and Alemán, J.D. 1992. Yielding of Mexico City Clay and Other Natural Clays. Journal of Geotechnical Engineering, Vol. 118, No. 7, 981-995.

Du, J., Zhu, X., Zhu, L., and Zhang, L. 1992. Some In-Situ and Laboratory Geotechnical Test Techniques Used in China. National Science Foundation Workshop: United States - China Cooperation in Geotechnical Engineering, Tongji University, Shanghai, China, 7 p.

East, D.R., Cincilla, W.A., Hughes, J.M.O., and Benoit, J. 1988. The Use of the Electric Piezocone for Mine Tailings Deposits. Penetration Testing 1988 (ISOPT-1), Balkema, Rotterdam, Vol. 2, 745-750.

East, D.R. and Ulrich, B.F. 1989. The Electric Piezocone for Profiling of Mine Tailings Deposits. Engineering Geology and Geotechnical Engineering, Balkema, Rotterdam, 35-38.

Elsworth, D. 1991. Dislocation Analysis of Penetration in Saturated Porous Media. Journal of Engineering Mechanics, ASCE, Vol. 117, No. 2, 391-408.

Elsworth, D. 1993. Analysis of Piezocone Dissipation Data Using Dislocation Methods. Journal of Geotechnical Engineering, ASCE, Vol. 119, No. 10, 1601-1623.

Finno, R.J. 1989. Subsurface Conditions and Pile Installation Data. Predicted and Observed Axial Behavior of Piles (GSP 23), ASCE, New York, N.Y., 1-74.

Franz, R.J. and Hull, J.A. 1993. Report of Geotechnical Exploration, Bowie, MD. Draft Report, Golder Associates, Mount Laurel, New Jersey.

Gillespie, D. and Campanella, R.G. 1981. Consolidation Characteristics from Pore Pressure Dissipation After Cone Penetration. Soil Mechanics Series No. 47, The University of British Columbia, Vancouver, B.C., 17 p.

Gillespie, D., Lunne, T., and Eidsmoen, T. 1984. In-Situ Site Investigation Techniques and Interpretation for Offshore Practice: Cone Penetration Tests at Haga. Report No. 40019-16, Norwegian Geotechnical Institute, Oslo, Norway, 90 p.

Gillespie, D., Lunne, T., and Eidsmoen, T. 1985. In-Situ Site Investigation Techniques and Interpretation for Offshore Practice; Cone Penetration Tests in Onsoy Clay. Report No. 40019-7, Norwegian Geotechnical Institute, Oslo, Norway, 92 p.

Graham, J., Crooks, J.H.A., and Bell, A.L. 1983. Time Effects on the Stress-Strain Behavior of Natural Soft Clays. Geotechnique, Vol. 33, No. 3, 327-340.

Greig, J.W., Campanella, R.G. and Robertson, P.K. 1988. Comparison of Field Vane Results with Other In-Situ Test Results. Vane Shear Strength Testing in Soils: Field and Laboratory Studies (STP 1014), ASTM, Philadelphia, 247-263.

Gupta, R.C. 1983. Determination of the In-Situ Coefficients of Consolidation and Permeability of Submerged Soils Using Electrical Piezoprobe Soundings. Ph.D. Thesis, University of Florida, Gainseville, 303 p.

Hawkins, A.B., Larnach, W.J., Lloyd, I.M., and Nash, D.F.T. 1989. Selecting the Location, and the Initial Investigation of the SERC Soft Clay Test Bed Site. Quarterly Journal of Engineering Geology, Vol. 22, No. 2, 281-316.

Hight, D.W., Bond, A.J., and Legge, J.D. 1992. Characterization of the Bothkennar Clay: An Overview. Geotechnique, Vol. 42, No. 2, 303-347.

Holtz, R.D., Jamiolkowski, M., and Lancellotta, R. 1986. Lessons From Oedometer Tests on High Quality Samples. Journal of Geotechnical Engineering 112 (8), 768-776.

Houlihan, M.F. and Blodgett, A.E. 1989. Landfill Geotechnical Evaluation - Charles City County Landfill. Draft Report No. P1123, Geosyntec Consultants, Inc., Atlanta, Georgia.

Houlsby, G.T. and Teh, C.I. 1988. Analysis of the Piezocone in Clay. Penetration Testing 1988 (ISOPT-1), Balkema, Rotterdam, Vol. 2, 777-783.

Houlsby, G.T. and Wroth, C.P. 1989. The Influence of Soil Stiffness and Lateral Stress on the Results of In-Situ Soil Tests. Proceedings, 12th International Conference on Soil Mechanics and Foundation Engineering, Rio de Janeiro, Brazil, Vol. 1, 227-232.

Houlsby, G.T. 1988. Piezocone Penetration Tests. Penetration Testing in the UK, Thomas Telford, London, 141-146.

Hughes, J.M.O., Jefferies, M.G., and Morris, D.L. 1984. Self Bored Pressuremeter Testing in the Arctic Offshore. Proceedings, 16th Offshore Technology Conference, Houston, Vol. 1, 255-264.

Huntsman, S.R., Mitchell, J.K., Klejbuk, L.W., and Shinde, S.B. 1986. Lateral Stress Measurement During Cone Penetration. Use of In-Situ Tests in Geotechnical Engineering, American Society of Civil Engineers, New York, 617-634.

ICSMFE. 1977. Subcommittee on Standardization for Europe - Report on the Penetration Test for Use in Europe. Proceedings, 9th International Conference on Soil Mechanics and Foundation Engineering, Tokyo, Vol. 3, 95-152.

Jacob, P.A. and Coutts, J.S. 1992. A Comparison of Electric Piezocone Tips at the Bothkennar Test Site. Geotechnique, Vol. 42, No. 2, 369-375.

Jaky, J. 1944. The Coefficient of Earth Pressures at Rest. Journal of the Society of Hungarian Architects and Engineers, Budapest, 355-358.

Jamiolkowski, M., Lancellotta, R., Tordella, L., and Battaglio, M. 1982. Undrained Strength from CPT. Proceedings, 2nd European Symposium of Penetration Testing, Amsterdam, Vol. 2, 24-27.

Jamiolkowski, M., Ladd, C.C., Germaine, J. and Lancellotta, R. 1985. New Developments in Field and Lab Testing of Soils. Proceedings, 11th International Conference on Soil Mechanics and Foundations Engineering, Vol. 1, San Francisco, 57-154.

Jamiolkowski, M., Ghionna, V.N., Lancellota, R., and Pasqualini, E. 1988a. New Correlations of Penetration Tests for Design Practice. Penetration Testing 1988 (ISOPT-1), Vol. 2, Balkema, Rotterdam, 263-296.

Jamiolkowski, M., Battaglio, M., and Bruzzi, D. 1988b. Discussion: Penetration Testing in the UK, Thomas Telford, London, 180-183.

Jamiolkowski, M., Lancellotta, R., and Pepe, C. 1993. Leaning Tower of Pisa - Updated Information. Proceedings, 3rd International Conference on Case Histories in Geotechnical Engineering, Vol. 2, St. Louis, 1319-1330.

Jamiolkowski, M., Leroueil, S., and LoPresti, D. 1991. Design Parameters From Theory to Practice. Proceedings, GeoCoast '91, Volume 2, Yokohama, Port and Harbor Research Institute, 877-917.

Jamiolkowski, M. and Marchetti, S. 1969. The Determination of Preconsolidation Load from a Controlled Gradient Consolidometer Device. Proceedings, 7th International Conference on Soil Mechanics and Foundations Engineering, Mexico City, Vol. 3, 523-524.

Janbu, N. 1969. The Resistance Concept Applied to Deformations of Soils. Proceedings, 7th International Conference on Soil Mechanics and Foundations Engineering, Mexico City, Vol. 1, 191-196.

Janbu, N. and Senneset, K. 1974. Effective Stress Interpretation of In-Situ Static Penetration Tests. Proceedings, 1st European Symposium on Penetration Testing, Stockholm, Vol. 2.2, 181-193.

Jefferies, M.G. and Funegard, E. 1983. Cone Penetration Testing in the Beaufort Sea. Proceedings, Geotechnical Practice in Offshore Engineering, ASCE, New York, 220-243.

Jefferies, M.G., Crooks, J.H.A., Becker, D.E., and Hill, P.R. 1987 Independence of Geostatic Stress from Overconsolidation in Some Beaufort Sea Clays. Canadian Geotechnical Journal, Vol. 24, No. 3, 342-356.

Jefferies, M.G., Ruffell, J.P., Crooks, J.H.A., and Hughes, J.M.O. 1987. Some Aspects of the Behavior of Beaufort Sea Clays. Strength Testing on Marine Sediments (STP 883), American Society for Testing Materials, Philadelphia, 487-514.

Jones, G.A. and Rust, E. 1982. Piezometer Penetration Testing. Proceedings, 2nd European Symposium on Penetration Testing, Amsterdam, Vol. 2, 607-613.

Jones, G.A. and Van Zyl, D.J.A. 1981. The Piezometric Probe - A Useful Investigation Tool. Proceedings, 10th International Conference on Soil Mechanics and Foundation Engineering, San Francisco, Vol. 2, 489-496.

Juran, I. and Tumay, M.T. 1989. Soil Stratification Using Dual Pore Pressure Piezocone Test. Transportation Research Record 1235, Washington, D.C., 68-78.

Juran, I. 1983. Application of the Piezocone Penetrometer to In-Situ Soil Investigations. Proceedings, International Symposium on In-Situ Testing, Paris, Vol. 2, 309-315.

Kabir, M. and Lutenegger, A.J. 1990. In-Situ Estimation of the Coefficient of Consolidation in Clays. Canadian Geotechnical Journal 27 (1), 58-67.

Keaveny, J.M. and Mitchell, J.K. 1986. Strength of Fine-grained Soils Using the Piezocone. Use of In-Situ Tests in Geot. Engrg. (GSP 6), ASCE, New York, 668-685.

Konrad, J.M. 1987. Piezo-Friction-Cone Penetrometer Testing in Soft Clays. Canadian Geotechnical Journal, Vol. 24, No. 4, 645-652.

Konrad, J.M. and Law, K.P. 1987a. Preconsolidation Pressure from Piezocone Tests in Marine Clays. Geotechnique, Vol. 37, No. 2, 177-190.

Konrad, J.M. and Law, K.T. 1987b. Undrained Shear Strength from Piezocone Tests. Canadian Geotechnical Journal, Vol. 24, No. 3, 392-405.

Koutsoftas, D. 1989. Factual Report: Site Investigation for Completion of Preliminary Design, Phase I, Muni Metro Turnaround Facility. Report No. 185-215-03, Dames & Moore, Inc., San Francisco, 3 volumes.

Koutsoftas, D. and Foott, R. 1982. Replacement Airport at Chek Lap Kok. Civil Engineering Design Studies Report. Dames & Moore, Inc., Hong Kong, 5 volumes.

Koutsoftas, D., Foott, R., and Handfelt, L.D. 1987. Geotechnical Investigations Offshore Hong Kong. Journal of Geotechnical Engineering, Vol. 113 (2), 87-105.

Kramer, S.L., Satari, R., and Kilian, A.P. 1990. Evaluation of In Situ Strength of a Peat Deposit from Laterally Loaded Pile Test Results. Transportation Research Record 1278, Transportation Research Board, Washington, D.C., 103-109.

Kulhawy, F.H., Birgisson, B., Grigoriu, M.D. 1992. Reliability-Based Foundation Design for Transmission Line Structures, Vol. 4: Transformation Models for In-Situ Tests. EPRI EL-5507, Electric Power Research Institute, Palo Alto, California, 58 p.

Kulhawy, F.H. and Mayne, P.W. 1990. Manual on Estimating Soil Properties for Foundation Design. Report EL-6800, Electric Power Research Institute, Palo Alto, 306p.

Kurfurst, P.J. and Woeller, D.J. 1988. Electric Cone Penetrometer - Development and Field Results from the Canadian Arctic. Penetration Testing 1988 (ISOPT-1), Balkema, Rotterdam, Vol. 1, 823-829.

Kurup, P.U. 1993. Calibration Chamber Studies of Miniature Piezocone Penetration Tests in Cohesive Soil Specimens. PhD Thesis, Department of Civil Engineering, Louisiana State University, Baton Rouge, Louisiana, 235 p.

Kurup, P.U., Voyiadjis, G.Z., and Tumay, M.T. 1994. Calibration Chamber Studies of Piezocone Test in Cohesive Soils. Journal of Geotechnical Engrg., Vol. 120 (1), 81-107.

Lacasse, S. and Lunne, T. 1982. Penetration Tests in Two Norwegian Clays. Proceedings, 2nd European Symposium on Penetration Testing, Amsterdam, Vol. 2, 661-669.

Ladd, C.C. and Foott, R. 1974. New Design Procedure for Stability of Soft Clays. Journal of Geotechnical Engineering, ASCE, Vol. 100, No. 7, 763-786.

Ladd, C.C., Foott, R., Ishihara, K., Schlosser, F., and Poulos, H.G. 1977. Stress Deformation and Strength Characteristics. Proceedings, 9th International Conference on Soil Mechanics and Foundation Engineering, Tokyo, Vol. 2, 421-494.

Ladd, C.C. and Edgers, L. 1972. Consolidated-Undrained Direct-Simple Shear Tests on Saturated Clays. Research Report R72-82, Mass. Inst. of Technology, Cambridge, 366 p.

Ladd, C.C. and T.W. Lambe, 1963. The Strength of Undisturbed Clay Determined from Undrained Tests. Laboratory Shear Testing of Soils (STP 740), ASTM, Phila., 342-371.

Lafleur, J., Silvestri, V., Asselin, R., and Soulie, M. 1988. Behavior of a Test Excavation in Soft Champlain Sea Clay. Canadian Geotechnical Journal, Vol. 25, No. 4, 705-715.

Lancellotta, R. and Pepe, C. 1990. Pisa Tower: Geotechnical Properties of Horizon A. Draft Preliminary Report 3234, Technical University of Torino, Italy, 55 p.

Landva, A.O., Valsangkar, A.J., Alkins, J.C., and Charalambous, P.D. 1989. Performance of a Raft Foundation Supporting a Multi-Storey Structure, Canadian Geotechnical Journal, Vol. 25, No. 1, 138-149.

LaRochelle, P., Zebdi, M., Leroueil, S., Tavenas, F., and Virely, D. 1988. Piezocone Tests in Sensitive Clays of Eastern Canada. Penetration Testing 1988 (ISOPT-1), Balkema, Rotterdam, Vol. 1, 831-841.

Larsson, R. 1980. Undrained Shear Strength in Stability Calculation of Embankments and Foundations on Soft Clays. Canadian Geotechnical Journal 17 (4), 591-602.

Larsson, R. and Mulabdić, M. 1991. Piezocone Tests in Clay. Swedish Geotechnical Institute Report No. 42, Linköping, Sweden, 240 p.

Leroueil, S. and Jamiolkowski, M. 1991. Exploration of Soft Soil and Determination of Design Parameters. Proceedings, GeoCoast '91, Volume 2, Yokohama, Port and Harbor Research Institute, 969-998.

Leroueil, S., Tavenas, F., Brucy, F., LaRochelle, P., and Roy, M. 1979. Behavior of Destructured Natural Clays. Journal of Geotechnical Engineering Division (ASCE), Vol. 105 (GT6), 759-780.

Leroueil, S., Tavenas, F., Samson, L., and Morin, P. 1983. Preconsolidation Pressure of Champlain Clays: Part II, Laboratory Determination. Canadian Geotechnical Journal, Vol. 20, No. 4, 803-816.

Levadoux, J.N. 1980. Pore Pressure in Clays due to Cone Penetration. Ph.D. Thesis, Department of Civil Engineering, Massachusetts Institute of Technology, Cambridge, Massachusetts, 753 p.

Levadoux, J.N. and Baligh, M.M. 1986. Consolidation After Undrained Piezocone Penetration I: Prediction. Journal of Geotechnical Engineering, Vol. 112 (7), 707-726.

Long, M.M. and O'Riordan, N.J. 1988. The Use of Piezocone in the Design of a Deep Basement in London. Penetration Testing in the UK, Thomas Telford, London, 173-176.

Lunne, T., Christoffersen, H.P. and Tjelta, T.I. 1985. Engineering Use of Piezocone Data in North Sea Clays. Proceedings, 11th International Conference on Soil Mechanics and Foundation Engineering, Vol. 2, San Francisco, 907-912.

Lunne, T., Eidsmoen, T., Gillespie, D., and Howland, J. 1986a. Laboratory and Field Evaluation of Cone Penetrometers. Use of In-Situ Tests in Geotechnical Engineering (GSP 6), American Society of Civil Engineers, New York, 714-729.

Lunne, T., Eidsmoen, T.E., Powell, J.J.M., and Quarterman, R.S.T. 1986b. Piezocone Testing in Overconsolidated Clays. Proceedings, 39th Canadian Geotechnical Conference, Ottawa, 209-218.

Lunne, T., Lacasse, S., and Rad, N. 1992. General Report: Discussion Session on SPT, CPT, PMT, and Recent Developments in In-Situ Testing. Proceedings, 12th International Conference on Soil Mechanics and Foundation Engineering (4), Rio de Janeiro, 2339-2403.

Lutenegger, A.J. and Kabir, M.G. 1987. Pore Pressures Generated by Two Penetrometers in Clays. Report No. 87-2, Department of Civil and Environmental Engineering, Clarkson University, Potsdam, New York, 44 p.

Lutenegger, A.J. and Kabir, M.G. 1988. Interpretation of Piezocone Results in Overconsolidated Clays. Penetration Testing in the UK, Thomas Telford, London, 43-46.

Mahar, L.J. and O'Neill, M.W. 1983. Geotechnical Characterization of Desiccated Clay. Journal of Geotechnical Engineering, ASCE, Vol. 109, No. 1, 56-71.

Marchetti, S. 1980. In Situ Test by Flat Dilatometer. Journal of Geotechnical Engineering, ASCE, Vol. 106, No. 3, 299-321.

Marsland, A. and Quarterman, R.S.T. 1982. Factors Affecting the Measurements and Interpretation of Quasi Static Penetration Tests in Clay. Proceedings, European Symposium on Penetration Testing (2), Amsterdam, Balkema Publishing, 697-702.

Martin, R.E. and Drahos, E.G. 1986. Pressuremeter Correlations for Preconsolidation Clays. Use of In-Situ Tests in Geotechnical Engineering (GSP 6), American Society of Civil Engineers, New York, 206-220.

Masood, T. and Mitchell, J.K. 1993. Estimation of In-Situ Lateral Stresses in Soils by Cone Penetration Test. Journal of Geotechnical Engineering, Vol. 119 (10), 1624-1639.

Masood, T., Mitchell, J.K., Lunne, T., and Hauge, E.A. 1988. In-Situ Testing at Hamilton Air Force Base and Bay Farm Island, California. Joint Report by University of California (Berkeley) and Norwegian Geotechnical Institute (Oslo), 15 p.

Matsumoto, T., Michi, Y., and Hirano, T. 1994. Performance of Axially Loaded Steel pipe Driven in A Soft Rock. Paper accepted April 13, Journal of Geotechnical Engineering.

Mayne, P.W. 1980. Cam Clay Predictions of Undrained Strength. Journal of Geotechnical Engineering, ASCE, Vol. 106, No. 11, 1219-1242.

Mayne, P.W. 1985. A Review of undrained Strength in Direct Simple Shear. Soils and Foundations, Vol. 25, No. 3, 64-72.

Mayne, P.W. 1986. CPT Indexing of In-situ OCR in Clays. Use of In Situ Tests in Geotechnical Engineering (GSP 6), ASCE, New York, 780-793.

Mayne, P.W. 1987. Determining Preconsolidation Stress and Penetration Pore Pressures from DMT Contact Pressures. ASTM Geotechnical Testing Journal, Vol. 10 (3), 146-150.

Mayne, P.W. 1988. Determining OCR from Laboratory Strength. Journal of Geotechnical Engineering, ASCE, Vol. 114, No. 1, 76-92.

Mayne, P.W. 1989. Preliminary Analysis of OCR Profile from Piezocone Data at Pyramid Carousel Center Site, Syracuse, N.Y.. Geotechnical Report for Stopen Engineering Partnership, Syracuse, NY., 24 p.

Mayne, P.W. 1989. Site Characterization of Yorktown Formation for New Accelerator. Foundation Engineering: Current Principles (GSP 22), ASCE, New York, Vol. 1, 1-15.

Mayne, P.W. 1991. Determination of OCR in Clays by Piezocone Tests Using Cavity Expansion and Critical State Concepts. Soil and Foundations, Vol. 31, No. 2, 65-76.

Mayne, P.W. 1992. Closure to Determination of OCR by Piezocone Tests. Soils and Foundations, Vol. 32, No. 4, 190-192.

Mayne, P.W. 1993. In-Situ Determination of Clay Stress History by Piezocone. Predictive Soil Mechanics (Proc. Wroth Memorial Symposium, Thomas Telford, London, 483-495.

Mayne, P.W. and Bachus, R.C. 1988. Profiling OCR in Clays by Piezocone. Penetration Testing 1988 (ISOPT-1), Balkema, Rotterdam, Vol. 2, 857-864.

Mayne, P.W. and Bachus, R.C. 1989. Penetration Pore Pressures from CPTU, DMT, and SBPMT. Proceedings, 12th International Conference on Soil Mechanics and Foundation Engineering, Vol. 1, Rio de Janeiro, 291-294.

Mayne, P.W. and Chen, B.S.Y. 1993. Effective Stress Method for Determining Undrained Strength Using Piezocones. Proceedings, 3rd International Conference on Case Histories in Geotechnical Engineering, ASCE, St. Louis, Vol. 2, 1305-1312.

Mayne, P.W. and Chen, B.S.Y. 1994. Preliminary Calibration of PCPT-OCR Model for Clays. Proceedings, 13th International Conference on Soil Mechanics and Foundation Engineering, New Delhi, Vol. 1, 283-286.

Mayne, P.W. and Frost, D. 1986. Geotechnical Report for WHCA Facility, Anacostia Naval Station, D.C. Report No. W6-5523, Law Engineering, McLean, Virginia, 222 p.

Mayne, P.W. and Gordon, D. 1987. Geotechnical Exploration - North Anna Radwaste Facility. Report No. W7-5768, Law Engineering, McLean, Virginia, 230 p.

Mayne, P.W. and Holtz, R.D. 1988. Profiling Stress History from Piezocone Soundings. Soils and Foundations, Vol. 28, No. 1, 16-28.

Mayne, P.W. and Kulhawy, F.H. 1990. Direct and Indirect Determination of In Situ K_o in Clays. Transportation Research Record 1278, Washington, D.C., 141-149.

Mayne, P.W. and Kulhawy, F.H. 1982. K_o-OCR Relationship in Soils. Journal of Geotechnical Engineering, ASCE, Vol. 108, No. 6, 851-872.

Mayne, P.W., Kulhawy, F.H., and Kay, J.N. 1990. Observations on the Development of Pore Water Stresses During Piezocone Penetration in Clays. Canadian Geotechnical Journal, Vol. 27, No. 4, 418-428.

Mayne, P.W., Kulhawy, F.H., and Trautmann, C.H. 1992. Experimental Study of Undrained Lateral and Moment Behavior of Drilled Shafts during Static and Cyclic Loading. Report TR-100221, Electric Power Research Institute, Palo Alto, 383 p.

Mayne, P.W. and Mitchell, J.K. 1988. Profiling of Overconsolidation Ratio in Clays by Field Vane. Canadian Geotechnical Journal 25 (1), 150-157.

Mayne, P.W. and Stewart, H.E. 1988. Pore Pressure Behavior of K_o-Consolidated Clays. Journal of Geotechnical Engineering, ASCE, Vol. 114, No. 11, 1340-1346.

McManis, K.L. and Arman, A. 1986. Sampling and Testing in Stiff Crustal Clays. Geotechnical Aspects of Stiff and Hard Clays (GSP 2), ASCE, New York, 1-13.

McManus, K.J. And Kulhawy, F.H. 1990. A Cohesive Soil for Large-size Laboratory Deposits. Geotechnical Testing Journal, ASTM, Vol. 14, No. 1, 26-36.

Mesri, G. and Abdel-Ghaffar, M.E.M. 1993. Cohesion Intercept in Effective Stress-Stability Analysis. Journal of Geotechnical Engineering, Vol. 119, No. 8, 1229-1249.

Mesri, G. and Choi, Y.K. 1979. Strain Rate Behavior of St-Jean Vianney Clay. Discussion, Canadian Geotachnical Journal, Vol. 16, No. 4, 831-834.

Moh, Z.C. and Hwang, R.N. 1993. Underground Construction of Taipei Transit System. Proceedings, 11th Southeast Asian Geotechnical Conference, Singapore, 15-24.

Nyirenda, Z.M. and Sills, G.C. 1988. Discussion on Piezocone Penetration Testing. Penetration Testing in the UK, Thomas Telford, London, 183-184.

Ohta, H., Iizuka, A., Nishihara, A., Fukagawa, R., and Morita, Y. 1991. Design Strength s_u Derived from Pressuremeter Tests. Computer Methods and Advances in Geomechanics, Balkema, Rotterdam, 273-278.

Ohta, H., Nishihara, A., and Morita, Y. 1985. Undrained Stability of K_o-Consolidated Clays. Proceedings, 11th International Conference on Soil Mechanics and Foundation Engineering, San Francisco, Vol. 2, 613-616.

Olsen, H.W., Rice, T.L., Mayne, P.W., and Singh, R.D. 1986. Piston Core Properties and Disturbance Effects. Journal of Geotechnical Engineering, Vol. 112 (6), 608-625.

Parry, R.H.G. 1970. Overconsolidation in Soft Clay Deposits. Geotechnique, Vol. 20, No. 3, 442-446.

Pelli, F. and Ottaviani, M. 1993. Definizione Della Resistenza non Drenata Delle Argille del Mare Adriatico Mediante Prove Penetrometriche Statiche. Rivista Italiana Di Geotechnica, pp. 157-171. (in Italian)

Penner, E. and Burn, K.N. 1978. Review of Engineering Behavior of Marine Clays in Eastern Canada. Canadian Geotechnical Journal, Vol. 15, No. 2, 269-282.

Powell, J.J.M. and Quarterman, R.S.T. 1988. The Interpretation of CPT in Clays With Rate Effects. Penetration Testing 1988 (ISOPT-1), Balkema, Rotterdam, Vol. 2, 903-910.

Powell, J.J.M., Quarterman, R.S.T. and Lunne, T. 1988. Interpretation and Use of the Piezocone Test in UK. Penetration Testing in the UK, Thomas Telford, London, 47-52.

Powell, J.J.M. and Uglow, I.M. 1985. A Comparison of Menard Self-boring and Push-in Pressuremeter Tests in a Stiff Clay Till. Advanced in Underwater Technology and Offshore Engineering, Vol. 3, Offshore Site Investigation, Graham and Trotman, London, 201-217.

Prevost, J.H. 1979. Undrained Shear Tests on Clays. Journal of Geotechnical Engineering, ASCE, Vol. 105, No. 1, 49-64.

Rad, N.S. and Lunne, T. 1986. Correlations Between Piezocone Results and Laboratory Soil Properties. Internal Report 52155-39, Norwegian Geot. Institute, Oslo, 87 p.

Rad, N.S. and Lunne, T. 1988. Direct Correlation Between Piezocone Test Results and Undrained Shear Strength of Clay. Penetration Testing 1988 (ISOPT-1), Balkema, Rotterdam, Vol. 2, 911-917.

Randolph, M., Carter, J., and Wroth, C.P. 1979. Driven Piles in Clay: Effects of Installation. Geotechnique 29 (4), 361-393.

Randolph, M. and Wroth, C.P. 1981. Application of the Failure State in Undrained Simple Shear. Geotechnique, Vol. 31, No. 1, 143-157.

Reid, J.M. and Turnbull, K.W. 1988. An Example of the Use of Cone Penetration Testing in the Design of Underground Structures and Temporary Works in Cohesive Soils. Penetration Testing in the UK, Thomas Telford, London, 227-230.

Richards, A. and Zuidberg, H. 1985. In-Situ Determination of the Strength of Marine Soils. Strength Testing of Marine Sediments, (STP 883), ASTM, Philadelphia, 11-40.

Robertson, P.K. 1990. Soil Classification Using the Cone Penetration Test. Canadian Geotechnical Journal, Vol. 27, No. 1, 151-158.

Robertson, P.K. and Campanella, R.G. 1983. Interpretation of Cone Penetration Tests. Canadian Geotechnical Journal, Vol. 20, No. 4, 734-745.

Robertson, P.K. and Campanella, R.G. 1985. Evaluation of Liquefaction Potential of Sand Using CPT. Journal of Geotechnical Engineering Division, Vol. 111, No. 3, 384-407.

Robertson, P.K. and Campanella, R.G. 1988. Guidelines for Using the CPT, CPTU and Marchetti DMT for Geotechnical Design. Report No. FHWA-PA-87-023-84-24, Federal Highway Administration, Washington, D.C.

Robertson, P.K. and Campanella, R.G. 1989. Guidelines For Geotechnical Design Using CPT and CPTU. Soil Mechanics Series No. 120, Department of Civil Engineering, University of British Columbia, Vancouver, B.C., 419 p.

Robertson, P.K., Campanella, R.G., Gillespie, D., and Greig, J. 1986. Use of Piezometer Cone Data. Use of In-Situ Tests in Geotechnical Engineering (GSP 6), American Society of Civil Engineers, New York, 1263-1280.

Robertson, P.K., Campanella, R.G., Gillespie, D., and By, T. 1988a. Excess Pore Pressures and the Flat Dilatometer Test. Penetration Testing 1988 (ISOPT-1), Balkema, Rotterdam, Vol. 2, 567-576.

Robertson, P.K., Campanella, R.G., Davies, M.P., and Sy, A. 1988b. Axial Capacity of Driven Piles in Deltaic Soils Using CPT. Penetrating Testing 1988 (ISOPT-1), Balkema, Rotterdam, Vol. 2, 919-928.

Robertson, P.K., Howie, J., Sully, J.P., Gillespie, D.G., and Campanella, R.G. 1988c. Discussion on Preconsolidation Pressures from Piezocone Tests in Marine Clay. Geotechnique, Vol. 38, No. 3, 455-465.

Robertson, P.K., Woeller, D.J., and Gillespie, D. 1989. Evaluation of Excess Pore Pressures and Drainage Conditions Around Driven Piles Using the Cone Penetration Test With Pore Pressure Measurements. Canadian Geotechnical Journal, Vol. 27 (2), 249-254.

Robertson, P.K., Sully, J.P., Woeller, D.J., Lunne, T., Powell, J.J.M., and Gillespie, D.G. 1992. Estimating Coefficient of Consolidation from Piezocone Tests. Canadian Geotechnical Journal, Vol. 29, No. 4, 539-550.

Rocha Filho, P. and Alencar, J. 1985. Piezocone Tests in Rio de Janeiro Soft Clay. Proceedings, 11th International Conference on Soil Mechanics and Foundation Engineering, San Francisco, Vol. 2, 859-862.

Roy, M., Tremblay, M., Tavenas, F., and La Rochelle, P. 1982. Development of a Quasi-Static Piezocone Apparatus. Canadian Geotechnical Journal, Vol. 19, No. 1, 180-188.

Saines, M., Strutynsky, A., and Lytwynyshyn, G. 1989. Use of Cone Penetration Testing in Hydrogeologic Investigations. Proceedings, First USA/USSR Hydrogeology Conference, Moscow, USSR, 16 p.

Sandven, R. 1990. Strength and Deformation Properties of Fine Grained Soils Obtained From Piezocone Tests. Ph.D. Thesis, Norwegian Institute of Tech., Trondheim, 337 p.

Sandven, R., Senneset, K. and Janbu, N. 1988. Interpretation of Piezocone Tests in Cohesive Soils. Penetration Testing 1988, Vol. 2, Balkema, Rotterdam, 939-953.

Saxena, S.K., Hedberg, J., and Ladd, C.C. 1978. Geotechncial Properties of Hackensack Valley Varved Clays of NJ. ASTM Geotechnical Testing Journal, Vol. 1 (3), 148-161.

Schiffman, R.L. and Aggarwala, B.D. 1961. Stresses and Displacements Produces in a Semi-Infinite Elastic Solid by a Rigid Elliptical Footing. Proceedings, 5th International Conference on Soil Mechanics and Foundation Engineering, Paris, Vol. 1, 795-801.

Schleede, S.C. 1985. Geotechnical Exploration for the Blue Water Plaza Project, Port Huron, Michigan. Report SHA 014075, Schleede-Hampton Associates, Inc., Naperville, Illinois, 4 Volumes.

Schmertmann, J.H. 1955. The Undisturbed Consolidation Behavior of Clay. Transactions Vol. 120, ASCE, New York, 1201-1233.

Schmertmann, J.H. 1978. Guidelines for Cone Penetration Test: Performance and Design. Report No. FHWA-TS-78-209, Federal Highway Administration, Washington, D.C., 145p.

Schmidt, B. 1966. Discussion: Earth Pressure at Rest Related to Stress History. Canadian Geotechnical Journal, Vol. 3, No. 4, 148-161.

Senneset, K. 1974. Penetration Testing in Norway. Proceedings, 1st European Symposium on Penetration Testing, Stockholm, Vol. 1, 85-89.

Senneset, K. and Janbu, N. 1985. Shear Strength Parameters Obtained from Static Cone Penetration Tests. Strength Testing of Marine Sediments: Laboratory and In-Situ Measurements (STP 883), ASTM, Philadelphia, 41-54.

Senneset, K., Janbu, N., and Svano, G. 1982. Strength and Deformation Parameters from Cone Penetration Tests. Proceedings, 2nd European Symposium on Penetration Testing, Vol. 2, Amsterdam, 863-870.

Senneset, K., Sandven, R., Lunne, T., By, T., and Amundsen, T. 1988. Interpretation of Piezocone Tests in Cohesive Soils. Penetration Testing 1988 (ISOPT-1), Balkema, Rotterdam, Vol. 2, 939-953.

Senneset, K., Sandven, R., and Janbu, N. 1989. Evaluation of Soil Parameters from Piezocone Tests. Transportation Research Record 1235, Washington, D.C., 24-37.

Shibata, T., Mimura, M., Shrivastava, A.K., and Nobuyama, M. 1992. Moisture Measurement by Neutron Moisture Cone Penetrometer: Design and Application. Soils and Foundations, Vol. 32, No. 4, 58-67.

Sills, G.C., May, R.E., Henderson, T., and Nyirenda, Z. 1988. Piezocone Measurements With Four Pore Pressure Positions. Penetration Testing in the UK, Thomas Telford, London, 247-250.

Silvestri, V. and Aubertin, M. 1988. Anisotropy and In-Situ Vane Tests. Vane Shear Strength Testing in Soils (STP 1014), ASTM, Philadelphia, 88-103.

Skempton, A.W. 1954. The Pore Pressure Coefficients A and B. Geotechnique, Vol. 4, No. 1, 143-147.

Skempton, A.W. 1961. Horizontal Stresses in a Overconsolidated Eocene Clay. Proceedings, 5th International Conference on Soil Mechanics and Foundation Engineering, Vol. 1, Paris, 352-357.

Skomedal, E. and Bayne, J.M. 1988. Interpretation of Pore Pressure Measurements From Advanced Cone Penetration Testing. Penetration Testing in the UK, Thomas Telford, London, 279-283.

Smits, F.P. 1982. Penetration Pore Pressure Measured with Piezometer Cones. Proceedings, 2nd European Symposium on Penetration Testing (2), Amsterdam, 871-876.

Smits, F.P. and Bruzzi, D. 1988. The Hocus Experiment: Investigation of Hole Closure Behind Falling Penetrators. Penetration Testing 1988 (2, Balkema, Rotterdam, 975-984.

Sowers, G.F. 1979. Introductory Soil Mechanics and Foundations: Geotechnical Engineering. MacMillan Publishing Co., New York, 621 p.

Stark, T.D. and Juhrend, J.E. 1989. Undrained Shear Strength From Cone Penetration Tests. Proceedings, 12th International Conference on Soil Mechanics and Foundation Engineering, Rio de Janeiro, Vol. 2, 327-330.

Sugawara, N. 1988. On the Possibility of Estimating In-Situ OCR Using Piezocone. Penetration Testing 1988 (ISOPT-1), Balkema, Rotterdam, Vol. 2, 985-991.

Sugawara, N. and Chikaraishi, M. 1982. On Estimation of ϕ' for Normally Consolidated Mine Tailings by Using the Pore Pressure Cone Penetrometer. Proceedings, 2nd European Symposium on Penetration Testing, Amsterdam, Vol. 2, 883-888.

Sully, J.P. 1991. Measurement of In Situ Lateral Stress During Full-Displacement Penetration Tests. Ph.D. Thesis, Department of Civil Engineering, The University of British Columbia, Vancouver, 485 p.

Sully, J.P. and Campanella, R.G. 1990. Measurement of Lateral Stress in Cohesive Soils. Transportation Research Record 1278, Washington, D.C., 164-171.

Sully, J.P. and Campanella, R.G. 1991. Effect of Lateral Stress on CPT Penetration Pore Pressures, Journal of Geotechnical Engineering, ASCE, Vol. 117, No. 7, pp. 1082-1088.

Sully, J.P. and Campanella, R.G. 1994. Evaluation of Field CPTU Dissipation Data in Overconsolidated Fine-Grained Soils. Proceedings, 13th International Conference on Soil Mechanics and Foundation Engineering (1), New Delhi, 201-204.

Sully, J.P., Campanella, R.G., and Robertson, P.K. 1988a. Interpretation of Penetration Pore Pressures to Evaluate Stress Histories in Clays. Penetration Testing 1988, Balkema, Rotterdam, Vol. 2, 993-999.

Sully, J.P., Campanella, R.G., and Robertson, P.K. 1988b. Overconsolidation Ratio of Clays from Penetration Pore Water Pressures. Journal of Geotechnical Engineering, ASCE, Vol. 114, No. 2, 209-215.

Sully, J. P. and Murria, J.M. 1987. Piezocone Testing in Lacustrine Soils. Proceedings, 8th Pan American Conf. on Soil Mechanics and Foundation Engrg (2), Cartagena, 177-189.

Sweeney, B.P. and Kraemer, S.R. 1993. Final Report on Special Laboratory and In Situ Testing Program - General Artery (I-93)/Tunnel (I-90) Project. Report No. 10360-40, Haley & Aldrich, Inc., Cambridge, Mass., 94 p.

Tanaka, A. and Diniz, A.M. 1993. Piezocone Tests in a Soft Clay Deposit. Proceedings, 11th Southeast Asia Geotechnical Conference, Singapore, 229-232.

Tanaka, Y. and Sakagami, T. 1989. Piezocone Testing in Underconsolidated Clay. Canadian Geotechnical Journal, Vol. 26, No. 4, 563-567.

Tang, S. and Zhu, X. 1988. Variations of the Subsoil Before and After Piling Measured by Piezocone Penetration Test. Penetration Testing 1988 (ISOPT-1), Balkema, Rotterdam, Vol. 2, 1007-1013.

Tavenas, F. 1981. Advantages and Limitations of the Piezocone. Proceedings, 10th International Conference on Soil Mechanics and Foundation Engineering (4), Stockholm, 769-773.

Tavenas, F., Blanchet, R., Garneau, R., and Leroueil, S. 1978. The Stability of Stage Constructed Embankments on Clay. Canadian Geotechnical Journal, Vol. 15 (3), 283-305.

Tavenas, F., Leroueil, S., and Roy, M. 1982. The Piezocone Test in Clays: Use and Limitations. Proceedings, 2nd European Symposium on Penetration Testing, Amsterdam, Vol. 2, 889-894.

Tavenas, F. and Leroueil, S. 1977. Effects of Stresses and Time in Yielding of Clays. Proceedings, 9th International Conference of Soil Mechanics and Foundation Engineering, Tokyo, Vol. 1, 319-326.

Tavenas, F. and Leroueil, S. 1979. Clay Behavior and the Selection of Design Parameters. Proceedings, 7th European Conference on Soil Mechanics and Foundation Engineering, Vol. 1, Brighton, England, 281-291.

Tavenas, F. and Leroueil, S. 1987. State-of-the-Art on Laboratory and In-Situ Stress-Strain-Time Behavior of Soft Clays. Proceeding, International Symposium on Geotechnical Engineering of Soft Soils, Mexico City, 1-146.

Taylor, B.B. 1993. Hibernia Development Project. Draft Report, Jacques/McClelland Geosciences, Inc., Dartmouth, Nova Scotia.

Teh, C.I. and Houlsby, G.T. 1988. An Analysis of the Cone Penetration Test by the Strain Path Method. Numerical Methods in Geomechanics, Vol. 1, (Proc. 6th NUMOG, Innsbruck), Balkema, Rotterdam, 397-402.

Teh, C.I. and Houlsby, G.T. 1991. An Analytical Study of the Cone Penetration Test in Clay. Geotechnique 41 (1), 17-34.

Torstensson, B.A. 1975. Pore Pressure Sounding Instrument. Proceedings, ASCE Specialty Conference on In-Situ Measurement of Soil Properties, Raleigh, NC, Vol. 2, 48-54.

Torstensson, B.A. 1982. A Combined Pore Pressure and Point Resistance Probe. Proceedings, 2nd European Symposium on Penetration Testing (2), Amsterdam, 903-908.

Tsuchiya, H., Muromachi, T., Sakai, Y., and Iwasaki, K. 1988. Penetration Testing 1988 (ISOPT-1), Balkema, Rotterdam, Vol. 2, 1021-1026.

Tumay, M.T., Acar, Y.B., Cekirge, M.H., and Ramesh, N. 1985. Flow Field Around Cones in Steady Penetration. Journal of Geotechnical Engineering, Vol. 111 (2), 193-204.

Tumay, M.T. and Acar, Y.B. 1985. Piezocone Penetration Testing in Soft Cohesive Soils. Strength Testing of Marine Sediments (STP 883), ASTM, Philadelphia, 72-82.

Tumay, M.T., Acar, Y., deSeze, E., and Yilmaz, R. 1982. Soil Exploration in Soft Clay with Electric Cone Penetrometer. Proceedings, 2nd European Symposium on Penetration Testing (2), Amsterdam, 415-921.

Tumay, M.T., Boggess, R.L., and Acar, Y.B. 1981. Subsurface Investigations With Piezo-Cone Penetrometer. Cone Penetration Testing and Experience, ASCE, New York, 325-342.

Tumay, M.T. and deSeze, E. 1983. Correlations of Undrained Shear Strength and QCPT Results Using SHANSEP Approach. Report No. FHWA/LA/LSU-GE-83/01, Federal Highway Administration, Washington, D.C., 166 p.

Ventura, P. 1983. Piezometer Cone Penetration Tests in Marine Subsoil Profiles. Proceedings, International Symposium on In-Situ Testing, Paris, Vol. 2, 425-427.

Vesić, A.S. 1972. Expansion of Cavities in Infinite Soil Mass. Journal of the Soil Mechanics and Foundations, ASCE, Vol. 98, No. 3, 265-290.

Vesić, A.S. 1975. Principles of Pile Foundation Design. Lecture Series on Deep Foundation, Boston Society of Civil Engineers, 46 p.

Vesić, A.S. 1977. Design of Pile Foundations. Synthesis of Highway Practice 42, Transportation Research Board, National Research Council, Washington, D.C., 68 p.

Villet, W.C.B. and Mitchell, J.K. 1981. Cone Resistance, Relative Density and Friction Angle. Cone Penetration Testing and Experience, ASCE, New York, 178-208.

Villet, W.C.B. and Darragh, R.D. 1985. Interpretation of Piezometric Cone Tests in Highly Overconsolidated Offshore Silts. Proceedings, 17th Offshore Technology Conference, Houston, Vol. 2, 187-200.

Vlasblom, A. 1985. The Electrical Penetrometer: A Historical Account of Its Development. Internal Publication, Delft Soil Mechanics Laboratory, P.O. Box 69, 2600 AB Delft, Netherlands, 52 p.

Whittle, A.J. 1990. A Constitutive Model for Overconsolidated Clays. Report No. MITSG 90-15, Massachusetts Institute of Technology, Cambridge, 25 p.

Whittle, A.J. 1993. Evaluation of a Constitutive Model for Overconsolidated Clays. Geotechnique, Vol. 43, No. 2, 289-313.

Whittle, A.J. and Aubeny, C.P. 1993. The Effects of Installation Disturbance on Interpretation of In-Situ Tests in Clay. Predictive Soil Mechanics (Proc. Wroth Memorial Symposium), Thomas Telford, London, 742-767.

Whittle, A.J. and Kavvadas, M.J. 1994. Formulation of MIT-E3 Constitutive Model for Overconsolidated Clays. Journal of Geotechnical Engineering, Vol. 120, No. 1, 173-198.

Wickremesinghe, D.S. and Campanella, R.G. 1991. Statistical Methods for Soil Layer Boundary Location Using the Cone Penetration Test. Proceedings, 6th Intl. Conf. on Applications of Statistics and Probability in Civil Engrg., Mexico City, Vol. 2, 636-643.

Wissa, A.E., Martin, R.T., and Garlanger, J.E. 1975. The Piezometer Probe. Proceedings, ASCE Conference on In-Situ Measurement of Soil Properties, Raleigh, Vol. 1, 536-545.

Woeller, D.J., Weemes, I., Kurfurst, P.J., and Robertson, P.K. 1991. Penetration Testing for Arctic Soil and Permafrost Conditions. Proceedings, 44th Canadian Geotechnical Conference, Calgary, Alberta, Vol. 1, 44-1 to 44-7.

Wroth, C.P. 1984. The Interpretation of In-Situ Soils Tests. Geotechnique, Vol. 34, No. 4, 449-489.

Wroth, C.P. 1988. Penetration Testing: A Rigorous Approach to Interpretation. Penetration Testing 1988 (ISOPT-1), Vol. 1, Balkema, Rotterdam, 303-311.

Wroth, C.P. and Houlsby, G. 1985. Soil Mechanics - Property Characterization and Analysis Procedures. Proceedings, 11th International Conference on Soil Mechanics and Foundation Engineering, Vol. 1, San Francisco, 1-54.

Zuidberg, H., Schaap, L., and Beringer, F. 1982. A Penetrometer for Cone Resistance and Dynamic Pore Pressure. Proceedings, 2nd European Symposium on Penetration Testing, Amsterdam, Vol. 2, 963-970.

Go UT!